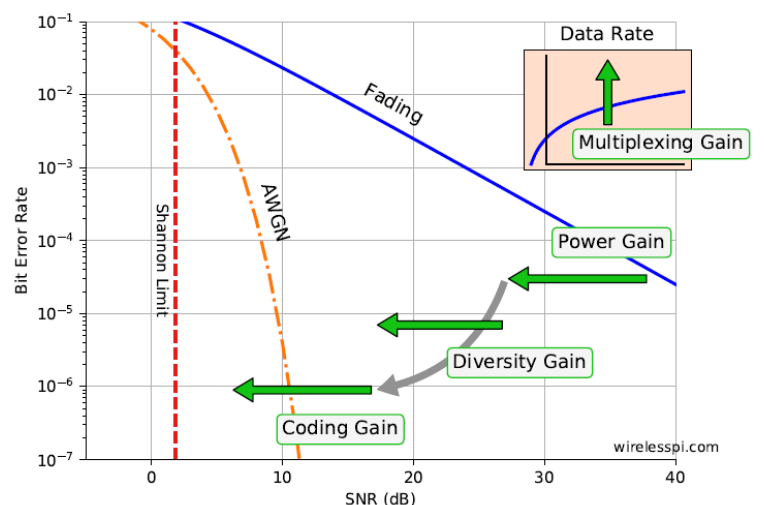
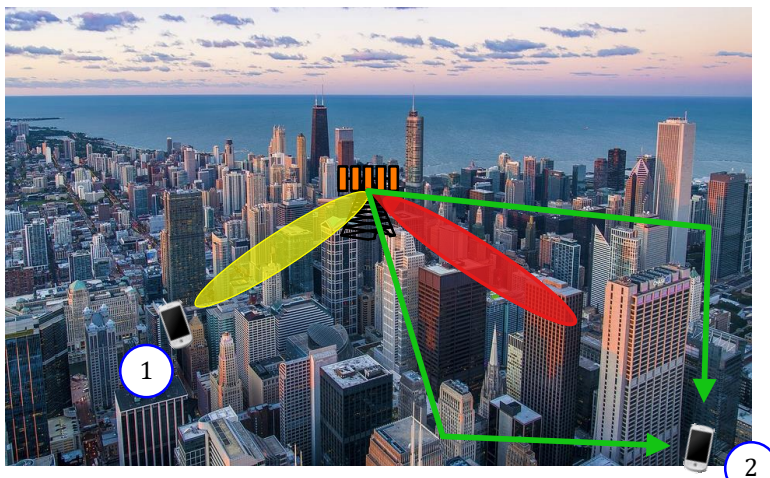


5G Physical Layer

An Easy Guide to Key Technologies



Qasim Chaudhari

5G Physical Layer

An Easy Guide to Key Technologies

Qasim Chaudhari

Copyright 2021 by Qasim Chaudhari

All rights reserved. This book or any portion thereof may not be reproduced or used in any manner whatsoever without the express written permission of the publisher. While we believe that the information given in this work is correct, all parties must rely upon their own skill and judgement when making use of them. We do not assume any liability to anyone for any loss or damage caused by any error or omission in the work, whether such error or omission is the result of negligence or any other cause. Any and all such liability is disclaimed.

For permission requests, contact info@wirelesspi.com.

Qasim Chaudhari
Melbourne, Australia
wirelesspi.com

Table of Contents

Preface	vii
1 Linking Data to Signals	1
1.1 The Big Picture	5
1.2 Complex Signals	8
1.3 Basics of Digital Communication	11
1.4 Quadrature Amplitude Modulation (QAM)	15
1.5 Appendix	19
2 Signal Transmission in a Wireless Channel	21
2.1 Large-Scale Fading	23
2.2 Small-Scale Fading	24
2.3 Diversity: A Dumb yet Clever Idea	37
2.3.1 The Anna Karenina Principle	38
2.3.2 The Inverse Anna Karenina Principle	40
2.3.3 Types of Diversity	44
2.4 Multiple Antenna Modes	47
3 Beamforming Demystified	51
3.1 Signal Model	54
3.2 Viewing Multiple Antennas through a Different Lens	57
3.3 Classical or Physical Beamforming	62
3.3.1 Superposition of Waveforms	64
3.3.2 Array Gain	67
3.3.3 The Origin of Beams	69
3.3.4 Beam Steering	90
3.4 Generalized or Virtual Beamforming	100
3.4.1 Maximum Ratio Combining (MRC)	101
3.4.2 Array Gain vs Diversity Gain	107
3.4.3 Maximum Ratio Transmission (MRT)	115

3.4.4	Precoding and Combining	118
3.5	The Small Picture	126
3.6	Appendix	126
4	Massive MIMO	131
4.1	Multi-User MIMO	135
4.2	Massive MIMO	138
4.3	Detection Algorithms	140
4.3.1	Spatial Matched Filtering (Maximum Ratio)	140
4.3.2	Zero-Forcing (ZF)	150
4.4	Acquiring Channel State Information (CSI)	155
4.5	Pilot Contamination	163
4.6	The Small Picture	165
5	Spatial Multiplexing	167
5.1	From Multi-User MIMO to Single-User MIMO	170
5.2	Detection with Tx Channel Knowledge	172
5.3	Detection with no Tx Channel Knowledge	186
5.3.1	Linear Detection	186
5.3.2	Successive Interference Cancellation	189
5.3.3	The Algorithm from a Clever Horse	194
6	Millimeter Wave (mmWave) Communication	201
6.1	Channel Propagation	205
6.2	Analog, Digital and Hybrid Beamforming	212
6.3	mmWave Massive MIMO	218
6.4	The Small Picture	220
7	Low Density Parity Check (LDPC) Codes	221
7.1	Encoding	225
7.2	Decoding	227
7.3	Appendix	242
8	Orthogonal Frequency Division Multiplexing (OFDM)	245
8.1	From the Printer Port	247
8.2	To a Sliced Bread	266
8.3	Why CP-OFDM?	274
8.4	Sub-Carrier Spacing (SCS)	275
8.5	DFT-Precoded OFDM	278
8.6	The Small Picture	279

TABLE OF CONTENTS

v

One Page Summary	281
Bibliography	283

Preface

The readers of my first book “Wireless Communications from the Ground Up - An SDR Perspective” know that a good explanation contains the following three features in my opinion: Lots of visualizations, easy mathematics and intuitive reasonings.

- In writing this book too, I focused on explaining the ideas through many figures which I hope are reasonably beautiful. Authors usually write the text and then draw figures. Since I learn the concepts through images in my mind, I draw a figure first and then explain it in the text. In the end, a reader is the best judge in regards to the quality of those figures.
- The mathematics part was a challenge because multiple antenna or MIMO systems are inherently tied up with matrices and linear algebra. I solved this problem through explaining a scalar case and then generalizing it to a matrix expression in the end. This approach kept this book clear of heavy matrix formulations. Also, at very few places where I used e and j to convey the concept, I confined them to a dedicated box that can be skipped without any discontinuity in exposition. Finally, some derivations have been given in appendices for interested readers in a small font.
- Most topics contain an intuitive description that makes them easier to understand. This is how a human mind works. For example, if I show you a number 1202, you will forget it in a few minutes. But with extra information that this number is the year 2021 in reverse, you will remember it for a long time. The link between 1202 and 2021 will keep the memory alive and correct.

An extra little bonus is a one page summary of the general direction of development in 5G cellular systems (in addition to one page for figures, it spans an extra page for a short and relevant description). A reader can see the big picture of the techniques employed and can also extrapolate the trends for future wireless networks.

On a personal note, I never thought that I would write a book ... again. The factors that led me towards this path are as follows. Multiple antenna systems and spatial signal processing are natural extensions of single-carrier systems we covered in the earlier book. In that sense, this work complements

and completes the first one. Nevertheless, the focus here is on how things work and not on algorithm development, the details of which can fit into another book. Furthermore, many of my readers asked me to write on 5G technologies. Finally, as the technology advances, two trends appear in general in any field. The science becomes more complicated after the low hanging fruit is picked up and hence only a few can master it. But if this technology has a real impact on our everyday lives (which the wireless systems do), the general public also gets interested in learning the fundamentals. In today's world, this diverse knowledge always proves to be the critical edge. I have tried to bridge this gap between the experts who are designing the systems and the learners who are eager to make sense of it.

On a final note, almost everything in this book comes from many engineers and researchers who have investigated and disseminated their ideas and they deserve the credits for the good part. Since this book is written, read and checked by a single person, there is a chance of technical errors and typos that are entirely my responsibility. If you find any such mistake, thank you for kindly informing me at info@wirelesspi.com.

Qasim Chaudhari
Melbourne, Australia
Oct 2021

Chapter 1

Linking Data to Signals



The first commercial cellular network was launched in Japan in 1979 and quickly proliferated in the rest of the world afterwards (that is what cells do). Very few people were able to visualize the oncoming revolution and the network was not even called 1G at that time. It made perfect sense for James Cameron to think of a future world where humans and machines will be fighting wars with *machine guns*. With the benefit of hindsight today, we know that this will never happen. The electronic side (the brain) of the technology has left its mechanical counterpart (the body) in the dust.



The Terminator (Image Credit: Orion Pictures)

The advancements in Gs has given rise to an increasingly connected world that is being taken to a new level by the 5G standard. With the Internet of Everything, smart grids, autonomous vehicles and transportation systems, financial and trading centers, or the security systems, information is constantly traveling in all directions across the globe at an unprecedented rate. It seems that everything that can be connected and automated will be connected and automated while complete ecosystems are being built on these oceans of information. It is possible to soon find ourselves living in a world where the symbolic butterfly flapping its wings in India can actually cause hurricanes in the United States. What will an antagonist Artificial Intelligence of the future need to bring the world to a halt and humans to their knees? Practically nothing. We would already have relinquished too much control, no machine guns required.

We are led on this path from an instinct to consume information. According to George Miller: "Just as the body survives by ingesting negative entropy, so the mind survives by ingesting information." Similar to the classification of animals into herbivores, carnivores and omnivores, modern cognitive scientists use the term *informavores* for humans. Information flow runs everything from our cell biology to our society to our economy. This information exchange is responsible for creating out of brain cells the experience of mind, making the weak homo sapiens the masters of the planet Earth, and transforming separate isolated worlds into a single global market. To extrapolate this trend, I quote a passage from *Sylvie and Bruno Concluded* by Lewis Carroll published in 1893. It tells us of a fictional map that had the scale of a mile to the mile.

"What a useful thing a pocket-map is!" I remarked.

"That's another thing we've learned from your Nation," said Mein Herr, "map-making. But we've carried it much further than you. What do you consider the largest map that would be really useful?"

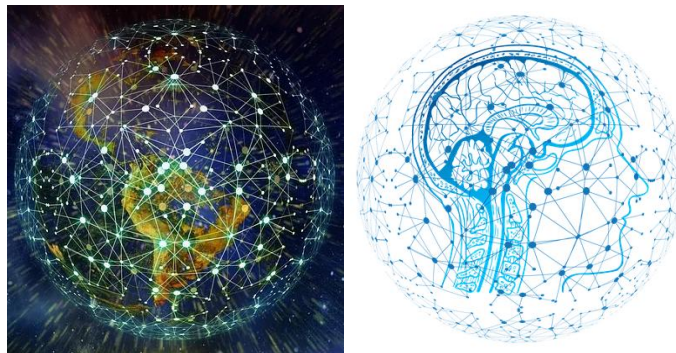
"About six inches to the mile."

"Only six inches!" exclaimed Mein Herr. "We very soon got to six yards to the mile. Then we tried a hundred yards to the mile. And then came the grandest idea of all! We actually made a map of the country, on the scale of a mile to the mile!"

"Have you used it much?" I enquired.

"It has never been spread out, yet," said Mein Herr: "the farmers objected: they said it would cover the whole country, and shut out the sunlight! So we now use the country itself, as its own map, and I assure you it does nearly as well."

Reality is complicated. We attempt to understand it through simpler models. Like the mile for mile map, we are also inadvertently building a huge brain on the scale of the planet itself by *connecting* as many nodes as possible. On the constructive side, this might help us understand the world in true depth. Moreover, it might subsequently give rise to an intelligence higher than humankind that could prove to be the greatest companion we have ever had. On the destructive side, that companion might turn against us one day as predicted by all the doomsday movies.



Connectivity implies building a brain as large as the planet itself

Today a large part of this information consuming behavior can be traced back to the ubiquitous wireless communication systems, what radio pioneer Lee De Forest called "an Invisible Empire of the Air, intangible, yet solid as granite". I suspect that at this point of our history, we are communicating more with electromagnetic waves than acoustic waves. Ever since we linked digital electronics to information exchange from one point to another without any physical medium, on-demand reception and transmission of data at any place and any time are exploding in an exponential manner. The roadblocks encountered on the growth curve of this invisible empire have consistently been overcome through invention of new technologies. These are the technologies you will learn about in this text that form the backbone of the physical layer (PHY) of 5G cellular systems.

1.1 The Big Picture

We now explore the big picture of information transfer on a wireless channel from both a single user and multiuser perspectives.

Single User Perspective

Let us start with the Bit Error Rate (BER) curve plotted against the Signal to Noise Ratio (SNR) in Figure 1.1. Even though the terminology used in this bird's eye view seems a little complicated, I do not assume any background knowledge on the reader's part. We will explore the interesting ideas behind each of them as we progress forward with the contents.

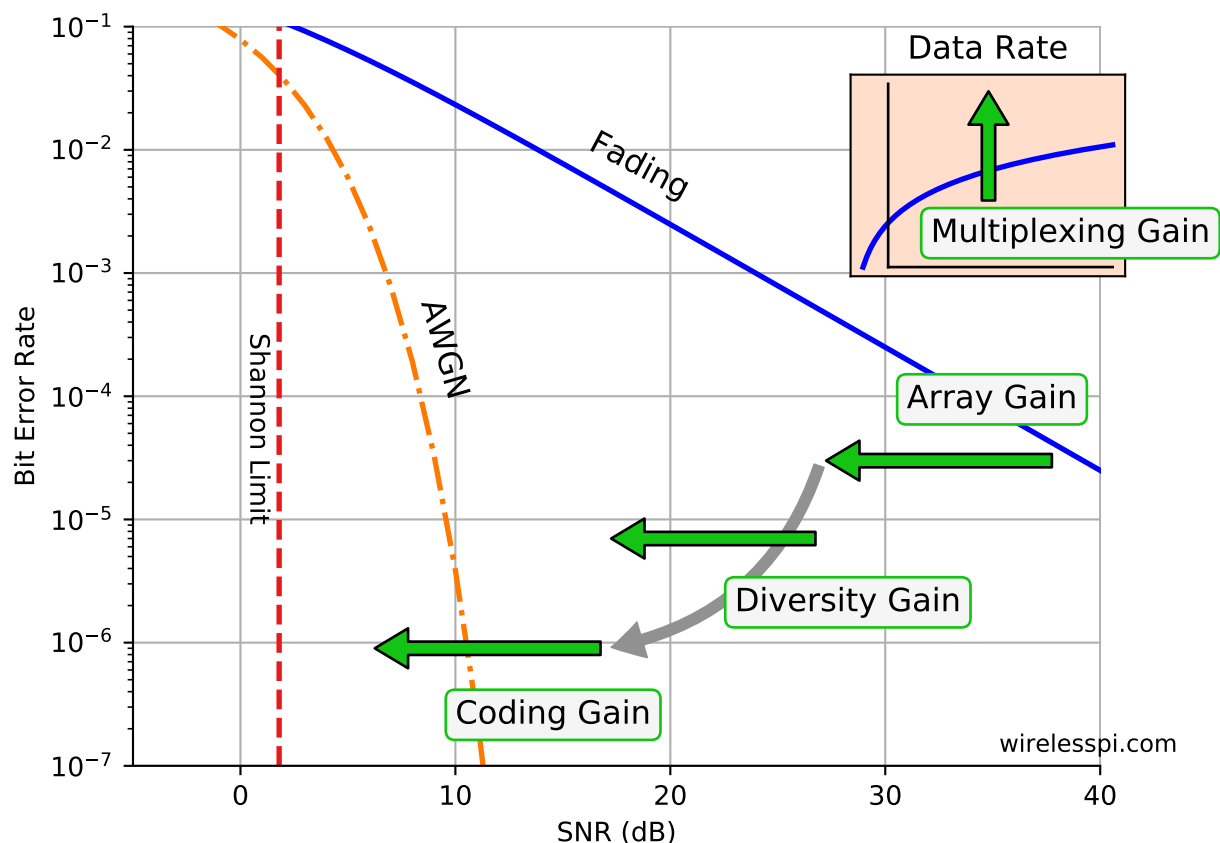


Figure 1.1: The big picture of wireless transmission from a single user perspective

- On the far left, the red dashed line is the Shannon limit on the SNR for a given data rate and bandwidth of the system. Error-free communication is not possible below this threshold.
- The orange dot-dashed line depicts the BER of the simplest digital modulation scheme in an Additive White Gaussian Noise (AWGN) channel. This is an idealized curve when no other

distortion affects the system performance.

- On the far right, the solid blue line shows the BER of the same digital modulation scheme operating in a wireless fading channel. Given a certain error rate (i.e., draw a horizontal line cutting all the curves for this purpose), the most remarkable feature here is the huge difference in SNR as compared to an AWGN channel. For instance, this difference is approximately $34 - 8 = 26$ dB at a BER of 10^{-4} !

The *array gain* shown in Figure 1.1 is obtained through processing the spatial samples at multiple antennas that is described in detail in Chapter 3. The *diversity gain* is achieved in several ways including time, frequency and space (i.e., antennas)[†] that is covered in different chapters. Moreover, we study clever techniques to acquire a *coding gain* such as Low Density Parity Check (LDPC) codes in Chapter 7 which pull this error rate closer to the Shannon limit. Finally, the curve in the inset of this figure draws the maximum achievable data rate for error-free communication known as the capacity of the channel. Increasing the rate of transmission in proportion to the number of deployed antennas, known as *multiplexing gain*, is one of the most attractive benefits of MIMO systems that is investigated in Chapter 5.

Multi-User Perspective

From a perspective of multiple users, there are three main themes that play a key role in increasing the data rate per unit area. It turns out that the area throughput can be broken as

$$\text{Area throughput (bits/s/km}^2\text{)} = \underbrace{\text{Spectral efficiency (bits/s/Hz/cell)}}_1 \times \underbrace{\text{Cell density (cells/km}^2\text{)}}_2 \times \underbrace{\text{Bandwidth (Hz)}}_3$$

In practice, network operators frequently measure the traffic density in units of Gigabits/s/km²/MHz of spectrum, abbreviated as GkM. The above expression tells us that these are the three areas where massive improvement is possible for 5G networks.

1. Spectral Efficiency

Better modulation and coding schemes as well as massive MIMO technology deal with increasing the spectral efficiency. Beamforming techniques described in Chapter 3 separate multiple users in spatial domain and allow them to transmit and receive at the same time on the same frequency. Massive MIMO is discussed in detail in Chapter 4 while Low Density Parity Check (LDPC) codes will be explained in Chapter 7.

[†]As shown in the figure with the main green arrow, the diversity gain is a shift towards the left or a decrease in SNR for the same bit error rate. However, we will learn later that diversity reduces the slope of this curve which has a drastic impact on system reliability. This is why I have drawn a grey arrow at an angle in the background representing the role of diversity in reduction of that slope.

2. Cell Density

A dense network serves the purpose of more efficient frequency reuse over a region, i.e., the same spectrum used over one limited geographical area can be reutilized in a neighboring area. As we will find out, higher frequencies in the mmWave band experience harsher propagation conditions than the lower microwave frequencies. Therefore, smaller cells are also better for communication in the mmWave spectrum that increase the cell density and lead to better frequency reuse.

3. Bandwidth

A wider bandwidth directly translates into higher throughput, just like increasing the number of lanes on a road directly impacts the traffic handled at peak times. This is the original reason for opening up the higher GHz and THz bands where vast amounts of empty spectrum is available. We cover communication in mmWave bands in Chapter 6.

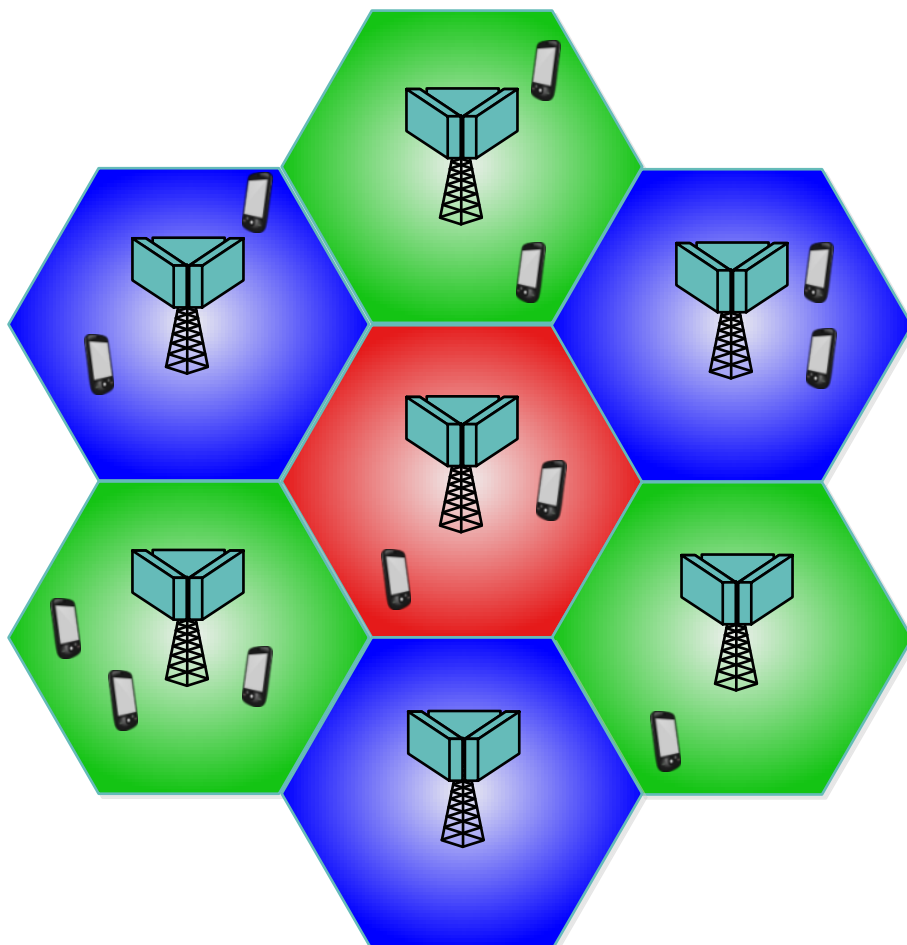


Figure 1.2: A cellular network

With this background, let us move towards the fundamental ideas behind waveform design. We begin with the concept of a complex sinusoid that forms the basis for all signal processing applications in communication systems, including the wireless signal that travels over the air from the Tx to the Rx side.

1.2 Complex Signals

Although complex notation is not complex to understand, one of the themes of this text is to avoid the usual notations e , i and j as much as possible. This is how we proceed next.

A Complex Number

We focus on a 2-dimensional plane with x or real-axis named as I (which stands for *inphase*) and y or imaginary-axis named as Q (which stands for *quadrature*), as shown in Figure 1.3. In Section 1.4, we will learn why these x and y components are called inphase and quadrature, respectively.

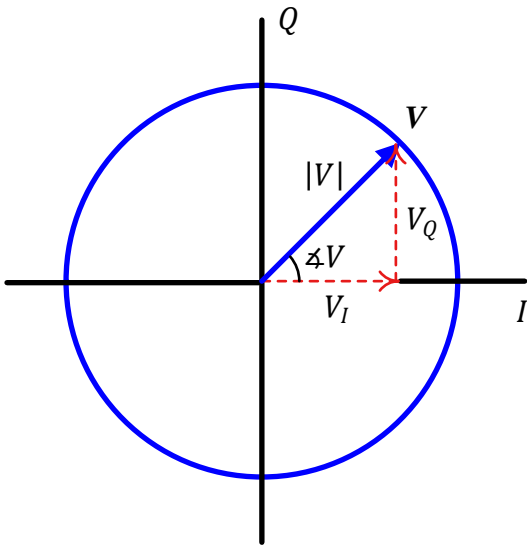


Figure 1.3: A complex number V in IQ -plane

In this IQ -plane, a complex number V is defined as a pair of real numbers (V_I, V_Q) , where V_I and V_Q are its I and Q components, respectively. This is known as a rectangular representation. From Figure 1.3, V can also be described in terms of its magnitude $|V|$ and phase $\angle V$, which is a polar representation. To convert from rectangular to polar coordinates, we apply results from simple geometry.

$$\begin{aligned} |V| &= \sqrt{V_I^2 + V_Q^2} \\ \angle V &= g\left(\frac{V_Q}{V_I}\right) \end{aligned} \tag{1.1}$$

where the function $g(\cdot)$ represents a simple \tan^{-1} for quadrants I and IV but incorporates the sign change for other quadrants. On the other hand, going from polar to rectangular coordinates implies

$$\begin{aligned} V_I &= |V| \cos \angle V \\ V_Q &= |V| \sin \angle V \end{aligned} \quad (1.2)$$

With this background, we explore the fundamental signal in signal processing applications: a complex sinusoid.

A Complex Sinusoid

Consider again a complex number V previously shown in Figure 1.3 in an IQ -plane. Now imagine V rotating anticlockwise in a circle at a constant rate with time as drawn in Figure 1.4. We note the following.

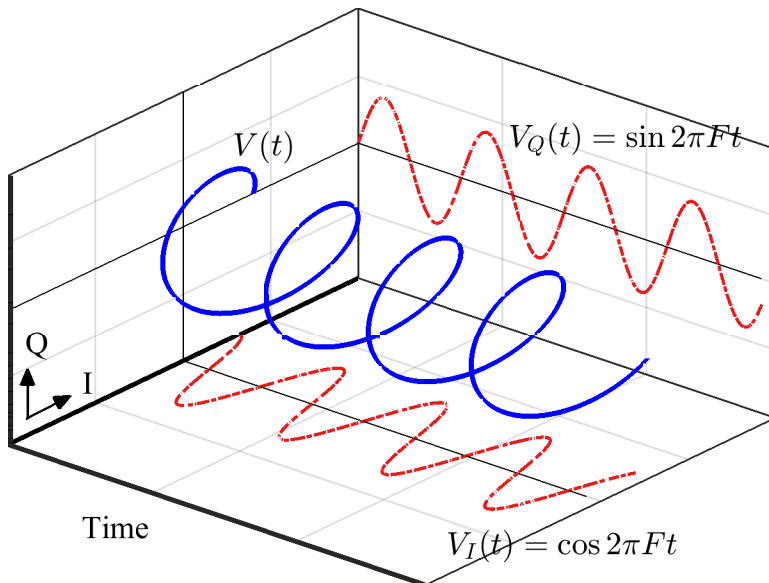


Figure 1.4: A complex sinusoid V rotating in time IQ -plane and generating a helix that projects two real sinusoids: $\cos 2\pi F t$ on I -axis and $\sin 2\pi F t$ on Q -axis

- The complex number V has become a signal $V(t)$ with time as independent variable. This complex signal rotating in time IQ -plane is called a **complex sinusoid**.
- A constant rotation rate implies that in any given duration Δt , the change in phase $\Delta\theta$ is a constant. This constant is known as the **angular velocity** that is defined as the rate of change in phase of this complex sinusoid, just like velocity is the rate of change of displacement.

$$\text{angular velocity} = \frac{\Delta\theta}{\Delta t}$$

- This angular velocity results in $V(t)$ generating a helix in the time IQ -plane, as shown in Figure 1.4.
- The **frequency** of this complex sinusoid is defined as this angular velocity normalized by 2π so that the units are cycles/second instead of radians/second.

$$F = \frac{1}{2\pi} \cdot \frac{\Delta\theta}{\Delta t}$$

Note that as time passes, $V(t)$ is shown in Figure 1.4 as coming out of the page. When its projection from a 3-dimensional plane to a 2-dimensional plane formed by time and I -axis is drawn downwards, we get its I part $V_I(t) = \cos 2\pi F t$. Similarly, when the projection is drawn on a 2-dimensional plane formed by time and Q -axis (on the back of the page), it generates the Q part $V_Q(t) = \sin 2\pi F t$. We will explain the terms I and Q shortly.

In conclusion, a complex sinusoid with frequency F is composed of two real sinusoids

I	\rightarrow	$V_I(t) = \cos 2\pi F t$ $V_Q(t) = \sin 2\pi F t$	(1.3)
Q	\uparrow		

where F is the continuous frequency with units of cycles/second or Hertz (Hz). The direction of rotation determines the sign of frequency as explained below.

Negative Frequency

Long ago, a lot of confusion clouded around negative numbers when numbers were used to count things. People could not understand how a person A can give -3 apples to a person B . It turned out that this can be accomplished by changing the direction of giving, i.e., A actually takes 3 apples from B .

Similarly, a frequency is usually defined as an inverse period $F = 1/T$ of a sinusoid. Naturally it becomes hard to visualize a negative frequency viewed as inverse period. Define it through the rate of rotation in an *anticlockwise* direction of a complex sinusoid $V(t)$ as in Figure 1.4, and it is evident that a negative frequency simply implies rotation of $V(t)$ in a *clockwise* direction. For example, the complex sinusoid

I	\rightarrow	$\cos 2\pi(-F)t = \cos 2\pi F t$
Q	\uparrow	$\sin 2\pi(-F)t = -\sin 2\pi F t$

has a frequency of $-F$. Here, we have used the identities $\cos(-\theta) = \cos \theta$ and $\sin(-\theta) = -\sin \theta$. With this understanding of complex signals, we are ready to move towards the basics of digital communication.

1.3 Basics of Digital Communication

“The fundamental problem of communication is that of reproducing at one point either exactly or approximately a message selected at another point.”

Claude Shannon - A Mathematical Theory of Communication [1]

This section briefly introduces what digital communication is about, see Ref. [2] for a detailed description. The main task of a digital communication system is to transfer a sequence of bits (0s and 1s) from one device to another through a channel. The most important parameter in this context is the data rate: the number of bits transmitted and received during one second. This is also called the *bit rate* and is denoted by R_b bits/second (b/s).

Amplitude Modulation

Since 0 and 1 bits have no physical form of their own, they are mapped to distinct voltage levels known as *symbols*, e.g.,

$$\begin{aligned} 0 &\longrightarrow +A \\ 1 &\longrightarrow -A \end{aligned}$$

at discrete time intervals $m = 0, 1, 2, \dots$. This process is called bit-symbol mapping and the time index m counts each such *symbol time*, T_M . A constellation of symbols is shown in Figure 1.5 which illustrates the relationship between bits $b[m]$ and symbols $s[m]$ as

$$s[m] = \begin{cases} +A, & b[m] = 0 \\ -A, & b[m] = 1 \end{cases} \quad (1.4)$$

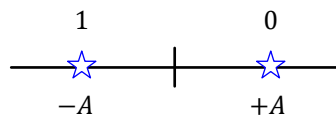


Figure 1.5: Two voltage levels or symbols representing 0 and 1

- This process of transforming bits of the maths world into symbols of the real world is given the name *modulation*. This also includes creating waveforms from these symbols that can travel down the channel between the Tx and Rx.
- Binary modulation implies that only two symbols are used here, one each for 0 and 1. For example, a binary 0 can be mapped to level $+A$ and a binary 1 can be mapped on symbol $-A$.

- Since the levels $+A$ and $-A$ refer to the amplitudes, this is a case of *pulse amplitude modulation*. Later, we will discuss phase modulation too that will lead us towards a combination of amplitude and phase modulations in Section 1.4 known as Quadrature Amplitude Modulation (QAM).

The received signal $r[m]$ is corrupted by the addition of random noise and given as

$$r[m] = s[m] + \text{noise}$$

As a consequence of noise addition, the received symbols are scattered around the actual symbol values. For the Rx to perform an inverse mapping from voltage levels or symbols back to bits, common sense dictates that symbol decisions $\hat{s}[m]$ should be taken according to the minimum distance rule:

Minimum distance rule

If $r[m]$ is closer to $-A$, it is decided that symbol $-A$ was sent at time m , and if it closer to $+A$, it is taken as symbol $+A$. To construct a general intuitive rule, the point in their middle is $(-A + A)/2 = 0$, and hence

$$\hat{s}[m] = \begin{cases} +A, & r[m] > 0 \\ -A, & r[m] < 0 \end{cases} \quad (1.5)$$

Let us now describe how more bits can be assigned to each symbol for faster transmission.

Higher Order Modulation

Notice that if a Rx can differentiate between two signal levels like a switch, it can certainly differentiate between more than two signal levels as well. Being able to do so can result in sending more data during the same amount of time. For example, Figure 1.6 shows four different symbols with the following bit assignments.

00	\longrightarrow	$-3A$
01	\longrightarrow	$-A$
11	\longrightarrow	$+A$
10	\longrightarrow	$+3A$

In this kind of a system, two bits can be collected during every unit of time (the symbol time T_M) and a symbol out of $-3A$, $-A$, $+A$, and $+3A$ can be accordingly selected for transmission. For example, a bit stream 01 00 10 can be represented by the symbol sequence $-A$, $-3A$, $+3A$. Higher order modulation implies that each symbol represents more than a single bit, as opposed to the binary modulation case. Keep in mind that the levels $+3A$ and $-3A$ are chosen instead of, say, $+2A$ and $-2A$ to maintain an equal distance between all the symbols, see Figure 1.6.

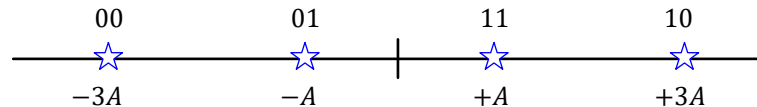


Figure 1.6: Two voltage levels or symbols representing 0 and 1

Extending the above procedure, a certain number of bits can be combined and represented by one symbol to transmit information during every symbol duration (T_M seconds). For instance, combining two bits generates $2^2 = 4$ symbols as we saw above. In general, $2^b = M$ symbols are required to transmit b bits of information. Taking \log_2 on both sides, an M -level modulation transmits $\log_2 M$ bits of information every T_M seconds. As an example, a modulation scheme with 8 symbols is efficient enough to send $\log_2 8 = 3$ bits each time. The advantage of higher order modulations is an increase in the data rate. For a symbol rate of $1/T_M$ symbols/second, the bit rate R_b becomes

$$R_b = b \cdot 1/T_M \quad \text{bits/second}$$

Increasing b (or bits per symbol) transmits more information bits during the same signaling interval.

Wireless Transmission

Until now, we only talked about bits (0s and 1s) and bit-symbol mapping to amplitude levels ($-A$ and $+A$). For transmission on a wireless channel, these symbols or amplitude levels must be modulated on an electromagnetic (EM) wave. Imagine a long straight wire with an AC source at its center shown in Figure 1.7. The source forces an acceleration and deceleration of charges in the forward and reverse directions. Since charges radiate whenever accelerated, the wire acts as an antenna in which

- an electric field is produced due to the charge distribution, and
- a magnetic field is produced due to the varying current in the antenna.

The resulting Electromagnetic (EM) wave exhibits a sinusoidal form because the charges periodically travel back and forth to the ends of the wire. This wave plotted in Figure 1.7 propagates away from the source close to the speed of light c in a direction perpendicular to both the electric and magnetic fields. A wireless signal is born.

A reverse process occurs on the receive side. The impinging EM wave influences the electrons in the antenna through its electric and magnetic fields. The acceleration and deceleration of these electrons under the influence of these fields creates a tiny electrical signal. This signal can be amplified and processed in any desirable manner. For an unmodulated EM wave, a general sinusoidal signal is given by

$$s(t) = A \cdot \cos(2\pi F t + \phi) \quad (1.6)$$

Here we can see that actually three different parameters can be altered to transmit information.

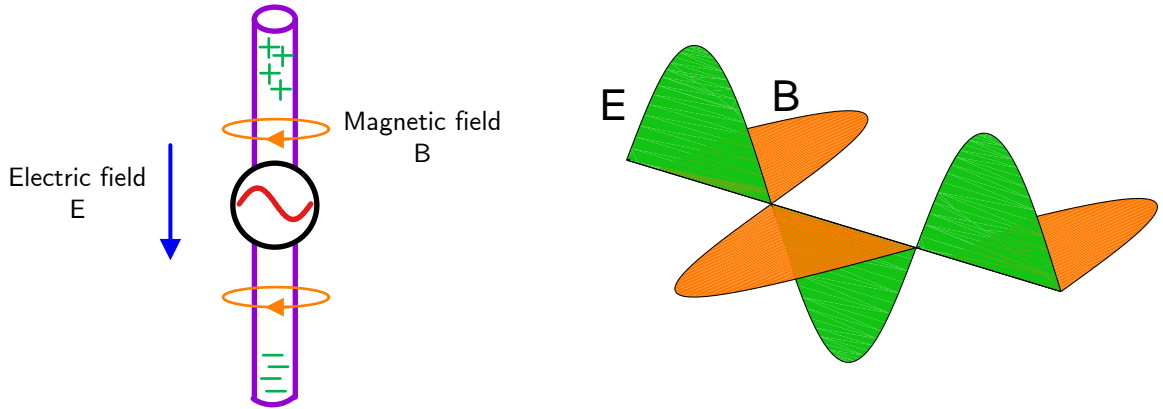


Figure 1.7: An electromagnetic wave is generated through acceleration of charged particles in a conductor in which the direction of propagation is perpendicular to both the electric and magnetic fields away from the source

- Amplitude A
- Frequency F
- Phase ϕ

In a binary amplitude modulation system, we can transmit a sinusoidal waveform with one amplitude (e.g., $-A$) for logic 0 and another amplitude (e.g., $+A$) for logic 1, as shown before in Figure 1.5. In each signaling interval m , the resulting waveform is given by

$$s(t) = A_m \cdot \cos(2\pi F t + \phi) \quad (1.7)$$

where A_m is either $-A$ or $+A$ according to the data bit. An Amplitude Modulated (AM) waveform is drawn in Figure 1.8 where we have neglected the pulse shaping operation for simplicity. The bit sequence is 0110 and therefore the chosen amplitudes according to Eq (1.4) are $+1$, -1 , -1 and $+1$. Observe that **only the amplitude** is utilized for data transmission in such a setup, although information could also be sent by varying other parameters such as phase and frequency.

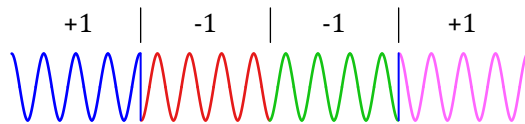


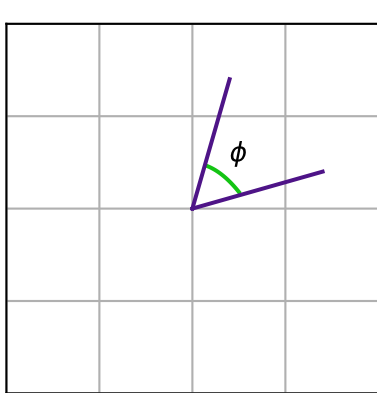
Figure 1.8: A simplified Amplitude Modulated (AM) waveform

1.4 Quadrature Amplitude Modulation (QAM)

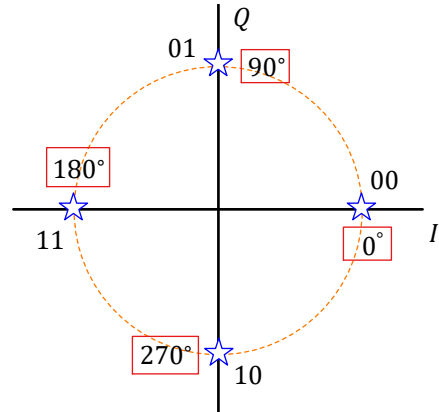
While amplitude modulation transmits information through amplitude scaling of a carrier wave according to the symbol value, it is also possible to transmit more data by changing the phase of that carrier wave at each signaling interval. Let us find out how.

Phase Modulation

For amplitude modulation, all the amplitudes still extend on the same axis of the constellation diagram such as the one drawn in Figure 1.6. On the other hand, for a phase modulated system, one axis is not enough because an actual angle is formed by *two lines*, not one. This is shown in Figure 1.9a. In other words, an amplitude modulation scheme has a 1-dimensional constellation diagram while a phase modulation scheme requires a 2-dimensional constellation diagram.



(a) An angle is formed by two lines, not one



(b) Constellation diagram with 4 symbols

Figure 1.9: Phase modulation

For a 4-phase modulation, we can send a set of two bits during each signaling interval as follows.

0°	\rightarrow	00
90°	\rightarrow	01
180°	\rightarrow	11
270°	\rightarrow	10

These phases are shown in the constellation diagram of Figure 1.9b along with their bit assignments. In general, phase modulation chooses a discrete set of points on the same circle.

I/Q Signals

If amplitude modulation sends the information on discrete amplitudes in one dimension and phase modulation chooses a set of discrete phases in two dimensions but on the same circle, both of these ideas

can be combined together in the form of *Quadrature Amplitude Modulation (QAM)*. For a practical implementation of this idea, we start with introducing the phase modulation ϕ_m in the amplitude modulation expression of Eq (1.7).

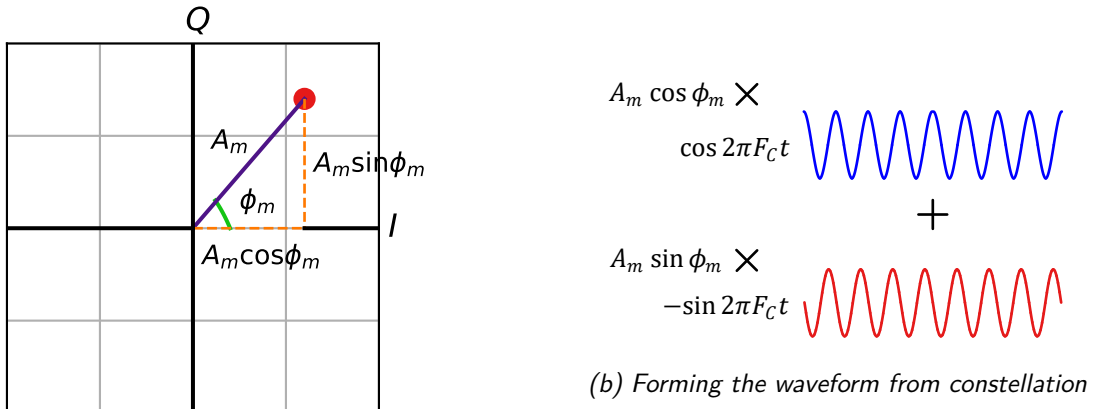
$$s(t) = A_m \cdot \cos(2\pi F t + \phi_m) \quad (1.8)$$

This is a waveform modulated in *both* amplitude and phase. Using the identity $\cos(\alpha + \beta) = \cos \alpha \cos \beta - \sin \alpha \sin \beta$, we open this up as

$$\begin{aligned} s(t) &= A_m \cdot \cos(2\pi F t) \cdot \cos \phi_m - A_m \cdot \sin 2\pi F t \cdot \sin \phi_m \\ &= \underbrace{(A_m \cos \phi_m)}_{\text{I part}} \cdot \cos(2\pi F t) - \underbrace{(A_m \sin \phi_m)}_{\text{Q part}} \cdot \sin 2\pi F t \end{aligned} \quad (1.9)$$

Here, the amplitude $A_m \cos \phi_m$ is the projection of the modulation point on x axis, while the amplitude $A_m \sin \phi_m$ is the projection of the modulation point on y axis. This is plotted in Figure 1.10a. These amplitudes are then modulated on two *quadrature* carriers, namely $\cos(2\pi F t)$ and $-\sin(2\pi F t)$ according to Eq (1.9) and summed together to be sent over the air as plotted in Figure 1.10b. Why are there two waveforms as opposed to one (before the summation)? Because

- constructing or measuring an angle requires two lines, and hence
- constructing or measuring a phase requires two waveforms, one for each line.



(a) I/Q plane and modulation parameters A_m and ϕ_m

Figure 1.10: QAM waveform generation

In the above description, we used the terms ‘inphase’ and ‘quadrature’ and also represented x and y axes in all the figures so far with notations I and Q , respectively. Why? Let us explain the answers in an intuitive sense from Eq (1.9).

- Recall that each phase, like each angle, needs a reference.

- For an angle, this reference is provided by the horizontal line connecting point $(0, 0)$ to point $(1, 0)$.
- For a phase, a cosine wave with phase 0° , i.e., $\cos(2\pi F t)$, is taken as the reference (an arbitrary choice) that is the first waveform in Eq (1.9).

Acting as an amplitude of this waveform $\cos(2\pi F t)$, the *symbol level* $A_m \cos \phi_m$ on the horizontal axis is known as the *In-Phase* component (in phase with a cosine), from which the notation I is extracted.

To understand the Q part, consider the following questions and answers.

Question:

How should we represent the amplitude on the vertical axis?

Answer:

We need another waveform!

Question:

If the horizontal axis links angle 0° on a 2-D plane to a cosine wave $\cos(2\pi F t)$ with the starting phase 0° , then the vertical axis at an angle 90° on a 2-D plane should be linked to which waveform?

Answer:

Another cosine wave with the starting phase of 90° .

Question:

What is a cosine wave with a starting phase of 90° ?

Answer:

Use the identity $\cos(\alpha + \beta) = \cos \alpha \cos \beta - \sin \alpha \sin \beta$.

$$\cos(2\pi F t + 90^\circ) = \cos 2\pi F t \cdot \underbrace{\cos 90^\circ}_0 - \sin 2\pi F t \cdot \underbrace{\sin 90^\circ}_1 = -\sin 2\pi F t$$

This second cosine wave comes out to be a negative sine wave!

In conclusion, in parallel with the cosine wave starting with a phase of 0° , we need another cosine wave at the Tx starting with a phase of 90° , which is a negative sine wave. This means that the *symbol level* $A_m \sin \phi_m$ on the vertical axis, acting as an amplitude of $-\sin(2\pi F t)$ in Eq (1.9), is known as the *quadrature* component, giving rise to the Q term. Quadrature in astronomy refers to the position of a planet when it is 90° from the sun as viewed from the earth.

In essence, we can combine any amplitude and any phase to create a symbol. In practice, we represent this symbol with two amplitudes: one on the horizontal axis and the other on the vertical

axis. Mathematically speaking, this is known as going from polar coordinates (A, ϕ) to rectangular coordinates (x, y) . This is why there is no mention of ‘phase’ in the expression Quadrature Amplitude Modulation.

QAM Constellations

Having seen how one QAM constellation point with an arbitrary amplitude and phase fits into this picture, some examples of QAM constellations are discussed now that allow efficient packing of modulation symbols. For an even power of 2, a **square QAM** is a constellation whose points are spaced on a grid in the form of a square. Some square QAM constellations are shown in Figure 1.11 from which we can observe the following.

- A tighter packing of symbols allows for higher data rates, e.g., 2 bits/symbol for 4-QAM, 4 bits/symbol for 16-QAM and 6 bits/symbol for 64-QAM. A 16-QAM constellation is made up of one 4-QAM in each of the 4 quadrants. Similarly, 64-QAM can be seen as an extension of 16-QAM scheme, one in each quadrant.
- To satisfy the same average power requirements, constellation points in higher-order QAM are closer to each other compared to lower-order QAM. An interested reader can see Appendix 1.5 for average energy computations. As a consequence, a smaller amount of noise power is enough to cause a decision error by moving the received symbol over the decision boundary. This is the cost of increasing data rate by packing more bits in the same symbol.

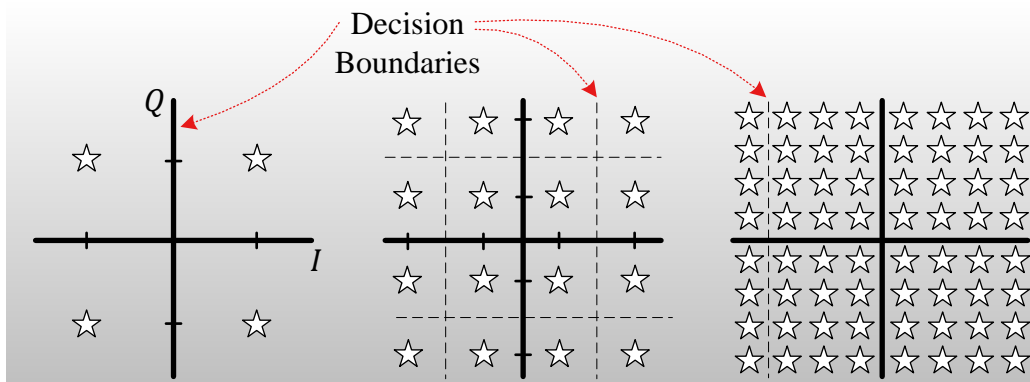


Figure 1.11: QAM constellation diagrams for $M = 4$, $M = 16$ and $M = 64$. Observe how points get closer for higher-order QAM and become prone to noise errors

5G systems support all the modulation schemes drawn in Figure 1.11, i.e., 4-QAM, 16-QAM and 64-QAM. To achieve higher data rates, 256-QAM (i.e., one 64-QAM in each of the 4 quadrants) is also part of the standard and it is expected to include even higher orders of QAM in the later stages.

1.5 Appendix

The most straightforward way to characterize an object under study is choosing its size as a criterion. For example, we measure the sizes of their areas or economies for comparing two countries, and sizes of their bodies for comparing two animals. Similarly, the energy of a signal is a measure of its size in signal processing applications. This energy is defined as the area under its *squared magnitude* which is computed through an integration in continuous-time signals and a summation in discrete-time signals.

Returning to the modulation, each constellation in Figure 1.11 has an average energy that can be computed from the *squared Euclidean distance* of each point or symbol s_i from the origin.

$$E_s = \text{Avg } |s_i|^2 = \frac{1}{M} \sum_{i=1}^M |s_i|^2$$

where M is the constellation size. For example, assume that the four symbols in 4-QAM constellation are given by

$$\text{4-QAM} \quad \longrightarrow \quad s_i = (+1, +1), \quad (+1, -1), \quad (-1, +1), \quad (-1, -1)$$

Applying the Pythagoras theorem, the squared distance of each point from the origin is $(\pm 1)^2 + (\pm 1)^2 = 2$. The average energy from 4 such symbols is then given by

$$E_s = \frac{1}{4} (2 + 2 + 2 + 2) = \frac{1}{4} (4 \cdot 2) = 2$$

We say that the constellation becomes normalized when scaled with square-root of this factor. For instance, a normalized 4-QAM constellation is scaled by $1/\sqrt{2}$ and written as

$$\text{Normalized 4-QAM} \quad \longrightarrow$$

$$s_i = \left(+\frac{1}{\sqrt{2}}, +\frac{1}{\sqrt{2}} \right), \quad \left(+\frac{1}{\sqrt{2}}, -\frac{1}{\sqrt{2}} \right), \quad \left(-\frac{1}{\sqrt{2}}, +\frac{1}{\sqrt{2}} \right), \quad \left(-\frac{1}{\sqrt{2}}, -\frac{1}{\sqrt{2}} \right)$$

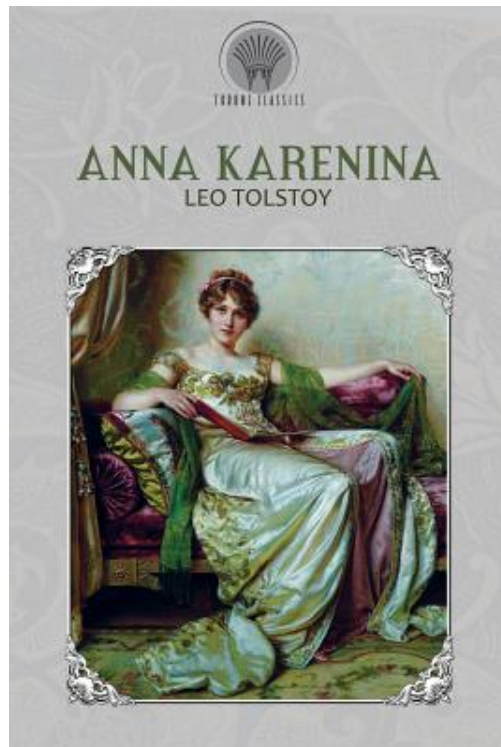
Thus, the average energy becomes equal to

$$E_s = \frac{1}{4} \cdot 4 \cdot \left(\frac{1}{\sqrt{2}^2} + \frac{1}{\sqrt{2}^2} \right) = 1 \quad (1.10)$$

With some effort, this average energy can be computed for 16-QAM and 64-QAM constellations in a similar manner. In this text, we only consider a normalized constellation with $E_s = 1$, unless otherwise stated.

Chapter 2

Signal Transmission in a Wireless Channel



Before we begin exploring how a wireless channel modifies the transmitted signal, I want to bring into the reader's attention a brief historical note. One of the very few people who saw the potential of a connected world was Mark R. Sullivan, president and director of the Pacific Telephone & Telegraph Co. He said in 1953 that the future phone might be carried by an individual like a watch (no wires) and the users would be able to see each other during the conversation. He even foresaw this phone translating from one language to another! Considering that the transistor was invented in 1947, he might have a hunch that the digital revolution was about to begin in a few years time.

Until now, we have focused on bits, symbols and the I and Q terms carrying the symbols on cosine and negative sine waves, respectively. For example, the amplitude A_m of the carrier waves depends on the value of the symbol at time m . In an actual transmission, the amount of power radiated into the air that satisfies a certain link budget to *close* the link depends on many other factors. For this purpose, we need to understand how the wireless channel acts on the Tx signal. Through extensive measurement campaigns, it has been found that the Tx signal undergoes two major kinds of fading in a wireless channel as follows.

2.1 Large-Scale Fading

Wave propagation in an ideal free space is the starting point from where the effect of a wireless channel can be analyzed under the following scenario.

- The region between Tx and Rx is considered free of all objects that might absorb or reflect RF energy.
- The atmosphere behaves as a uniform and nonabsorbing medium.
- The earth is treated as being far away from the signal path.

In such a setup, we assume that a Tx radiates P_{Tx} watts of power uniformly spreading in all spatial directions which is known as isotropic radiation. Taking the Tx as a point source, the ideal radiated wavefront advances in a spherical shape, similar to an expanding balloon when filled with air (or knowledge, according to Blaise Pascal: "Knowledge is like a sphere; the greater its volume, the larger its contact with the unknown."). Then, the power density at a distance d from the Tx point source is the



A wireless prophecy

ratio of the Tx power P_{Tx} to the surface area of the sphere $4\pi d^2$.

$$\text{Power density} = \frac{P_{\text{Tx}}}{4\pi d^2} \quad \text{Watts}/m^2 \quad (2.1)$$

Therefore, the Tx power decays with inverse of squared distance in free space and the corresponding loss is termed as *path loss*. This is drawn in Figure 2.1 for a sphere with radius d . It is evident that only a small fraction of the radiated power is actually intercepted by the receiving device.

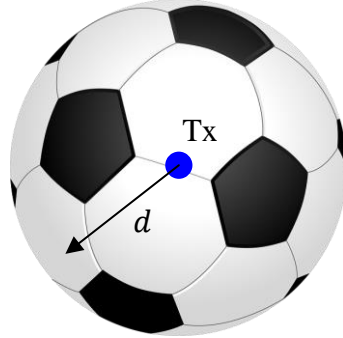


Figure 2.1: Free space path loss at a distance d from the Tx antenna

For most practical channels, the free space path loss is an idealized simplification because the medium is not empty and a signal can reach the Rx after getting reflected, diffracted or scattered from multiple objects in the surroundings as well as the ground. For example, a single reflection from the ground can degrade the Rx power as much as the fourth power of the inverse distance – as opposed to the squared distance in free space. Different environments exhibit different such coefficients appearing as a power to the inverse distance. As a general rule,

$$P_{\text{Rx}} \propto \frac{1}{d^\beta}$$

with the value of β dictated by the environment and empirically determined through an experimental campaign.

In addition to this path loss, the large-scale fading includes *shadowing* caused by buildings and other obstacles affecting the wave propagation (the term is borrowed from the sunlight shadowed by the clouds). Combined path loss and shadowing represent the changes in average signal power over a large area. Since large-scale fading is useful for estimating average Rx power over a certain distance, it is mostly utilized in configuring the power budget of a communication link and cell site planning in mobile radio systems.

2.2 Small-Scale Fading

Small-scale fading is a phenomenon that arises due to the unguided nature of the wireless medium. Dramatic variations in signal amplitude occur at the Rx from constructive and destructive interference

of multipath components originating from the surrounding environment that give rise to small-scale fading. This is the main challenge for designing efficient high-rate wireless communication systems [2] which spawned an array of research activities in the past 50 years aimed to bring the wireless transmission rates closer to their wire counterparts. The technologies for 5G systems have been chosen with the benefit of experience gained from actual implementations over these years.

Delay Spread

To understand how the channel fading phenomenon arises in a wireless channel, consider a modulated waveform in Figure 2.2 that is sent over the air at a particular carrier frequency F_C . This signal arrives at the destination after traversing several different routes. The wireless channel is represented in Figure 2.2 through a set of unit impulses with different amplitudes which come together to form our basic channel impulse response.

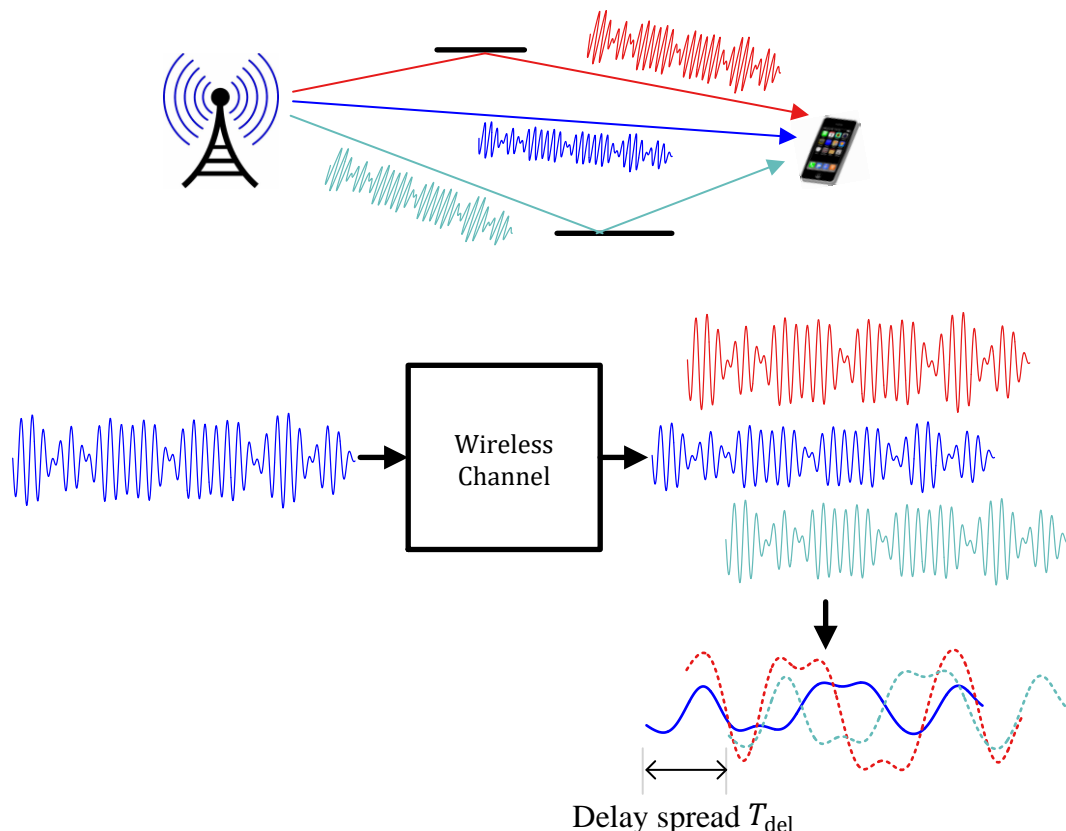


Figure 2.2: A wireless channel consisting of N_p paths with amplitudes ρ_i and delays τ_i

- The first of these paths is the direct path with a relative amplitude of $\rho_0 = 1$ and a relative delay of $\tau_0 = 0$.

- The second of these paths arrives with an amplitude ρ_1 and a delay τ_1 with respect to τ_0 .
- There are a total of N_p such paths with relative amplitudes and delays denoted by ρ_i and τ_i , respectively, where $i = 0, 1, \dots, N_p - 1$.
- The amplitudes ρ_i are determined through large-scale fading phenomenon discussed before.
- The delay spread T_{Del} of a wireless channel is roughly defined as the time difference between the first and the last significant path.

$$T_{\text{Del}} = \tau_{(N_p-1)} - \tau_0 \quad (2.2)$$

We now describe the effect of movement in the channel.

Doppler Spread

With the introduction of motion in the channel, interesting things happen due to a phenomenon known as **Doppler shift**, a concept taught in high school physics. Some people have actually paid 300 dollars to learn this concept from the sirens of the police car approaching behind them for a ticket.

Imagine an unmodulated carrier wave $s(t) = \cos 2\pi F_C t$ impinging on the antenna of a mobile in a parked car as drawn in Figure 2.3. The signal arrives at the Rx τ_0 seconds later when the electromagnetic wave travels a distance of d_0 m at a speed of approximately $c = 3 \times 10^8$ m/s. From the time reference of the Tx, this signal is a delay (a right shift) and can be written as

$$\rho_0 \cos 2\pi F_C (t - \tau_0) = \rho_0 \cos 2\pi F_C \left(t - \frac{d_0}{c} \right)$$

where $\tau_0 = d_0/c$.

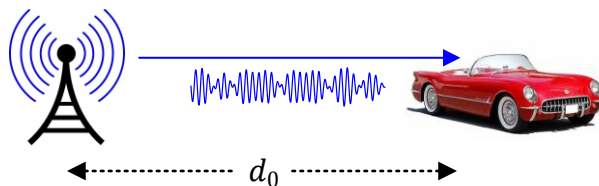


Figure 2.3: Movement of either the Tx, the Rx or any object within the channel causes a Doppler shift in the signal frequency

Now imagine that the car is started and is driven at a constant velocity of ν m/s directly opposite to the antenna. For all further times t , the electromagnetic wave that had to travel d_0 m now has to cover a distance of $d_0 + \nu t$.

$$\begin{aligned} \rho_0 \cos 2\pi F_C \left(t - \frac{d_0 + \nu t}{c} \right) &= \rho_0 \cos 2\pi F_C \left(t - \frac{\nu}{c} t - \frac{d_0}{c} \right) \\ &= \rho_0 \cos 2\pi \left\{ \left(F_C - \frac{\nu}{c} F_C \right) t - F_C \tau_0 \right\} \end{aligned} \quad (2.3)$$

Some comments are now in order.

- As encountered before, the term $-2\pi F_C \tau_0$ is a constant phase shift that arises due to the delay between the Tx and the Rx.
- The frequency of a signal is the term that appears with variable t , except the factor 2π . We conclude that the new frequency of the signal is

$$F_C^{\text{new}} = F_C - \frac{\nu}{c} F_C$$

Consequently, there is a shift in frequency which is known as **Doppler shift**. Here, the Doppler shift, also commonly known as Doppler frequency F_D , is

$$F_D = -\frac{\nu}{c} F_C \quad (2.4)$$

- From the above expression, the Doppler shift depends on the carrier frequency F_C : the higher the frequency, the higher the Doppler shift and vice versa.
- The Doppler shift also depends on the velocity of the Rx antenna ν . In fact, rewriting the relation as

$$\frac{F_D}{F_C} = -\frac{\nu}{c}$$

reveals that as a fraction of carrier frequency F_C , it is just a ratio of the velocities between the mobile and the electromagnetic wave.

- Recall that the expression $d_0 + \nu t$, i.e., an increasing distance, implies that the car in Figure 2.3 started moving away from the Tx antenna at an angle of π radians. Therefore, the wave has to travel a larger distance and hence the minus sign with the Doppler shift. We can write the actual shift in frequency as

$$-\frac{\nu}{c} F_C = \frac{\nu \cos \pi}{c} F_C$$

Subsequently, for a general angle ϕ with respect to the axis of propagation of the wave, the Doppler shift is written as

$$F_D = \frac{\nu \cos \phi}{c} F_C = F_{D,\max} \cos \phi \quad (2.5)$$

In other words, we only take into account the velocity component in the direction of arrival of the wave[†].

[†]Many scientists write the relation using $c = F_C \lambda_C$ where λ_C is the carrier wavelength. Then, the Doppler shift becomes

$$F_D = \frac{\nu \cos \phi}{c} F_C = \frac{\nu \cos \phi}{F_C \lambda_C} F_C = \frac{\nu \cos \phi}{\lambda_C}$$

Channel Gains

To determine an expression for the accumulated multipath effect at the Rx, let us simplify the scenario by considering a sinusoidal wave that is sent over the air without any modulation. We can write it as

$$s(t) = \cos(2\pi F_C t)$$

where F_C is the carrier frequency of the electromagnetic wave. Although unrelated to the modulated data, the choice of carrier frequency F_C plays a significant role in determining the overall channel effect, as we see now. Nature adds up all these reflected paths at the Rx antenna. Assuming for a moment that there is no movement in the channel, we can write

$$\begin{aligned} r(t) &= \rho_0 \cos 2\pi F_C(t - \tau_0) + \rho_1 \cos 2\pi F_C(t - \tau_1) + \cdots + \rho_{N_p-1} \cos 2\pi F_C(t - \tau_{N_p-1}) \\ &= \sum_{i=0}^{N_p-1} \rho_i \cos 2\pi F_C(t - \tau_i) \end{aligned}$$

Using the identity $\cos(A - B) = \cos A \cos B + \sin A \sin B$, we can write the above equation as

$$r(t) = \sum_{i=0}^{N_p-1} \underbrace{\rho_i \cos 2\pi F_C \tau_i}_{\gamma_{i,I}} \cdot \cos 2\pi F_C t - \sum_{i=0}^{N_p-1} \underbrace{-\rho_i \sin 2\pi F_C \tau_i}_{\gamma_{i,Q}} \cdot \sin 2\pi F_C t$$

This is the standard representation of an I/Q signal, e.g., see Eq (1.9). From the above expression, the coefficients of a complex baseband wireless channel can be described as

$I \quad \rightarrow$	$\gamma_{i,I} = \rho_i \cdot \cos 2\pi F_C \tau_i$	
$Q \quad \uparrow$	$\gamma_{i,Q} = -\rho_i \cdot \sin 2\pi F_C \tau_i$	(2.6)

Here, we can see why the wireless channel exhibits a complex response even though the Tx signal is real. Any sinusoidal wave with a non-zero phase can be represented as having both a cosine (horizontal) and sine (vertical) component, see Section 1.4. The modulated data travels on a sinusoidal wave which arrives at the Rx through multiple delays. This implies that each wave undergoes a different phase shift. Consequently, a summation of sinusoidal waves with different phase shifts gives rise to a final sinusoidal wave that has both a cosine and a sine component[†].

Many readers find it easier to understand these summation patterns by drawing the path amplitudes and phases as vectors and then doing vector addition and subtraction. One such example is shown in Figure 2.4 for a relatively mild channel. This is also known as a *phasor diagram*.

What exactly is the effect of such vector summations on the actual waveform? Let us explore the answer to this question below.

[†]The above description also shows that the channel response is in general a complex function of frequency and time, even if an inphase only modulation such as BPSK is employed for transmission. Therefore, a BPSK Rx has to employ a *Q* arm as well to scavenge energy lost from the *I* arm.

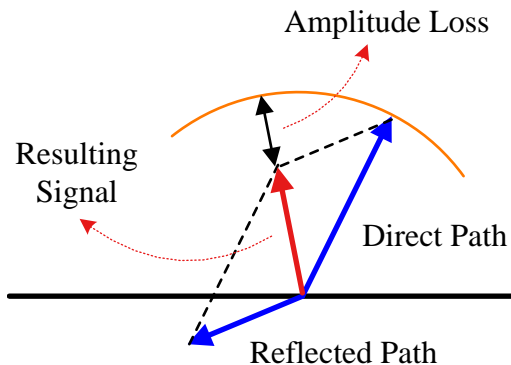


Figure 2.4: A vector sum representation of multipath addition

Constructive and Destructive Interference

To see how detrimental this wireless channel is, consider the fact that even a slight change in the environment causes a significant change in the channel response. To understand the reasoning below, recall that $\cos(\theta + 2\pi) = \cos \theta$, i.e., a phase change of 2π implies one full cycle. In a similar manner, a phase change of π implies half a cycle.

Constructive Interference

Concentrating on the term $2\pi F_C \tau_i$ in Eq (2.6), the phase of each path completes a full cycle whenever $F_C \cdot \tau_i = 1$. Why? Because whenever $2\pi F_C \tau_i$ changes by 2π , the part $F_C \cdot \tau_i$ changes by 1.

$$\text{variation in } \tau_i = \frac{1}{F_C} \rightarrow \text{Phase change} = 2\pi$$

As an example, if the carrier frequency F_C is 1.9 GHz, $1/F_C = 0.5263 \text{ ns}$ which at the speed of electromagnetic wave c is a distance of 15.8 cm. In this two-path channel, if the second path length is either of the same length or different by a mere 15.8 cm, the two waves add constructively to boost the signal amplitude as shown in Figure 2.5a. The vertical line is drawn to identify the similar phases in the two waveforms.

Destructive Interference

On the other hand, assume that the Rx moves a distance such that the phase of each path undergoes a shift of π for each $F_C \cdot \tau_i = 1/2$.

$$\text{variation in } \tau_i = \frac{1}{2F_C} \rightarrow \text{Phase change} = \pi$$

In the example above, if the second path length is different by just 7.9 cm, the two waves add destructively causing the signal amplitude to plummet as shown in Figure 2.5b. The vertical line is drawn to identify the opposite phases in the two waveforms. This happens for a time variation

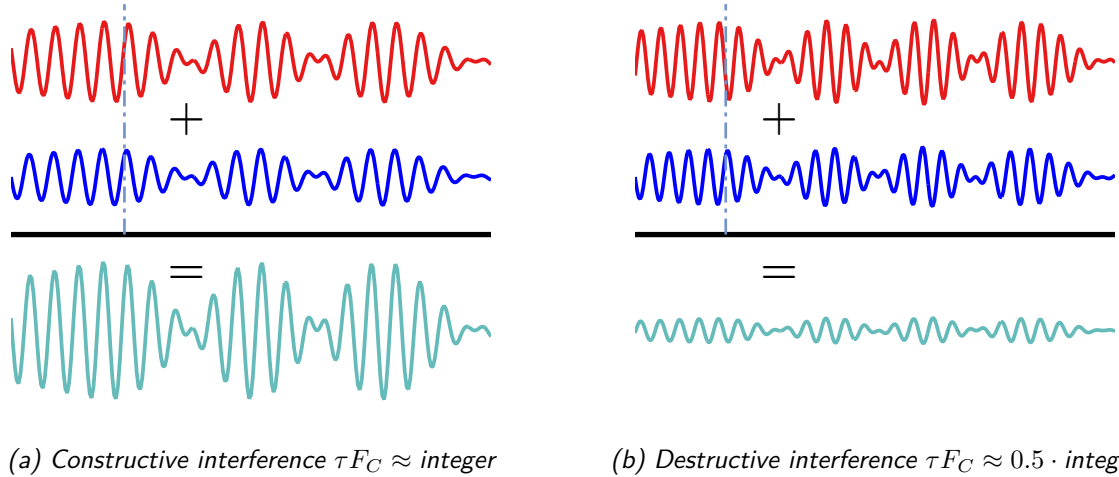


Figure 2.5: Constructive and destructive interference arising from the different delays of multipath

going from $1/F_C$ to $1/2F_C$. Using $c = F_C \cdot \lambda$, this happens from λ/c to $(\lambda/2)/c$. We conclude that *a displacement of $\lambda/2$ meters* is the limit beyond which the channel response changes.

For obvious reasons, most of the actual interference patterns lie in between these two extremes.

Coherence Time and Coherence bandwidth

From the above example, we saw that the channel undergoes a phase shift of π over a distance of $\lambda/2$ meters. In other words, if the phase change remains within π , the channel may be considered time-invariant. This leads to the idea of *coherence time T_C* as the interval over which the channel response stays nearly constant in time because the wireless device does not go beyond $\lambda/2$ meters. Traveling at a speed of v m/s and using $d = v \cdot t$, this comes out to be

$$T_C = \frac{\lambda}{2v} \quad (2.7)$$

This is an approximation that holds well in empirical observations.

Let us now consider the frequency domain. Since the magnitude response of such a wireless channel also varies with frequency, the range of frequencies over which this magnitude can be assumed approximately constant is termed as *Coherence Bandwidth B_C* of the channel.

- From frequency domain characteristics[†], we know that a signal spread in time causes a faster variation in the spectrum.

[†]The Fourier Transform of an impulse signal:

$$\underbrace{\delta(t - t_0)}_{\text{Delayed unit impulse}} \xleftrightarrow{\text{FT}} \underbrace{e^{-j2\pi F t_0}}_{\text{A Complex sinusoid}}$$

- This means that a larger τ_i produces a faster rotation than a smaller τ_i .
- This in turn results in sharp transitions from high/low to low/high magnitudes in frequency domain.
- Therefore, coherence bandwidth is inversely proportional to the delay spread T_{Del} (time difference between the first and the last significant path).

$$B_C \propto \frac{1}{T_{\text{Del}}} = \frac{1}{\tau_{(N_p-1)} - \tau_0} \quad (2.9)$$

where the definition of delay spread is used from Eq (2.2).

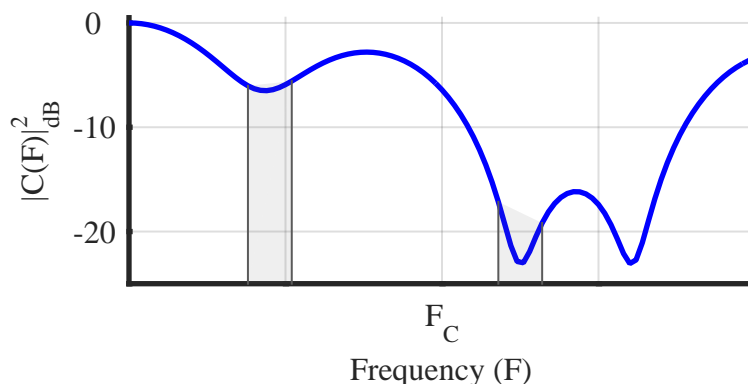


Figure 2.6: Coherence bandwidth B_C of a channel

The coherence bandwidth B_C for our example channel $C(F)$ in frequency domain is redrawn as shaded regions in Figure 2.6. If we split the channel magnitude response in discrete components, then the portions within a B_C exhibit a strong magnitude correlation, i.e., their magnitudes attain values near to each other. Two such instances are drawn in the figure as shaded regions.

- When the channel is good, it is good for almost all spectral components within B_C .
- When a deep fade occurs, it drowns almost the complete region within B_C .

Coherence Interval

The ideas of coherence time and coherence bandwidth can be combined into a single factor known as *coherence interval* which basically is a time-frequency span of T_C seconds over a bandwidth of B_C Hz.

In general, for a signal $x(t)$, we have the time shift property of Fourier Transform as

$$x(t - t_0) \xleftrightarrow{\text{FT}} \underbrace{e^{-j2\pi F t_0}}_{\text{A Complex Sinusoid}} \cdot X(F) \quad (2.8)$$

This phase shift being a function of frequency F represents *multiplication of the signal spectrum with a complex sinusoid of inverse period t_0* . The larger this delay t_0 , the faster the rotation. This is *the* most important property of Fourier Transform but textbooks have a tendency to mention it as just another property without emphasizing this enough.

The main attraction behind defining a coherence interval is that if the channel does not vary much over T_C seconds and its spectrum does not undergo significant alterations within B_C Hz, then it can be assumed nearly constant on a time-frequency grid without any time or frequency variations.

According to sampling theorem in DSP, the sample rate $1/T_S$ of a signal spanning a bandwidth B Hz should be greater than $2B$ Hz in terms of real samples. For complex samples with both an I and Q part, this turns out to be

$$\frac{1}{T_S} \geq B \text{ samples/second}$$

i.e., for a waveform constrained in B_C Hz, we need B_C samples every second. The number of samples collected over an interval of T_C seconds is a coherence interval given by

$$X = B_C \cdot T_C \text{ samples} \quad (2.10)$$

This is drawn in Figure 2.7. It is evident that the coherence interval is a time-frequency grid with duration T_C and bandwidth B_C .

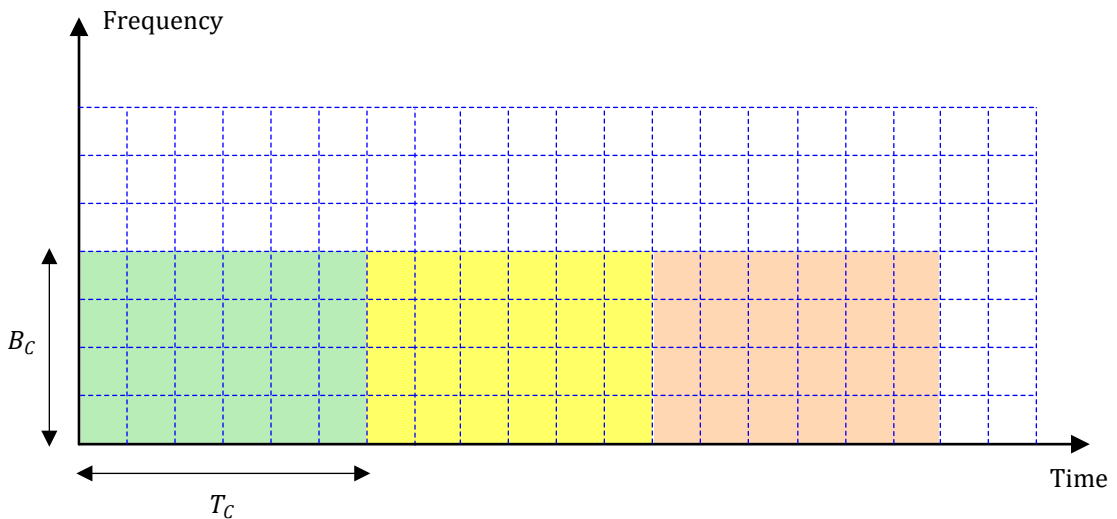


Figure 2.7: Coherence interval of a channel is a time-frequency grid with duration T_C and bandwidth B_C

Let us use the definitions of T_C and B_C to construct an example. For a carrier frequency $F_C = 1\text{GHz}$ (i.e., wavelength $\lambda = c/F_C = 0.3$ m), walking at a speed of $v = 5 \text{ km/hr}$ or 1.39 m/s yields T_C from Eq (2.7) as

$$T_C = \frac{\lambda}{2v} \approx 107 \text{ ms}$$

On the other hand, for a displacement $c(\tau_2 - \tau_1) = 50$ m between two paths, we write from Eq (2.9)

$$B_C = \frac{c}{c(\tau_2 - \tau_1)} = 6 \text{ MHz}$$

The coherence interval is now given by

$$X = T_C \cdot B_C = 642000 \text{ samples}$$

This can be a low value for large distances and/or higher carrier frequencies, e.g., at mmWave bands. Next, we turn towards the frequency flat and frequency selective channels.

Frequency Flat Fading

A carrier wave modulated at a low data rate is depicted in Figure 2.8 where the first and second multipath are shown above and below the main signal for clarity. Also, the vertical line is drawn to identify the phases in the waveforms at the same point in time.

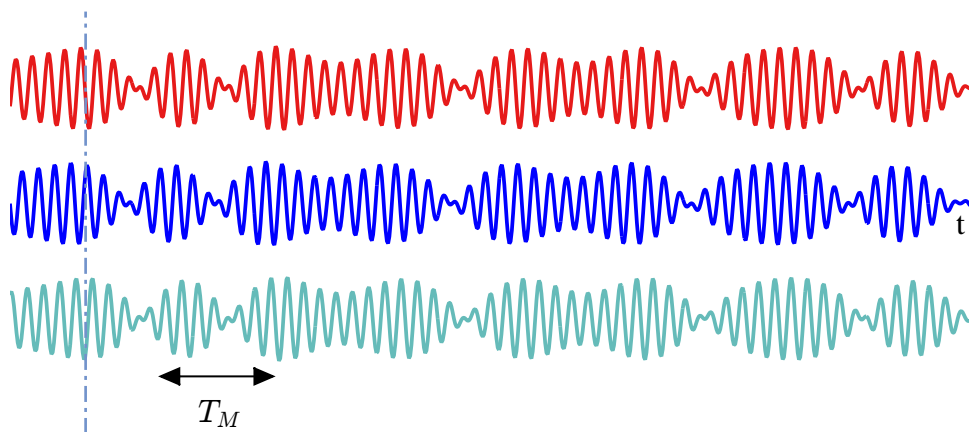


Figure 2.8: First and second multipath components arriving τ_1 and τ_2 seconds after the direct path, respectively. With these delays much less than symbol time T_M , the phases are different but the data symbol values are almost the same

As plotted in Figure 2.5 before, the phases of these paths might add constructively or destructively or somewhere in between. However, as long as the delay of the second and third paths with respect to the first one is small, the data symbol values of these paths are still (almost) the same and hence *there is very low Inter-Symbol Interference (ISI)* that shows up on top of those path phases. By ISI, we imply that one symbol does not interfere with the future symbols (e.g., when a path delay is longer than a symbol time). In this sense, the data symbols are all in this together. Depending on the phases of the paths, all the data symbols either experience the same boost or suffer a similar attenuation. The fate of the whole signal is the same.

Before we find the rationale behind the terminology ‘frequency flat’, let us explore the mathematics behind it. The channel impulse response is given by

$$c(t) = \sum_{i=0}^{N_p-1} \gamma_i \cdot \delta(t - \tau_i)$$

where γ_i are channel gains defined in Eq (2.6), N_p is the number of paths and $\delta(t)$ is the unit impulse signal. When τ_i are fairly close to each other, the impulses can be taken out as a common factor due to their similarity $\delta(t - \tau_i) \approx \delta(t)$.

$$c(t) \approx \sum_{i=0}^{N_p-1} \gamma_i \cdot \delta(t) = h \cdot \delta(t) \quad (2.11)$$

where h is a complex constant expressed as

$$h = \sum_{i=0}^{N_p-1} \gamma_i \quad (2.12)$$

Here, Eq (2.11) reinforces the concept of the whole signal experiencing the same fate decided by h . To summarize, as long as the delay spread is a small fraction of the symbol time, i.e., the signal is not too far spread in time with respect to signal bandwidth, all such summations give rise to only one channel tap h . For a modulation symbol s sent over the air, the received signal r is thus given by

$$r = s \cdot h + \text{noise}$$

This is the model mostly followed in most infrastructure based wireless systems. A simple block diagram of such a setup is drawn in Figure 2.9.

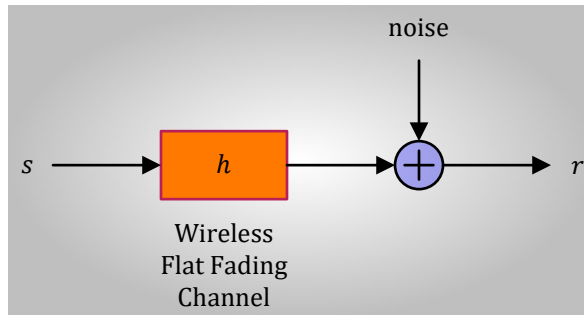


Figure 2.9: A flat fading channel model

To view this concept in frequency domain, start with a small delay spread, i.e., the signal copies are arriving close to each other at the Rx. Clearly, when the delays τ_i are small, the rotation periods of [frequency domain complex sinusoids](#) in Eq (2.8) are large (because the period in frequency domain is given by $1/t_0$ in that equation, just like the period in a time domain sinusoid is $1/F_0$). Not much rotation occurs across the signal bandwidth thus leading to a relatively flat gain. We say that the channel reduces to almost a single complex constant.

A frequency flat fading scenario is drawn in Figure 2.10 as an example. Notice that the whole signal bandwidth almost fits within the coherence bandwidth of the channel. Hence, the Rx magnitude depends on the multiplication between the full signal spectrum and (almost) a single attenuation factor

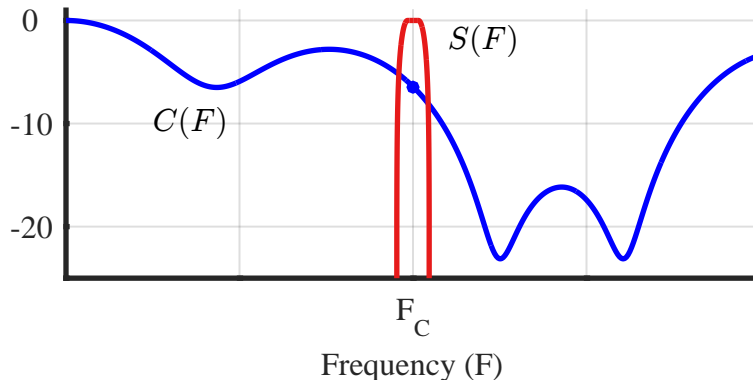


Figure 2.10: Signal bandwidth within the channel coherence bandwidth B_C gives rise to frequency flat fading. The term flat implies multiplication of the spectrum with (almost) a single attenuation factor shown as the blue dot here

shown as a blue dot at F_C . This is why it is known as frequency flat fading. Clearly, this blue dot representing the channel attenuation is nothing but $C(F_C)$.

To see how detrimental the effect of fading is on the average bit error probability of digital modulation schemes, consider a wireless channel with no fading and only Additive White Gaussian Noise (AWGN) as the disturbance. The bit error rate is then given by

$$P_b \propto e^{-\text{SNR}} \quad (2.13)$$

Here, the constants appearing before e and SNR in the exponent are omitted for simplicity. This P_b is drawn for a range of SNR in Figure 2.11 where an exponential trend quickly drops the error rate even at moderate SNR. For example, the required SNR at 10^{-4} is around 8 dB for an AWGN channel.

Now a flat fading channel is usually modeled as following a Rayleigh distribution. What this means is that channel gain γ in Eq (2.12) is a complex Gaussian random variable (whose magnitude is Rayleigh distributed and phase is uniformly distributed between 0 and 2π). In this case, the bit error rate is only *inversely* proportional to the SNR.

$$P_b \propto \frac{1}{\text{SNR}} \quad (2.14)$$

This trend is also drawn in Figure 2.11 for a comparison with the AWGN channel. It is clear that the bit error rate is much worse here due to the inability of the inverse relationship to bring the error rate down quickly enough. As an example, the required SNR at 10^{-4} is around 34 dB for a fading channel – approximately 26 dB difference from an AWGN channel!

Next, we explore the topic of frequency selective fading.

Frequency Selective Fading

A carrier wave modulated at a high data rate is depicted in Figure 2.12 where the first and second multipath are shown above and below the main signal for clarity. The phases of these paths might

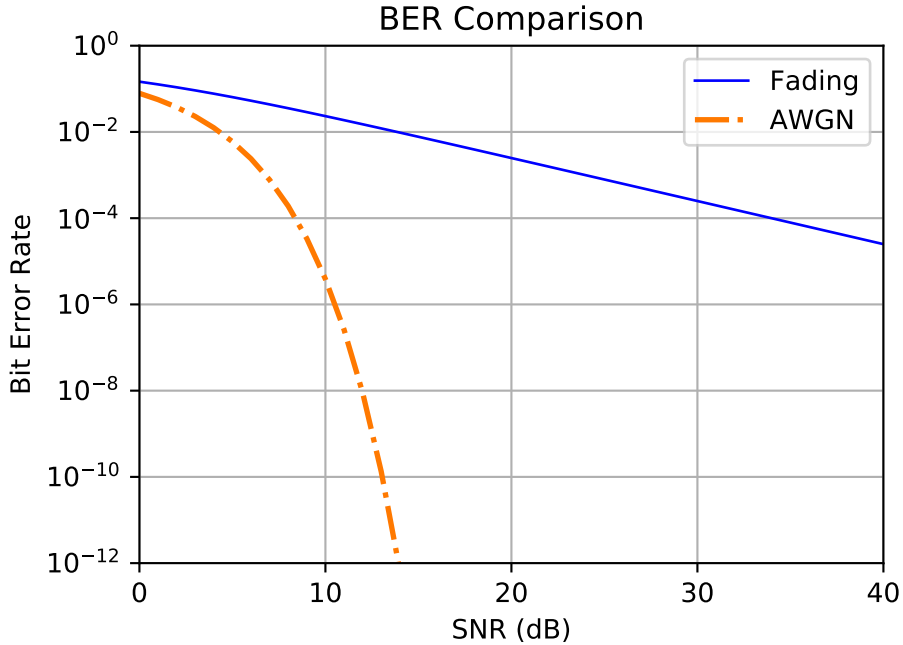


Figure 2.11: A Bit Error Rate (BER) comparison between AWGN and fading channels

add constructively or destructively or somewhere in between. Moreover, due to the long delay of the second and third paths with respect to the first one, the data symbol values of these paths adding up at random instants generate *a tremendous amount of Inter-Symbol Interference (ISI)* that shows up on top of those path phases. This happens because the random data symbols get summed up into other symbols long after they were actually transmitted. In this sense, there are two phenomenon, and not one, that contribute towards the constructive and destructive interference:

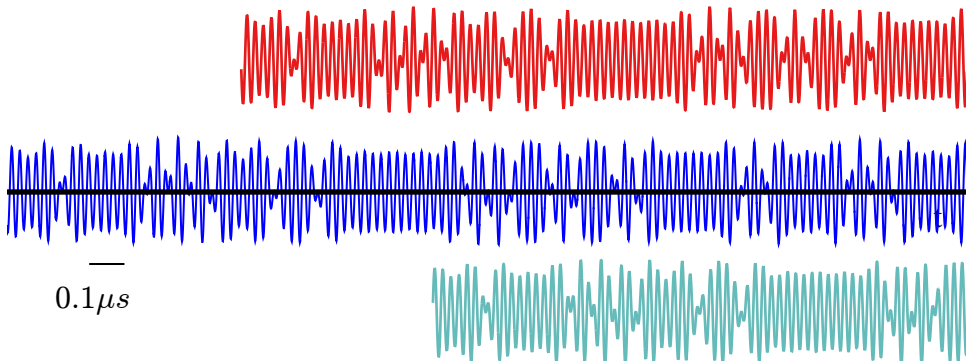


Figure 2.12: First and second multipath components arriving τ_1 and τ_2 seconds after the direct path, respectively. With these delays equal to or higher than a symbol time, not only the phases are different but the data symbol values also randomly add to form the cumulative signal

1. path delays, and
2. symbol values

As before, recognizing the frequency selective fading is a straightforward task in frequency domain. The spectra of all incoming signal paths are the same but different delays in time give rise to complex sinusoids with different inverse periods, see Eq (2.8). When these inverse periods are large (due to long time delays), a faster rotation occurs across the signal bandwidth thus leading to spectral selectivity. We conclude that a larger delay spread implies increased frequency selectivity and a smaller coherence bandwidth.

A frequency selective fading scenario is drawn in Figure 2.13 as an example where the shaded box represents the coherence bandwidth B_C . Notice that due to the high data rate and hence large signal bandwidth, the whole bandwidth extends beyond the coherence bandwidth of the channel and the Rx magnitude is distributed across a wide spectral region. This is not necessarily bad. As the term selectivity implies, when some part of the signal spectrum is in a deep fade, the rest of the portion is not and hence we are able to achieve *frequency diversity* through this selective behaviour if we employ an equalizer at the Rx. We investigate the general idea behind diversity in the next section.

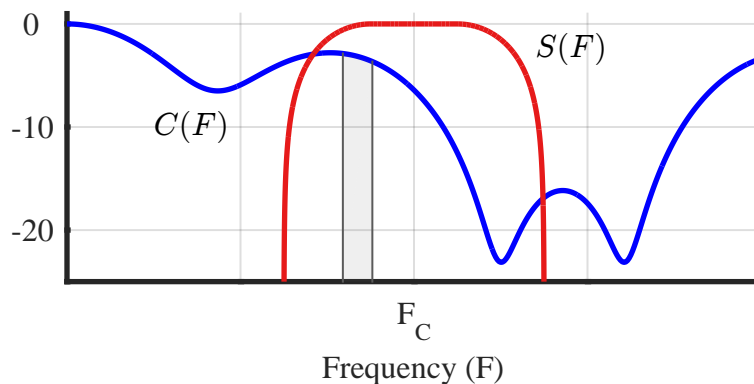


Figure 2.13: Signal bandwidth extending beyond the channel coherence bandwidth B_C gives rise to frequency selective fading. The term selective implies discriminatory treatment of different portions of the signal spectrum by the channel

2.3 Diversity: A Dumb yet Clever Idea

Diversity is one of those few ideas that are extremely dumb and extremely clever at the same time. It can be explained in one sentence as well as in a whole book. Let us find out the basic concept.

2.3.1 The Anna Karenina Principle

Understanding the idea of diversity starts with the Anna Karenina principle introduced in Jared Diamond's 1997 book *Guns, Germs and Steel: The Fates of Human Societies*. It comes from the famous first sentence of the great novel *Anna Karenina* written by Leo Tolstoy in 1877.

The Anna Karenina Principle

"Happy families are all alike; every unhappy family is unhappy in its own way."

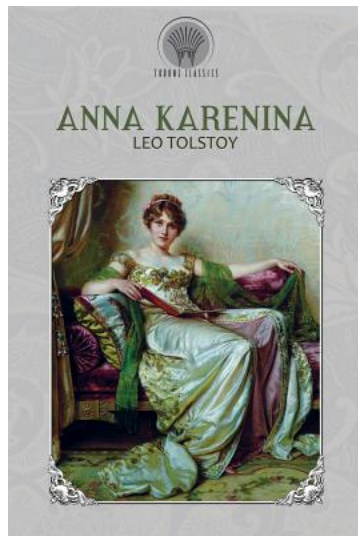


Figure 2.14: *Anna Karenina* by Leo Tolstoy

According to Diamond, what Tolstoy meant from this sentence was that a marriage must succeed in many different aspects of life to be counted as happy such as sexual attraction, agreement about money, child discipline, religion, in-laws and other vital issues. Failure in a single item of the above list can ruin a marriage even if it has all the other ingredients needed for happiness. Diamond extended this principle to understanding many different aspects of life. He concluded that instead of seeking easy, single-factor explanations for the route to success, one must avoid several separate possible causes of failure because failure in one of them is the failure of the whole. This is the general idea behind the Anna Karenina principle.

There are numerous examples of this phenomenon in our everyday life. For instance, for life to exist in the cold and dark universe, we need a star to provide energy as heat. A planet is also required as a home. Furthermore, this planet must reside in the Goldilocks Zone of that star. Similar to the baby bear's porridge in the story *Goldilocks and the Three Bears*, this is the habitable zone around the

star where the temperature is just right – neither too hot, nor too cold – for liquid water to exist, see Figure 2.15. This planet must also inhibit several specific elements in the right proportions at the right places. As another example, many vital body organs such as heart and brain must function properly for a person to live. If any of them fails, there is no more life.

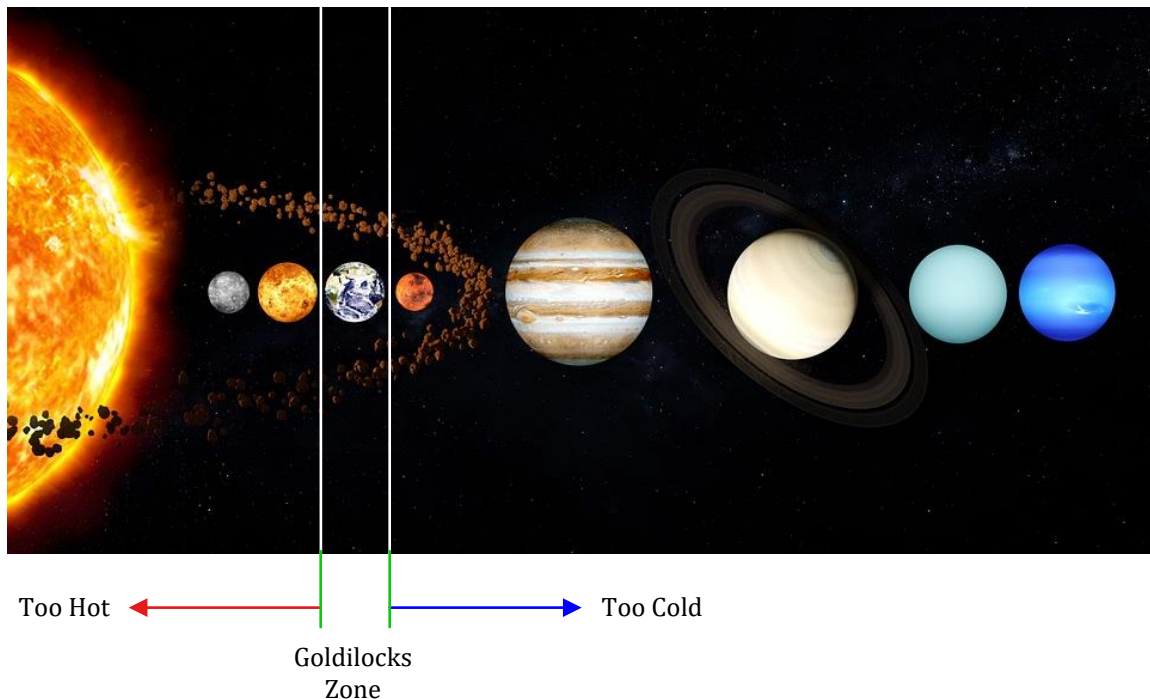


Figure 2.15: Earth lies in the Goldilocks Zone of our solar system

Speaking in mathematical terms, we can say that if the requirements A, B, C, etc. in the above examples are all independent to each other, and we denote their probabilities as P_A , P_B , P_C , etc., then the probability of a successful outcome is

$$P(\text{success}) = P_A \cdot P_B \cdot P_C \cdots \quad (2.15)$$

Clearly, when any single term on the right side becomes zero, the chance of success on the left side becomes zero too. If the probability of all the terms is the same, given by p , and there are L such participating factors, then the above equation yields

$$P(\text{success}) = p^L \quad (2.16)$$

All this comes from the the 2nd law of thermodynamics, according to which the failure cases (disorganized states) should be much higher than the success cases (organized states). This is how Anna Karenina principle also dominates most (but not all) of the natural world. Nature is more of a tinkerer than an engineer, as it adopts a slow and steady trial and error approach for creation purpose. The

variations from one state to the next at each instant are so subtle that they are almost negligible. Over insanely long periods of time, almost all cases lead to failure, see the probability of success above. For instance, more than 99% of the earth's species have gone extinct and there were countless others outside our sphere of knowledge. However, for some cases, these small variations accumulated like compound interest and produced creatures of majestic beauty and complexity. While the downside is the extent of time required (in millions and billions of years), the upside is exquisitely efficient systems with little room to improve. Compare the remarkable energy efficiency of a human body with a machine performing the same range of tasks.

Let us now find out about the inverse of this principle next.

2.3.2 The Inverse Anna Karenina Principle

Most people on the planet are born with two kidneys and two lungs. If one of them fails, they can still live a healthy life with some precaution. This is the essence of diversity. Now consider the main active agent in the known world: a human mind. With the ability to make decisions and influence outcomes as well as iterate over the design in a short time span, human designs can be made more resilient than those of nature. Let us take a simple analogy. If you toss a coin, you only have a 50% (i.e., $1/2$) chance of getting a head.

$$\underbrace{\{H\}, \{T\}}_{1 \text{ out of } 2}$$

However, if you toss two coins, there is a 75% (i.e., $3/4$) chance that you will have at least 1 head as the outcome.

$$\underbrace{\{H, H\}, \{H, T\}, \{T, H\}, \{T, T\}}_{3 \text{ out of } 4}$$

These odds increase in your favor with more coins. For 4 coins shown in Figure 2.16, there are $2^4 = 16$ possible outcomes and the probability of at least one of them having a head improves to around 94% (i.e., $15/16$).

What does this mean in the context of wireless communications? Consider the block diagram of a simple communication system in Figure 2.17 depicting three main blocks involved as well as the wireless channel. Notice that everything is in the hands of the system designer except the wireless channel that depends on large-scale and small-scale fading (as well as all the distortions encountered in the Tx/Rx frontends). These blocks, namely coding + decoding, modulation + demodulation and Tx/Rx frontends, can be optimized with the most ingenious of ideas. Nevertheless, a wireless channel in a bad state can still break the system. This is because when a number (or in our case, a waveform) is multiplied with zero, all we get is a zero without knowing if that number was 7, 16 or 21. This is why the bit error probability in Figure 2.11 for a fading channel is significantly worse than that for the AWGN case.



Figure 2.16: Basic concept of diversity: the more coins you have, the higher the odds that at least one of them is a head

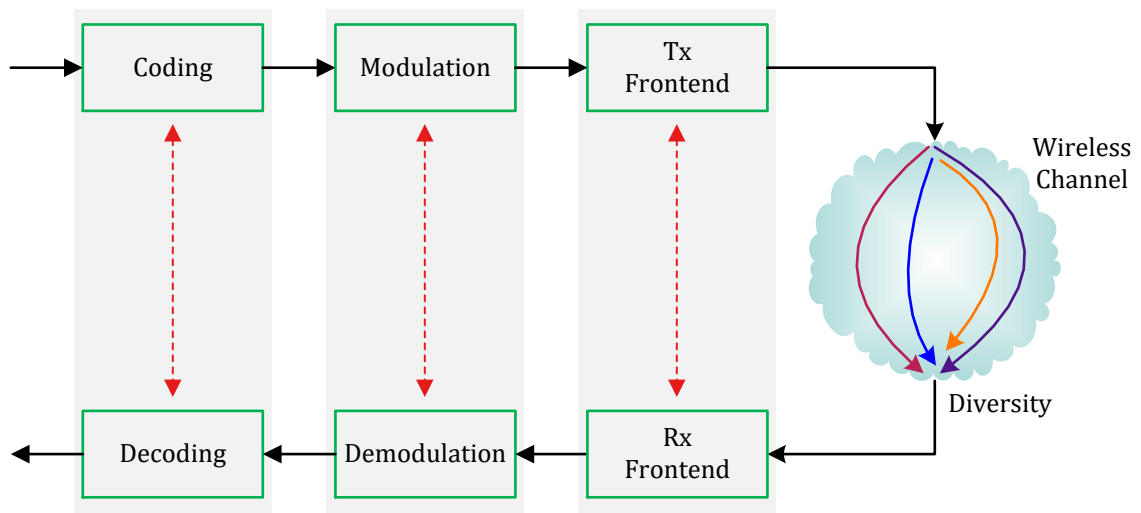


Figure 2.17: Block diagram of a simple communication system. Everything is in the hands of the designer except the wireless channel

Diversity implies using two or more statistically independent replicas for the transfer of the same information. This improves the reliability of the received message because nothing can recover the data signal in a deep fade except getting more copies of the same message. Just like the probability of at least one head in coin tosses increases with the number of coins, the probability of at least one copy out of a fade increases with the number of diverse copies. This is shown as the signal traversing multiple routes within the wireless channel in Figure 2.17 (as a reminder, this is a different concept than multipath studied before because the term route here can denote a simple retransmission in time or reception from

another antenna, for example). As long as any one of these copies enables the signal reception at a sufficient SNR, the system operation is a success. This message replication can be provided in different forms (e.g., time, frequency, polarization, space) but a simple illustration of how combining the same signal from two different antennas improves the signal part is drawn in Figure 2.18.

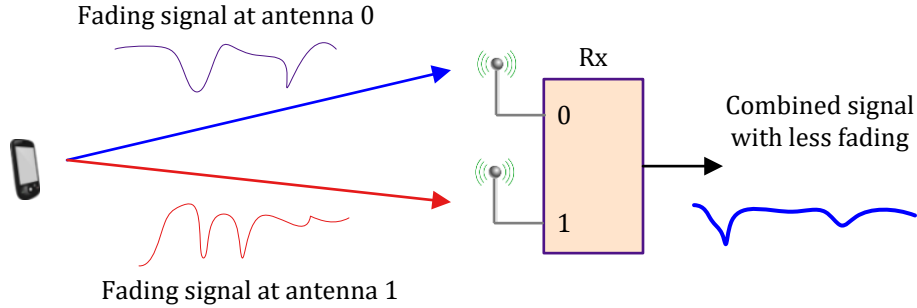


Figure 2.18: Diversity implies two or more independent replicas of the same information

Coming to the mathematical side, if the probability of each copy being rendered useless by channel fading is P_A , P_B , P_C , and so on, the transmission will only fail if *each and every one of them* experiences fading at the same time. We can write

$$P(\text{failure}) = P_A \cdot P_B \cdot P_C \cdots$$

Extending this idea further, if the probability of an individual fade given by p is the same for all the replicas (a realistic assumption), the probability of overall link failure with L diverse copies is given by

$$P(\text{failure}) = p^L \quad (2.17)$$

And the corresponding probability of success is given by

$$P(\text{success}) = 1 - P(\text{failure}) = 1 - p^L \quad (2.18)$$

Compare this with Eq (2.16) and notice how the relation is completely reversed. I like to call this *The Inverse Anna Karenina Principle* that originates from the active role of an intelligent agent in the design. We conclude that the higher the number of diverse replicas L , the lower the chances of a failed transmission. This number L is known as *diversity order*. This diversity is the fundamental reason behind how cellular networks like 5G have overcome the harsh wireless channel for high speed data transmission. In fact, you can easily extrapolate the idea here to grasp how massive MIMO systems in Chapter 4 with a large number of antennas (i.e., a large L in the above expression) effectively transform a fading channel into a simple AWGN one.

Organisms and Super-Organisms

Wireless transmission is not the only area where a careful human design can beat the odds of success. In the field of biology, it was always known that bigger animals live longer than smaller animals. But their lifespan increases in proportion to mass raised to an exponent *smaller* than 1 (approximately 1/4). For example, a whale is 100,000,000 times bigger than a shrew and lives on average 100 times longer. A few decades ago, a scientist named Geoffrey West investigated whether the same law applies to the super-organisms of human-built cities and found a similar pattern repeated for infrastructure based quantities such as the number of gas stations, length of electricity cables and the surface area of the roads, etc. However, when several figures directly related to creativity and innovation such as patents, R&D budgets, inventions and crime were collected, the results were unlike anything seen in the biology world. Cities scale in a super-linear fashion with an exponent *greater* than 1.



Figure 2.19: Human ingenuity significantly raises the odds of success

Now without proof, we state that the probability p of a deep fade in a Rayleigh fading channel is inversely proportional to the Signal to Noise Ratio (SNR).

$$p \approx \frac{1}{\text{SNR}} \quad (2.19)$$

where the exact constant that depends on the modulation scheme is ignored for simplicity. Therefore,

Eq (2.17) tells us that the probability of failure or Bit Error Rate (BER) is related to SNR as

$$\text{BER} \propto p^L = \frac{1}{\text{SNR}^L} \quad (2.20)$$

This is an interesting result revealed by the above expression: an increasing diversity order affects the BER in an *exponential* fashion! In Section 3.4, we will relate this trend to the slope of the BER curve. While we did not go into fancy derivations proving this result due to the limited mathematical scope of this text, this is a rather neat way of comprehending the role of diversity in a wireless system.

2.3.3 Types of Diversity

You might have noticed above that the idea of diversity is quite simple. In a technologically advanced world today, it is hard to imagine that no better solution could be devised to combat multipath fading than to provide additional copies of the signal. But this is true. The best defense against a fading channel built by the best minds of the world is to provide these multiple replicas so that the probability of all of them simultaneously drowning by fading becomes quite low.

That was the dumb part of diversity. The clever part arises from the fact that these multiple copies are not simply repeated transmissions. Instead, mathematicians and engineers have devised brilliant strategies in various forms of diversity that are practically employed.

Time Diversity

In the simplest case, a wireless signal can be sent twice over the same channel at two different time instants. The gap between these instants should be slightly longer than the average duration of a fading event. In real world, however, this technique is wasteful of resources available at the disposal of a communication system designer. Therefore, a clever scheme known as Forward Error Correction (FEC) is used instead of simply repeating the original transmission. During the coding process, redundant bits are added to the information bits in a deterministic manner. At the Rx, a decoder runs suitable algorithms to figure out the transmitted bits even when the received signal has suffered from multiple errors. This was shown as coding and decoding blocks in Figure 2.17. A state-of-the-art coding scheme known as Low Density Parity Check (LDPC) codes has been chosen for 5G data channels which is discussed in detail in Chapter 7.

Interleaving is another form of time diversity. To combat a long series of errors during the same fading event known as burst errors, the information bits are interleaved at the Tx side and de-interleaved at the Rx side. For example, one method of interleaving is to read the bits in rows and write them out in columns so that two adjacent bits in the information stream are actually one column apart at the input of the coder. This prevents the burst from erasing an adjacent set of bits.

Frequency Diversity

The destructive interference at the antenna we mentioned earlier causes a fade in the received power because the phase difference between the two paths is either (close to) 180° or a multiple thereof. Clearly, the frequency F sets the number of wavelengths that fit into the length of the transmission path. The fraction left thereafter determines the arriving phase at the Rx. Opposite phases of two such paths cancel the received signal.

Now if we send another copy of the signal at a slightly different frequency, the phase difference between the two paths will not be close to 180° as long as the other frequency is more than the coherence bandwidth apart. It just becomes similar to the two coins example we saw above and the probability of phases canceling out for *both* of these frequencies is low. This gives rise to frequency diversity utilized by wideband signals. When one part of the spectrum is in fade, the other part of the spectrum is not affected and usually provides enough information for signal recovery.

Equalizers in wireless communication systems exploit this frequency diversity to mitigate the channel effect. For instance, a RAKE receiver is a special kind of equalizer in Code Division Multiple Access (CDMA) systems, the technology behind 3G cellular networks. In 4G and 5G systems, equalization in frequency domain has been adopted due to its superiority over time domain equalization. We discuss this idea further in Chapter 8.

Spatial Diversity

When some people first hear the term *space*, it causes some confusion in regards to what the concept of diversity has to do with space! For clarification purpose, space refers to the diversity provided by another antenna at a different position. The idea is similar to human ears in the form of two receive antennas that help us not only to capture sounds from different locations but also to estimate their directions.

The starting point is the realization that multipath fading cannot take away energy that has already been injected into the air. Since the signal is traveling in time and space, the energy has simply been redistributed in three spatial dimensions. The only problem is the fraction of energy impinging on the Rx antenna where wave summation occurs in a destructive manner. This fraction of energy can be significantly increased by tapping into a different part of space. For example, if there is a second antenna placed at the Rx sufficiently apart from the first antenna, the phase relationship between the two paths would be different over there.

In major cellular and wireless networks of the past, space diversity has been employed with the help of multiple Tx antennas and/or multiple Rx antennas giving rise to Multiple Input Multiple Output (MIMO) systems. The interesting thing about spatial diversity is that signal transmission takes place at the same time over the same frequency band. In comparison, both time and frequency diversity require additional bandwidth, an increasingly scarce resource. The benefits thus provided are worth the material cost of additional antennas, their RF chains and associated signal processing. We explain the idea of

space diversity with the help of a simple scheme: Selection Combining (SC).

Consider a wireless link with 1 Tx antenna and 2 (or more) Rx antennas as shown in Figure 2.20. At each symbol time, a data symbol s is transmitted which belongs to a Quadrature Amplitude Modulation (QAM) scheme. To focus on the events happening within one symbol time only, we have dropped the time index m from the modulation symbol $s[m]$ here.

- In this setup, r_1 is the signal received by the first antenna while r_2 is the signal received by the second antenna.
- h_1 is the flat fading channel gain[†] between the Tx antenna and the first receive antenna.
- h_2 is the flat fading channel gain between the Tx antenna and the second receive antenna.

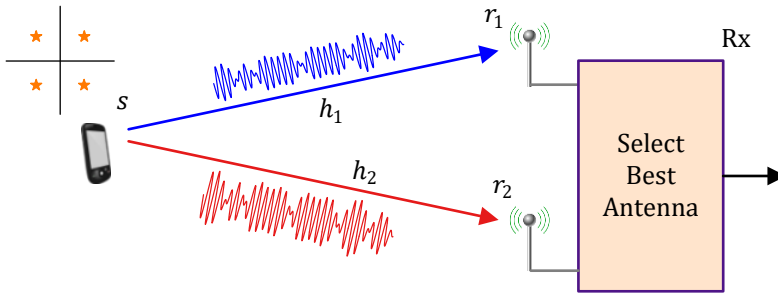


Figure 2.20: Selection combining implies choosing the antenna with the highest instantaneous strength

In selection combining, the Rx computes the instantaneous signal strength at each of the antennas and selects the one with the highest power. In other words, the branch with the best channel gain h_i is chosen for demodulation. This exploitation of channel knowledge at the Rx provides a significant *diversity gain*, a concept we will explore in detail later.

To see how the performance is enhanced with selection combining, the average bit error rate is drawn in Figure 2.21 for a Rayleigh fading channel with $N_R = 1, 2$ and 3 Rx antennas where ideal bit error rate for an AWGN channel is also shown. This bit error performance from selection diversity improves with increasing number of antennas. For instance, by adding a second antenna at the Rx at a target bit error rate of 10^{-4} depicted by the ellipse, the average SNR requirement in a flat fading scenario drops from around 34 dB to less than 20 dB. This is further reduced to less than 15 dB when a third antenna is also available. We conclude that the improvement is substantial for the first few antennas before the law of diminishing returns flattens the marginal gain from each additional antenna.

One drawback of selection combining is that it discards the useful energy arriving at the other antennas at the expense of simple hardware requirements and computational simplicity. In many situations,

[†]Remember that there is a difference between channel paths and channel taps. The bandwidth of our signal determines the number of channel taps in our system, regardless of the actual number of channel paths. These taps are usually denoted by $h[n]$ in wireless literature. More details on this can be found in Chapter 8 of Ref. [2].

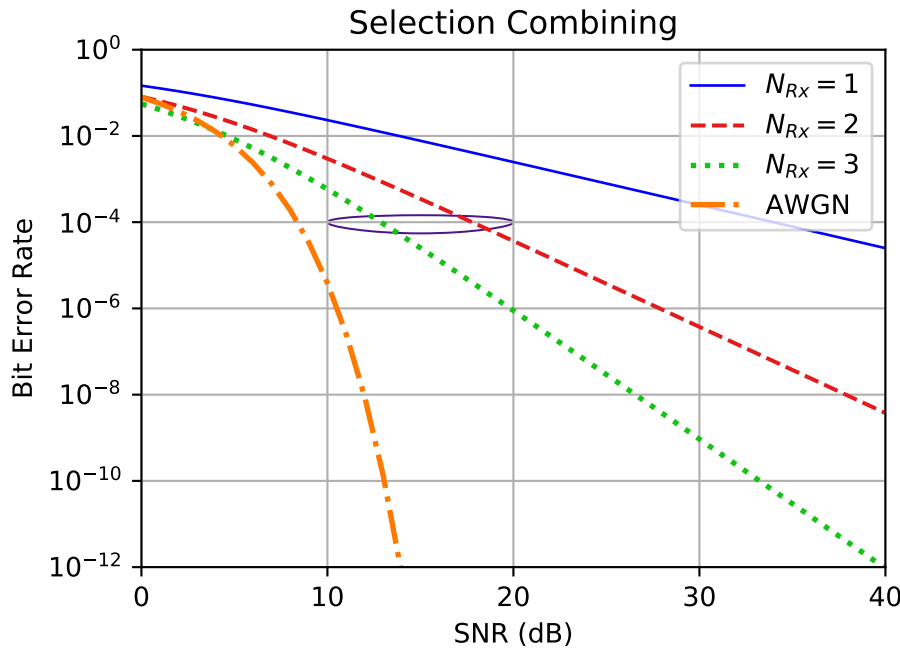


Figure 2.21: Average bit error rate for selection combining with 1, 2 and 3 Rx antennas

such a trade-off is desirable. Otherwise, a better approach known as maximal ratio combining can be employed which we study in Section 3.4. In the next section, we explore different modes in which multiple antennas can be deployed.

2.4 Multiple Antenna Modes

When computing approaches the physical limits of clocking speeds, we turn towards multi-core architectures. When communication approaches the physical limits of transmission speeds, we turn towards multi-antenna systems. What exactly are the benefits that led to scientists and engineers choosing multiple antennas as the foundation of 4G and 5G PHY layers? While having spatial diversity was the original incentive for adding antennas at the base stations, it was discovered in mid 1990s that multiple antennas at Tx and/or Rx sides open up other possibilities not foreseen in single antenna systems.

Let us now describe three main techniques in this context.

Beamforming

Beamforming is the principal technology on which physical layer of 5G cellular networks is based. There are two different kinds of beamforming:

- Physical beamforming, also known as Line of Sight (LoS) or classical beamforming

- Virtual beamforming, also known as Non-Line of Sight (NLoS) or generalized beamforming[†]

Interestingly, there has been a longstanding confusion between them although both of these types are radically different from one another. The main idea in both cases is to employ multiple antennas to enhance the signal strength from particular users while suppressing the signals from interferers. As an analogy, a digital filter alters the signal contents in frequency domain, a process known as *spectral filtering*. In a similar manner, beamforming alters the signal contents in spatial domain. This is why it is also known as *spatial filtering*. The method of choosing suitable weights to accomplish this task depends on whether the beamforming is physical or virtual.

Physical beamforming has a rich history in signal processing algorithms for sonar and radar systems. It creates actual beams in space for transmission or reception and hence closely associated with Angle-of-Arrival (AoA) or Angle-of-Departure (AoD) of the signals. Similar to OFDM covered in Chapter 8 that creates parallel streams in frequency domain, physical beamforming creates parallel beams in angular domain.

On the other hand, virtual beamforming in the simplest scenario implies that the same signal is emitted (or received) from each of the Tx (or Rx) antenna with appropriate phase and gain weighting such that the signal power is maximized for a particular user. Unlike steering the physical beam in a particular direction, the transmission or reception occurs in all directions but the main emphasis is on constructively adding multiple copies of the signal at the Rx thus reducing the multipath fading impact.

Both of these types of beamforming are discussed in detail in Chapter 3.

Spatial Multiplexing

In spatial multiplexing mode, an input data stream is split into multiple parallel streams in space domain, i.e., each of these streams is then transmitted through a different Tx chain. As long as the channel paths arrive from a multitude of directions exhibiting little correlation at the Rx antennas, Digital Signal Processing (DSP) techniques can be applied to transform one wireless medium into independent parallel channels. This MIMO mode was a major factor behind orders of magnitude higher data rates in the modern wireless systems because independent information is sent from multiple antennas at the same time over the same bandwidth. We study spatial multiplexing in Chapter 5.

Space-Time Coding

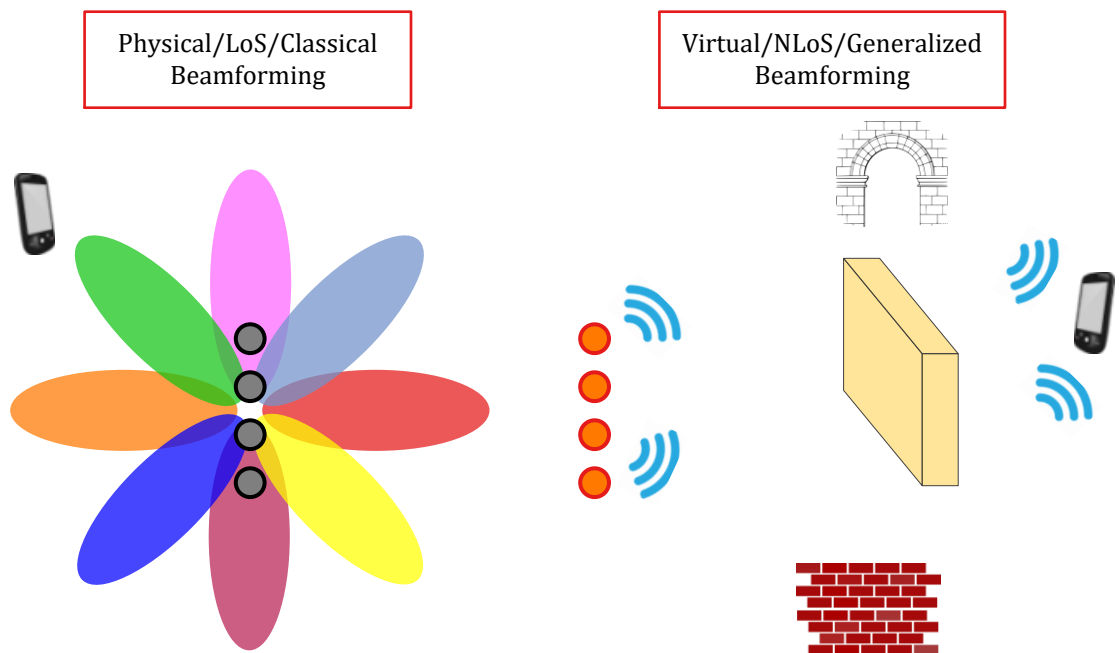
In this mode, special coding schemes are utilized in time and across antennas in a manner that signal diversity is enhanced at the Rx without any data rate penalty as compared to a single antenna

[†]Borrowing from real and imaginary parts of a complex number, I think that *real* beamforming and *imaginary* beamforming would have been even better terminologies. As we explore in Chapter 3, the former actually creates real beams while the latter performs mathematical operations after which the radiation pattern has no resemblance with a beam. But I settled on the expressions physical and virtual to avoid any confusion while still conveying the basic idea.

system. Space-time codes enhance spatial diversity without any requirement for availability of channel estimates at a Tx possessing multiple antennas.

Chapter 3

Beamforming Demystified



Beamforming through multiple antennas had long been used by signal processing engineers for radio applications. Even Marconi used four antennas to increase the gain of signal transmissions across the Atlantic in 1901. Directional beamforming from an antenna array was proposed in 1919 as a solution to spectrum scarcity. It has also been known since 1970s that multiple antennas at the base station help simultaneous communication with several users. But beamforming only became a household terminology after its incorporation in 5G standard. After the advent of MIMO concept in mid 1990s, the majority of research and implementation efforts were focused towards point-to-point spatial multiplexing mode which allows the transmission of multiple independent streams in a simultaneous manner to a single user (discussed in Chapter 5). It was only with time that beamforming (with all its variants) was adopted as the main MIMO technique for NR standard, although spatial multiplexing is still a part of 5G systems. To give you the intuition behind two kinds of beamforming, Figure 3.1 demonstrates how the beams are pointed towards the intended users. How is the yellow beam directed towards user 1 formed? How does the green beam connect the base station with user 2 although the red beam is blocked by the building between the two? These are the questions we answer in this chapter.

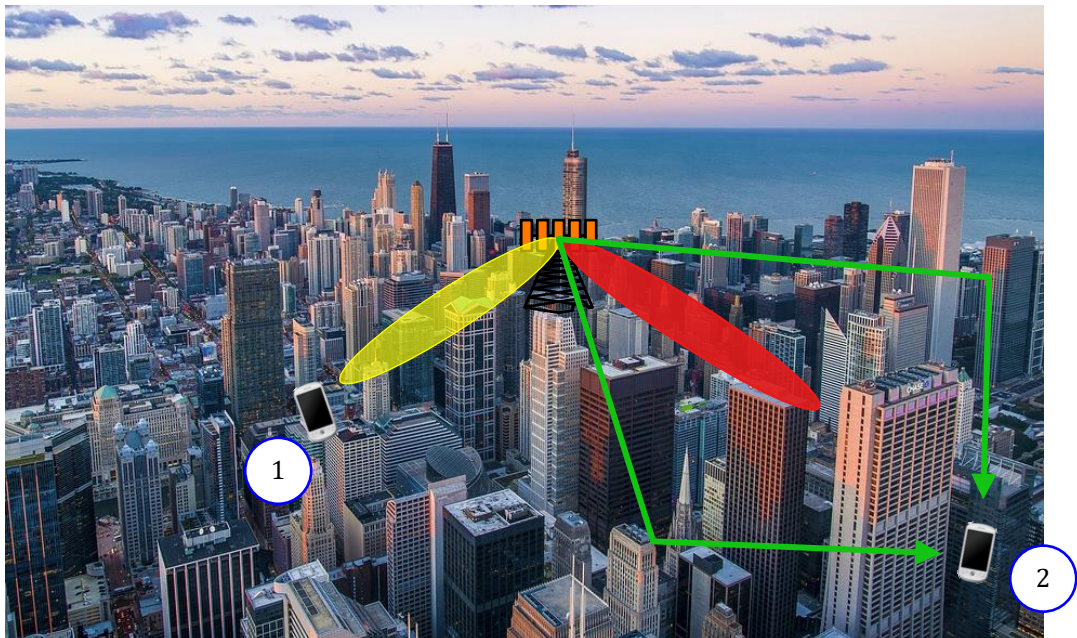


Figure 3.1: Two types of beamforming

Let us cover some preliminaries before moving towards the more interesting part. Keep in mind that the scope of this text is focused on a signal processing viewpoint instead of more detailed electromagnetic mechanisms and therefore the effects of polarization are ignored in the discussion.

3.1 Signal Model

As a starting point for examining the idea behind beamforming in wireless systems, we turn our attention towards a single antenna system.

A Single Antenna System

Consider a single antenna system shown in Figure 3.2 which is also known as a *Single-Input Single-Output (SISO)* system. We can temporarily remove any time index to focus on only one data symbol denoted by s . Furthermore, the received signal at the Rx antenna is denoted by r while the flat fading channel gain is written as h . Then, for this 1 Tx and 1 Rx system, we can write

$$r = h \cdot s + \text{noise} \quad (3.1)$$

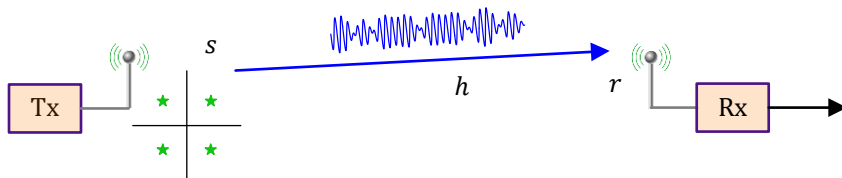


Figure 3.2: A Single Input Single Output (SISO) system with 1 Tx and 1 Rx antenna

This simple expression is the signal model used in modern communication systems, the reasons for which we saw in Section 2.2. Interestingly, these infrastructure-based systems are expensive to build and run but they deliver relatively simple signals at the Rx if the interference contribution is ignored. On the other hand, the signal expression for a conventional (single carrier) point-to-point radio link between a Tx and a Rx is quite complicated, and given by

$$r(t) = \sum_m s(m)g(t - mT_M)$$

Here, $g(t)$ is a convolution between the pulse shape $p(t)$ and the frequency selective wireless channel $h(t)$, or $g(t) = p(t) * h(t)$, and T_M is a symbol time described in Section 1.3. Design of such systems from a signal processing perspective was the topic of my earlier book [2].

Next, we describe some signal normalizations that are important for a performance comparison between single and multiple antenna systems.

Some Normalizations

We said before that energy of a discrete-time signal is the sum of its magnitude squared samples. A related parameter is the power of a signal that is simply the energy per unit time. From Eq (3.1), the

average signal power at the Rx is given by

$$\text{Signal Power} = \text{Avg } |s|^2 \cdot \text{Avg } |h|^2 = E_s \cdot \text{Avg } |h|^2 \quad (3.2)$$

where E_s is the symbol energy. For all the discussions in this text, we assume the following.

Signal Energy

Modulation symbols are unit energy, i.e., $E_s = 1$, as derived in Eq (1.10) before. This implies that these symbols are ± 1 for BPSK where E_s comes out to be $\frac{1}{2}(+1)^2 + \frac{1}{2}(-1)^2 = 1$. Similarly, for QPSK, we have the symbols $(\pm \frac{1}{\sqrt{2}}, \pm \frac{1}{\sqrt{2}})$ [†], and so on. Consequently, the signal power corresponds to only the channel gain h at the Rx which is also normalized next.

Channel Normalization

Since $|h|^2$ is a random number, an averaging operation is performed to obtain the expression for the average signal power. Just like the modulation, the average power for h can be fixed at unity, or $\text{Avg } |h|^2 = 1$, the reasons of which are shortly explained (for the sake of correctness, note that the random processes here are assumed to be ergodic which implies that time averages and statistical averages are the same).

The above results can be summarized in the following expressions that will be used later.

$$\begin{aligned} E_s &= 1 \\ \text{Avg } |h|^2 &= 1 \end{aligned} \quad (3.3)$$

The consequence of the above settings on signal power are as follows. For a unit energy transmission symbol and normalized channel gain as above, the signal power for a *single antenna* from Eq (3.2) also gets normalized to 1.

$$\text{Signal Power} = E_s \cdot \text{Avg } |h|^2 = 1 \quad (3.4)$$

With the Gaussian noise power denoted by its variance σ^2 , we can write the average Signal to Noise Ratio (SNR) at Rx antenna as

$$\text{SNR} = \frac{\text{Signal Power}}{\text{Noise Power}} = \frac{1}{\sigma^2} \quad (3.5)$$

This SNR is the benchmark against which we compare the gains in multiple antenna systems. At this stage, a few comments are in order.

- The normalization of symbol energy, $E_s = 1$, is a frequently used practice and can be accommodated in a straightforward manner.

[†]In complex notation, these symbol values for QPSK are $(\pm \frac{1}{\sqrt{2}}, \pm j \frac{1}{\sqrt{2}})$.

- Channel normalization is obviously not true for physical wireless channels as both the large-scale and small-scale fading determine the eventual Rx power. However, it is done for performance comparisons in computations of Signal to Noise Ratio (SNR) while the actual power differences are shifted to a separate factor as we see next.
- If both the constellation energy and the channel power are normalized to 1, what is the expression for a signal that is radiated into the air with a power of P watts? The answer is that we can simply multiply the modulation symbols by a factor of \sqrt{P} that combines all the channel gains and attenuation from the Tx to the Rx into a single factor while still maintaining the symbols s and the channel gain h into their normalized forms.
- The large-scale factor \sqrt{P} is important from a power control perspective where users at different locations in a cell adjust their respective power levels through a feedback procedure from the base station to keep the interference under control. It also plays a crucial role in performance analysis of a multi-user system. However, the equations look more complicated after the inclusion of this factor. Therefore, I will ignore power control throughout this text.

In summary, the normalizations done here are for comparing multiple antenna gains with respect to a single antenna system.

A Multiple Antenna System

With this background in place, let us now describe a multiple antenna system, also known as an antenna array. The most common configuration for a set of antennas is to arrange them at regular spacing in either one (Uniform Linear Array or ULA) or two dimensions (rectangular array). Conformal arrays with curved surfaces are also common. Smart antennas is another term associated with antenna arrays equipped with signal processing algorithms on the backend. In this text, we will mainly focus on a one-dimensional or linear arrangement to grasp the fundamental aspects of this technology instead of more practical planar (e.g., rectangular) and conformal (e.g., cylindrical) arrays. The lessons learned here can be mapped on these more complicated array geometries.

A multiple antenna system with 1 Tx and N_R Rx antennas shown in Figure 3.3 called a *Single-Input Multiple Output (SIMO) system*. Again, we temporarily remove any time index to focus on only one data symbol denoted by s . The received signal at the Rx antenna is denoted by r_j while the flat fading channel gain is written as h_j . Then, the expression for r_j becomes

$$r_j = h_j \cdot s + \text{noise}, \quad j = 0, 1, \dots, N_R - 1 \quad (3.6)$$

In the context of multiple antennas, the flat fading setup can be justified as follows.

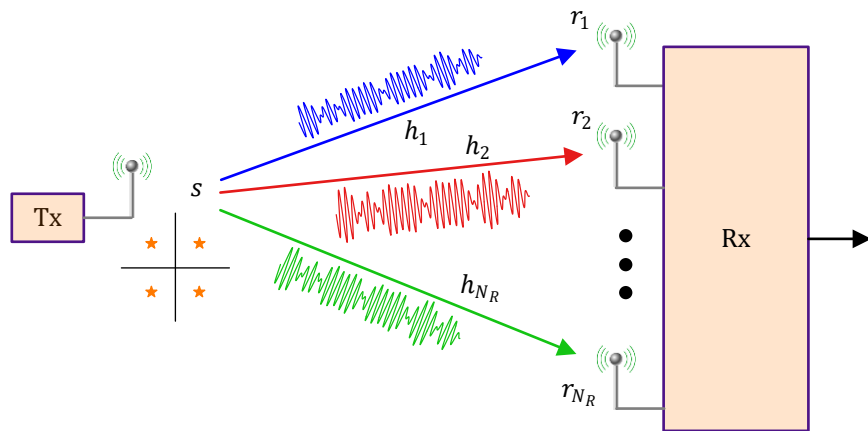


Figure 3.3: A Single Input Multiple Output (SIMO) system with 1 Tx and N_R Rx antennas

Why Flat Fading?

As discussed in Section 2.2, high data rate transmissions in general exhibit a frequency selective channel. However, in most of the literature as well as this text, the system model is expressed with a flat fading gain. This is because both 4G and 5G systems employ OFDM technique explained in Chapter 8 which converts a frequency selective channel into many parallel frequency flat fading channels. This also accounts for inter-antenna interference in a MIMO system. Furthermore, massive MIMO covered in Chapter 4 significantly reduces time and frequency variations of the wireless channel. Therefore, we will continue to assume a flat fading channel with gain h_j for each antenna in this study.

What can be achieved with the additional antennas? To answer this question, let us view multiple antennas through a different lens.

3.2 Viewing Multiple Antennas through a Different Lens

Once upon a time, an antenna was viewed as a simple device to transmit and receive an electromagnetic wave, much like a battery the sole purpose of which is to provide electrical power. A set of antennas, however, can be viewed from a new angle as follows.

Sampling in Time Domain

An Analog-to-Digital Converter (ADC) is a device that samples an analog signal in time domain to create a corresponding sequence of numbers. Similarly, a Digital-to-Analog Converter (DAC) gets a sequence

of numbers as an input to generate a reconstructed analog signal. As an example, a rectangular pulse shape is shown in Figure 3.4 which is sampled at regular intervals separated by T_S seconds. The length of the pulse is equal to one *symbol interval* in continuous time domain.

$$T_M = NT_S$$

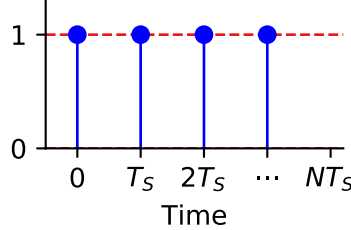


Figure 3.4: A rectangular pulse shape sampled in time domain at intervals of T_S seconds

The sampling interval T_S is chosen according to the bandwidth B of the arriving signal. Sampling theorem in DSP tells us that the sampling rate $F_S = 1/T_S$ required to capture all the information in an analog signal should be greater than twice the bandwidth B , or $1/T_S \geq 2B$. In other words, the spacing between two samples T_S should be less than half the inverse bandwidth.

$$T_S \leq \frac{1}{2B} \quad (3.7)$$

For a sinusoidal wave as an example, we require at least two samples within each cycle. The question now is how to choose the right sample spacing T_S .

- If T_S is chosen as much smaller than in the above expression (a high sample rate), then we have many more samples to process than required. This adds to the system cost through extra storage and signal processing as well as reduced efficiency.
- On the other hand, a value for T_S greater than $1/2B$ implies a violation of sampling theorem. This gives rise to *aliasing* in frequency domain which are spectral replicas of the original waveform appearing within the band. A set of aliases arising as a result of aliasing is shown in Figure 3.5.

Sampling in Space Domain

In a manner analogous to sampling by the ADC and reconstruction by the DAC in time domain, the signals arriving at an antenna array can be visualized as being *sampled in space domain*. Similar to the discrete-time sampling, the bottom part of Figure 3.6 depicts an antenna array sampling the signal at a regular spacing of d meters.

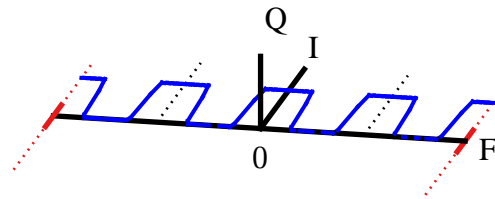


Figure 3.5: Aliases arise in frequency IQ plane as a result of violating the sampling theorem which are simply the replicas of the original spectrum at integer multiples of sample rate

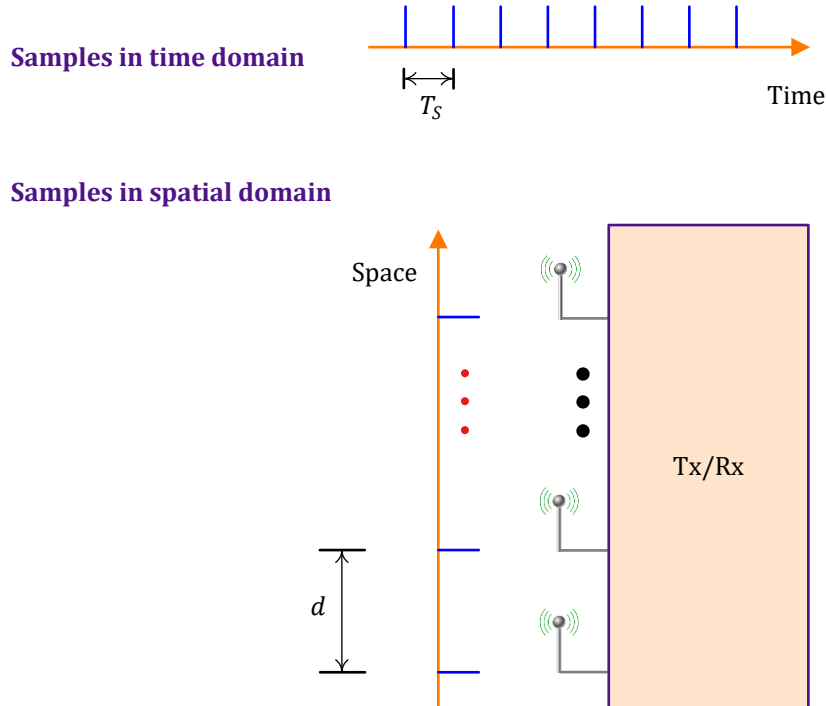


Figure 3.6: Multiple antennas can be thought of sampling the signal in space dimension, very similar to how an Analog-to-Digital Converter (ADC) samples the signal in time domain

Here, the spacing d between the elements is chosen according to the wavelength λ of the target signal. Similar to sampling theorem in time domain, we have the following relation

$$d \leq \frac{\lambda}{2}$$

This is called critically spaced antenna spacing and corresponds to the time domain condition $1/2B$. In Eq (3.66) of Appendix 3.6, we derive another condition for the spacing between antenna elements.

$$d \leq \frac{\lambda}{1 + \sin \theta_0} \quad (3.8)$$

where θ_0 is the direction of the array pattern peak. Why is there a difference between $\lambda/2$ and the above expression? As we will see soon during physical beamforming, the directional response of the array as a result of spatial sampling is analogous to frequency response in time sampling but the correspondence is between the sine of angle, $\sin(\theta)$, instead of θ alone and the frequency variable ω during the transformation.

- If the antenna spacing d is lesser than the above value, it is like collecting more samples in space than necessary. Such a small spacing is expensive from a hardware viewpoint, increases mutual coupling and reduces spatial diversity between channels.
- If the spacing is larger than the above value, then there are less number of elements for the same array length that reduces manufacturing costs and the associated feeding circuitry. Nonetheless, these advantages come at the cost of *grating lobes*, a phenomenon similar to spectral aliases for time domain sampling. Suffice it to say here that the normal operation of an array is to pick up signals from desired directions and attenuate the rest. Instead, grating lobes pick up signals from some undesired directions as well without attenuation.

In the light of the above, the goal is to design antenna arrays with the widest possible spacing until the effect of grating lobes starts to appear. The relation in Eq (3.8) is derived for the peak of the grating lobe, not the middle between the main and grating lobes. Therefore, many multiple antenna systems are designed as a series of identical elements separated by a distance of 0.5λ to 0.7λ .

Time-Frequency Grid

Shown at the left of Figure 3.7 is a *time-frequency grid* where the available resources of time and frequency are sliced in discrete intervals. While the rise of digital computing made it straightforward to produce discrete time domain samples, the frequency part did not offer any such convenience. For most of the history of wireless communications, designers did not know how to slice the frequency domain at discrete points. This was due to the definition of frequency based on time itself, i.e., frequency is inversely proportional to time $T = 1/F$. It was only after the formulation of Orthogonal Frequency Division Multiplexing (OFDM) technique that frequency domain could also be discretized in a convenient manner. This was one of the major reasons for adoption of OFDM systems in 4G and then 5G cellular standards.

Time-Frequency-Space Grid

Availability of multiple antennas on wireless devices adds another dimension to the resources at the disposal of the system designer. While frequency is dependent on time, there is no such limitation for space. Extra antennas can be utilized to sample additional versions of the same signal which can be exploited in a variety of manners. The right part of Figure 3.7 illustrates one time-frequency grid associated with each antenna. Consequently, instead of a time-frequency square as before, we have

a time-frequency-space cube which can be employed for communication enhancement, reliability or directivity.

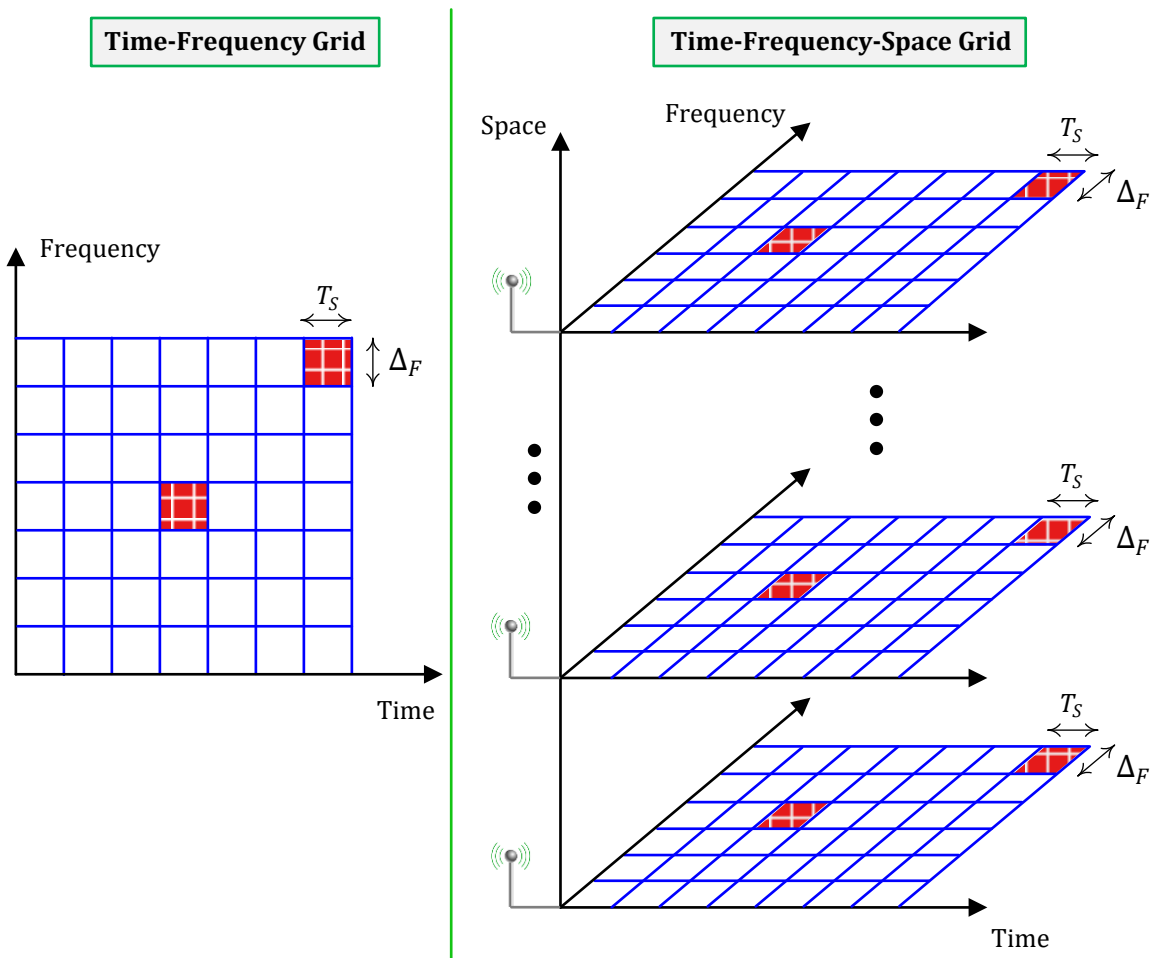


Figure 3.7: A view of time-frequency-space grid in a communication system

The initial trend in developing MIMO systems was to maximize the data rate. This technique is known as spatial multiplexing which was the main thrust behind the accelerated adoption of MIMO systems in wireless standards. The basic idea is to equip both sides of a communication link with some antennas and fill each element of this grid with a unique modulation symbol. This was an excellent idea for point-to-point links where the only purpose is raw throughput maximization. On the other hand, a cellular network achieves an entirely different goal: to maximize the overall throughput for a number of users within a geographical area. Such a goal requires increasing the individual data rates while simultaneously decreasing the interference among the users. This objective can be better accomplished through beamforming from a large antenna array by directing user signals in their own directions (whether physical or virtual) thus automatically reducing the interference part. The asymmetric nature of the links, where more data is downloaded than uploaded, also plays a factor in the push towards installing

a large number of antennas at the base station while keeping the mobile terminals simple. The NR standard now utilizes both beamforming and spatial multiplexing to serve the users.

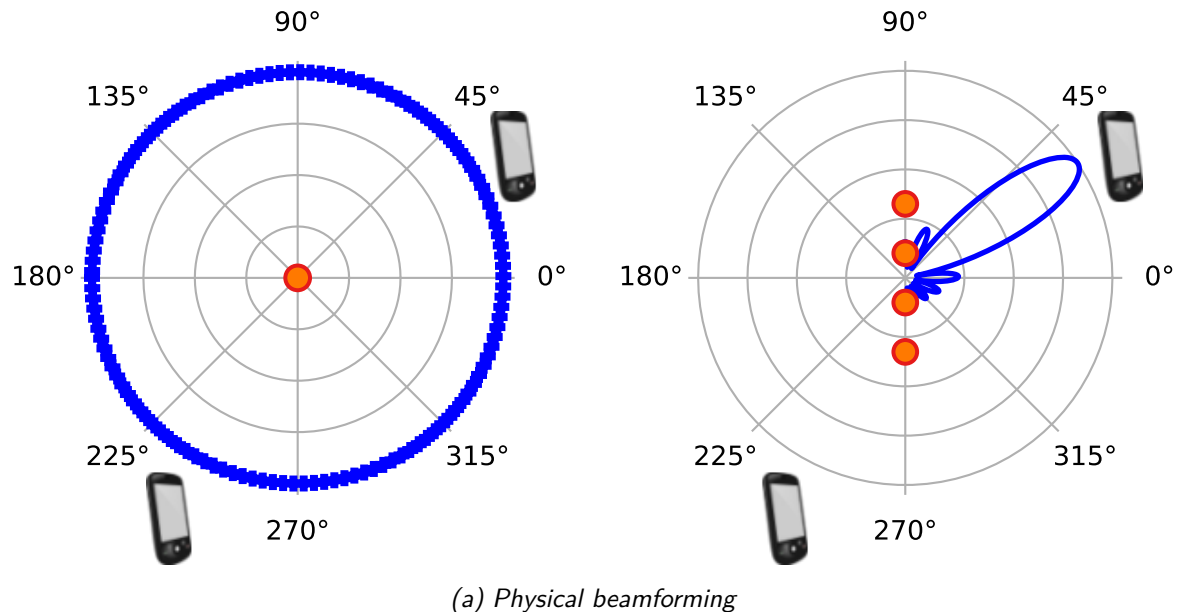
Next, we turn our attention towards the two major types of beamforming: physical and virtual. Physical beamforming actually steers the signal energy in a particular direction while virtual beamforming exploits the knowledge of channel gains to coherently combine the energy arriving at the Rx from different directions. Let us explore these two methods in detail. For most of what follows, we assume that the Tx has knowledge about channel gains.

3.3 Classical or Physical Beamforming

In a cellular network, the electromagnetic energy emanating from the Tx antennas or arriving at the Rx antennas consists of the desired signal and interference signals from the perspective of a certain user. If only a Line of Sight (LoS) exists between the base station and that user, the angles in a geometrical space can act as suitable differentiators. In other words, the desired signal and interference can be separated at the Rx if the signals can be characterized in terms of their Direction of Arrival (DoA), also known as Angle of Arrival (AoA). A similar characterization in the Tx case holds in terms of Direction of Departure (DoD) or Angle of Departure (AoD).

- For instance, on the left of Figure 3.8a is a radiation pattern of a single isotropic antenna which radiates or receives an equal amount of power from all directions, very similar to a light bulb. In a cellular network, a device (whether base station or mobile) not intended to receive that signal still had to deal with interference coming from the transmissions directed at another device. We conclude that lots of energy is wasted in unwanted directions that could instead be utilized to boost the power to the desired user. This is where the power of focus comes in.
- Every child has this experience of burning a paper with a magnifying glass under the sun as illustrated in Figure 3.8b. This demonstrates the power of focus that spreads thinner with increasing number of targets. Space based solar power might one day beam the energy harvested in space back to earth based on a similar principle (as Isaac Asimov suggested in his story *The Last Question*: All Earth ran by invisible beams of sunpower coming from a small station, one mile in diameter, circling the Earth at half the distance of the Moon).

Now shown on the right side of Figure 3.8a is an antenna array that ‘looks’ only into a particular intended direction thus minimizing the interference for other users in the same area. This is the essence of physical beamforming. The case where there is no direct Line of Sight (LoS) path from the Tx to the Rx will be discussed in virtual beamforming. Both of these strategies are implemented through varying the phase and/or amplitude of the signal at each antenna which form the ‘spatial samples’ described in the last section.



(b) A demo of the power of focus: burning a paper through a magnifying glass

Figure 3.8: Physical beamforming directs transmission and reception patterns in an intended direction thus minimizing the interference for other users in the network

3.3.1 Superposition of Waveforms

This brings us to the question about the origin of beams. Why do multiple antennas ‘look’ into particular directions and why the final radiation pattern comes from the Fourier Transform? Why do the overall radiation characteristics depend on both the individual elements as well as the size and configuration of the antenna array? This is what we explain next from a fundamentals viewpoint. For an in-depth study of antenna design and arrays, see Ref. [14].

Set Up

The discussion below is based on the following setup.

Linear Array

In our example, an array consists of equally spaced antennas along a horizontal or vertical straight line, a configuration commonly known as a Uniform Linear Array (ULA). Similar ideas can be extended to other array geometries.

Far Field

The signal is transmitted from a far-field region which implies that the source and destination are sufficiently distant from each other. This leads to the following consequences.

- In reality, each antenna element encounters a slightly different angle due to the spherically expanding wavefront. From the Rx perspective in the far field drawn in Figure 3.9, the angle differences between the source and individual antenna elements are negligible and the signal can be treated as a planar wavefront (the last red line) arriving at *one* particular angle. This means that the green lines shown in the figure are (almost) parallel and differences between distances from the Tx to the antenna elements depend on their common angle at the Rx. This is an approximation that holds quite well in most practical situations with great results.
- As far as channel gains at individual antenna elements are concerned, the path loss from *large-scale fading* is nearly the same for each element of the array. Therefore, the only difference in channel gains at the antennas arises from the array geometry itself, as we see later.

Radiation Pattern

Each element in this array exhibits an isotropic radiation pattern. While an isotropic antenna is an ideal reference, such an assumption helps in focusing on the radiation part played by a collection of antennas instead of those from the individual elements. Such an isotropic characteristic holds whether the array is in transmission or reception mode. For practical non-isotropic antennas (e.g.,

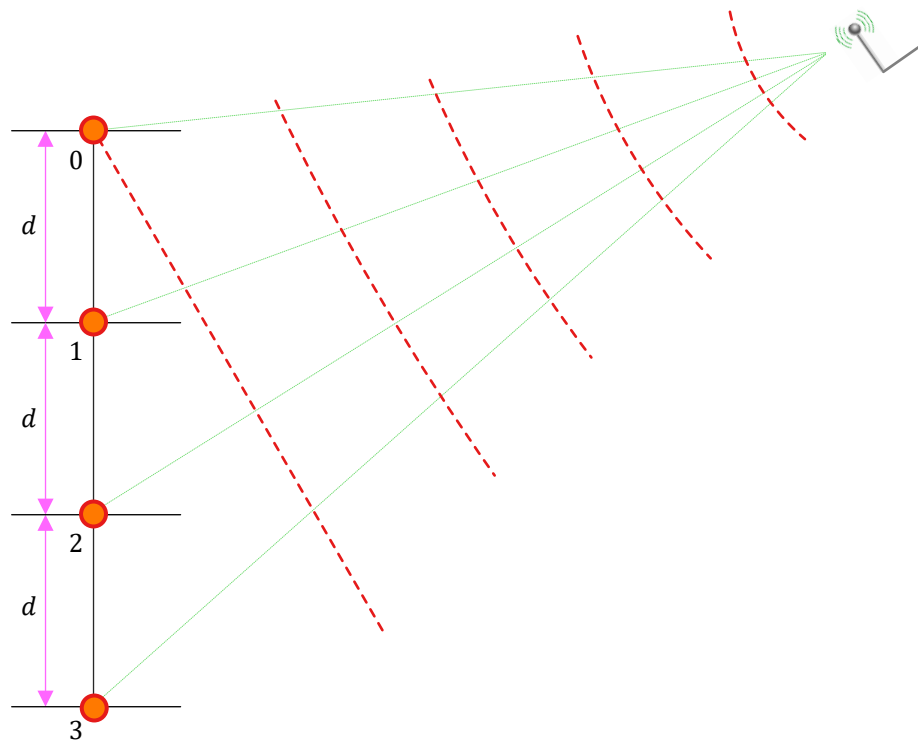


Figure 3.9: A planar wavefront in the far field region of the antenna array

dipole or microstrip antennas), the cumulative pattern is a multiplication between the individual pattern with that of the array, as we see later in Figure 3.22c.

Next, we look into a signal level view arising from the above mentioned framework.

A Signal Level View

At the Tx side, this implies that the antenna array is excited by a current source according to the modulated information riding on a carrier frequency and then each element radiates equal energy in all directions. Such isotropic radiation patterns are illustrated in Figure 3.10 for a 4-element array. It is evident that the maximum gain occurs in the direction where their patterns overlap with each other. This angle is 0° in the scenario shown here. Also notice from the figure that a mirror beam, known as a *backlobe*, should be created in the opposite direction (i.e., 180°) due to the isotropic antennas assumption. In practice, this backlobe is suppressed by the use of more directional antenna elements. Coming back to our setup, the unique range for the array pattern is from -90° to $+90^\circ$. The reason why such a superposition results in shaped beams will be discussed shortly.

At the Rx side, the array of isotropic antennas is equally receptive to planar waves arriving from all

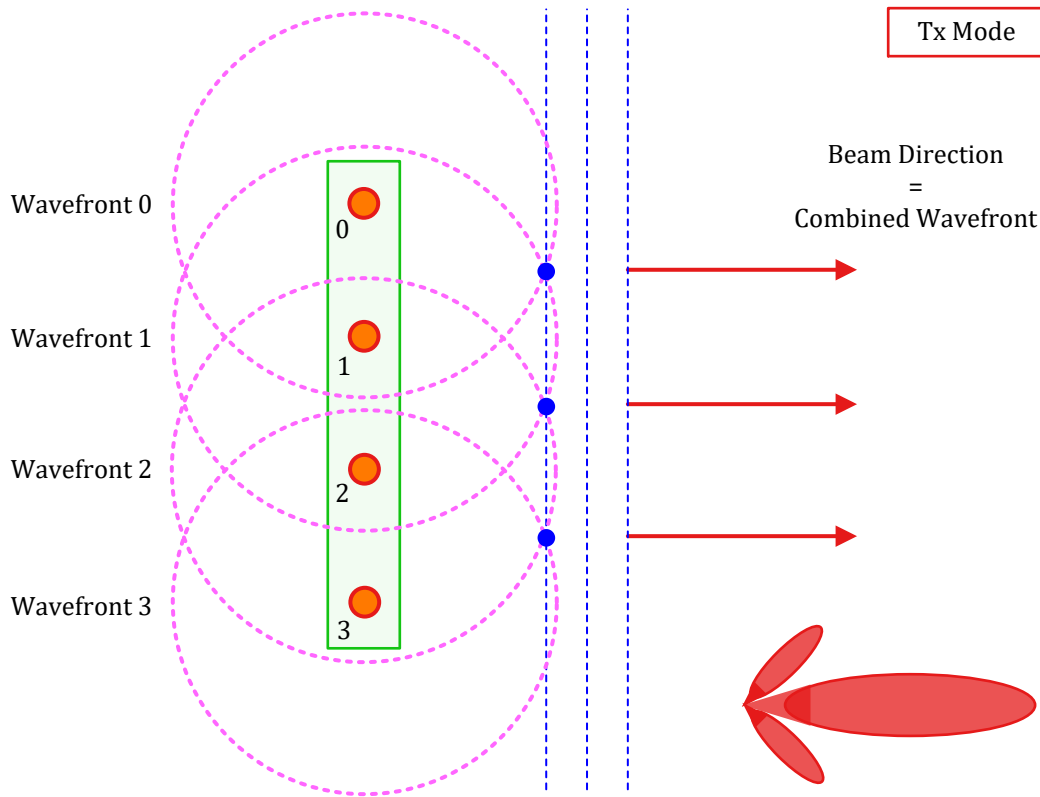


Figure 3.10: Actual formation of the wavefront from isotropic antenna elements

directions which excites each element in proportion to the variations in the incoming electromagnetic wave. A signal level interpretation of the beamforming process is illustrated in Figure 3.11 from a Rx viewpoint. The signal processing operations are drawn from right to left to stay consistent with 0° on the right side as the angle of arrival. Here, a sinusoidal wavefront representing the amplitude variations arrives at our antenna array from an angle of 0° . This means that the signals generated in each element are in phase with each other. This phase relation is shown with the help of a dashed red line in the figure crossing the respective waveforms. Therefore, when the outputs from each antenna are added together, there is a coherent summation that increases the output amplitude. In our simplistic scenario, they are all the same signal r_0 !

$$z = \sum_{n=0}^3 r_n = \sum_{n=0}^3 r_0 = 4r_0$$

Clearly, this cumulative signal carries an amplitude in proportion to the size of the antenna array, a factor of 4 in this figure. This is represented by a larger beam at 0° and smaller beams on the sides in Figure 3.10. We will now formally compute the array gain thus achieved.

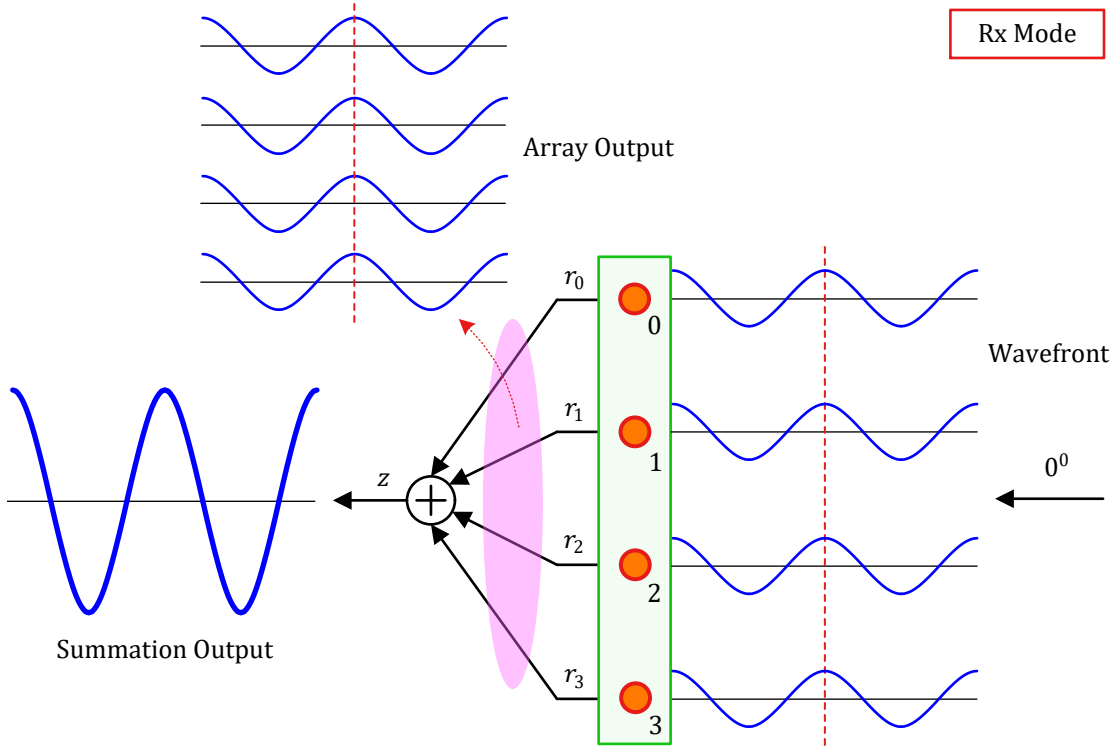


Figure 3.11: Signal level interpretation of the wavefront

3.3.2 Array Gain

If the array size in Figure 3.11 is N_R , observe the following.

- The signal is amplified by a factor of N_R due to phase-aligned or coherent summation.
- The signal power grows as N_R^2 because power is proportional to amplitude squared.
- The noise power only increases by a factor of N_R (instead of N_R^2). The intuitive reason is that the noise in each array element is independent of the noise in other elements and hence there is no *phase-aligned summation* for the noise waveform, as opposed to the signal. The mathematical reason is shortly described.
- Based on the above two observations, the SNR increase is therefore $N_R^2/N_R = N_R$.

After establishing the intuitive part, let us now derive the same results with the help of a little maths. In the simplistic scenario of Figure 3.11 under consideration, all the channel coefficients are the same, so we put $h_j = h$ in Eq (3.6) to get r_0 . Thus, the Rx signal at each branch is

$$r_n = r_0 = \underbrace{h \cdot s}_{\text{signal}} + \text{noise}, \quad n = 0, 1, \dots, N_R - 1 \quad (3.9)$$

Now as seen in Figure 3.11, a simple summation is performed at the Rx. The resulting signal at the output is

$$z = \sum_{n=0}^{N_R-1} r_n = \sum_{n=0}^{N_R-1} \{ h \cdot s + \text{noise} \} = \underbrace{N_R (h \cdot s)}_{\text{signal}} + \sum_{n=0}^{N_R-1} \text{noise} \quad (3.10)$$

A minimum distance rule can be applied to estimate the modulation symbol \hat{s} here[†]. The question is how to compute the array gain in this scenario.

- Since the average power in a single antenna $E_s \cdot \text{Avg } |h|^2$ is normalized to unity in Eq (3.4), the array signal power in Eq (3.10) is seen to be

$$\text{Avg Signal Power} = N_R^2 \cdot E_s \cdot \text{Avg } |h|^2 = N_R^2$$

- The total variance in case of the sum of N_R independent and identically distributed Gaussian random variables is equal to N_R times the variance of a single Gaussian random variable. Thus, the total noise power, given by the total variance after summation, is

$$\text{Noise Power} = N_R \cdot \sigma^2$$

From the above two observations, the combined SNR for an array of antennas is

$$\text{SNR}_{\text{Array}} = \frac{\text{Avg Signal Power}}{\text{Noise Power}} = \frac{N_R^2}{N_R \cdot \sigma^2} = N_R \cdot \frac{1}{\sigma^2} = N_R \cdot \text{SNR} \quad (3.11)$$

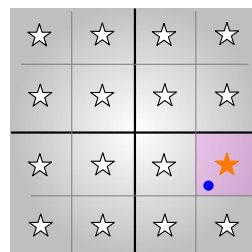
Comparing with Eq (3.5) where the SNR is given by $1/\sigma^2$, this extra factor of N_R appearing here is the well known *array gain* provided by the additional antennas. We can write the following expression from the above equation.

$$\text{Array Gain} = \frac{\text{SNR}_{\text{Array}}}{\text{SNR}} = N_R \quad (3.12)$$

Array gain is sometimes also known as *power gain*.

[†]For known normalized h and a zero noise scenario, the estimate of the modulation symbol \hat{s} is given from Eq (3.10) as

$$\hat{s} = \frac{z}{N_R \cdot h} = \frac{\sum_{n=0}^{N_R-1} r_n}{N_R \cdot h} \quad \rightarrow$$



and this estimate \hat{s} maps exactly on one of the modulation symbols. When noise or other distortions are present, a 16-QAM example is also shown above where a decision is made in favour of the star nearest to the blue point \hat{s} .

Role of Array Gain in the Big Picture

The power or array gain described in Eq (3.11) provides a multiplicative factor of N_R to the SNR of a single antenna system. Consequently, as far as the bit error rate is concerned, it provides a *linear* increase in performance with the number of Rx antennas. To see why, recall Eq (2.14) where the average bit error probability P_b decays in an inverse relationship with the SNR. For an array or array gain of N_R as above, this comes down to

$$P_b \propto \frac{1}{\text{SNR}_{\text{Array}}} = \frac{1}{N_R \cdot \text{SNR}} \quad (3.13)$$

Let us take the logarithm on the right side above because the BER is plotted on a log-log scale.

$$\log\left(\frac{1}{\text{SNR}_{\text{Array}}}\right) = \log\left(\frac{1}{N_R \cdot \text{SNR}}\right) = -\log N_R - \log \text{SNR} \quad (3.14)$$

Comparing with a linear equation $y = m \cdot x + c$ where x corresponds to the log of SNR, the array gain brings the y-intercept of the BER curve down by a factor of $\log N_R$. This can be interpreted as shifting the curve to the left for the same SNR and the relation is linear with the number of antennas on a log scale. These findings can be confirmed from Figure 3.12 where every doubling of the number of antennas N_R provides a gain of

$$10 \log_{10}(2) \approx 3 \text{ dB}$$

Also observe in Figure 3.12 that the array gain is impressive in the sense that it shifts the BER curve to the left but the result is still far away from the BER curve for an AWGN channel (also shown in the same figure), let alone reduce it even further towards the Shannon limit described through Figure 1.1. The fundamental difference is the *slope* of the curves being compared. Any strategy that would help us accomplish our goal of approaching the Shannon limit necessarily needs to *bend* the BER curve downwards! We conclude that the array gain does not change the slope of the BER curve under Rayleigh fading itself. That is accomplished by diversity gain explored later in Section 3.4.2.

3.3.3 The Origin of Beams

One problem in the set up of Figure 3.11 is that coherent summation with aligned phases happens only if the signal arrives at an angle of 0° . From the Tx perspective, how should we focus the signal energy towards a Rx at another angle? To answer these questions, we first find out what happens when the signal arrives from a different angle.

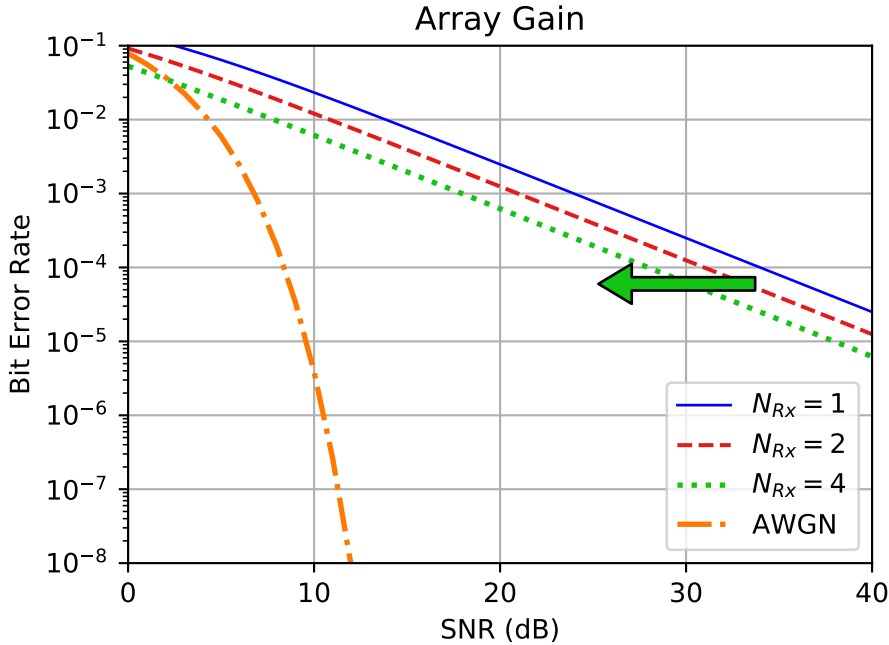


Figure 3.12: Array gain for $N_R = 1, 2$ and 4 antennas

Phase Misalignment

Recall from Figure 3.9 a planar wavefront arriving from a sufficiently distant Tx towards the Rx array at one particular angle. In such a scenario, there will be a relative delay in the wavefront reaching each antenna element and therefore coherent summation is not possible. As an example, Figure 3.13 draws a plane wave arriving at an angle of 26° with the antenna array. If $\tau_0 = 0$ is the time at which the wavefront reaches the topmost reference element 0, the time delays it takes to reach the antenna elements 1, 2 and 3 are given by τ_1 , τ_2 and τ_3 , respectively. This causes a misalignment of the signal copies out of each array element and at the input of the summation block. This phase misalignment is indicated by a slanted dashed line going through the waveforms in Figure 3.13. As a consequence, all the waveforms add without phase alignment and there is no array gain achieved at the final output, illustrated through a low amplitude signal as the output waveform.

Nonetheless, this does not mean that an antenna array can ‘look’ for the target signal into one fixed direction only, as we find out next.

From Mechanics to Electronics

One solution is to mechanically steer the beam in a desired direction through an electronically controlled motor. Systems with mechanical beam steering have been extensively used in the past and are still used in particular applications. You might have seen rotating air surveillance radars at the airports similar to the one shown in Figure 3.14. However, a gradual shift towards electronic steering happened due to the

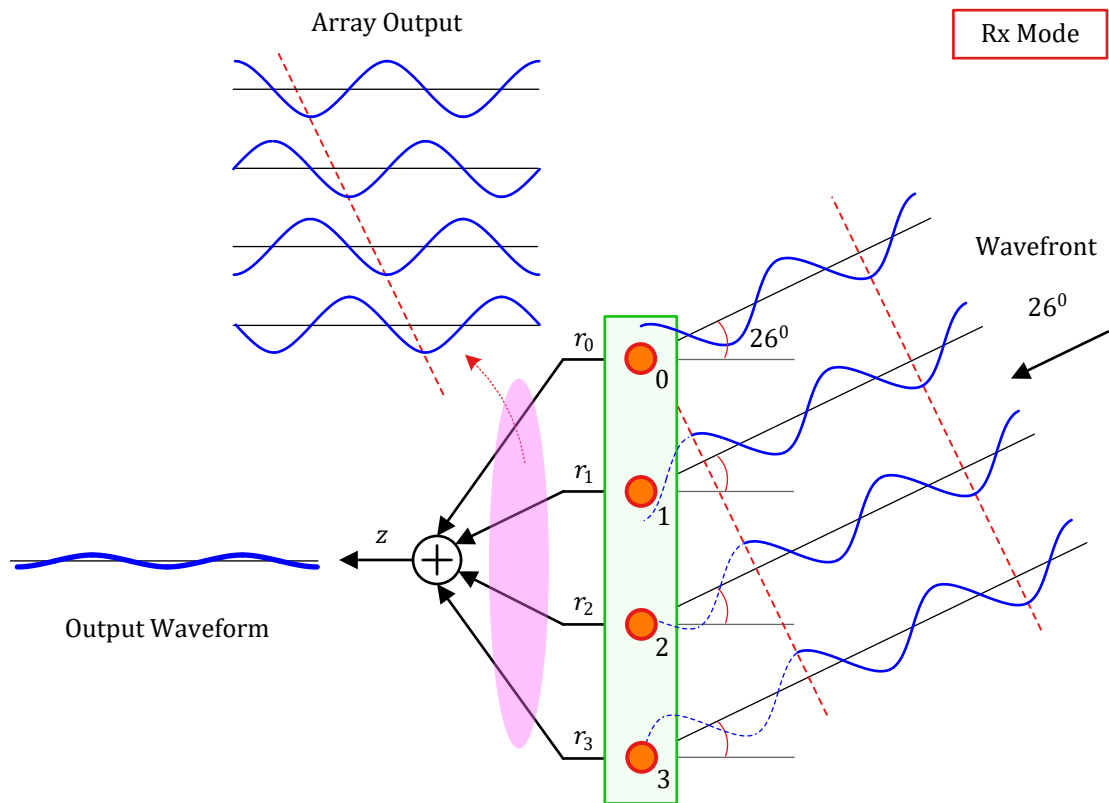


Figure 3.13: A signal arriving at an angle of 26° at an antenna array

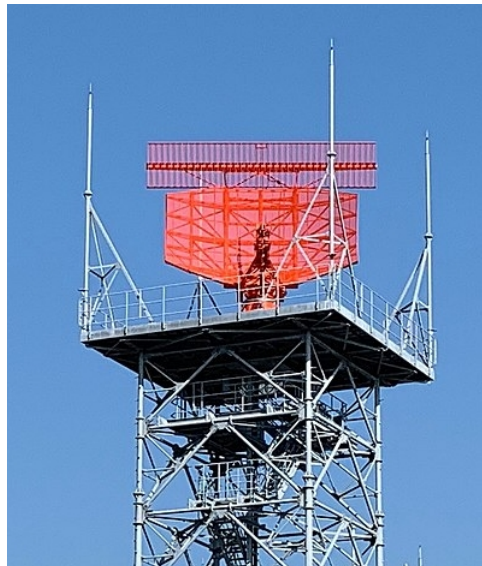


Figure 3.14: An airport surveillance radar with mechanical steering (image credit: Project Kei, CC BY-SA 4.0 via Wikimedia Commons)

several advantages it offers over the mechanical counterpart.

- Electronic scanning inherently maintains all the benefits of digital processing, e.g., flexibility, adaptability and better immunity to noise and components variations.
- Mechanical scanning techniques are slow due to inertia, time lags and vibrations of mechanical systems. In contrast, blazing fast switching of the transistors enables virtually instantaneous beam steering and tracking in highly dynamic environments.
- Electronic beam control has the capability to form multiple beams simultaneously to communicate with several transmitters and/or receivers.

In this regard, simple signal processing techniques can be applied to steer the beam in any direction with maximum gain while placing nulls in the directions of interference. This is one of main benefits of an antenna array (i.e., a spatially sampled signal analogous to time domain sampling) over a single large antenna (i.e., a continuous spatial signal analogous to a continuous-time signal).

Introducing Time Delays

To see how beam formation works, refer to Figure 3.15 and suppose that the antenna array is in transmission mode.

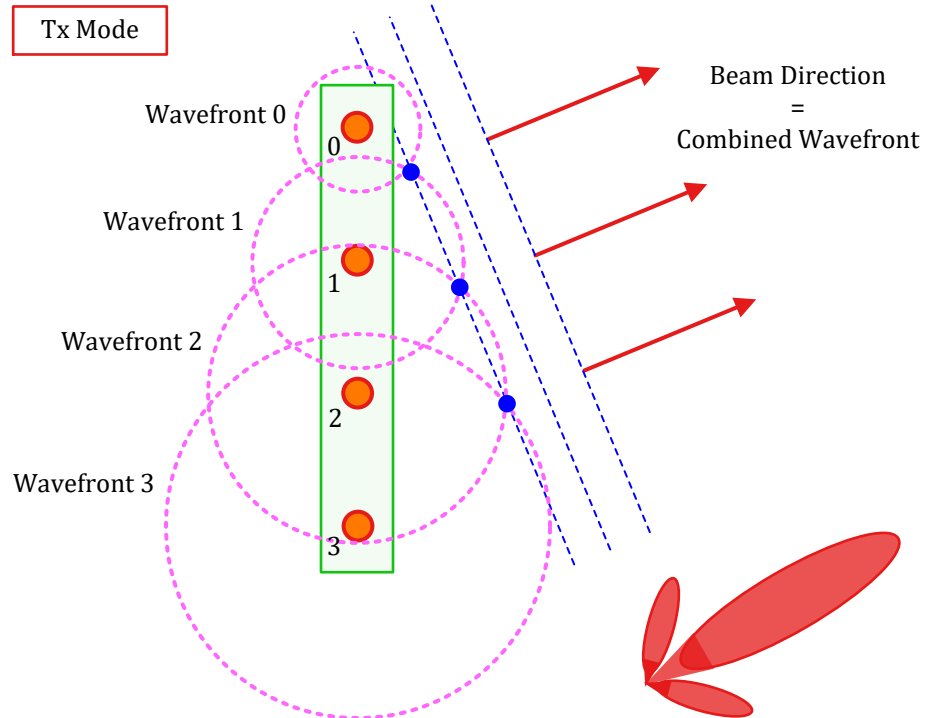


Figure 3.15: Actual formation of the wavefront from isotropic antenna elements

- The last array element, 3 in this figure, sends the signal first.
- The second last element 2 starts transmitting with a delay of τ_1 seconds.
- The elements 1 and 0 subsequently delay their transmissions by τ_2 and τ_3 seconds, respectively.

How are these delays computed such that the antenna array looks at a target direction will be discussed shortly. Here, notice that although these waves are still traveling in all directions due to the isotropic nature of the individual elements, the overlapping points representing the same phase of the waves are now tilted towards a direction of 26° . We say that the combined wavefront travels at an angle of 26° and the antenna array is now ‘looking’ into that particular direction.

Water Beams

You can see this beam formation process yourself by conducting a little experiment at home. Take a bucket of water (or a pool of water somewhere after rainfall) and throw two stones in it in succession at slightly different places. Holding the two stones together in one hand and releasing them at the same time from a vertically tilted position is also possible for a shorter delay. The water waves will spread out in all directions but the crest and trough formation will show a direction in proportion to the delay between the two stones.



Figure 3.16: A beam formation process can be seen in water waves by throwing two stones

It is clear from Figure 3.15 that the element delays are integer multiples of a single delay τ between any two adjacent antennas. This is only true for a uniform array, for which we shortly compute these

delay values. Non-uniform arrays are also used in some applications where general notations for delays, i.e., τ_n , are used.

To understand the signal level interpretation of this phenomenon, consider the array in Figure 3.17 from a Rx viewpoint now where the signal is arriving from the same angle.

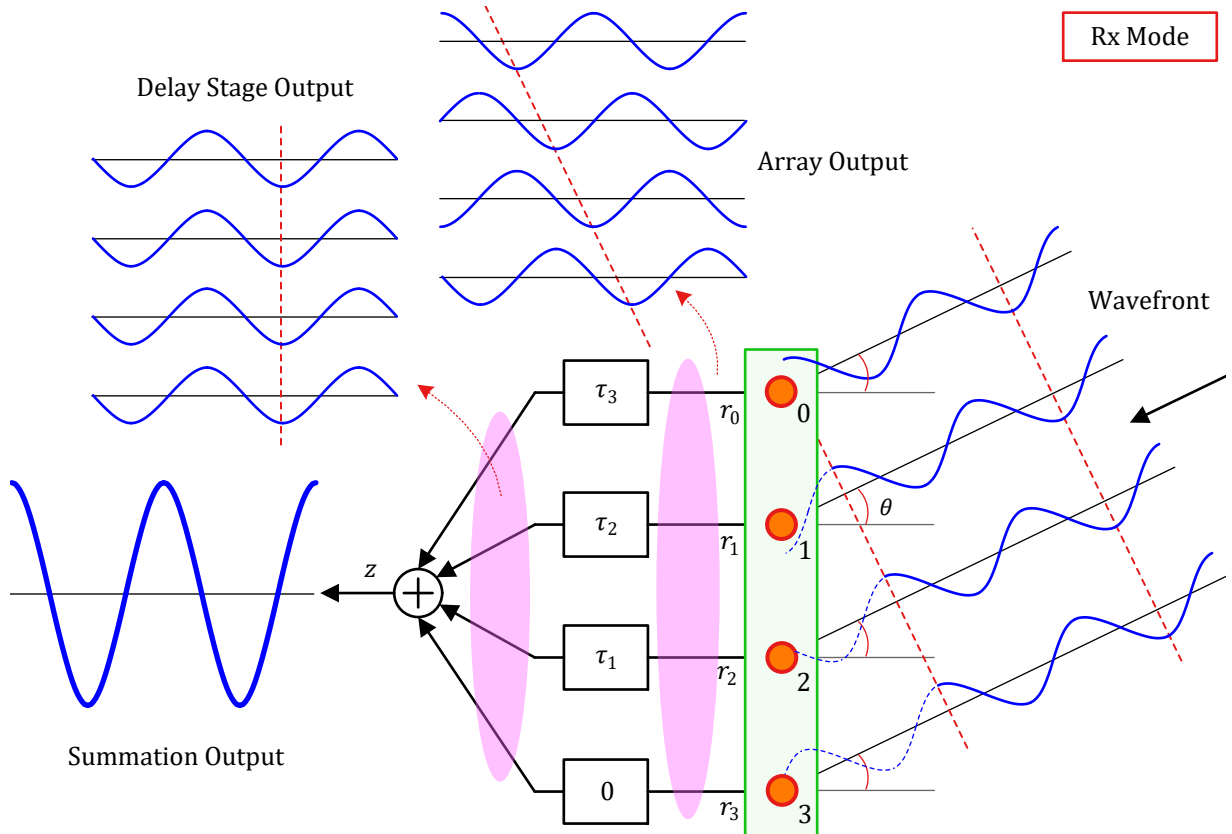


Figure 3.17: Signal level interpretation of the wavefront

Reference Time

Assign time $\tau_0 = 0$ to the instant the wavefront reaches the reference element 0.

Arriving Delays

Let times τ_1 , τ_2 , and τ_3 denote the instants the wavefront reaches the array elements 1, 2 and 3, respectively. This means that with respect to element 0, the signal is delayed by τ_1 at antenna 1, τ_2 at antenna 2 and τ_3 at antenna 3 (as a word of caution, these times of arrival are *not* the ones shown in delay blocks after the array output in Figure 3.17).

Steering Delays

Remember that we can delay a signal in time but cannot advance it in a strictly real-time appli-

cation. The strategy hence is to introduce the steering delays in reverse order of arriving delays.

- Taking the last element 3 as a reference for steering delays, we can assign a steering delay of $\tau_0 = 0$ to antenna 3 in Figure 3.17.
- Similarly, a delay of τ_1 is inserted at antenna 2 which aligns its waveform in phase with that at antenna 3.
- Finally, the signals at antennas 1 and 0 can be delayed by τ_2 and τ_3 seconds, respectively.

Observe the output signal of delay blocks in Figure 3.17 where they are all aligned to waveform at antenna 3 (shown by the vertical dashed line), not with the waveform at antenna 0.

Coherent Summation

Now the waveforms out of all the time delay blocks are phase aligned with each other. A summation block produces a coherent summation with an amplitude gain according to the number of antennas. This is shown as the waveform at the right of Figure 3.17.

A symbolic depiction of the waveforms in such a setup is also drawn in Figure 3.18. The top figure illustrates a phase coherent summation in a given direction. One can imagine the steering delay block as a device that blocks the waveform for a fixed amount of time τ , represented by a stop sign here. The individual signals can be seen as phase aligned at the output of the delay blocks before their final summation.

On the other hand, a depiction of an interference signal coming from an undesired direction is also drawn at the bottom of Figure 3.18. It can be seen that the signal from an unintended direction reaches antenna 3 first and is already delayed by some amount at the reference antenna 0. It gets further delayed by τ_3 in the steering delay stage thus widening the time gap with respect to the waveform at antenna 3. A similar scenario holds for the remaining antennas 1 and 2. This unaligned summation at the combiner generates a non-coherent output with a magnitude much lesser than that obtained for the target waveform before.

We saw before that the array gain or array gain for N_R Rx antennas was given in Eq (3.12) as N_R for an angle of 0° . With the successive time delay insertion technique up the array, this array gain becomes valid for any angle of arrival or departure in an ideal case. Next, to apply the steering delays described above, we need to compute the expressions for the time delays τ_1, τ_2, \dots , required at each antenna element. This is what we do now.

Computing the Time Delays

To initially keep the description simple, a d -spaced vertical array with two antenna elements is drawn in Figure 3.19a. A planar wave (implying that the source is situated at a large distance from this array) arrives at an angle θ with the upper antenna chosen as the reference point. It is clear that the wave has

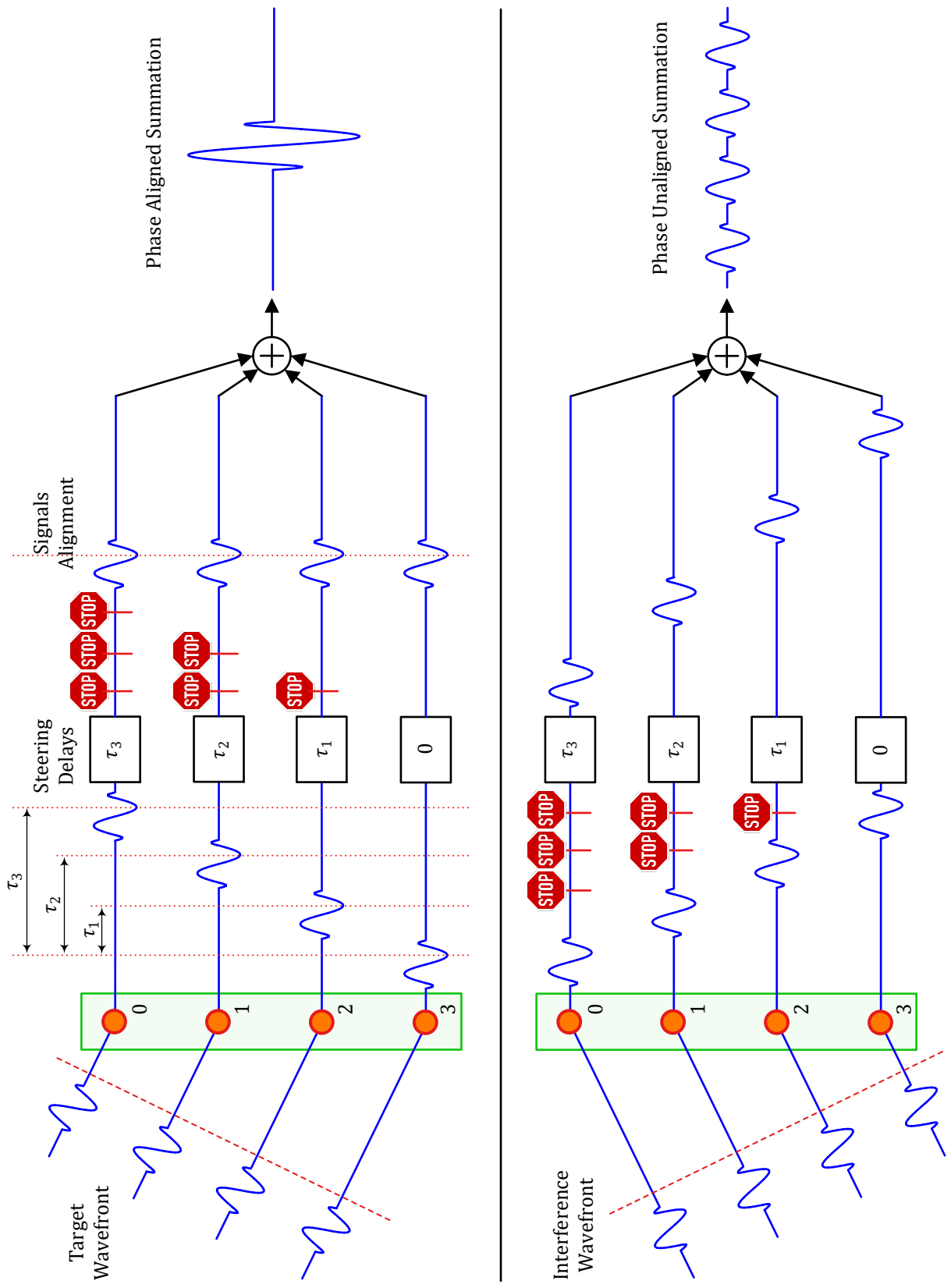


Figure 3.18: Steering the beam in a particular direction through time delay blocks

to travel an extra distance to reach the lower antenna as compared to the reference point. How is this distance computed?

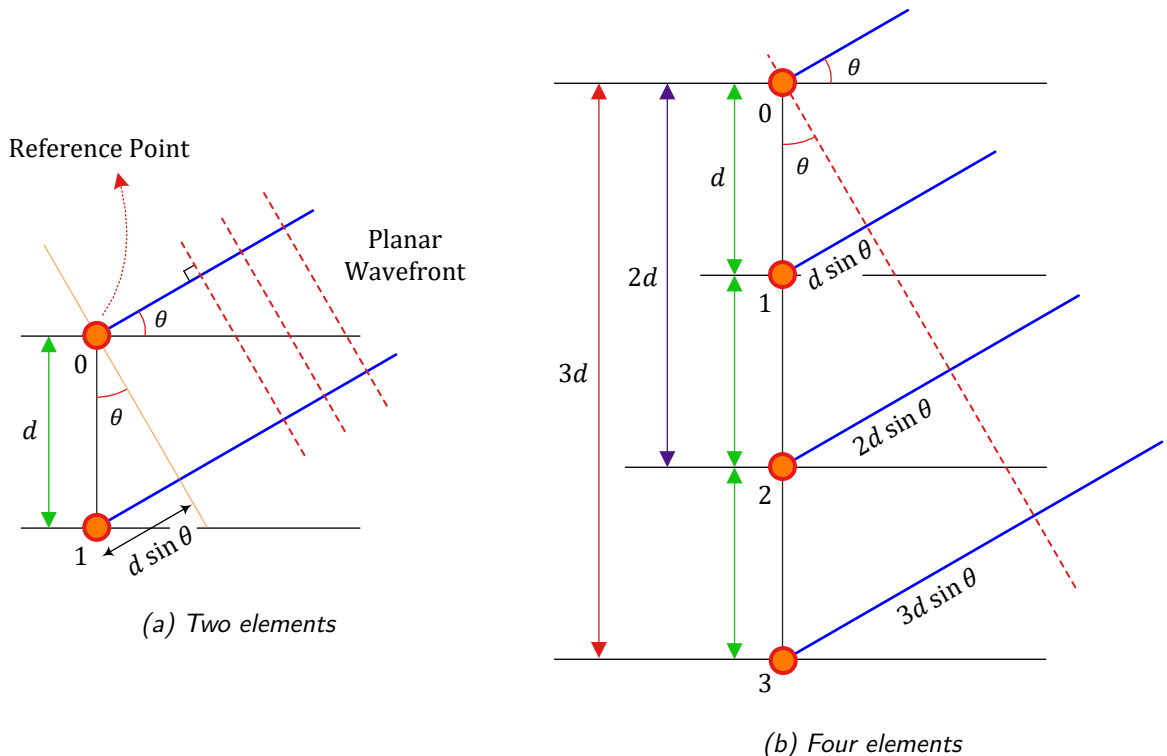


Figure 3.19: Delay computation for a d -spaced vertical antenna array

For this purpose, first notice that the angle between the vertical array axis and the arriving wavefront is the same as the angle of arrival θ between the horizontal axis and the direction of travel of that wave. This is because an angle between two lines is equal to the angle between their respective perpendiculars. From simple trigonometry, the extra distance traveled by the wave in Figure 3.19a to reach the lower antenna element is given by

$$\text{Extra distance} = d \sin \theta$$

Keep in mind that when the wavefront makes an angle θ with respect to the *perpendicular* to the array axis, the incremental distance term is expressed by $\sin \theta$ as above. You will see an alternative term $\cos \theta$ in many resources that arises from θ being defined as an angle with respect to the array axis itself.

If c is the speed of an electromagnetic wave in the air, then the extra time to travel is the ratio of the extra distance to this speed and is denoted by τ . With reference to antenna 1, we call it τ_1 as well.

$$\tau = \tau_1 = \frac{\text{Distance}}{\text{Speed}} = \frac{d \sin \theta}{c} \quad (3.15)$$

In a similar manner, Figure 3.19b draws an antenna array with four elements. Let us take into account the bigger triangle now formed by the antenna elements 0 and 2 with the wavefront and apply

the same trigonometric principles. It is easy to see that the extra distance traveled by the wave is $2d \sin \theta$ to reach element 2 and $3d \sin \theta$ to arrive at element 3. From here, we can write the time delays at array elements 2 and 3 as

$$\begin{aligned}\tau_2 &= 2 \frac{d \sin \theta}{c} = 2\tau \\ \tau_3 &= 3 \frac{d \sin \theta}{c} = 3\tau\end{aligned}$$

Here, the delays are integer multiples of a single value τ due to the uniformity of the array. In general,

$$\tau_n = n\tau = n \frac{d \sin \theta}{c} \quad (3.16)$$

The array response is made up of these delays as below.

Array Response

Now we explore the breakdown of the fractional delays discussed above into a simple multiplication of the arriving narrowband signal at each antenna with a complex number. For this purpose, the question we face is the following.

If the signal arriving at the reference point (antenna element 0) is denoted as $r_0(t)$, how exactly is it related to the signal expression arriving at antenna element 1 and given by $r_1(t)$? Taking into account the extra travel time of τ as compared to the reference, we can write this expression from Eq (3.15).

$$r_1(t) = r_0(t - \tau) = r_0 \left(t - \frac{d \cdot \sin \theta}{c} \right) \quad (3.17)$$

Let us take $r_0(t)$ as the most general narrowband signal, i.e., a complex sinusoid with frequency F . We first learn through complex signals notation why the delays (an undesirable option) can be converted into multiplications (well suited to our digital processing architectures).

Delays in Complex Notation

For a narrowband transmission, the signal $r_0(t)$ as a complex sinusoid can be written as

$$r_0(t) = e^{j\omega t}$$

Now the signal $r_1(t)$ with a delay of τ seconds is given by

$$r_1(t) = e^{j\omega(t-\tau)} = \underbrace{e^{j\omega t}}_{r_0(t)} \cdot \underbrace{e^{-j\omega\tau}}_{a_1} \quad (3.18)$$

which is simply a product between the original signal $r_0(t)$ and a *complex constant* $e^{-j\omega\tau}$! This is really the crux of the whole thing: a time delay inserted by physics *can be seen* as a product

between the same signal $r_0(t)$ and a complex number! Let us denote this number by a_1 as

$$a_1 = e^{-j\omega\tau} \quad (3.19)$$

In conclusion, a phase shift of $\omega\tau$ occurs at the first antenna element.

To avoid e and j , we repeat the same procedure with real signals next. As explained in Section 1.2, a complex sinusoid is formed by two real sinusoids: a cosine in I arm and a sine in Q arm. Using $\omega = 2\pi F$,

$$\begin{array}{ll} I & \rightarrow \\ Q & \uparrow \end{array} \quad \begin{array}{l} r_{0,I}(t) = \cos \omega t \\ r_{0,Q}(t) = \sin \omega t \end{array} \quad (3.20)$$

When this signal is delayed by an amount τ , we get $r_1(t)$ as

$$\begin{array}{ll} I & \rightarrow \\ Q & \uparrow \end{array} \quad \begin{array}{l} r_{1,I}(t) = r_{0,I}(t - \tau) = \cos \omega(t - \tau) \\ r_{1,Q}(t) = r_{0,Q}(t - \tau) = \sin \omega(t - \tau) \end{array} \quad (3.21)$$

Using the trigonometric identities $\cos(A - B) = \cos A \cos B + \sin A \sin B$ and $\sin(A - B) = \sin A \cos B - \cos A \sin B$,

$$\begin{array}{ll} I & \rightarrow \\ Q & \uparrow \end{array} \quad \begin{array}{l} r_{1,I}(t) = \underbrace{\cos \omega t}_{r_{0,I}(t)} \cdot \underbrace{\cos \omega\tau}_{a_{1,I}} - \underbrace{\sin \omega t}_{r_{0,Q}(t)} \cdot \underbrace{(-\sin \omega\tau)}_{a_{1,Q}} \\ r_{1,Q}(t) = \underbrace{\sin \omega t}_{r_{0,Q}(t)} \cdot \underbrace{\cos \omega\tau}_{a_{1,I}} + \underbrace{\cos \omega t}_{r_{0,I}(t)} \cdot \underbrace{(-\sin \omega\tau)}_{a_{1,Q}} \end{array}$$

We know that when two complex numbers are multiplied, the I part of the result is given by $I \cdot I - Q \cdot Q$ while the Q part of the result is expressed as $Q \cdot I + I \cdot Q$. Comparing this with the above equation, we realize that this expression is nothing but the multiplication of two complex signals:

$$r_1(t) = a_1 \cdot r_0(t) \quad (3.22)$$

One of them is the complex sinusoid $r_0(t)$ as in Eq (3.20) while the other is a complex number a_1 given by

$$\begin{array}{ll} I & \rightarrow \\ Q & \uparrow \end{array} \quad \begin{array}{l} a_{1,I} = \cos \omega\tau \\ a_{1,Q} = -\sin \omega\tau \end{array}$$

which is the same as Eq (3.19). The reason time delays appear as phase shifts is now clear. Compare Eq (3.21) with Eq (3.22) and see how a delay in time domain has been transformed into a product! This is a beautiful result which forms the basis for implementation of physical beamforming in most practical antenna arrays.

Let us define this *antenna phase shift* as $u = \omega\tau$. With such a substitution, we get the above complex number a_1 as

$$\begin{array}{ll} I & \rightarrow \\ Q & \uparrow \end{array} \quad \begin{aligned} a_{1,I} &= \cos \omega\tau = \cos u \\ a_{1,Q} &= -\sin \omega\tau = -\sin u \end{aligned} \quad (3.23)$$

From Eq (3.15), recall that $\tau = d \sin \theta / c$. Moreover, the wavelength λ of the complex sinusoid is related to the frequency F and the speed of an electromagnetic wave c by $\lambda \cdot F_C = c$. As a consequence, $\omega = 2\pi F = 2\pi c / \lambda$ and

$$u = \omega\tau = 2\pi F \frac{d \sin \theta}{c} = 2\pi \frac{d \sin \theta}{\lambda}$$

The variable u then becomes[†]

$$u = 2\pi \frac{d \sin \theta}{\lambda} \quad (3.24)$$

I could have denoted this antenna phase shift u with something like ϕ but that could potentially cause confusion in reader's mind with the *actual* beam direction θ .

The above description was for one additional antenna. This can be generalized to include the effect of more antennas as below.

An Array of Complex Scalars

A complex sinusoid $r_0(t)$ appearing at the reference antenna 0 also appears at the reference antenna 1 but with a slight difference. It is

- delayed by τ , or equivalently,
- phase shifted by $u = \omega\tau$, or equivalently,
- multiplied with a complex number a_1 given by Eq (3.23).

Generalizing this observation, the complex sinusoid $r_0(t)$ also appears at antennas 2, 3, ..., $N_R - 1$ but it is multiplied with a complex scalar a_n that

[†]As we find in Appendix 3.6, the exact relation is given by

$$u = 2\pi \frac{d}{\lambda} \left(\sin \theta - \sin \theta_0 \right)$$

where θ_0 is a reference direction.

can be given by using $\tau_n = n\tau$ and hence $\omega\tau_n = \omega\tau n = un$.

$$\begin{array}{ll} I & \rightarrow \\ Q & \uparrow \end{array} \quad \boxed{\begin{aligned} a_{n,I} &= \cos un = \cos \left(2\pi \frac{d \sin \theta}{\lambda} n \right) \\ a_{n,Q} &= -\sin un = -\sin \left(2\pi \frac{d \sin \theta}{\lambda} n \right) \end{aligned}} \quad (3.25)$$

where $n = 0, 1, 2, \dots, N_R - 1$. These complex scalars – combined in a vector form – are known as an *array response vector* which can be written in complex notation as

$$a_n = e^{-j2\pi \frac{d \sin \theta}{\lambda} n} = e^{-jun} \quad (3.26)$$

In summary, these delays can be seen as an array response vector for narrowband signals that induce a multiplication of element output $r_n(t)$ with a complex scalar a_n of Eq (3.25). Physical beamforming deals with compensating for these complex products.

Beam Shape

While we have discussed the interaction of the electromagnetic waves with the antenna array, we have not yet discovered what the beam shape looks like. This is something almost all textbooks and tutorials on beamforming explore at the start of their introductions. The reason I did not bring it up earlier is that although the beam shape is given by the Fourier Transform of individual antenna intensities, it is not always explained why. Where exactly does Fourier Transform, a conversion tool from time t to frequency ω domain, come into the picture? And how does the frequency ω for time domain correspond to phase shift u of the array?

Coming back to our analogy between time domain and space domain sampling described in Figure 3.6, let us find out the cumulative radiation pattern of a particular arrangement for a group of antennas. This is commonly known as the *array factor* and it can be derived through the techniques borrowed from time to frequency transformation.

Main Lobe in Frequency Domain

The tool we use for going into frequency domain is the Discrete-Time Fourier Transform (DTFT).

It defines the spectral representation of a signal $x[n]$ as

$$\begin{aligned} I \rightarrow & X_I(e^{j\omega}) = \sum_n [x_I[n] \cos \omega n + x_Q[n] \sin \omega n] \\ Q \uparrow & X_Q(e^{j\omega}) = \sum_n [x_Q[n] \cos \omega n - x_I[n] \sin \omega n] \end{aligned} \quad (3.27)$$

where ω is the discrete frequency variable. The complex version of this definition is shown below.

The Discrete-Time Fourier Transform

In terms of complex signals, the DTFT is defined as

$$X(e^{j\omega}) = \sum_n x[n] e^{-j\omega n} \quad (3.28)$$

For a rectangular pulse, $x[n]$ is an all-ones sequence.

$$X(e^{j\omega}) = \sum_n e^{-j\omega n} \quad (3.29)$$

The frequency response or spectrum of the rectangular pulse of Figure 3.4 is derived in Appendix 3.6 as

$$|X(e^{j\omega})| = \frac{\sin N \frac{\omega}{2}}{\sin \frac{\omega}{2}} \quad (3.30)$$

The above spectrum is known as an *aliased sinc* signal that includes the aliases arising from finite sample rate (we have a violation of sampling theorem here because spectrum of a rectangular signal is a sinc signal that has infinite bandwidth). As N becomes large (i.e., sample rate goes to infinity), we can apply the approximation $\sin A \approx A$ in the denominator and the spectrum approaches that of an actual sinc signal. This is drawn in Figure 3.20 where a main lobe appears at index 0 while the sidelobes decay as we move away from zero on either side. Keep in mind that as more samples are collected, the main lobe of the sinc signal becomes more concentrated around index 0.

Spectral Filtering

With the discrete-time samples available, DSP algorithms can be applied to modify the output spectrum in frequency domain as desired. This is known as *spectral filtering*. Interestingly, even a simple sinc filter shown in Figure 3.20 has a lowpass response! It passes the frequencies around zero with little distortion and blocks the frequencies further away. We can say that it acts as a spectral filter.

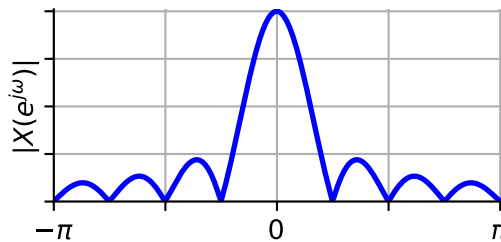


Figure 3.20: A sinc signal is the DTFT of a rectangular signal

The main lobe of the sinc signal does not have to be at zero frequency. Recall the modulation property of Fourier Transform introduced in Eq (3.31) according to which multiplication of individual samples with a complex sinusoid in time domain shifts the signal in frequency domain.

Shifting the Sinc Main Lobe

Let us reproduce the frequency domain version of Eq (2.8) here.

$$x[n] \cdot e^{j\omega_0 n} \quad \xrightarrow{\text{FT}} \quad X((e^{j(\omega-\omega_0)})) \quad (3.31)$$

We see that multiplying the signal $x(t)$ with the samples of a complex sinusoid shifts the spectrum at ω_0 .

This is plotted in Figure 3.21 where the main lobe of the sinc has been shifted to $\omega = \pi/2$ as a result of such multiplication. Now the frequencies around that value can pass unhindered but rest of the frequencies, both above and below, are attenuated. We have a bandpass response. For a practical implementation with low sidelobe levels in the spectrum, there are several techniques, such as windowing (e.g., Hamming, Blackman-Harris, Kaiser-Bessel), that can be applied to the time domain signal.

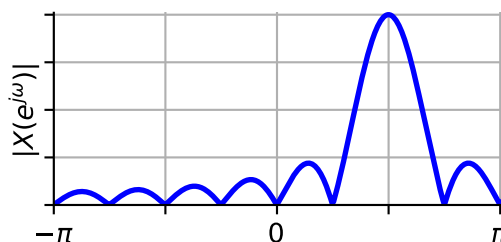


Figure 3.21: Main lobe shifted in frequency by multiplication with a complex sinusoid

Main Lobe in Spatial Domain

This is an interesting idea due to the analogy between samples in time forming a sinc signal and samples in space forming a directional beam. If each antenna exhibits an ideal omnidirectional pattern, then their equal intensities can be represented as a series of constants. Now when each antenna successively delays its waveform, the resultant field formed at any angle θ in space comes from their *superposition in that direction!* The mathematical expressions are as below.

Recall Eq (3.24) that describes the *antenna phase shift* for each successive element.

$$u = \omega\tau = 2\pi \frac{d \sin \theta}{\lambda} \quad (3.32)$$

where the variable u is the spatial counterpart of the frequency variable ω in time sampling. Again, it is not denoted with something like ϕ to avoid confusion with the *actual* beam direction θ .

Direction θ and Fourier Transform

We learned in Eq (3.18) that a complex sinusoid $e^{j\omega t}$ delayed by τ is given by

$$r_1(t) = e^{j\omega(t-\tau)} = e^{j\omega t} \cdot e^{-j\omega\tau}$$

This can be generalized to form $r_n(t)$ involving $\tau_n = n\tau$ by using $\omega\tau_n = \omega\tau n = un$. When signals from N array elements are added together with their respective delays, we have

$$\begin{aligned} \text{Superposition of Waves} &= \sum_n r_n(t) = \sum_n e^{j\omega(t-\tau_n)} = e^{j\omega t} \sum_n e^{-j\omega\tau_n} \\ &= e^{j\omega t} \sum_n e^{-jun} \end{aligned}$$

where the last step follows from the definition of u . The first factor above is the input sinusoid and the second is known as the *array factor* (AF) defined as

$$\text{AF} = \sum_n e^{-jun} \quad (3.33)$$

Compare the above expression with Eq (3.29). They are very similar! This is the reason why directional response of an antenna array is given by the Fourier Transform of the array amplitude distribution. In words, we have seen that time delays for narrowband signals can be represented as products with complex scalars and hence their superposition at any point in space can be written as a sum of those complex scalars!

For a uniform intensity distribution of the isotropic case, we can simply write the array factor from

Eq (3.30).

$$\text{AF} = \frac{\sin N \frac{u}{2}}{\sin \frac{u}{2}} \quad (3.34)$$

This is also an aliased sinc signal but in space domain! Let us now see some figures related to this concept.

- The equal weight given by each antenna in spatial direction is shown as a constant signal in Figure 3.22a, the same as an array emitting a continuous wave with uniform amplitude distribution.
- The array factor with respect to phase shift u is drawn in Figure 3.22b which approaches a sinc signal for large N (as described in time domain analogy).
- The overall radiation pattern is the product between the individual antenna pattern and the array factor as drawn in Figure 3.22c.

$$\text{Overall Pattern} = \text{Element Pattern} \times \text{Array Factor}$$

The array factor is an interesting characteristic of the system because it arises from a particular configuration of participating elements and acts beyond their individual radiation patterns[†]. Keep in mind that for non-planar arrays (such as a base station with a circular or ring array) in general, the element pattern cannot be factored out of the cumulative expression.

- When this sinc signal is bent into a polar pattern just like you wear a belt around your waist, a beam is formed where the main lobe points in a given direction: $u = 0$ in this case. This is drawn in Figure 3.22e.
- Continuing from the frequency shift analogy in time domain samples that was shown in Figure 3.21, individual samples in space domain (i.e. antenna inputs or outputs) can be multiplied with a complex sinusoid to shift the beam direction in spatial domain as illustrated in Figure 3.22d.

Spatial Filtering

Analogous to spectral filtering we saw before, the beams in space can be shifted to produce a desired spatial response where the larger lobe produces a higher gain. Signals arriving from one or more directions can be blocked or passed by careful design of these complex multipliers. This is known as *spatial filtering*. Furthermore, just like the windowing functions in time domain, the beam can be modified with reduced sidelobe levels through analogous weighting functions.

[†]This also helped me understand why a group, team, organization or a nation is not a simple sum of their parts, e.g., why organizations with efficient employees might not be productive, or why nations with peace loving citizens can wage wars in far away countries.

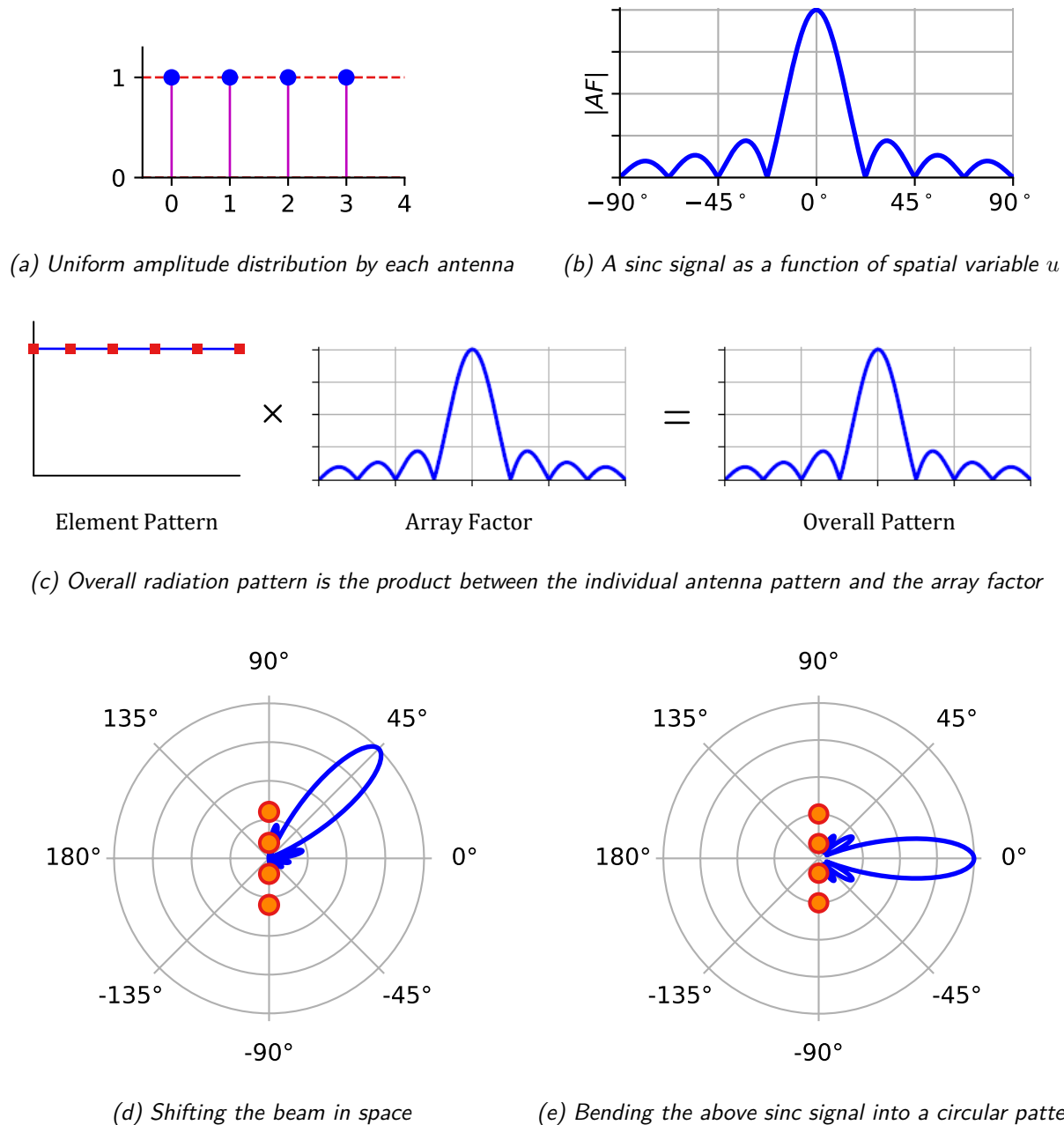


Figure 3.22: Illustration of how a spatial sinc signal, or a beam, is formed

Role of Number of Elements N

Let us now observe the behavior of the antenna array for the number of elements N with antenna spacing d . For this purpose, Figure 3.23 plots the array factor $|AF|$ introduced in Eq (3.34) at a frequency of 60 GHz by varying N and d . We observe the following.

- Drawn in Figure 3.23a is the array factor for $N = 4$ antennas at a spacing of $d = \lambda/2$. A single wide main lobe of a sinc function is visible in the look range of $\theta = -90^\circ$ to $+90^\circ$. Let us determine the zero crossing locations with respect to beam direction θ . For this purpose, notice that the numerator and denominator in Eq (3.34) are both zero at $u = 0$. Therefore, the array factor magnitude crosses zero again when the numerator $Nu/2$ becomes π . This yields

$$u = \frac{2\pi}{N}$$

Plugging in the value of u from Eq (3.24),

$$2\pi \frac{d \sin \theta}{\lambda} = \frac{2\pi}{N} \quad (3.35)$$

For $d = \lambda/2$, this turns out to be

$$\sin \theta = \frac{2}{N}$$

For $N = 4$, our first zero crossing appears where $\sin \theta = 1/2$. Consequently, it can be located in Figure 3.23a at $\theta = \sin^{-1}(1/2) = 30^\circ$. The main lobe width is twice this value.

The right side shows the same function bent into a polar pattern. We say that the array has a main beam at 0° or it transmits and receives maximum amount of energy at 0° .

- When the number of elements is increased from $N = 4$ to $N = 8$, the sinc main lobe becomes narrow. Plugging $N = 8$ with $d = \lambda/2$ in Eq (3.35), we get $\theta = 14.5^\circ$ as seen in Figure 3.23b.

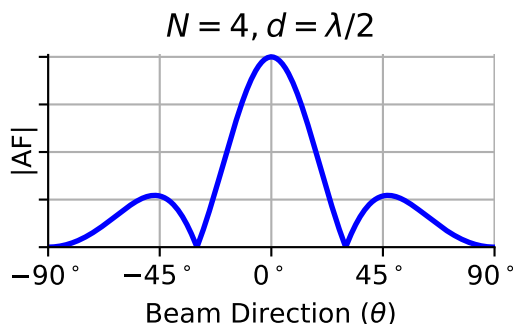
The effect of increase in N is visible on the right side polar plot with a narrower beam. In systems where users are separated in spatial dimension, these narrow beams result in less interference, both within the same signal (ISI) and from the remaining users.

Role of Antenna Spacing d

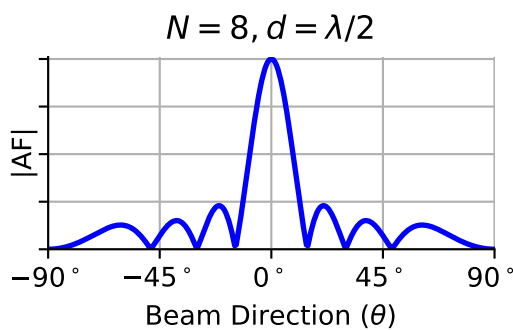
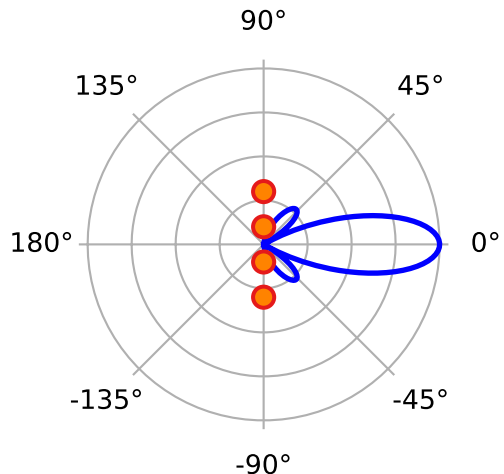
Increasing the number of elements N is not the only way to achieve narrow beams. Let us fix the number of elements $N = 4$ and modify the antenna spacing d to $3\lambda/2$. The resulting array factor is drawn in Figure 3.23c where one can observe a narrower main beam as compared to $d = \lambda/2$ in Figure 3.23a. Why two new lobes have arisen will be discussed shortly. The first zero crossing can be derived as before from Eq (3.35). Plugging $N = 4$ and $d = 3\lambda/2$, we have

$$\sin \theta = \frac{2}{3N} = \frac{1}{6}$$

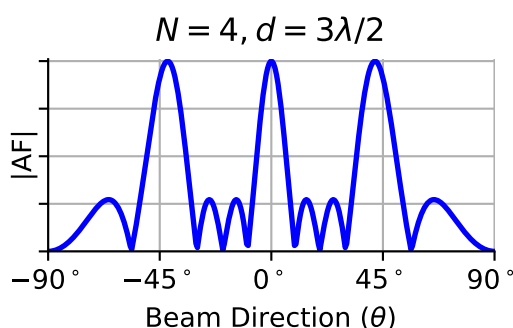
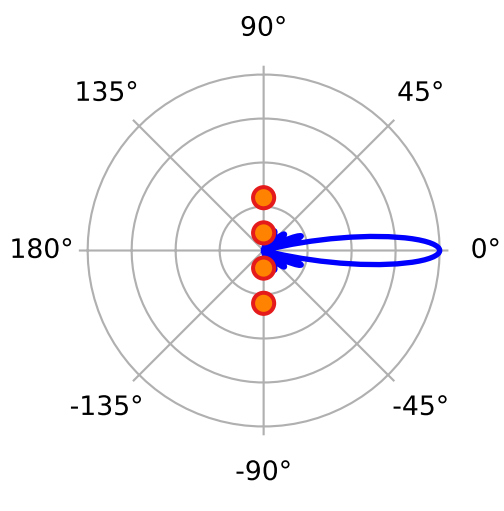
Here, θ turns out to be 9.6° . Shown on the right side is the polar plot with this narrow beam even though the number of elements is still $N = 4$. We realize the following.



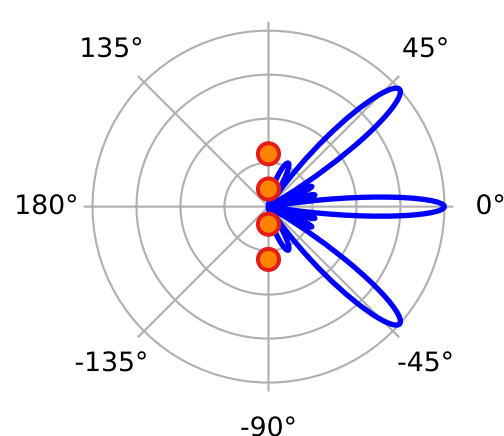
(a) Single and wide main lobe



(b) Single and narrow main lobe



(c) Two grating lobes on the sides

Figure 3.23: Effect of varying the array size N and antenna spacing d

Array Length

It was observed that the beamwidth (here, null-to-null spacing of the main lobe) depends on both the number of elements N and antenna spacing d . Looking back, we can see that the real parameter of interest here is the array length L that is a product of these two variables. The array length is defined as

$$L = (N - 1)d$$

which you can easily verify by looking at a uniform linear array. On a side note, I personally like to view the array length as $L = Nd$ due to the analogy from time domain sampling. Recall from Figure 3.4 that a discrete-time pulse with N samples at a spacing of T_S is said to have a length of NT_S because going into discrete spectrum virtually constructs periodic copies starting at time NT_S (which has the same signal value as time 0). This is known as input periodicity of the Discrete Fourier Transform (DFT). Furthermore, many derivations in analysis of antenna arrays are simplified by taking the length as Nd instead of $(N - 1)d$.

Returning to the additional two lobes in Figure 3.23c, these are called *grating lobes* that arise due to violating the spatial sampling theorem as $d = 3\lambda/2$. Recall the sampling theorem in time domain, $T_S \leq 1/2B$ where B is the signal bandwidth. We can write an analogous expression as

$$d \leq \frac{\lambda}{2}$$

Appendix 3.6 derives the exact relationship for this spacing for a reference look direction θ_0 of the array.

The S-Curve

Let us plot the antenna phase shift u with respect to beam direction θ for different values of d [9]. The resulting graph is drawn in Figure 3.24 for $d = 0.4\lambda, 0.5\lambda$, and 0.6λ that resembles an S-curve encountered in carrier and timing synchronization loops of single carrier systems.

- The plot for $d = 0.5\lambda$ is straightforward. For a full spatial scan of $\theta = -90^\circ$ to $+90^\circ$, the antenna phase shifts are from $u = -180^\circ$ to $+180^\circ$. This only holds in theory and can only be approximated with real antennas.
- For $d = 0.4\lambda$, full spatial scan can be implemented through relevant phase shifts that do not even span the full range of u .
- For $d = 0.6\lambda$, even a $\theta = 60^\circ$ scan angle cannot be achieved with full range of phase shift u . This is in violation of array sampling theorem above and this gives rise to grating lobes we saw in

Figure 3.23c. It is evident from the corresponding polar plot that grating lobes release or pick up energy from some undesired directions too, creating interference between users in the system.

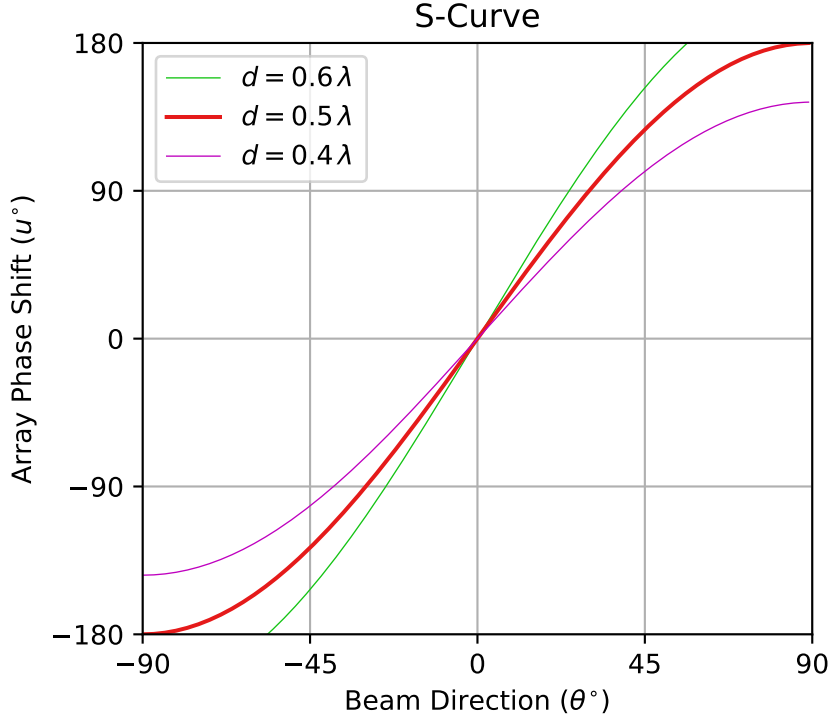


Figure 3.24: S-curve of the phase shift

As derived in Appendix 3.6 for an interested reader, we can visualize that the grating lobes just start appearing at $d = \lambda/(1 + \sin \theta_0)$ for a reference direction θ_0 . Therefore, as long as we keep the spacing 5-10% below that point, there will be no interference. Unlike frequency domain, the actual beam direction θ is not proportional to the antenna phase shift u due to the sine involved in the direction of arrival and departure of electromagnetic waves.

3.3.4 Beam Steering

For a target θ , one can easily compute the delays that enable a coherent summation of signals from all the antennas for one particular direction. Physical beamforming is based on calculating these differences in wave arrival times between antenna array elements and compensating for these delays through signal processing techniques that steer the beams in any desired direction. There are two main candidates for this purpose: True Time Delays (TTD) and phase shifting. The former is a general solution while the latter works for narrowband signals only.

Transmission Lines and Fractional Delay Filters

There are two main technologies available for inserting the above mentioned time delays: analog and digital. An analog solution to introduce the above mentioned time delays is to insert a set of switched transmission lines with incremental lengths behind each antenna element or a group of elements. However, there are two main problems with this approach.

- A large number of such delay lines requires a complex switching network and the resultant switched lines make the equipment bulky and expensive, particularly for 5G systems incorporating massive MIMO at the base stations.
- No component is perfect and the differences in dispersion in various transmission line sections lead to inaccurate beamforming.

Coming to the digital side, a bank of time domain Finite Impulse Response (FIR) filters can be used that progressively delays the incoming waveforms at their respective antennas. One such example is shown in Figure 3.25. From the impulse responses above, it is clear that the zeroth filter produces a sample that is exactly at the peak (i.e., there is no delay introduced). For each successive array element n , there is a shift in the peak towards the left that can be set as τ_n , as shown by dashed green lines in Figure 3.25. This is why these filters are said to provide linear phase shifts producing the time delays that perform a beamforming task similar to multi-rate filters. The drawback is that processing the signal out of each antenna through a digital filter is prohibitively complex. For this and other reasons beyond the scope of this text, implementing fractional delay filters to process a waveform is less desirable than a simpler solution such as a simple multiplication with a complex number. This is possible with narrowband signals as explained below.

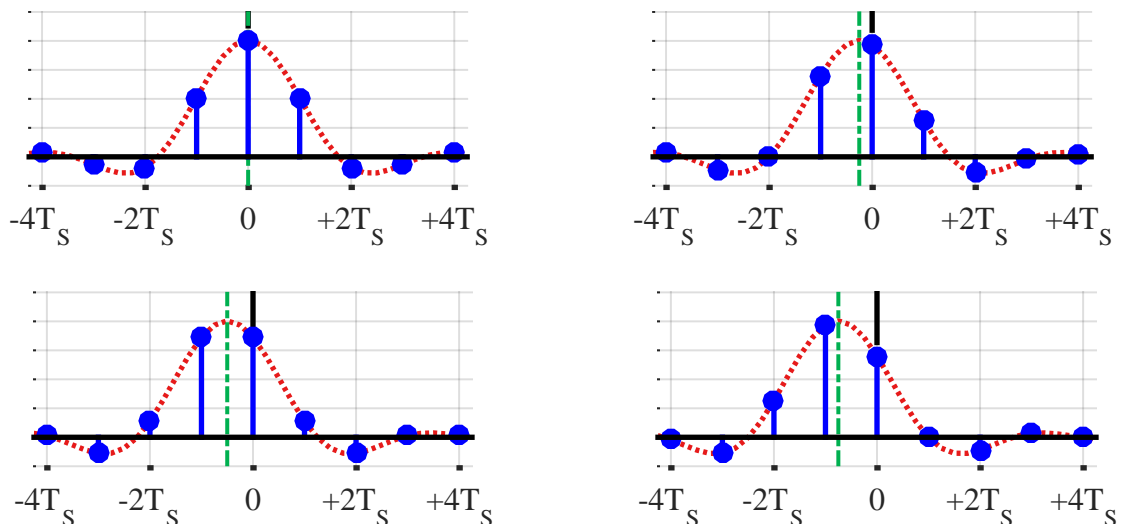


Figure 3.25: A bank of fractional delay filters

Phase Shifters

As discussed before, the beams in space can be shifted to produce a higher gain in certain directions and low gains in some others. In fact, a null response can also be simultaneously obtained to block the signals from interferers in a cellular network. We first describe the phase shifting for a desired signal first and then see how to handle the interfering users.

There are several statistical signal processing techniques that qualify for the actual algorithms implementation, most of which are derived through fancy mathematics. Due to the limited scope of this text, we consider here a simple technique which is sufficient to gain a broad understanding of the subject.

We return to the array response derived in Eq (3.25) for real signals and Eq (3.26) for complex signals. This is reproduced below.

$$\begin{aligned} I \rightarrow & \quad a_{n,I} = \cos\left(2\pi \frac{d \sin \theta}{\lambda} n\right) = \cos un \\ Q \uparrow & \quad a_{n,Q} = -\sin\left(2\pi \frac{d \sin \theta}{\lambda} n\right) = -\sin un \end{aligned} \quad (3.36)$$

If our ultimate target is coherent summation of the waveforms, then there should be no delays out of any of the antenna elements. In other words, no such complex scalar as in Eq (3.36) should appear at each element. When that happens, all the signals before the summation block appear fully in-phase with each other. For this purpose, we can multiply the incoming signal $r_n(t)$ from each array element i with another complex scalar w_n that has an exact *opposite phase* from a_n . This is accomplished through a conjugate product.

To see why this is so, first refer to the complex notation.

Phase Cancellation

If the complex weights w_n are designed as complex conjugates of array response a_n , the phases cancel out. From Eq (3.26),

$$w_n \cdot a_n = e^{+j\theta n} \cdot e^{-j\theta n} = 1$$

In terms of real signals to avoid e and j , let us write the polar representation of a_i from Eq (3.36).

$$\begin{aligned} |a_n| &= \cos^2 un + \sin^2 un = 1 \\ \angle a_n &= \tan^{-1} \left\{ \frac{-\sin un}{\cos un} \right\} = -un \end{aligned}$$

Now recall from the definition of a conjugate of a complex number that the magnitude stays the same while the phase reverses its sign.

$$|a_n^*| = |a_n| \quad \angle a_n^* = -\angle a_n$$

Since our purpose is to remove this phase shift arising from the arriving time delays, the weights w_n are chosen as conjugates of a_n in this scheme, $w_n = a_n^*$.

$$\boxed{|w_n| = |a_n^*| = |a_n| = 1}$$

$$\angle w_n = \angle a_n^* = -\angle a_n = +un$$

A multiplication of two complex numbers implies a product of their magnitudes while addition of their phases. Applying this rule to multiply a_n with w_n , we get

$$|w_n \cdot a_n| = |a_n^* \cdot a_n| = |a_n|^2 = 1$$

$$\angle(w_n \cdot a_n) = \angle w_n + \angle a_n = +un - un = 0$$

for each array element n . The effect of delays has vanished! The product $w_n \cdot a_n$ simply becomes a real number 1 with zero phase that can be compactly written as

$$w_n \cdot a_n = 1 \quad (3.37)$$

A major consequence of the above result is that the output from each antenna has the delay arising from the extra distance $d \sin \theta$ removed and all the waveforms can be added in phase. Importantly, as opposed to Figure 3.25, this is accomplished through much simpler complex multiplications performing the same function as time delays for narrowband signals. A block diagram for this approach is illustrated in Figure 3.26 along with the waveforms involved at various stages. Here is a simple mathematical derivation for the gain.

- From Eq (3.17), we know that the signal at each antenna $r_n(t)$ is a delayed version of the narrowband signal $r_0(t)$ arriving at the reference antenna.

$$r_n(t) = r_0(t - \tau_n)$$

- Also, Eq (3.22) can be generalized to represent that delay as a complex product.

$$r_n(t) = a_n \cdot r_0(t)$$

- The beamformer multiplies the antenna signals $r_n(t)$ with complex weights w_n followed by a summation.

$$z = \sum_{n=0}^3 w_n \cdot r_n(t)$$

- Therefore, the resultant signal at the beamformer output is given by

$$\begin{aligned} z &= \sum_{n=0}^3 w_n \cdot r_0(t - \tau_n) = \sum_{n=0}^3 w_n \cdot a_n \cdot r_0(t) \\ &= \sum_{n=0}^3 r_0(t) \quad \text{as } w_n \cdot a_n = 1 \text{ from Eq (3.37)} \\ &= 4 \cdot r_0(t) \end{aligned}$$

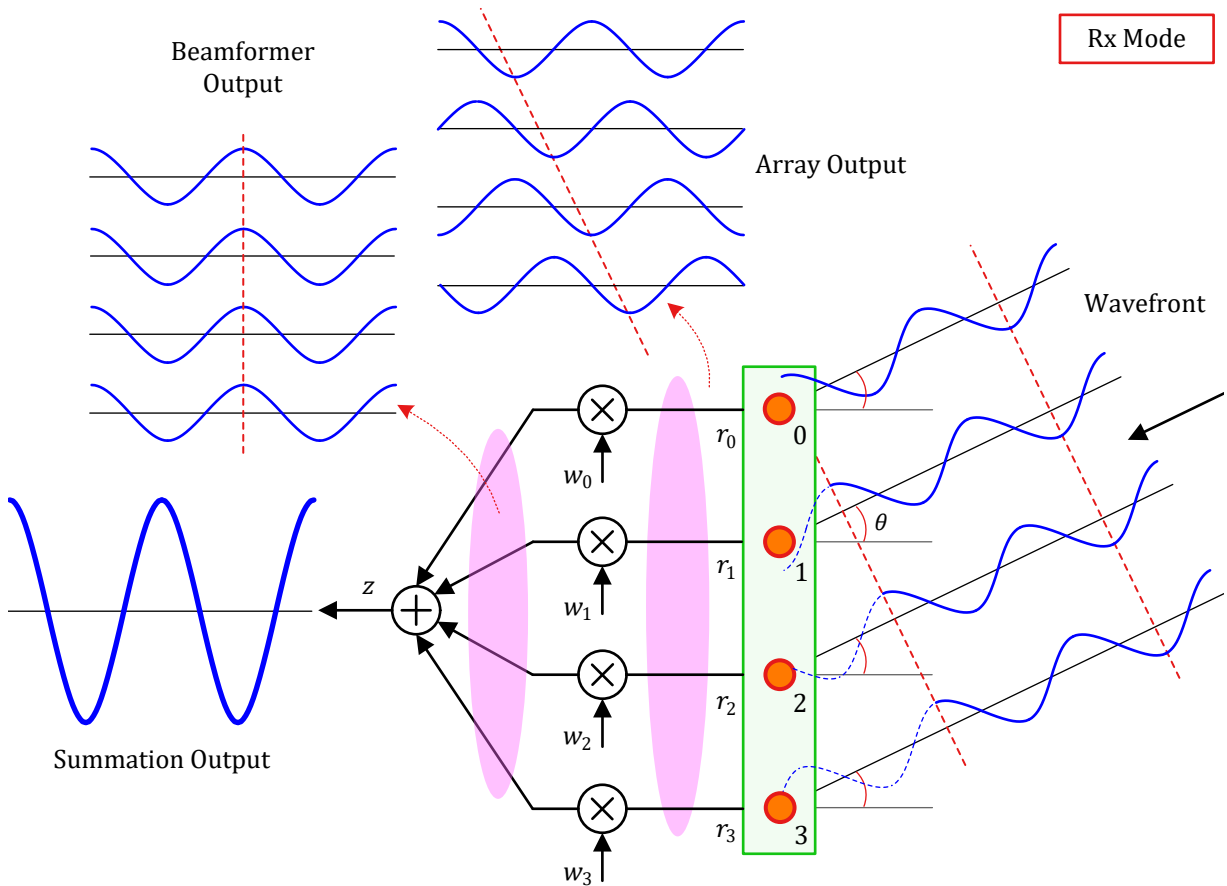


Figure 3.26: Implementation of delay compensation through complex multipliers

thus yielding a gain of 4 here.

Now we can see why the resulting array is also known as a [phased array](#): This is due to phase shifting the output of each element prior to summation. For narrowband signals, this phase shifting is an approximation but it is widely used and gives very good results in most situations. For broadband signals on the other hand, the phase shifts alone are insufficient and filters are required in each path that perform the equivalent of time-delay beamforming task, as described next.

Broadband Beamforming

We saw above that phase shifts alone are incapable of beamforming over the entire bandwidth. Why? The intuitive reason comes from a signal level view. In the narrowband scenario, the same signal reached the array with no change except a progressive delay from one antenna to the next. As we see in Figure 3.27, the baseband signal arriving at the reference antenna 0 has changed during the time interval τ it takes to reach antenna 1. As a consequence, individual array elements here observe different versions of the complex baseband signal, resulting in a phenomenon known as [beam squint](#). There are

two main techniques to form beams of broadband signals.

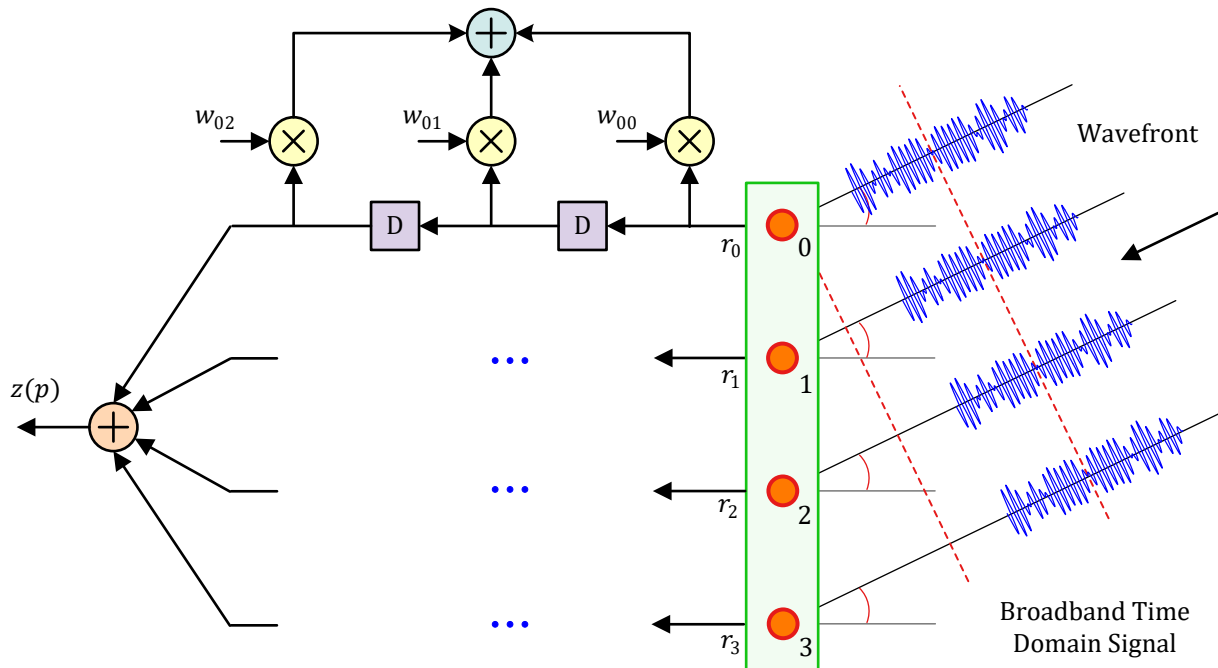


Figure 3.27: Broadband beamforming treats the entire bandwidth instead of a single frequency

Spatial Filtering

In addition to the narrowband beamforming that caters for the center frequency through spatial sampling, an architecture shown in Figure 3.27 samples the signal in both space and time. This enables two-dimensional filtering and combines regular narrowband beamforming with time domain filtering, similar to how a Finite Impulse Response (FIR) filter is implemented in DSP applications. Observe that each antenna element is attached to its own filter due to which the weights $w_{n,l}$ are denoted by two indices, the first across space and the other across time. The cumulative signal out of all the branches is given by

$$z(p) = \sum_{n=0}^3 \sum_{l=0}^2 w_{nl} \cdot r_n(p-l)$$

where the index l indicates time indices and p denotes the current time. This is also known as a tapped delay line structure. Each such branch by necessity needs to have separate RF electronics and ADC forming an efficient yet expensive fully digital solution.

Next, I describe a beautiful downsampling analogy to this beamforming process.

A Downsampling Analogy

This methodology is the space counterpart to downsampling a digital signal in time domain (feel free to skip this note if you do not have a background in DSP). Readers with a DSP knowledge will enjoy comparing the successive delays in the previous beamforming figures with a downsampling architecture shown in Figure 3.28 which is taken from Ref. [2]. The signal delivered to the bottom path is the current input sample. The signal delivered to the filter one path up is the next input sample. With each clock cycle, the commutator moves upwards traversing the successive paths of the polyphase partition and delivering next arriving samples with one sample delay. The final summation at the end produces the desired signal at a reduced rate. This can be considered as beamforming in delay domain. If you are thinking why filters are absent in the beamforming architecture in space, this is because we are considering narrowband inputs here (think of them as close to sinusoidal signals). For broadband input signals, such filters are required to form the beam.

A reader with DSP background will recognize the similarity to sample rate conversion in time domain.

“This phase sensitive summation aligns contributions from the desired alias to realize the processing gain of the coherent sum while the remaining alias terms, which exhibit rotation rates corresponding to M roots of unity, are destructively canceled in the summation.”

fred harris

Frequency Domain Beamforming

The spatial filtering structure is more complex than simple narrowband beamforming which generates an interest in an architecture that handles broadband signals in a manner similar to a narrowband structure. This is accomplished through frequency domain beamforming in Figure 3.29. in which a Discrete Fourier Transform (an efficient implementation of which is the Fast Fourier Transform, or FFT) is taken at the output of each element. This data is processed through its own beamformer before returning to time domain through an iFFT. While both time domain and

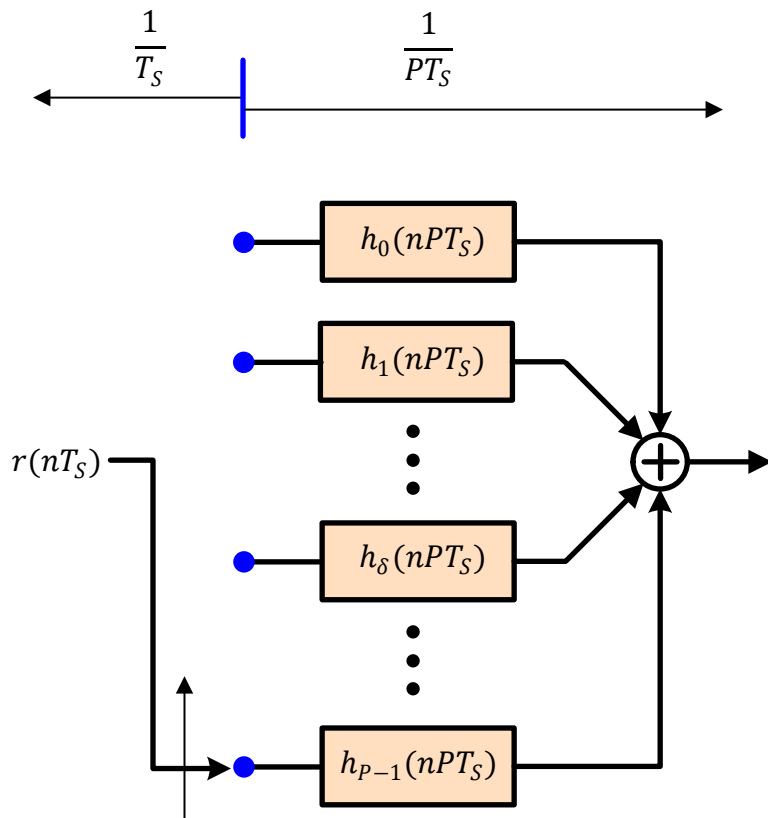


Figure 3.28: The beamforming process in space through introducing successive delays up the line is similar to a downsampling a digital signal in time domain. This figure is taken from Ref. [2]

frequency domain beamformers achieve the same purpose, frequency domain solution is more efficient beyond a certain filter order. Moreover, it has been shown to be less sensitive to coefficient quantization and more suited to VLSI implementation. We will encounter the frequency domain beamforming in the context of OFDM systems in Chapter 6.

Handling Interference

In a cellular network, the target is not to maximize the SNR for one user but also to nullify the interference generated from other mobile users (keep in mind that desired signal for one user is interference for the other, and vice versa). For this purpose, the above method of array weights simply matching to the conjugate of array response vector is not enough. Instead, a combined response needs to be developed with a large gain towards the target signal and nulls towards interfering stations. This is analogous to bandpass and bandstop filtering techniques in digital signal processing applications. In a strict sense, we are no longer forming 'beams' but instead filtering in angular domain.

For this purpose, it is evident that changing only the antenna phases is not enough because this only

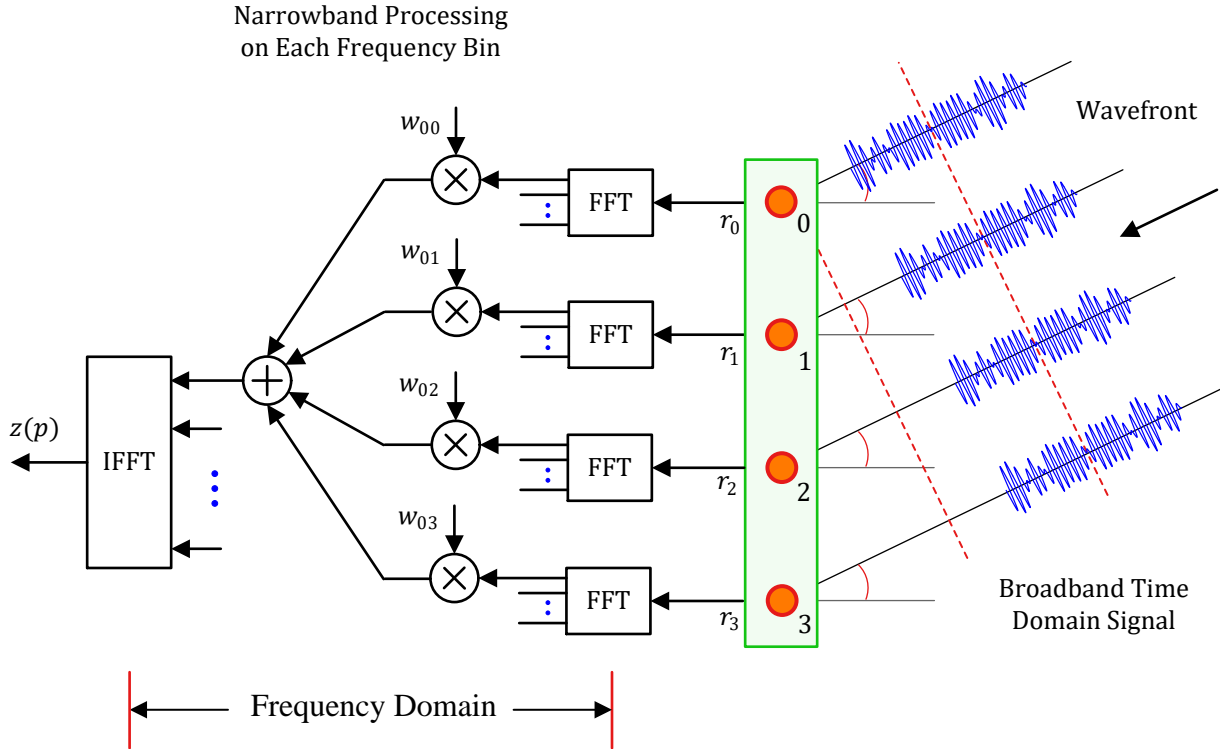


Figure 3.29: Frequency domain beamforming implements a procedure for broadband signals that resembles the conventional narrowband beamformers

changes the look direction while the shape of the overall pattern remains unchanged. This is similar to a mechanical rotation of the antenna array described earlier in Figure 3.14. Now the shape of the overall pattern can be modified through employing *both* the phases and the amplitudes. This is essential for handling interference by creating nulls in the directions of unwanted signals while simultaneously boosting the desired signal. A change in both the amplitude and phase of the complex antenna weights is an idea that is extended further in Section 3.4.

Consider the following example for this purpose in which we need to choose the weights w_n that approximate a desired response. This can be accomplished through either simple FIR filter design techniques or formal optimization design methods. Here, we describe a simple zero forcing solution to illustrate the general concept which is also known as *null steering beamformer*.

As illustrated in Figure 3.30, there are three elements in a uniform antenna array with spacing $d = \lambda/2$ where λ is the signal wavelength. There is one target user along with two interferers at the following angles: user at 50° and interferers at -10° and -70° . The array response vectors for all these directions are given by their corresponding complex scalars given in Eq (3.25). At an angle θ for

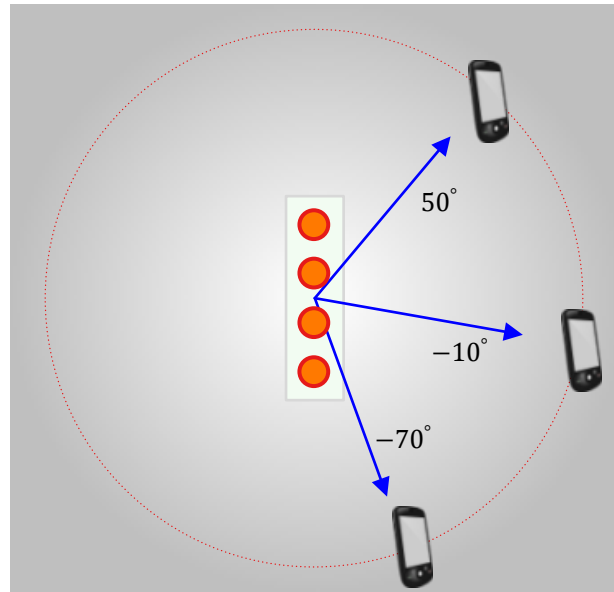


Figure 3.30: A network scenario with a user at angle 50° with two interferers at angles -10° and -70°

instance, and using $u = 2\pi d \sin \theta / \lambda$, we have

$$\begin{array}{ll} I \rightarrow & a_{n,I} = \cos \left(2\pi \frac{d \sin \theta}{\lambda} n \right) = \cos (\pi \sin \theta n) \\ Q \uparrow & a_{n,Q} = -\sin \left(2\pi \frac{d \sin \theta}{\lambda} n \right) = -\sin (\pi \sin \theta n) \end{array}$$

where $d = \lambda/2$ is utilized and $n = 0, 1, 2$, and 3 . So the array response vectors are given in the following table obtained through plugging in the values for i and θ in the above relation.

	$\theta_0 = 50^\circ$	$\theta_1 = -10^\circ$	$\theta_2 = -70^\circ$
$(a_{n,I}, a_{n,Q})$	$i = 0$ (1, 0)	$i = 1$ (-0.74, -0.67)	$i = 2$ (1, 0)
		$(0.85, 0.52)$	$(-0.98, 0.19)$
		$(0.10, 0.99)$	$(0.46, 0.89)$

Now in physical beamforming, the complex weights w_n should do the following:

- Enhance the signal strength in the direction of desired user, i.e., at 50° . This can be accomplished by choosing maximum gain values there.
- **Simultaneously** minimize the signal strengths from the directions of interfering users, i.e., at -10° and -70° . This can be accomplished by choosing minimum gain values there.

Thus, a null steering beamformer weights can be chosen to satisfy the following expressions.

$$\begin{aligned} w_n \times (a_n \text{ for } 50^\circ) &= 1 \\ w_n \times (a_n \text{ for } -10^\circ) &= 0 \\ w_n \times (a_n \text{ for } -70^\circ) &= 0 \end{aligned}$$

where gain 1 on the right side implies maximum gain and 0 implies suppression of transmission or reception. Solving this set of equations generates the following set of weights.

$$\begin{aligned} w_{0,I} &= 0.30 & w_{0,Q} &= 0.48 \\ w_{1,I} &= -0.30 & w_{1,Q} &= 0.27 \\ w_{2,I} &= -0.44 & w_{2,Q} &= -0.34 \end{aligned}$$

This forming of the beams can be used both at the Tx for directional transmission as well as the Rx for directional reception. In conclusion, instead of simply changing the phase, we can also alter the amplitude to create desirable radiation patterns. The cost of this additional constraint of creating nulls in certain directions is the reduction of available gain in the desired direction.

Until now, we have assumed a direct line of sight between the Tx and Rx where the directional response can be designed. Physical beamforming is viable only in these kinds of environments (or in a limited scattering scenario). A different solution is needed where the signal arrives at the Rx through reflected and scattered paths without any direct line of sight. For this purpose, we turn our attention towards virtual beamforming.

3.4 Generalized or Virtual Beamforming

During the discussion on physical beamforming, we assumed that the signals from desired and interfering signals are arriving in their own particular directions. However, recall from Chapter 2 that a wireless channel involves transmission from a Tx to a Rx along multiple paths that are often impinging on the Rx antenna from *several different directions or angles*.

- Even if no other objects were present in the surroundings, the electromagnetic waves from the wireless tower experience difference angles of reflections when they hit the ground. The mobile, in addition to a direct signal from the base station, receives secondary waves coming from an apparently semi-infinite image of the source. This is similar to a vertically elongated image of the sun over a rippled body of water as illustrated in Figure 3.31.
- For other objects in the surroundings, the multipath add up at the Rx antenna to form *channel gains h_j* as explained in Section 2.2. A zoomed-in view of channel gains h_j is drawn in Figure 3.32. While these channel gains are shown as straight arrows from the Tx to the Rx in block diagrams, the reality behind each of them consists of several multiple paths coming from different angles and adding up with different amplitudes and phases.



Figure 3.31: Even with no other objects, there is a secondary wave coming from the semi-infinite image of the source

Consequently, it is not possible to associate a single Angle of Arrival (AoA) to the signals from a particular user, limiting the application of physical beamforming to line of sight and limited scattering scenarios. To overcome this hurdle, virtual beamforming is a solution to enhance the signal strength from desired users while suppressing the signals from the interferers, even when they are coming from numerous angles in rich scattering environments. To find out how this works, we start with the idea of maximum ratio combining.

3.4.1 Maximum Ratio Combining (MRC)

In Section 2.3, we described in detail the idea of space diversity through an example of Selection Combining (SC). Maximum Ratio Combining (MRC) is another space diversity scheme that embodies the concept behind virtual beamforming. Let us find out how.

Setup

Consider a wireless link with 1 Tx antenna and 2 (or more) Rx antennas as shown in Figure 3.33. At each symbol time, a data symbol s is transmitted which belongs to a Quadrature Amplitude Modulation (QAM) scheme. To focus on the events happening within one symbol time only, we have dropped the time index m from the modulation symbol $s[m]$ here.

- In this setup, r_1 is the signal received by the first antenna while r_2 is the signal received by the second antenna.
- h_1 is the flat fading channel gain between the Tx antenna and the first receive antenna.

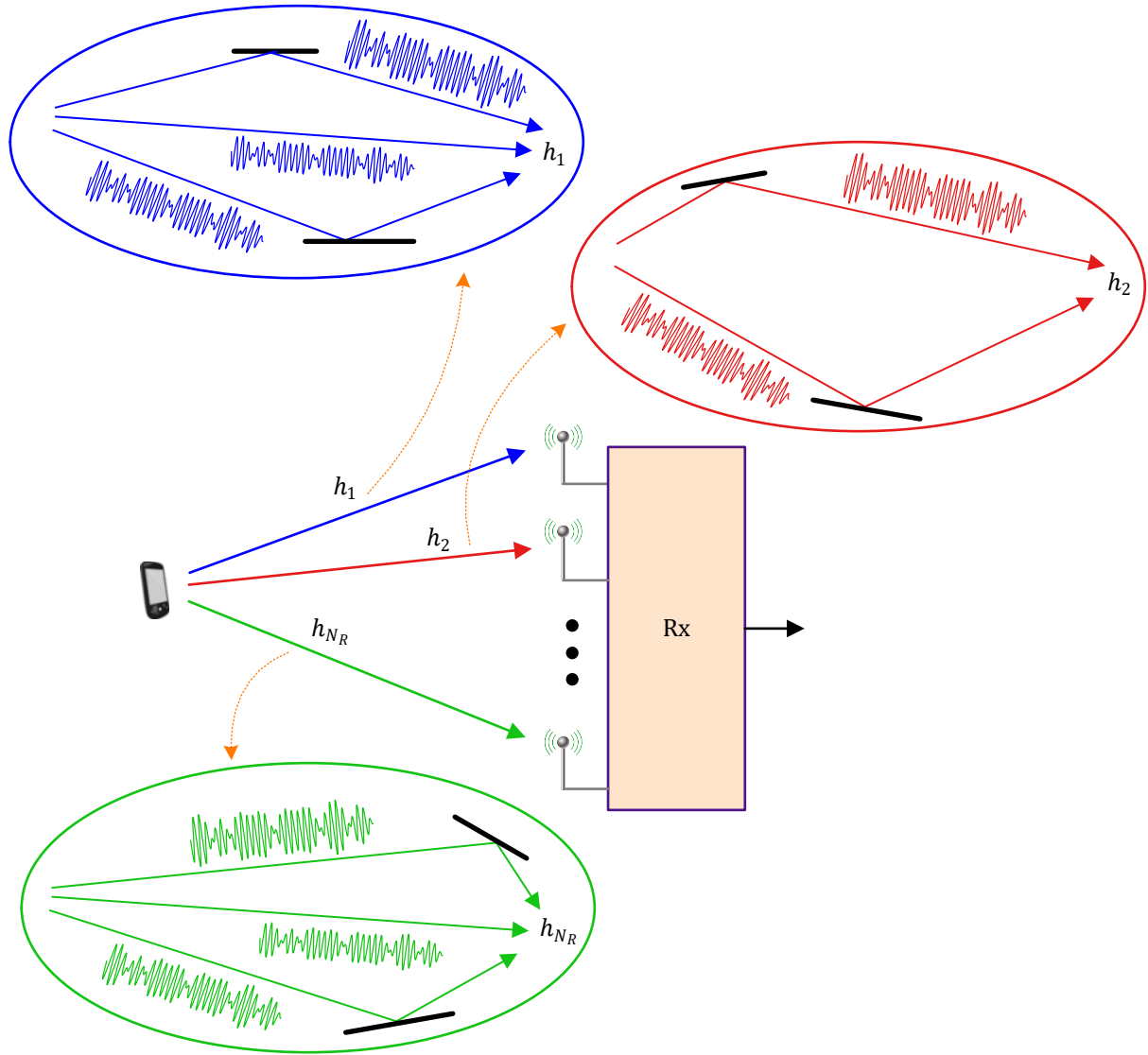


Figure 3.32: In most practical wireless channels, the signals arrive at the Rx through several different angles and combine to form the gains h_i

- h_2 is the flat fading channel gain between the Tx antenna and the second receive antenna.

Consequently, the expressions for the signals at the Rx is given by

$$\begin{aligned} r_1 &= h_1 \cdot s + \text{noise} \\ r_2 &= h_2 \cdot s + \text{noise} \end{aligned} \tag{3.38}$$

Here, the channel gains h_1 and h_2 are usually modeled as complex Gaussian random variables.

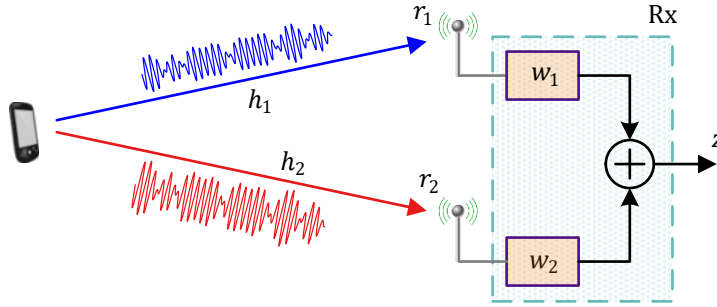


Figure 3.33: Maximum ratio combining implies matching the antenna weights w_1 and w_2 to the conjugates of flat fading channel coefficients h_1 and h_2 , respectively

Why a Simple Summation Will Not Work

In selection combining, we simply scan the power arriving at each antenna and choose the one with the highest SNR. However, selecting the antenna with the best SNR implies that energy at the other antennas is neglected. Instead, the design goal can be modified to maximize the SNR by scavenging the energy from all Rx antenna streams. As we now see, picking additional spatial samples from the air is not enough. We must know how to efficiently utilize them.

The first idea then is to sum the signal from all these antennas. Recall that the channel gains h_1 and h_2 are complex Gaussian random variables here. This in turn implies that their magnitudes are Rayleigh distributed and phases are uniformly distributed between 0 and 2π . Therefore, adding several complex numbers with random phases tends to average out the summation! Moreover, we have already seen during a discussion on physical beamforming that the strategy that would help us accomplish our goal of approaching the Shannon limit necessarily needs to *bend* the BER curve downwards. This is done by reducing the slope of the BER curve and that is where the maximum ratio combining enters the picture. Although selection combining covered in Section 2.3.3 also bends this BER curve but not up to an optimal level.

Computing the Weights w_i

In this spirit, a Maximum Ratio Combining (MRC) receiver is also drawn in Figure 3.33 that forms the decision through a linear combination of r_1 and r_2 after weighting them with complex scalars w_1 and w_2 , respectively. The output signal z is given by

$$z = w_1 \cdot r_1 + w_2 \cdot r_2 + \text{noise} \quad (3.39)$$

$$\begin{aligned} &= w_1 \cdot h_1 \cdot s + w_2 \cdot h_2 \cdot s + \text{noise} \\ &= s \cdot \{w_1 \cdot h_1 + w_2 \cdot h_2\} + \text{noise} \end{aligned} \quad (3.40)$$

Here, the effect of scaling by w_j on the noise samples will be explored later. Also, while the parameters w_j in physical beamforming were selected according to the signal direction of arrival or departure, a

different criterion is chosen in virtual beamforming due to the absence of a single such direction owing to multipath nature of the wireless channel.

Each channel gain h_j is a complex number with magnitude $|h_j|$ and phase $\angle h_j$. Magnitudes and phases of w_j can be represented in a similar manner. Then, we can write their complex product (in which magnitudes are multiplied while phases are added) below[†].

$$\begin{aligned} |w_j \cdot h_j| &= |w_j| \cdot |h_j| \\ \angle(w_j \cdot h_j) &= \angle w_j + \angle h_j \end{aligned} \quad (3.41)$$

To see how optimal w_j are chosen, assume that the channel gains h_j are known at the Rx. In practice, this is usually accomplished by inserting a training sequence or periodic pilot symbols known at the Rx in the information stream. Then, we can proceed as follows.

Cancelling the Phase

If the weight w_j has an opposite phase as compared to that of h_j , we have $\angle w_j = -\angle h_j$ and the complex multiplication will cancel out the phases, see Eq (3.41). On the other hand, noise samples simply add without any phase alignment. With this substitution, the combiner output from Eq (3.40) becomes

$$z = s \sum_{j=1}^{N_R} |w_j| \cdot |h_j| + \text{noise} \quad (3.42)$$

where the effect of scaling by w_j on the noise samples as well as their summation is described in Appendix 3.6. This phase cancellation is shown on the left of Figure 3.34. All channel gains are said to be aligned at the Rx in the same direction. Since we have not yet modified the magnitude of w_j , all w_j have unit magnitude here. This scheme is known as Equal Gain Combining (EGC).

Grading the Magnitude

It is obvious that the branches with better SNR provide a more reliable contribution towards making the modulation symbol decision. Therefore, the branches with higher SNRs should be given more weight as compared to the ones with less signal energy. I call this grading the magnitudes which is shown on the right of Figure 3.34, similar to how the courses with higher credit hours contribute more towards a student's GPA. In the algorithm, this can be accomplished by choosing $|w_j|$ the same as $|h_j|$ which is a *measure of confidence* for the channel gain at i -th Rx antenna.

$$|w_j| = |h_j|$$

[†]In complex notation, this is written as

$$w_j \cdot h_j = |w_j| \cdot |h_j| \cdot e^{j(\angle w_j + \angle h_j)}$$

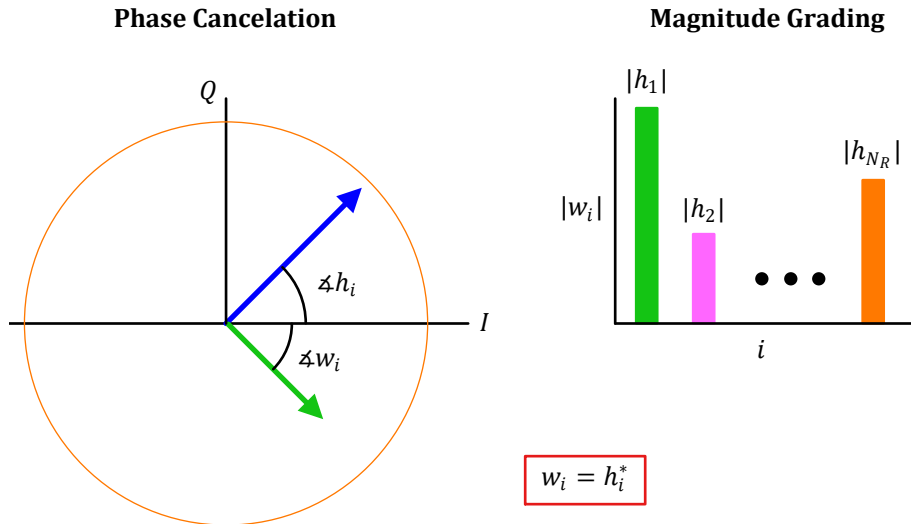


Figure 3.34: Maximum Ratio Combining (MRC) cancels the phase and grades the magnitudes according to each channel gain

When the magnitudes of w_j are chosen according to the above expression, Eq (3.42) becomes

$$z = s \sum_{j=1}^{N_R} |h_j|^2 + \text{noise} \quad (3.43)$$

Notice how the energy from all the Rx branches is being summed in the above expression (without any detrimental effects that come from out-of-phase summations); this is virtual beamforming! As a consequence, this is the optimal approach for signal processing decisions and hence MRC performance is better than every other Rx diversity scheme.

The Brexit Vote

This reminds me of the Brexit vote. Famous biologist Richard Dawkins said that the majority of the British public (including himself) should never have been asked to participate in that referendum. In his opinion, this decision was only up to those with necessary expertise in economics and history.

Taking an analogy from maximum ratio combining, estimation theory tells us that neither the public referendum nor Dawkins' selective suggestion is an optimal approach. Instead, here is what should be done. Given the options in light of a common reference such as a country's ideology or long term goals, **everyone** should vote in such decisions and

each vote should be weighted (on a scale from 0 to 1) in proportion to the person's expertise in the relevant matter.



Figure 3.35: Maximum Ratio Combining (MRC) technique hints towards optimal decision making in public matters

In summary, since the conjugate of a complex number inverts its phase but leaves the magnitude unchanged, the optimal w_j can be chosen as complex conjugates of h_j .

$$w_j = h_j^* \quad (3.44)$$

To keep the expressions simple here, I have deliberately skipped the power normalization part where these h_j^* are scaled by $1/\sqrt{\sum_{j=1}^{N_R} |h_j|^2}$. That factor will be included when we explore the array gain in virtual beamforming.

While complex conjugates are used for selecting the weights w_j , recall that a similar conjugate product was taken for physical beamforming scenario too! Nevertheless, there are two main differences here.

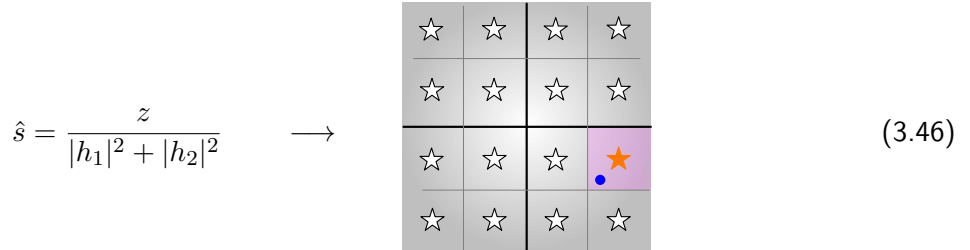
- In physical beamforming, the weights w_i were chosen as conjugates in relation to the angle of arrival of the wave manifested by array response vector formed by a_i , thus enabling the beam to 'look' into particular directions. In virtual beamforming on the other hand, the weights w_j are chosen as conjugates of the overall flat fading channel gains h_j . This introduces diversity in the system.

- Due to a planar wavefront assumption, the Rx signal at each antenna differed in phase only (and hence the terms $\tau, 2\tau, 3\tau, \dots$) with no difference in magnitude. So the product $w_i \cdot a_i$ had a magnitude of 1 as seen in Eq (3.37). On the other hand, all channel gains h_j are not the same and therefore a conjugate operation produces w_j with varying magnitudes.

Having worked out the antenna weights w_j , let us apply the results to our initial setup of 1 Tx antenna and 2 Rx antennas of Figure 3.33. When these weights $w_j = h_i^*$ are applied to the Rx signal branches as in Eq (3.40), the resulting signal available for demodulation becomes

$$z = \{h_1^* \cdot h_1 + h_2^* \cdot h_2\} \cdot s + \text{noise} = \{|h_1|^2 + |h_2|^2\} \cdot s + \text{noise} \quad (3.45)$$

since the product of a complex number with its conjugate cancels the phase and squares the magnitude. Here, the noise term here is actually a superposition of two individual noise terms. For known normalized channel gains and a zero noise scenario, the symbol estimate \hat{s} can be written from Eq (3.45) as



and this estimate \hat{s} maps exactly on one of the modulation symbols. When noise or other distortions are present, a 16-QAM example is also shown above where a decision is made in favour of the star nearest to the blue point \hat{s} . This is because the modulation symbol with the minimum distance from z is the most likely candidate for a Gaussian noise distribution (recall that there is a squared Euclidean distance term in Gaussian probability density function).

3.4.2 Array Gain vs Diversity Gain

Let us now explore different kinds of gains achieved through virtual beamforming, which in this scenario is done through maximum ratio combining. The same basic ideas can be extended to other smart techniques employed in 5G cellular systems.

Array Gain

The array gain for physical beamforming was derived before in Eq (3.12) and was given by N_R . For virtual beamforming case here, we proceed as follows.

- For a single antenna system with a normalized constellation, the SNR is given in Eq (3.5) as

$$\text{SNR} = \frac{\text{Avg Signal Power}}{\text{Noise Power}} = \frac{1}{\sigma^2}$$

This is the benchmark against which the performance of any beamforming system will be compared.

- The average signal power in Eq (3.43) is derived in Appendix 3.6 as

$$\text{Avg Signal Power} = E_s \cdot \sum_{i=1}^{N_R} \text{Avg } |h_j|^2 = 1 \cdot \sum_{i=1}^{N_R} 1 = N_R$$

where we have assumed unit energy modulation symbols as well as normalized channel gains, see Eq (3.3).

- The total noise power is also derived in Appendix 3.6 as σ^2 .

From the above observations, the combined SNR for an array of antennas is

$$\text{SNR}_{\text{Array}} = \frac{\text{Avg Signal Power}}{\text{Noise Power}} = \frac{N_R}{\sigma^2} = N_R \cdot \frac{1}{\sigma^2} = N_R \cdot \text{SNR} \quad (3.47)$$

This extra factor of N_R appearing here is the well known *array gain* provided by the additional antennas. We can write the following expression from the above equation.

$$\text{Array Gain} = \frac{\text{SNR}_{\text{Array}}}{\text{SNR}} = N_R \quad (3.48)$$

which is exactly the same as obtained in a physical beamforming scenario.

In Eq (3.13), we said that the average bit error probability P_b decays in an inverse relationship with $\text{SNR}_{\text{Array}}$. On a logarithmic scale for the bit error rate, this becomes

$$\log \left(\frac{1}{\text{SNR}_{\text{Array}}} \right) = \log \left(\frac{1}{N_R \cdot \text{SNR}} \right) = -\log N_R - \log \text{SNR} \quad (3.49)$$

Comparing with a linear equation $y = m \cdot x + c$ where x corresponds to the log of SNR, the array gain brings the y-intercept of the BER curve down by a factor of $\log N_R$ for a given SNR. This can be interpreted as shifting the curve to the left (i.e., a reduction in SNR) for the same BER. This was plotted before in Figure 3.12 in the context of physical beamforming and reproduced in Figure 3.36 for virtual beamforming where $N_R = 1, 2$ and 4 antennas. It is evident from the plots (and array gain expression) that each doubling of the number of antennas gains 3 dB in terms of the required SNR. This is why there the required SNR for a BER value of 10^{-2} is given by 14 dB for 1 antenna and 11 dB for 2 antennas. This further reduces to 8 dB for 4 antennas as evident in the figure.

Diversity Gain

We saw above that the array gain only shifts the error curve to the left but does not change the *slope* of the curve itself. The story for the diversity gain is a little different.

Diversity gain is achieved by providing multiple copies of the signal in some format such as time, frequency or space. This replication reduces the chances of a deep fade as explained in Section 2.3

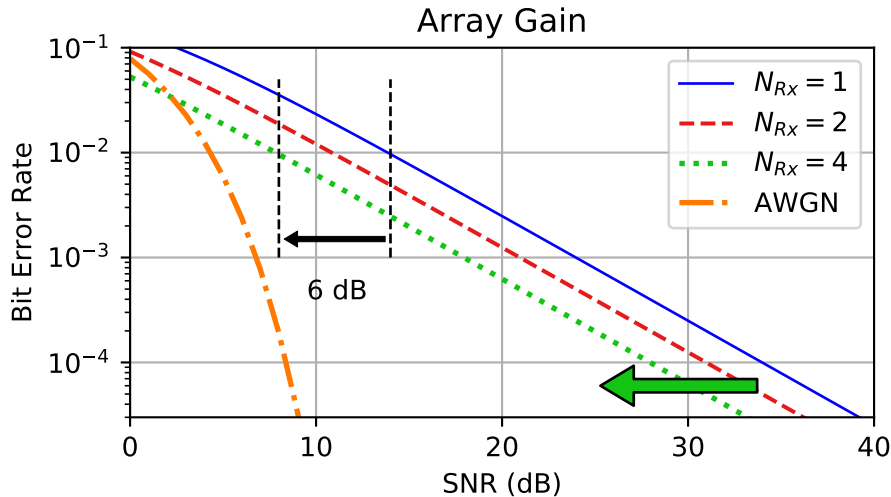


Figure 3.36: Array gain for $N_R = 1, 2$ and 4 antennas

during the discussion on Anna Karenina principle and coin tosses. We saw there that a transmission only fails if *all* L diverse paths simultaneously go in a deep fade. If p is the probability of a deep fade in a Rayleigh fading channel, then the probability of all L paths going down is proportional to p^L . Since p is inversely proportional to the SNR, $p \propto 1/\text{SNR}$ from Eq (2.19), the probability of failure or BER is related to array SNR as

$$\text{BER} \propto p^L = \frac{1}{\text{SNR}^L}$$

This number L is known as *diversity order*. The higher the diversity order L , the lower the chances of a failed transmission.

To view the role of diversity order in the big picture, let us view this expression on a logarithmic scale.

$$\log\left(\frac{1}{\text{SNR}^L}\right) = \log\left(\text{SNR}^{-L}\right) = -L \cdot \log \text{SNR} \quad (3.50)$$

Comparing with a linear equation $y = m \cdot x + c$ where x corresponds to the log of SNR, the diversity order L is clearly seen as the negative slope of the curve. This is why the diversity order is defined as the *slope* of the bit error rate curve if plotted logarithmically against the average SNR.

To see the effect of this reduction in slope, the average bit error rate for maximum ratio combining is drawn in Figure 3.37 for a Rayleigh fading channel with $N_R = 1, 2$ and 4 Rx antennas. The ideal bit error rate for an AWGN channel is also shown. The bit error performance from maximum ratio combining improves with increasing number of antennas. For instance, by adding a second antenna at the Rx at a target bit error rate of 10^{-4} , the average SNR requirement in a flat fading scenario drops from around 34 dB to approximately 16 dB. This is further reduced to 7 dB when two more antennas are also available. The improvement is even more dramatic for lower bit error rate values. This shows

one piece of the puzzle regarding how the bit error rate plotted in Figure 1.1 is brought down from a simple Rayleigh fading scenario towards the Shannon limit.

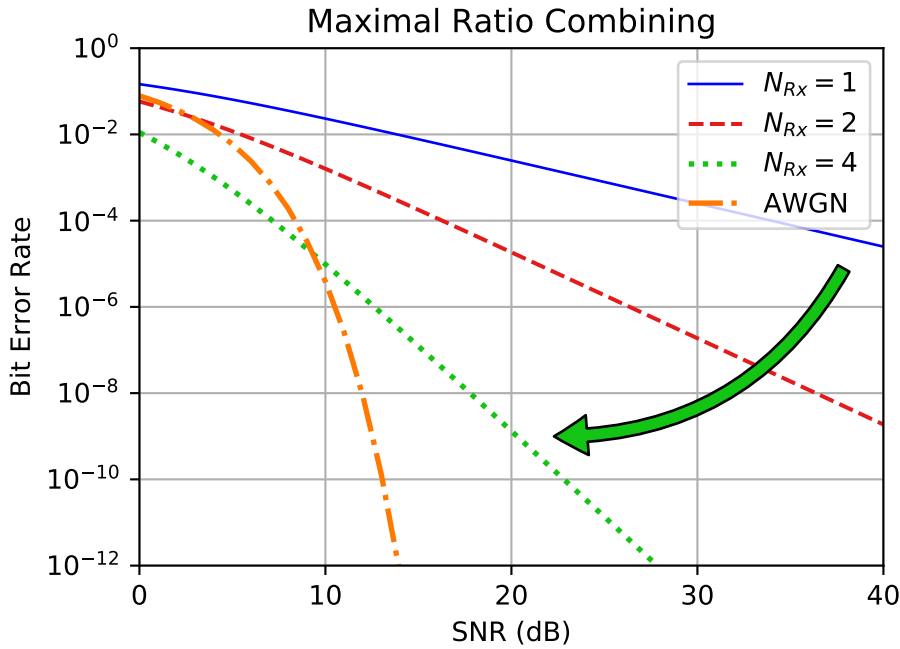


Figure 3.37: Average bit error rate for Maximum Ratio Combining (MRC) with 1, 2 and 4 Rx antennas

The important question now is how to quantify this left shift in the BER curve arising from the impact of diversity. In this regard, sometimes the diversity order L is taken as the diversity gain. In my opinion, we should differentiate between the diversity order and diversity gain. A gain is usually described in terms of reduction in SNR for the same BER, while the factor L only represents a decrease in slope. Therefore, I prefer to define the diversity gain as a reduction in SNR for a fixed BER that comes through employing additional diversity branches. This is not an easy task and hence a common notion of *outage capacity* is often utilized. Leaving rigor aside, we can see a little approximation with the help of BER slopes to grasp the idea.

If SNR_1 and SNR_L are the two SNR values at that BER for number of diversity branches 1 and L , respectively, we can define

$$\text{Diversity Gain} = \text{SNR}_1 - \text{SNR}_L \quad \text{at a fixed BER} \quad (3.51)$$

For example, in case of one additional antenna, $L = 2$ and this value can be modified as $\text{SNR}_1 - \text{SNR}_2$. This is in line with how we defined the array gain as a left shift of the BER curve. For this purpose, Figure 3.38 draws two curves, one with $L = 1$ and the other with $L = 2$. There are a few assumptions in this figure that must be taken into account while interpreting the results.

- Since engineering community often turns to approximations for rough estimates, one popular approach in this context is to analyze the asymptotic performance in the high SNR region. At

high SNRs, the BER curve forms straight lines with the slope depending on the diversity order L of the system.

- There is another constant factor that depends on L and appears as a multiplicative factor in BER expression. On a logarithmic scale, that constant slightly changes the y-intercept of the straight line (in addition to the array gain). Nevertheless, that constant is ignored here to focus only on slope reduction.
- There is no array gain included while drawing the curve.

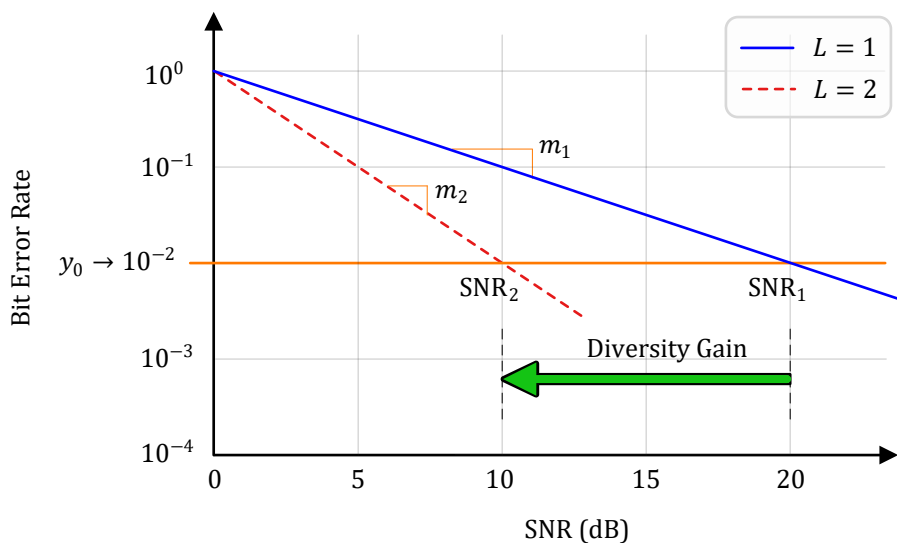


Figure 3.38: Defining diversity gain as a reduction in SNR for a fixed BER by employing additional diversity branches L

In this setting, the diversity gain can be computed as follows. For a fixed BER, say y_0 at 10^{-2} in Figure 3.38 with zero y-intercept, we can write the following expression for $L = 1$ (no extra branches).

$$y_0 = m_1 \cdot \text{SNR}_1 \quad \Rightarrow \quad \text{SNR}_1 = \frac{y_0}{m_1}$$

which comes from the linear equation $y = m \cdot x + c$. Since the second curve for $L = 2$ also cuts through the same y_0 line,

$$y_0 = m_2 \cdot \text{SNR}_2 \quad \Rightarrow \quad \text{SNR}_2 = \frac{y_0}{m_2}$$

From the definition of diversity gain in Eq (3.51), we have

$$\text{Diversity Gain} = \text{SNR}_1 - \text{SNR}_2 = y_0 \left(\frac{1}{m_1} - \frac{1}{m_2} \right) \quad (3.52)$$

Recalling from Eq (3.50) that the diversity order comes with a negative slope, the gain between having no diversity $m_1 = -1$ and that of order $m_2 = -2$ comes out to be $y_0 \left(-1 + \frac{1}{2} \right)$. This can be generalized

for $m_2 = -L$ as

$$\text{Diversity Gain} = \text{SNR}_1 - \text{SNR}_L = y_0 \left(-1 + \frac{1}{L} \right) \quad (3.53)$$

Again as a reminder, this expression for diversity gain is a simplified approximation based on the some assumptions described before. To verify the results, let us plug $L = 2$ in the above equation for y_0 at 10^{-2} which on a logarithmic scale becomes $10 \cdot \log 10^{-2} = -20$.

$$\text{Diversity Gain} = -20 \left(-1 + \frac{1}{2} \right) = 10 \text{ dB}$$

As is evident from Figure 3.38, this is the amount of SNR gained by introducing an additional diversity branch, i.e., one more antenna in our case. With $L = 4$, this turns out to be

$$\text{Diversity Gain} = -20 \left(-1 + \frac{1}{4} \right) = 15 \text{ dB}$$

For a lower BER value, this would have been even larger as the resultant diversity gain depends on the point on the BER curve at which the above expression is computed. In contrast, the array gain stays the same for all BER values, irrespective of where you draw a horizontal line to cut the BER curve.

Comparison Between Array Gain and Diversity Gain

For a comparison between array and diversity gains, these bit error rate relations are drawn in Figure 3.39 in a normalized sense (without including any constants). It is clear that while array gain is simply an offset from the case of no diversity, diversity gain actually reduces the slope of the curve with increasing number of antennas. This improvement arises from the fact that the probability of all L paths having a low SNR is quite small, see Eq (3.50). Consequently, the BER drops much quicker with the diversity gain as compared to the simple linear decrease with the array gain.

The interesting part is that multiple antennas still provide additional signal energy, whether we extract diversity or not. In other words, diversity gain is achieved over and above the array gain. Let us reproduce the signal part of Eq (3.68) below derived in Appendix 3.6 where N_R antennas in space diversity case have been changed to L diversity branches. Then, we can write

$$z = s \sqrt{\sum_{j=1}^L |h_j|^2}$$

The total signal power conditioned on channel gains is clearly $\sum_{j=1}^L |h_j|^2$ (since $E_s = 1$). While SNR refers to a single antenna system, the instantaneous SNR here or $\text{SNR}_{\text{Array}}$ is given by

$$\text{SNR}_{\text{Array}} = \text{SNR} \cdot \sum_{j=1}^L |h_j|^2 = \underbrace{\left[L \cdot \text{SNR} \right]}_{\text{Array Gain}} \cdot \underbrace{\left[\frac{1}{L} \sum_{j=1}^L |h_j|^2 \right]}_{\text{Diversity Gain}} \quad (3.54)$$

The following comments are in order regarding this expression [5].

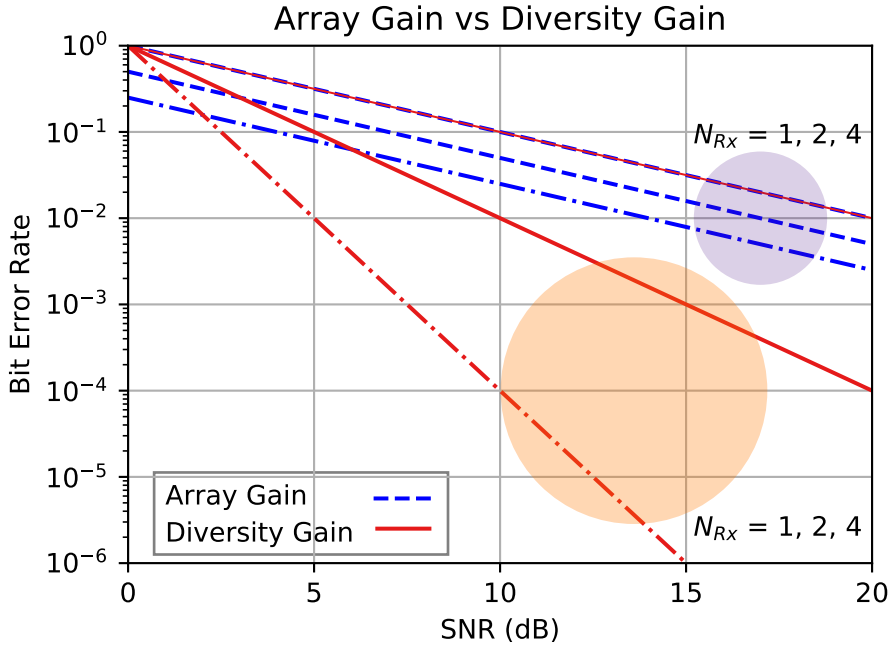


Figure 3.39: Array gain versus diversity gain (with normalized constants to show the trend only) for $N_R = 1, 2$ and 4

- The first term on the right hand side above represents the power or array gain, compare it with Eq (3.47). Physically speaking, this is accomplished through coherent combining with multiple antennas at the Rx. As mentioned before, the array gain increases linearly with L , i.e., doubling the number of antennas provides a 3 dB array gain. In terms of the logarithmic graph of the bit error rate versus SNR, this array gain decreases the y-intercept of the linear curve and is given by the left shift or reduction in SNR for the same BER.
- Loosely speaking, the second term above represents the diversity gain. After taking the average value with respect to all channel realizations, this is expressed by the diversity order L as the exponent of SNR on a normal scale or the slope of the curve on a logarithmic scale. Strictly speaking, the diversity gain is the left shift or reduction in SNR at a certain BER as a result of diversity combining.
- Although array gain remains fixed for all BER values, the diversity gain is different at each BER value due to the modified slope.
- If the channel gains are completely correlated, i.e., $h_j = h$, then from Eq (3.54), we have

$$\left[L \cdot \text{SNR} \right] \cdot \frac{1}{L} \sum_{j=1}^L |h|^2 = \left[L \cdot \text{SNR} \right] \cdot |h|^2$$

We still have the array gain but no diversity gain! Where did we encounter such a situation (i.e.,

$h_j = h$) before? Recall from Eq (3.9) that this is the physical beamforming scenario with one wavefront arriving at or departing from all the antennas in a particular direction. There is indeed no diversity gain in such Line of Sight (LoS) conditions.

- Even when all h_j are independent from each other, there is a limit to the diversity gain that can be obtained. The improvement provided by $L = 2$ over $L = 1$ is significantly greater than the marginal gain provided by $L = 4$ over $L = 2$. For instance, in Figure 3.39 at a BER of 10^{-2} ,

$$L = 1 \longrightarrow L = 2 \quad \text{SNR Gain} = 20 - 10 = 10 \text{ dB}$$

$$L = 2 \longrightarrow L = 4 \quad \text{SNR Gain} = 10 - 5 = 5 \text{ dB}$$

This is a general rule as *the law of diminishing returns* sets in that puts a cap on uninhibited growth of any phenomenon. There are manifestations of this law everywhere in our world. For example, when the number of blades on a razor went from one to two, it produced a marked improvement in the quality of shaving. However, addition of every extra blade brought less marginal refinement and very few razors today have more than three blades.

1. Against our intuition, this law of diminishing returns is not necessarily bad. When we have a large L (e.g., a large number of antennas), Eq (3.54) tells us that

$$\frac{1}{L} \sum_{j=1}^L |h_j|^2 \longrightarrow \text{Avg} \left\{ |h_j|^2 \right\} \longrightarrow 1 \quad (3.55)$$

This is because summing a large number of channel gains on the left side becomes the arithmetic mean or average value over those gains. Consequently, the right side converges towards a constant number which is 1 in this case due to the normalization set in Eq (3.3). This phenomenon transforms a Rayleigh fading channel to more like an AWGN one and the fading vanishes! This is one of the key attractions behind the adoption of massive MIMO systems in 5G standard, a topic we cover in Chapter 4.

2. Remember that the idea of pointed beams in physical beamforming explained earlier goes against exploiting the full multipath and hence *decreases* the spatial diversity available. However, there are other sources of diversity in a communication system (e.g., time diversity obtained through channel coding and frequency diversity through an equalizer) that contribute towards the initial large gain.

- As a consequence of the above discussion, the diversity gain available in the system is utilized to a reasonable extent. Remember that the array gain does not hit such a ceiling of diminishing returns. Each doubling of the number of antennas keeps yielding a 3 dB gain. Since diversity gain is the reduction in SNR for a given bit error rate, it has a *maximum* limit of the fading margin at that BER irrespective of the number of antennas used. We conclude that the diversity gain saturates at the fading margin and hence smaller than array gain for a large number of antennas. On the other hand, the array gain keeps growing and surpasses the diversity gain for a large number of antennas.

This completes the second piece of the puzzle regarding how the bit error rate plotted in Figure 1.1 is brought down from a simple Rayleigh fading scenario towards the Shannon limit.

3.4.3 Maximum Ratio Transmission (MRT)

Until now, our focus was on combining the signals from multiple antennas at the Rx side. Can a similar system be developed with multiple antennas at the Tx side?

As our first consideration, we attempt to replicate the results of Rx diversity in a scenario where there are multiple Tx antennas and a single Rx antenna. This is commonly known as a *Multiple-Input Single Output (MISO)* system. Assume that there are N_T Tx antennas available and only a single Rx antenna as shown in Figure 3.40. This is a dual problem of 1 Tx antenna and multiple Rx antennas we saw before for a SIMO system in Figure 3.3.

- Since our focus is on one symbol, we can temporarily remove the time index m and denote the data symbol by s only.
- At this stage, no knowledge about the channel gains is assumed at the Tx. Therefore, the power is equally divided among the two antennas and hence amplitude of the signal (which is the square root of power) is given by $1/\sqrt{2}$.
- Each Tx antenna emits the same signal which encounters the flat fading channel gain h_j on its way to the Rx.

Now the nature adds the signals impinging at the single Rx antenna allowing us to write

$$\begin{aligned} r &= h_1 \cdot \frac{s}{\sqrt{2}} + h_2 \cdot \frac{s}{\sqrt{2}} + \text{noise} = \underbrace{\frac{h_1 + h_2}{\sqrt{2}} s}_{h} + \text{noise} \\ &= h \cdot s + \text{noise} \end{aligned} \quad (3.56)$$

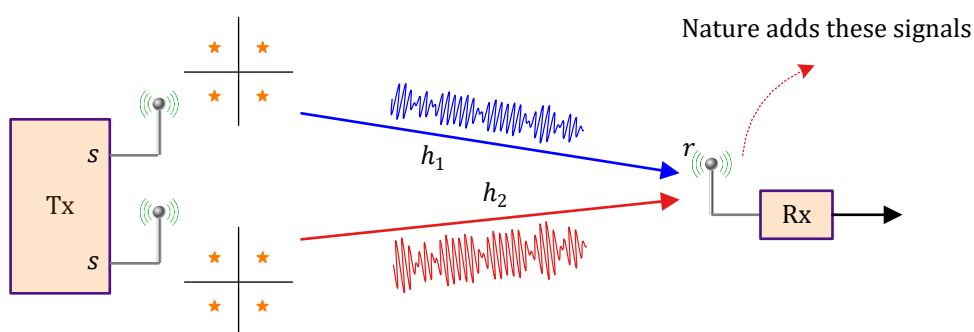


Figure 3.40: A *Multiple-Input Single Output (MISO)* system with 2 Tx antennas and 1 Rx antenna

As explained before, the channel gains h_1 and h_2 are complex Gaussian random variables with uniformly distributed phases between 0 and 2π . Their sum also follows a Gaussian distribution with a uniform phase. We are facing the same situation in Eq (3.56) as a simple Rayleigh fading wireless channel! The conclusion is that there is no diversity gain in this setup.

To do better, the trick is to copy the same architecture employed for MRC before but reverse the roles of antennas if the channel knowledge is available at the Tx. The resulting technique is known as Maximum Ratio Transmission (MRT)[†]. A block diagram of this scheme for 2 Tx antennas and 1 Rx antenna is drawn in Figure 3.41, a dual of the MRC block diagram at the Rx in Figure 3.33. Here, the modulation symbol s is weighted by w_1 and w_2 before sending it through the first and second Tx antennas, respectively. Nature adds these signals at the Rx antenna and the result can be expressed as

$$\begin{aligned} r &= w_1 \cdot h_1 \cdot s + w_2 \cdot h_2 \cdot s + \text{noise} \\ &= s \cdot \{w_1 \cdot h_1 + w_2 \cdot h_2\} + \text{noise} \end{aligned}$$

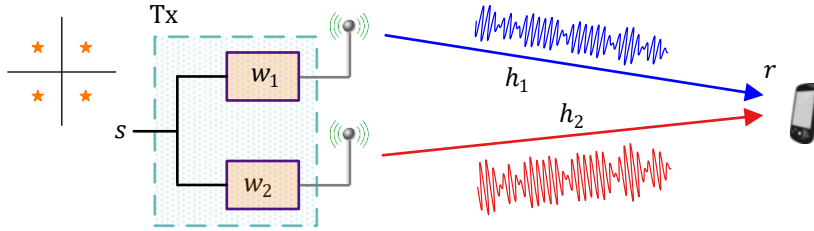


Figure 3.41: Maximum Ratio Transmission (MRT) with 2 Tx antennas and 1 Rx antenna where the antenna weights w_1 and w_2 must be matched to flat fading channel coefficients h_1 and h_2 , respectively

This is exactly the same equation as Eq (3.40) encountered for MRC at the Rx before and hence the same analysis can be applied here. Consequently, if we choose random and fixed w_i , their sum would neither cancel the phases nor grade the magnitudes. Instead, the modulation symbol s must be weighted by w_i in each branch such that the natural summation at Rx antenna coherently adds electromagnetic energy emanating from each Tx antenna. This can be accomplished by implementing the same solution as in the case of MRC at the Rx, i.e., optimal weights w_i are complex conjugates of channel gains h_i .

$$w_i = h_i^* \tag{3.57}$$

where I have again ignored the scaling factor $1/\sqrt{\sum_{i=1}^{N_T} |h_i|^2}$ to keep the expressions simple. When optimal w_i are chosen, the signal at the Rx antenna becomes

$$r = \{h_1^* \cdot h_1 + h_2^* \cdot h_2\} \cdot s + \text{noise} = \{|h_1|^2 + |h_2|^2\} \cdot s + \text{noise} \tag{3.58}$$

[†]The term Maximum Ratio Transmission (MRT) is also used for maximizing diversity reception through linear precoding when both the Tx and the Rx are equipped with multiple antennas. I choose the more common and simpler use of the terminology here for ease of understanding.

which we found in MRC scenario at the Rx as well, see Eq (3.45). The improvement as compared to Eq (3.56) lies in the multiplicative factor with the modulation symbol s . Previously it was a fading coefficient h that was the sum of h_1 and h_2 that could potentially bring each other down. Now the factor appearing with data symbol s is $|h_1|^2 + |h_2|^2$. Here, not only that the contribution from each channel gain h_i is taken according to its own energy but also the magnitude squared operation completely cancels the phase for each h_i . This is the best we can do in focusing the energy towards the intended destination.

To get an intuitive sense of how this choice works at the Tx side, an example of a simple manipulation is drawn in Figure 3.42. Without any weighting at the Tx, the two signals from both antennas will mostly cancel each other at the Rx. However, utilizing the channel knowledge, the Tx adjusts its phase at second antenna before the transmission such that signals from both antennas now arrive at the Rx in phase with each other. In 5G systems with a large number of base station antennas and a simple user terminal, this is how beamforming is implemented in non-LoS scenarios.

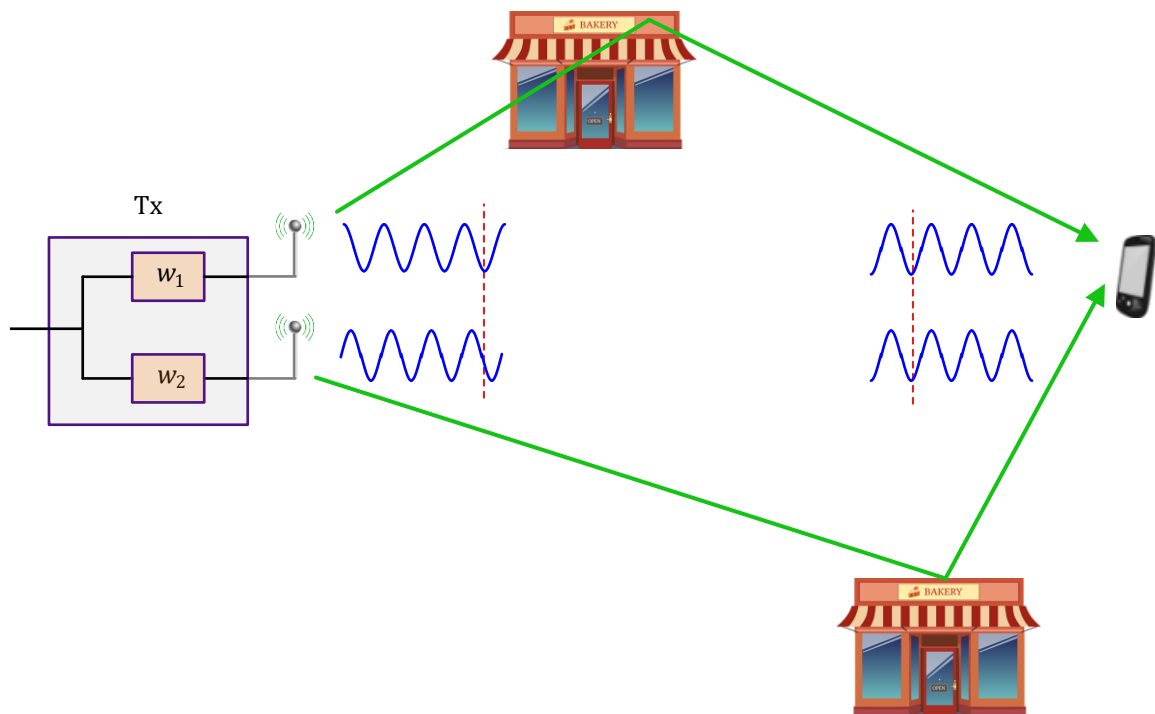


Figure 3.42: An intuitive way to understand the maximum ratio transmission. The Tx utilizing the channel knowledge adjusts its phase at second antenna before sending the signal such that signals from both antennas arrive at the Rx in phase with each other

3.4.4 Precoding and Combining

Having covered both physical and virtual beamforming, we can step back a little and look at the concept of beamforming from a general perspective.

- We start with a single antenna that has a fixed radiation pattern.
- An array of those antennas can transmit or receive a signal together in unison. If no other processing is done, the radiation pattern of such an array is also fixed (e.g., a main lobe at 0°).
- A successive delay in each antenna of the array results in a superimposed signal, the direction of which depends on the value of those delays.
- For narrowband signals, delays can be replaced by phase shifts implemented by complex multiplications.
- Since the scalars are complex-valued, the amplitude can also be modified that can be used to handle interference and multipath scenarios.
- With both amplitude and phase changes, virtual beams can be created. Assuming a flat fading channel mode, each antenna handles a signal distorted by a complex scalar channel coefficient. The array can then focus on canceling the phase of flat fading coefficient and grade their channel coefficients according to their magnitudes. We say that the array is focused on some desired (mathematical) directions in transmitting or receiving a signal.

This generalized view of beamforming is called *precoding* at the Tx side and *combining* at the Rx side. This terminology is widely used in 3GPP specifications and standards. It can be confusing but we can simplify it as follows. For all practical purposes, there is no difference between beamforming and Tx precoding/Rx combining. However, the latter terms are more general and hint towards the idea of radiation patterns other than pencil beams. For a single user scenario, the terms imply a product between its symbol stream with an antenna weight vector. These terms become more relevant when we talk about multiple users in a Multiuser-MIMO (MU-MIMO) system. In this scenario, the symbol streams are multiplied with a matrix to generate a complicated pattern that simultaneously enhances the Signal to Interference plus Noise (SINR) ratio for all users according to a chosen criterion.

Single User Scenario

We now describe the precoding and combining tasks from a single user perspective. The multi-user scenario will be described in the next subsection.

Tx Precoding

In the case of a single user communicating with a multiple antenna Tx, the symbol stream s is

multiplied with the weight w_i and delivered to the corresponding Tx antenna i that emits the signal x_i as

$$x_i = w_i \cdot s \quad i = 1, 2, \dots, N_T$$

This is illustrated in Figure 3.43. To simplify the block diagram in preparation of the matrix

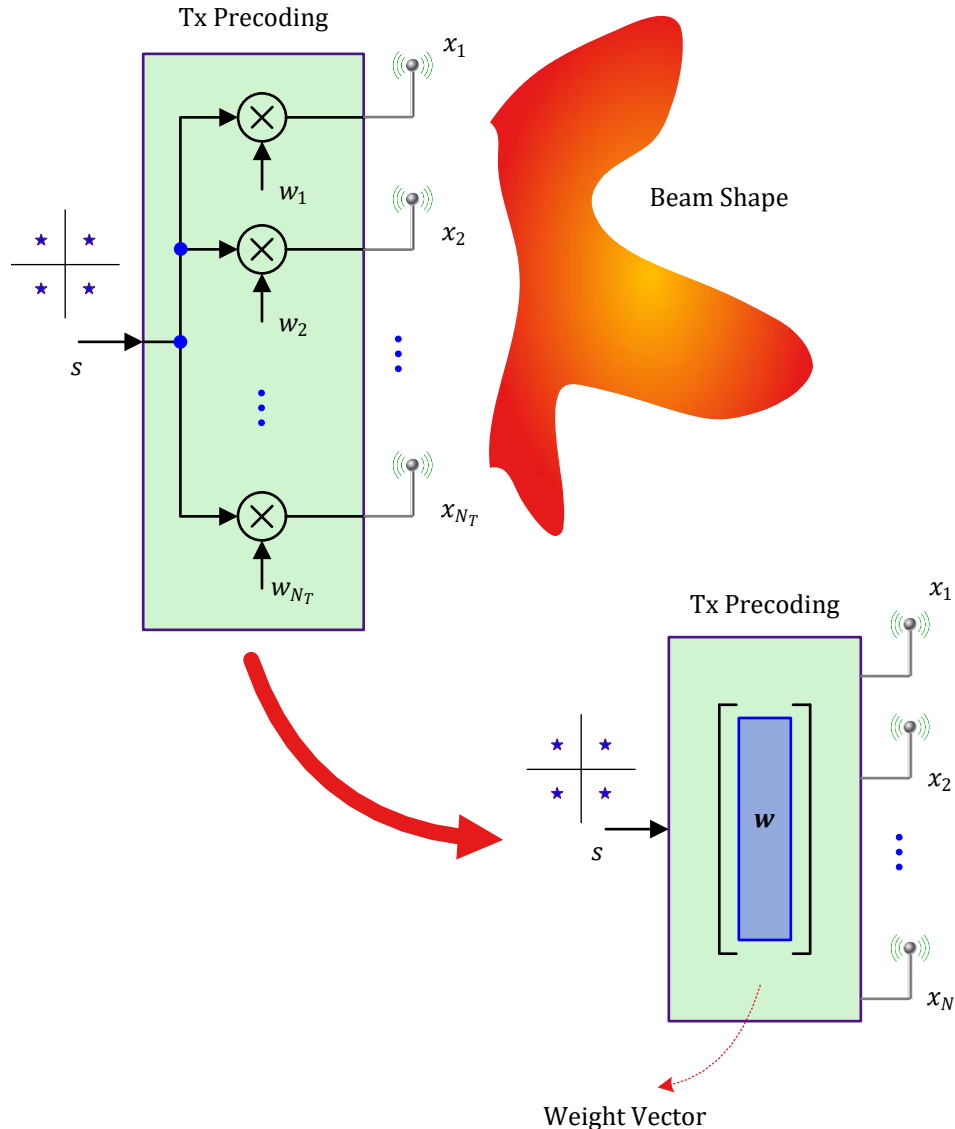


Figure 3.43: Tx precoding implies multiplying the symbol stream s with antenna weight factors w_i

precoding coming next, we can show the vector of weights w_i as a vertical box in the bottom right figure. The signal emitted from the Tx antenna is not the modulation symbol s but instead its scaled version x_i (the modulation symbols are not sent to the antennas in any case but instead wrapped in a single or multi-carrier waveform). The weights w_i adjust the amplitude and phase

of the input signal before sending them in the air.

Rx Combining

The Rx operation is a dual of the Tx operation. In forming duals, the following steps are involved.

- Nodes are replaced with summations and summations with nodes.
- Direction of the signal flow is reversed.
- Input and output ports are interchanged.

This is what is done in Figure 3.44 where the arriving signal r_j is sent to scaling factors w_j before a final summation that produces an estimate \hat{s} for the symbol.

$$\hat{s} = \sum_{j=1}^{N_R} w_j \cdot r_j$$

In preparation of matrix operations coming next, the vector product between r_j and w_j is shown as a horizontal box since matrix multiplication implies products between respective elements of rows of one matrix with columns of the other.

From Figure 3.43 and Figure 3.44, we can now expand our view of beamforming and see how precoding and combining are slightly more suitable terms to use. This is because the antenna array is not forming physical main beams in space but instead its complicated radiation pattern is a function of amplitudes and phases applied through the complex-valued weights. This makes the beamforming concept work in multipath environments as well as different transmission bandwidths (keep in mind that the radiation pattern applies to both Tx and Rx roles). The analogy with time domain filtering is also more clear here and hence this process was called spatial filtering earlier. This difference between strong physical lobes explained earlier and a complicated (but desired) radiation pattern is the biggest source of confusion in beamforming literature.

Multi-User Scenario (MU-MIMO)

In the above discussion, a multi-antenna Tx communicates with a single user by forming a particular beam pattern and a multi-antenna Rx receives signal from a single user through beams suited to that user. Now we explain this idea for the scenario where there are multiple users in the network, e.g., in a cell, simultaneously communicating with a base station equipped with an antenna array. This is known as a Multi-User MIMO (MU-MIMO). Here, we will give a brief description of MU-MIMO from a beamforming perspective. A comparison of MU-MIMO with massive MIMO will be presented in Chapter 4.

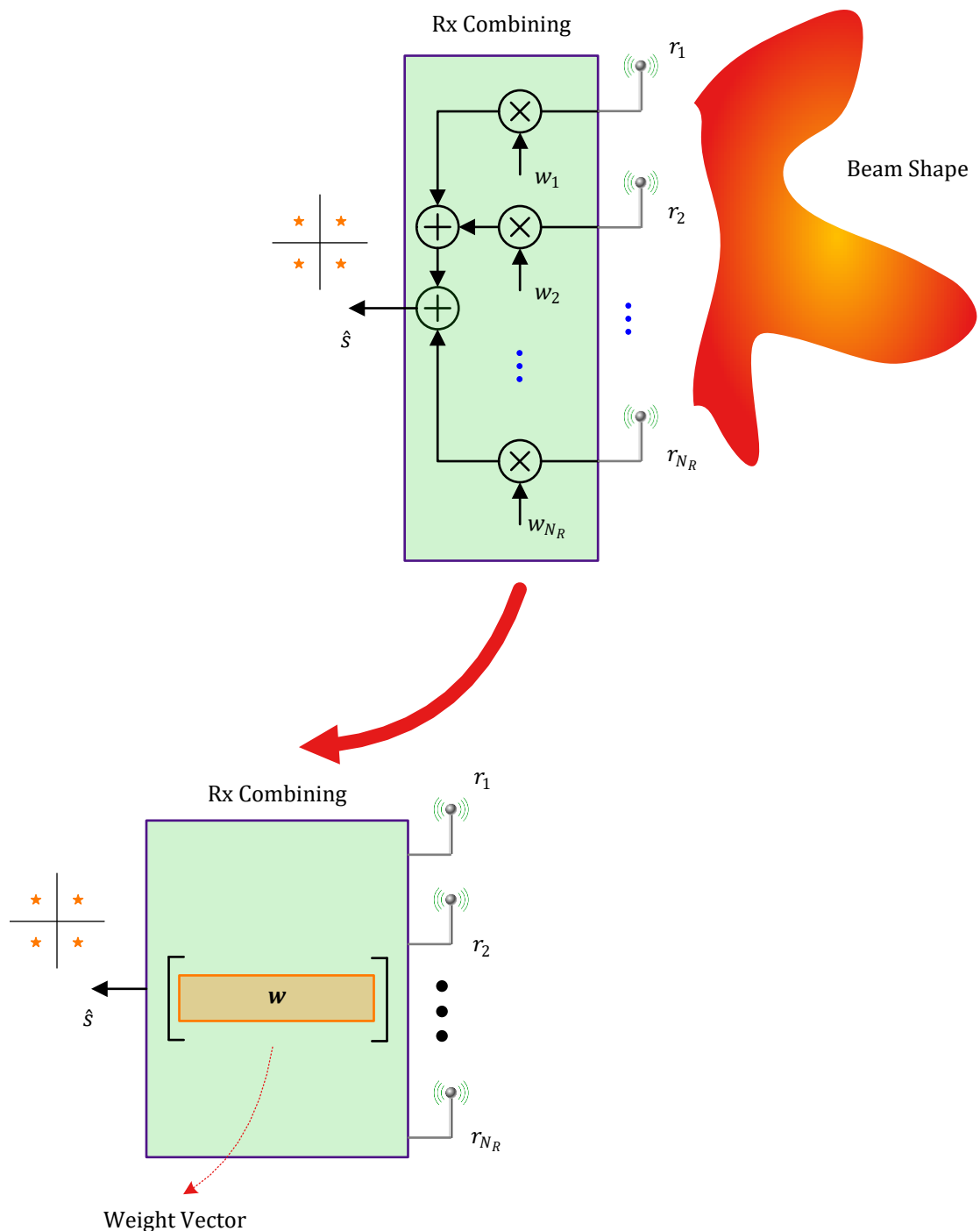


Figure 3.44: Rx combining implies multiplying the received signal r_j with antenna weight factors w_j before a final summation, i.e., a dot product of these two vectors is taken

Tx Precoding

As with the single user case, we will consider a simplified version of the Tx and the Rx. We will zoom in the detailed signal level operations in Chapter 8 on OFDM. This simplified Tx antenna array sending a signal to K users is drawn in Figure 3.45. In the top figure, a real scenario is depicted where a base station has a set of symbol streams s_i that it prepares to send to K individual users through N_T antennas. How should the mapping from modulation symbols s_i ($i = 1, 2, \dots, K$) to emitted signals x_m ($m = 1, 2, \dots, N_T$) be done to maintain a target Signal to Interference plus Noise Ratio (SINR) at each user? This is where a whole set of Tx precoding vectors enter the picture and join together to form a *precoding matrix*.

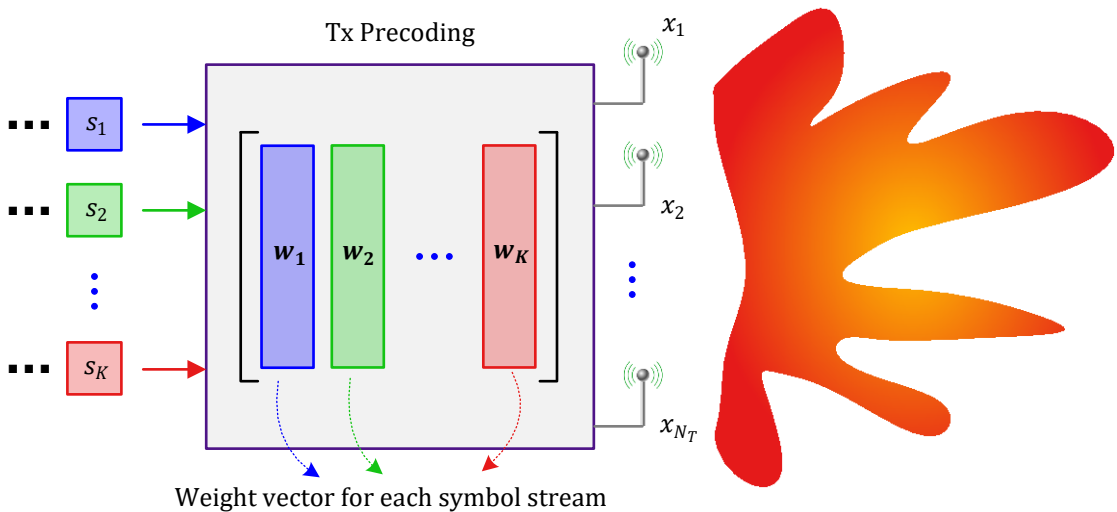
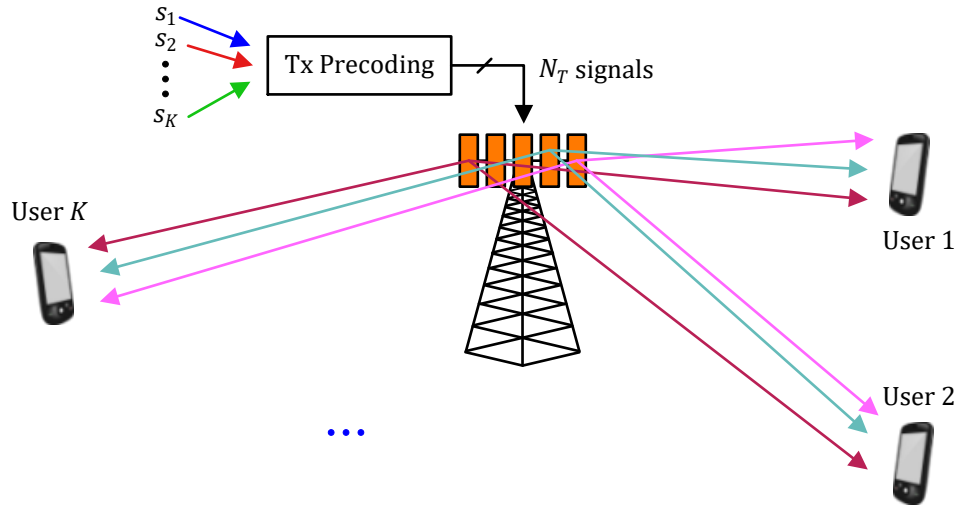


Figure 3.45: Tx precoding implies multiplying the symbol streams s_i with their respective antenna weight factors $w_{m,i}$ for mapping to N_T antennas

This precoding matrix is illustrated at the bottom of Figure 3.45. Observe that independent symbol streams s_1, s_2, \dots , are input to this matrix and each user is assigned a particular precoding vector that consists of the sets of weights $w_{m,i}$. For example, the signal at first antenna can be written as

$$x_1 = \sum_{i=1}^K w_{1,i} \cdot s_i$$

To see how the final beam is formed, consider the following expression.

$$\begin{matrix} x_1 \\ x_2 \\ \vdots \\ x_{N_T} \end{matrix} = \sum_{i=1}^K \left\{ \begin{array}{l} w_{1,i} \\ w_{2,i} \\ \vdots \\ w_{N_T,i} \end{array} \right\} \times s_i$$

There are K individual streams that need to be mapped to N_T antennas. This is done by multiplying the individual symbol streams s_i with their *respective* antenna weight factors $w_{m,i}$ where the index m represents a Tx antenna and ranges from 1 to N_T . Recall that the radiation pattern formed by a single stream was shown in Figure 3.43. The present pattern is then the summation of K such patterns that is the generalized version of a ‘beam’. Since vector multiplication is a linear process, the superposition principle holds and the cumulative beam is the summation described in the above expression. This is plotted at the bottom of Figure 3.45. This is how the base station focuses energy in particular directions such that the signal at each user i is (ideally) independent of the other symbol streams. As with other figures in this text, color coding should be closely observed (e.g., blue, green and red symbol streams are mapped to their respective columns). Many a times the term precoding is specifically associated for multiple beamforming vectors, one for each stream to be sent over the air.

Rx Combining

The combining operation is again a dual of the precoding operation and drawn in Figure 3.46. At the top, a base station array with N_R antennas is receiving signals from K users with symbols s_i . How should the base station perform a linear operation (combining) such that each symbol comes out (ideally) independent of the other symbols at the output? This is done through a *combining matrix*.

This combining matrix is depicted at the bottom of Figure 3.46. There are N_R individual Rx signals (one at each antenna) that need to be mapped to K symbol streams. This is done by multiplying the combination of signals r_j with their *respective* antenna weight factors $w_{m,j}$ where the index m represents a symbol stream and ranges from 1 to K . This can be written as

$$\hat{s}_j = \sum_{j=1}^{N_R} w_{1,j} \cdot r_j$$

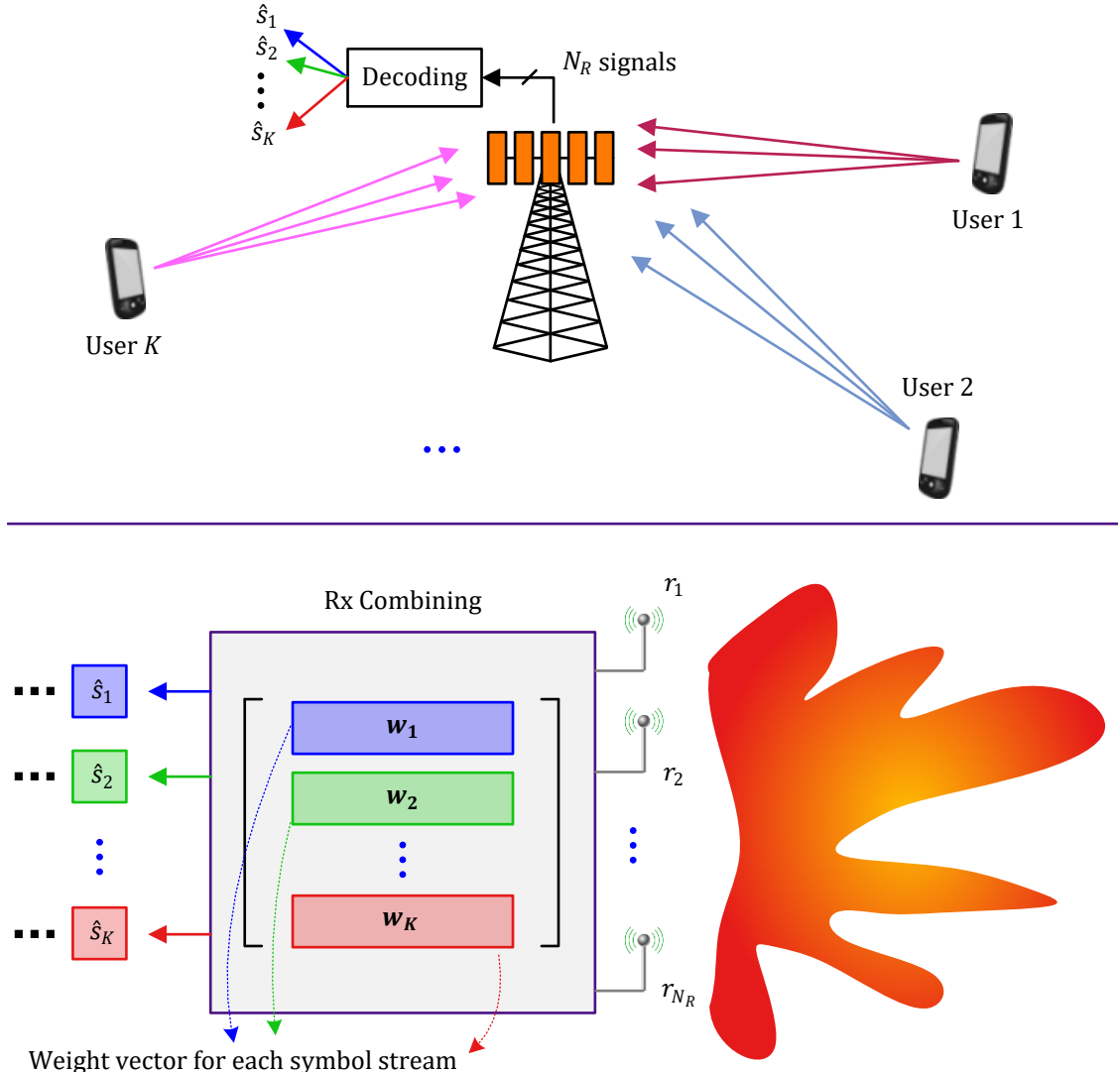


Figure 3.46: Rx combining implies multiplying the incoming signal r_j with their respective antenna weight factors $w_{m,j}$ for mapping to K symbol streams

Why is there a summation here as compared to a simple scaling in Tx case? The answer lies in single user cases of Figure 3.43 and Figure 3.44, respectively, where the Rx operation was shown to be a dual of Tx operation and the dual of a simple node is an adder. This is how the base station receives energy from particular directions such that the signal at each user i is (ideally) independent of the other symbol streams. As with other figures in this text, color coding should be closely observed (e.g., blue, green and red symbol streams originate from their respective rows).

In summary, each weight vector represents its own spatial signature that determines its contribution in

the overall radiation pattern. As long as each symbol stream uses a weight vector that can be sufficiently separated from the other weight vectors, all the symbol streams (i.e., all the user terminals) can share the same resource in time-frequency grid encountered earlier. This is a very important result: users are not separated in time (Time Division Multiple Access, TDMA), in frequency (Frequency Division Multiple Access, FDMA) or in code (Code Division Multiple Access, CDMA), as was the case with earlier generations of cellular networks. Instead, the users are separated in space through the precoding and combining vectors. This gives rise to a concept of cellular systems where users are individually served. Figure 3.47 illustrates this difference between the older generations as compared to 5G. The upper cell is divided into sectors and several users share the same signal in space while being separated through some other resource. On the other hand, beamforming in the lower cell directs the energy directly to the intended user, thus increasing the desired signal gain and reducing interference at the same time. Keep in mind that physical beams are shown in the figure although they can be virtual too in a mathematical sense as described before.

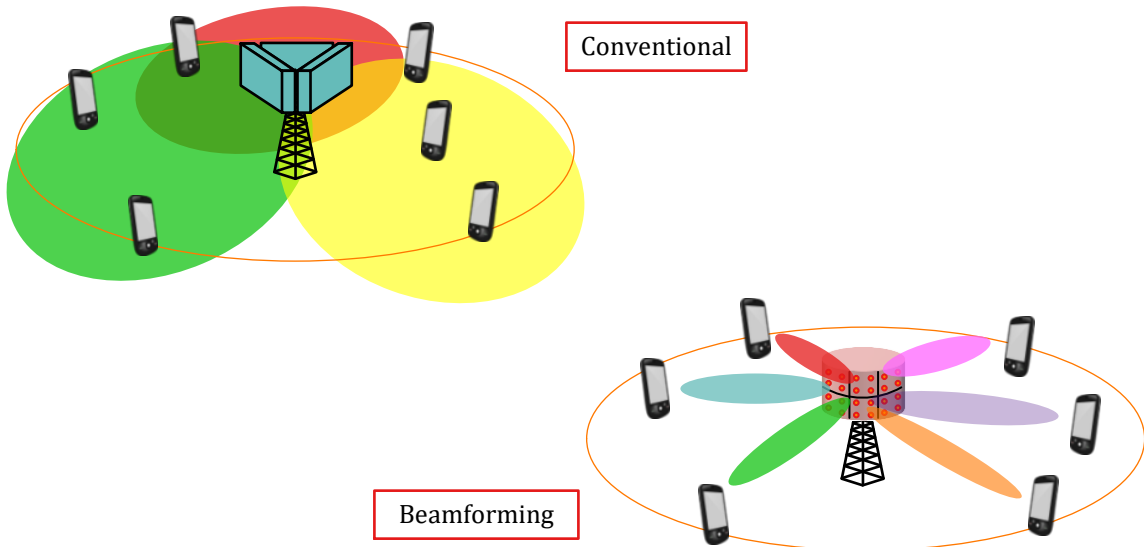


Figure 3.47: A view of conventional vs 5G systems

Sending and receiving separate data streams to or from multiple users at the same time and within the same bandwidth is known as *spatial multiplexing* in the context of MU-MIMO. The idea of spatial multiplexing in the context of Single-User MIMO (SU-MIMO) is covered in Chapter 5. The topics covered in the next two chapters also include how some of the precoding and combining vectors are computed when we cover singular value decomposition, maximum ratio and zero-forcing schemes.

3.5 The Small Picture

The signals arriving at each antenna have different complex multiplicative factors h_i contributed by nature that destroy the phase coherence.

$$z = \sum_{i=0}^3 r_i = \sum_{i=0}^3 r_0 \cdot \underbrace{h_i}_{\text{contributed by nature}} \neq 4r_0 \quad (3.59)$$

Nevertheless, thanks to the sampling view of the array, we will have the opportunity to compensate for these natural multiplicative factors by inserting multiplications of our own, denoted by w_i , which are designed to restore the lost phase coherence.

$$z = \sum_{i=0}^3 r_i \cdot w_i = \sum_{i=0}^3 r_0 \cdot \underbrace{h_i}_{\text{contributed by nature}} \cdot \underbrace{w_i}_{\text{compensated by signal processing}} = 4r_0 \quad (3.60)$$

In both physical and virtual beamforming, the signal in each branch is weighted by a complex scalar w_i such that the final summation coherently adds electromagnetic energy departing from or arriving at each antenna. The difference between them lies in the way this summation is made coherent, see Figure 3.48.

Physical Beamforming

In a Line of Sight (LoS) situation, the complex scalars w_i are chosen according the direction of arrival of the signal such that the *delay* at each antenna is equalized before the final summation. This creates a narrow angular window centered around the direction towards the source or destination.

Virtual Beamforming

In the situation of a multipath channel, the complex scalars w_i are chosen according to the channel gains experienced by the signal. This adjustment of phases and amplitudes creates a *constructive superposition* of many independently arriving paths at the destination. A word of caution regarding Figure 3.48: While two distinct paths are shown for illustration purpose, in practice the cumulative signal is a summation of several paths with no clear directionality.

3.6 Appendix

In this appendix, we derive the mathematical results that otherwise break the flow of the topics under discussion.

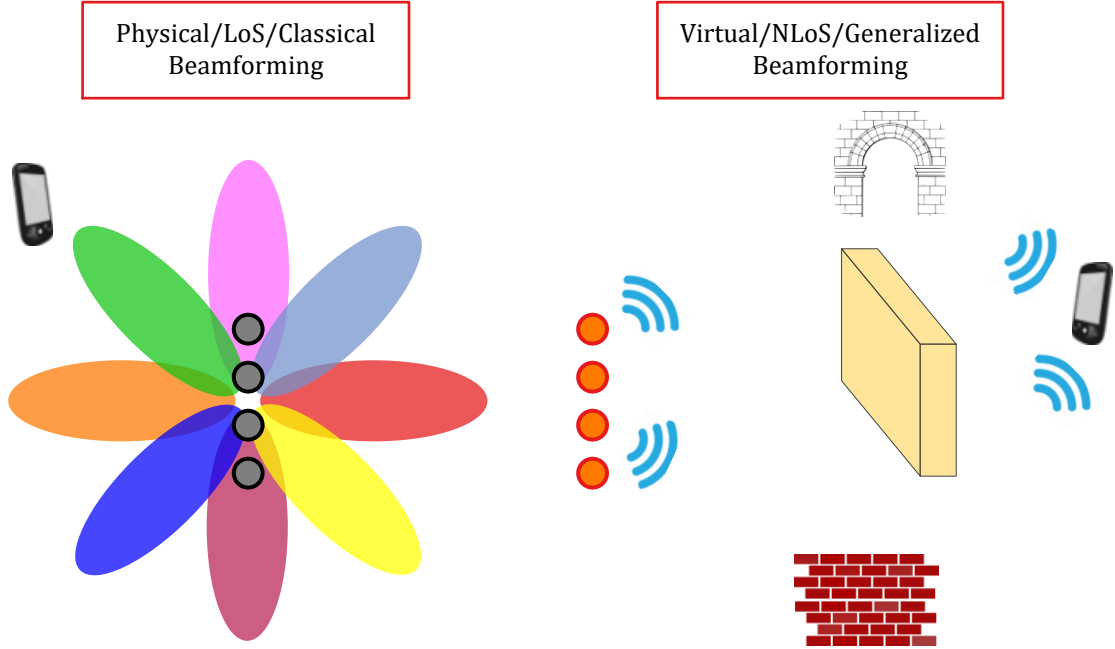


Figure 3.48: A summary of physical vs virtual beamforming

The Spectrum of a Rectangular Pulse

Consider a signal $x[n]$ of length N with I and Q components given as $x_I[n]$ and $x_Q[n]$. The Discrete-Time Fourier Transform (DTFT) $X(e^{j\omega})$ is defined as

$$\begin{aligned} I \rightarrow & X_I(e^{j\omega}) = \sum_{n=-\infty}^{\infty} [x_I[n] \cos \omega n + x_Q[n] \sin \omega n] \\ Q \uparrow & X_Q(e^{j\omega}) = \sum_{n=-\infty}^{\infty} [x_Q[n] \cos \omega n - x_I[n] \sin \omega n] \end{aligned} \quad (3.61)$$

Now let us compute the DTFT of a length- N rectangular pulse shown before in Figure 3.4. For convenience, we assume that N is even.

$$x_I[n] = \begin{cases} 1, & 0 \leq n \leq N-1 \\ 0, & \text{otherwise} \end{cases}$$

Since this sequence is real with no Q component in time domain, the frequency domain I component from the DTFT definition of Eq (3.61) can be expressed as

$$\begin{aligned} I \rightarrow & X_I(e^{j\omega}) = \sum_{n=0}^{N-1} x_I[n] \cos \omega n = \sum_{n=0}^{N-1} \cos \omega n \\ & = \sum_{n=0}^{N-1} \cos \omega n \frac{\sin \frac{\omega}{2}}{\sin \frac{\omega}{2}} \end{aligned} \quad (3.62)$$

where $x_I[n] = 1$ for all n in the first step above. Using the identity $\cos A \sin B = \frac{1}{2}\{\sin(A+B) - \sin(A-B)\}$, we get

$$\begin{aligned} I &\rightarrow X_I(e^{j\omega}) = \frac{1}{2 \sin \frac{\omega}{2}} \sum_{n=0}^{N-1} \left[\sin\left(n + \frac{1}{2}\right) \omega - \sin\left(n - \frac{1}{2}\right) \omega \right] \\ &= \frac{1}{2 \sin \frac{\omega}{2}} \left[\sin\left(N - \frac{1}{2}\right) \omega - \sin\left(-\frac{1}{2}\right) \omega \right] \end{aligned}$$

where only the first and last terms survive and the remaining terms in the summation cancel out (e.g., put $N = 4$ in the top expression above to get the second). Using the same identity as before with $A = (N-1)/2$ and $B = N/2$,

$$\begin{aligned} I &\rightarrow X_I(e^{j\omega}) = \frac{1}{\sin \frac{\omega}{2}} \cos\left(\frac{N-1}{2}\right) \omega \cdot \sin\left(\frac{N}{2}\right) \omega \\ &= \frac{\sin N \frac{\omega}{2}}{\sin \frac{\omega}{2}} \cos\left(\frac{N-1}{2}\right) \omega \end{aligned} \quad (3.63)$$

Similarly, Q component can be found from the DTFT definition as well.

$$Q \rightarrow X_Q(e^{j\omega}) = \sum_{n=0}^{N-1} -x_I[n] \sin \omega n = \sum_{n=0}^{N-1} -\sin \omega n$$

Following the same procedure as I component, and using another identity $\sin A \sin B = \frac{1}{2}\{\cos(A-B) - \cos(A+B)\}$, the Q component of its DTFT is given by

$$Q \rightarrow X_Q(e^{j\omega}) = -\frac{\sin N \frac{\omega}{2}}{\sin \frac{\omega}{2}} \sin\left(\frac{N-1}{2}\right) \omega \quad (3.64)$$

From Eq (3.63) and Eq (3.64), and using $\cos^2 \theta + \sin^2 \theta = 1$, we get the magnitude of the DFT as

$$|X(e^{j\omega})| = \frac{\sin N \frac{\omega}{2}}{\sin \frac{\omega}{2}} \quad (3.65)$$

This is known as a *sinc* signal. A rectangular and a sinc signal are the two most important signals utilized in DSP applications. The magnitude response $|S[k]|$ is drawn in Figure 3.20.

Spatial Sampling

Let us derive the exact relation introduced in Eq (3.8) during the spatial sampling theorem.

- Start with a general reference angle θ_0 to gauge the response with respect to that direction. Directing to a desired angle θ implies adjusting u as

$$u = 2\pi \frac{d}{\lambda} (\sin \theta - \sin \theta_0)$$

- Assuming $\theta_0 \geq 0$, the maximum for $|u|$ occurs at $\theta = -\pi/2$ given by

$$|u|_{\max} = 2\pi \frac{d}{\lambda} (1 + \sin \theta_0)$$

- Eq (3.65) has the spatial counterpart given by

$$AF = \frac{\sin N \frac{u}{2}}{\sin \frac{u}{2}}$$

This tells us that the denominator is zero only at $u = 0$ where the numerator is also zero. This forms the maximum gain that can be found in the limit. However, the position of grating lobe lies where this maximum is reached *again*, i.e., *both* the numerator and the denominator are again zero. This happens for $u = 2\pi$.

- There are no grating lobes as long as $|u|_{\max}$ is less than this value.

$$2\pi \frac{d}{\lambda} \left(1 + \sin \theta_0\right) \leq 2\pi$$

This leads us to the final expression.

$$d \leq \frac{\lambda}{1 + \sin \theta_0} \quad (3.66)$$

Figure 3.49 illustrates this concept for a main lobe that points at $\theta_0 = 30^\circ$ for $N = 32$ antennas at the frequency $F = 60$ GHz. Can you guess the element spacing d just by looking at the figure?

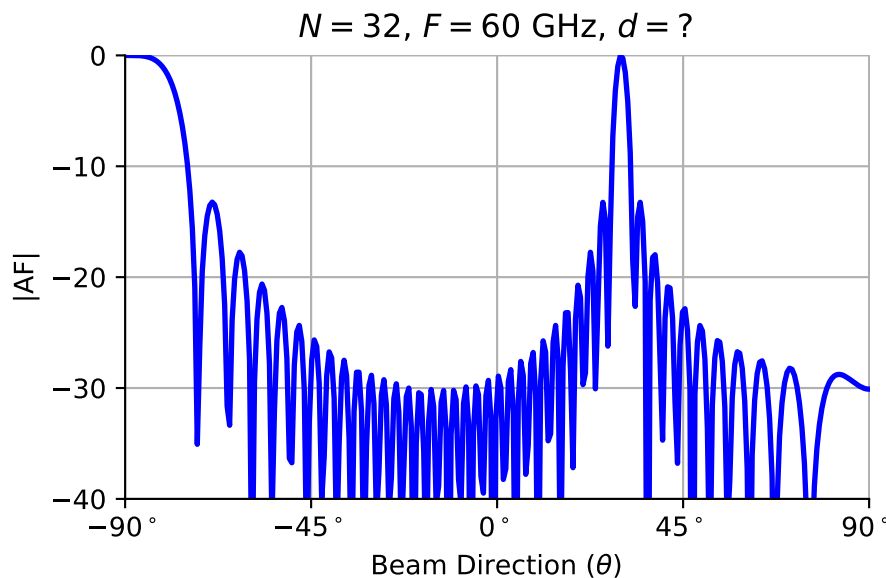


Figure 3.49: The instant a grating lobe starts to appear

Sine the grating lobe has just started to appear at the left edge, the relation in Eq (3.66) is at the boundary, i.e., it satisfies the equality. With $\theta_0 = 30^\circ$, we have

$$d = \frac{\lambda}{1 + \sin(30^\circ)} = 0.67\lambda$$

Average Signal and Noise Power in MRC

During the derivation of optimal weights $w_i = h_i^*$, I ignored the following two factors to keep the expressions simple.

1. A scaling by w_i on the noise samples also occurs because any factor applied to received signal r_i will also impact the noise contained within those samples. Eq (3.39) can now be modified as

$$\begin{aligned} z &= \sum_{i=1}^{N_R} w_i \cdot r_i = \sum_{i=1}^{N_R} w_i \cdot (h_i \cdot s + \text{noise}) \\ &= s \sum_{i=1}^{N_R} w_i \cdot h_i + \sum_{i=1}^{N_R} w_i \cdot \text{noise} \end{aligned} \quad (3.67)$$

2. A normalization factor for each w_i given by

$$w_i = \frac{h_i^*}{\sqrt{\sum_{i=1}^{N_R} |h_i|^2}}$$

needs to be included. The role of this normalization factor is to keep the total power in the output samples the same as in input samples. Remember that this affects both the signal and noise power in the same manner. The advantage, however, is that the detection symbol estimates become independent of the variations in channel gain magnitudes that is necessary for their mapping on the same Rx constellation. A practical and more important benefit is the utilization of full dynamic range of the word lengths offered by the Analog-to-Digital Converter (ADC). With this modification also taken into account, the expression in Eq (3.67) changes as

$$\begin{aligned} z &= s \sum_{i=1}^{N_R} \frac{h_i^*}{\sqrt{\sum_{i=1}^{N_R} |h_i|^2}} \cdot h_i + \underbrace{\sum_{i=1}^{N_R} \frac{h_i^*}{\sqrt{\sum_{i=1}^{N_R} |h_i|^2}} \cdot \text{noise}}_{\text{modified noise}} \\ &= s \frac{\sum_{i=1}^{N_R} |h_i|^2}{\sqrt{\sum_{i=1}^{N_R} |h_i|^2}} + \text{modified noise} = s \underbrace{\sqrt{\sum_{i=1}^{N_R} |h_i|^2}}_{\text{Signal}} + \text{modified noise} \end{aligned} \quad (3.68)$$

Taking into account the above relations, the average signal power is obtained through a squaring and averaging operation.

$$\text{Avg Signal Power} = E_s \cdot \sum_{i=1}^{N_R} \text{Avg } |h_i|^2 = 1 \cdot \sum_{i=1}^{N_R} 1 = N_R$$

where we have assumed unit energy modulation symbols as well as normalized channel gains, see Eq (3.3).

Noise in a single antenna has a power equal to its variance σ^2 . After virtual beamforming, each noise sample in Eq (3.68) has a power given by $(|h_i|^2 / \sum_{i=1}^{N_R} |h_i|^2) \cdot \sigma^2$. Since these samples in space are uncorrelated to each other, the total noise power in N_R samples can be written as

$$\text{Noise Power} = \sum_{i=1}^{N_R} \frac{|h_i|^2}{\sum_{i=1}^{N_R} |h_i|^2} \cdot \sigma^2 = \sigma^2$$

These signal and noise power values help us determine the array gain for the MRC case.

Chapter 4

Massive MIMO



In the spring of 2009, the popular IEEE Vehicular Technology Conference (VTC) was held in Barcelona, Spain. In a panel discussion during this conference titled “Is PHY layer dead?”, several experts from the wireless community explored in great depths whether research on the physical layer (PHY) of wireless communication systems has hit a performance wall and the amount of funding and efforts into this area can be justified through the quantifiable gains from this research. The findings from this discussion were summarized in a paper [6] from which an excerpt is quoted below.

Number of Antennas Approaching Infinity

Hitting the aforementioned performance wall, or approaching it closely enough, the community has accepted the posing and answering of questions that do not relate to exact expressions but rather to bounds and asymptotic operating conditions. For instance, it is natural today to develop mathematical expressions for the cases of SNR approaching zero or *the number of antennas approaching infinity* (emphasis mine). Is PHY research getting lost in asymptopia?

As irony would have it, the very next year Thomas Marzetta from Bell Labs published a paper “Non-cooperative Cellular Wireless with Unlimited Number of Base Station Antennas” [7] which originated the idea of Massive MIMO. In the paper, he theorized that “in the limit of an infinite number of antennas, the effects of uncorrelated noise and fading vanish, throughput and the number of user terminals are independent of the size of the cells, spectral efficiency is independent of the bandwidth and the required transmit energy per bit goes to zero”. Based on these results, he proposed adopting massive MIMO as a desirable direction for 5G systems that implies having 64 or more antennas at the base stations. This is exactly where the standardization went in the coming years.

- The above conclusions seem too good to be true. And that is correct. They are based on simplified assumptions, all of which do not hold in real cellular networks. This is why some discrepancies were found in actual implementations of massive MIMO technology as compared to academic simulations that will be discussed in Section 4.4. Nevertheless, the gains thus obtained were beneficial enough to warrant its adoption in the standard.
- Going into higher mmWave bands (upwards of 24 GHz) also helped massive MIMO achieve traction in the wireless industry. As we explore mmWave communication in Chapter 6, the wavelength at those frequencies is quite small. Since the antenna spacing is directly proportional to the operating wavelength, many more antennas can be packed in the same physical area as compared to sub-6 GHz bands. Therefore, massive MIMO is a natural partner to mmWave communications.

In their book “Fundamentals of Massive MIMO” [8], Marzetta et al. described three timeless

truths in the field of wireless communications. I reproduce those observations below with some relevant remarks.

1. *Demand for wireless throughput, both mobile and fixed, will always increase.*

This reminds me of the exchange between the android David and Dr. Holloway in the great movie Prometheus.

Holloway: What we hoped to achieve was to meet our makers. To get answers. Why they even made us in the first place.

David: Why do you think your people made me?

Holloway: Because we could....



Exchange between android David and Dr. Holloway

A common pattern throughout the human history, including the wireless networks, has been the following: we do many things only because we can. During the development, we are unaware of their long term consequences on this planet in general and life in particular. Fortunately, 5G is the first cellular standard in which energy efficiency was set as one of the major goals and it is expected that future wireless systems will eventually operate in an environmentally sustainable mode.

2. *The quantity of available electromagnetic spectrum will never increase, and most desirable frequency bands that can propagate into buildings and around obstacles and that are unaffected by weather constitute only a small fraction of the entire spectrum.*

This is why low ranges of the spectrum are commonly known as *beachfront spectrum*. In the real-estate market, the property closer to the beach is highly valued and priced accordingly while those willing to own a large farmhouse have to go further inland. On the spectrum side, lower frequencies can easily penetrate the buildings and are largely unaffected by weather but to satisfy demand for

wireless data rate close to wireline communication, a large amount of spectrum is required that is available on the higher side of 30 GHz called mmWave band (actual spectrum allocation starts from 24 GHz). We will discuss mmWave communication in Chapter 6. In addition, there is a lot of research going on towards the next frontier in wireless communications, namely the Tera Hertz band, for 6G standard where the frequencies above 100 GHz are loosely termed as THz frequencies.

3. *Communication theorists and engineers will always be pressured to invent or discover breakthrough technologies that provide higher spectral efficiency.*

While there have been innovations in the wireless field every few years, the truth is that in a cellular network, most of the increase in data rates resulted from wider spectrum and reduced cell sizes. This holds despite the fact that both the wider spectrum and reduced cell sizes directly increase the capital expenditure. The reason behind this is a natural human tendency to spend towards a one-off cost rather than incurring regular overheads. In the adoption of massive MIMO and mmWave systems as well, the trend has been towards spending a larger amount once in terms of hardware and spectrum instead of paying for recurring costs of smart but highly complex signal processing algorithms. In a way, it is similar to purchasing versus leasing a car where most people prefer to pay more upfront and buy the product once rather than incurring regular costs of a lease in the foreseeable future. It will be interesting to see if and when this trend can be broken.

Next we discuss the idea behind multi-user MIMO before moving towards massive MIMO [8].

4.1 Multi-User MIMO

At the end of Chapter 3, we discussed how multiple users in the network, e.g., in a cell, can simultaneously communicate with a base station equipped with an antenna array. This is known as a Multi-User MIMO (MU-MIMO). For efficiency reason, it is desirable to keep the user terminals simple from both hardware and signal processing perspectives while assigning the cost and complexity of both the hardware and signal processing to the base station with multiple antennas. This idea behind MU-MIMO forms the basis for massive MIMO later. Since the users are geographically separated, their flat fading channel gains or spatial signatures are different from each other. This can be exploited by the base station array to generate multiple streams directed towards the users in an individual manner. This is also sometimes called Space Division Multiple Access (SDMA). MU-MIMO has long been used in satellite communications. Since the terminals on ground have Line-of-Sight (LoS) paths to the satellite, there is hardly any scattering or angle spread. Therefore, the satellite can communicate simultaneously with multiple well-separated users through physical beamforming described in Section 3.3.

In a cellular network setting, a single base station equipped with N_B antennas[†] serves K user

[†]In a cellular scenario, I am not denoting the number of antennas at the base station with N_T because it has to both send and receive the signals.

terminals, each of which consists of one or more antennas. In both downlink and uplink settings below, we ignore the power control coefficient for keeping the mathematical expressions simple.

- A block diagram of a multi-user MIMO system in a downlink setup is shown in Figure 4.1a. Data streams for each user are available at the base station that implements a precoding algorithm (similar to what we studied in generalized beamforming) by summing the weighted signals over K users before transmitting the output signal from its N_B antennas. This precoding requires Channel State Information (CSI) availability at the base station.
- On the uplink shown in Figure 4.1b, K users can transmit their data during the same time and frequency with no multiuser signal processing. The base station with N_B antennas can use the CSI to separate each data stream from the cumulative signal using advanced signal processing algorithms.

Benefits and Drawbacks

A multi-user MIMO system offers some advantages as well as some drawbacks as follows. There are two main benefits of this approach.

- Customer terminals with a few antennas are simple in terms of hardware complexity, battery life and cost.
- We will see in Chapter 5 that a rich scattering channel supports multiple data streams from multiple antennas. In most cases, multi-user MIMO automatically satisfies the rich scattering environment assumption for spatially multiplexing individual streams because the user terminals are geographically scattered around the cell.

On the other hand, the drawbacks are as follows.

- While the hardware complexity is avoided in simple terminals, signal processing complexity at the user end still remains. For instance, users need to implement computationally intense detection algorithms (e.g., successive interference cancellation described in Chapter 5). This puts a drain on power budget of the user equipment.
- Not only the base station but each user must also know the channel coefficients for decoding the data in the downlink transmission. This reduces the spectral efficiency as several pilot symbols need to be allocated for this purpose in each direction! This is why Figure 4.1a shows CSI requirement at the terminals as well as the decoding procedure.

This leads us towards the massive MIMO concept.

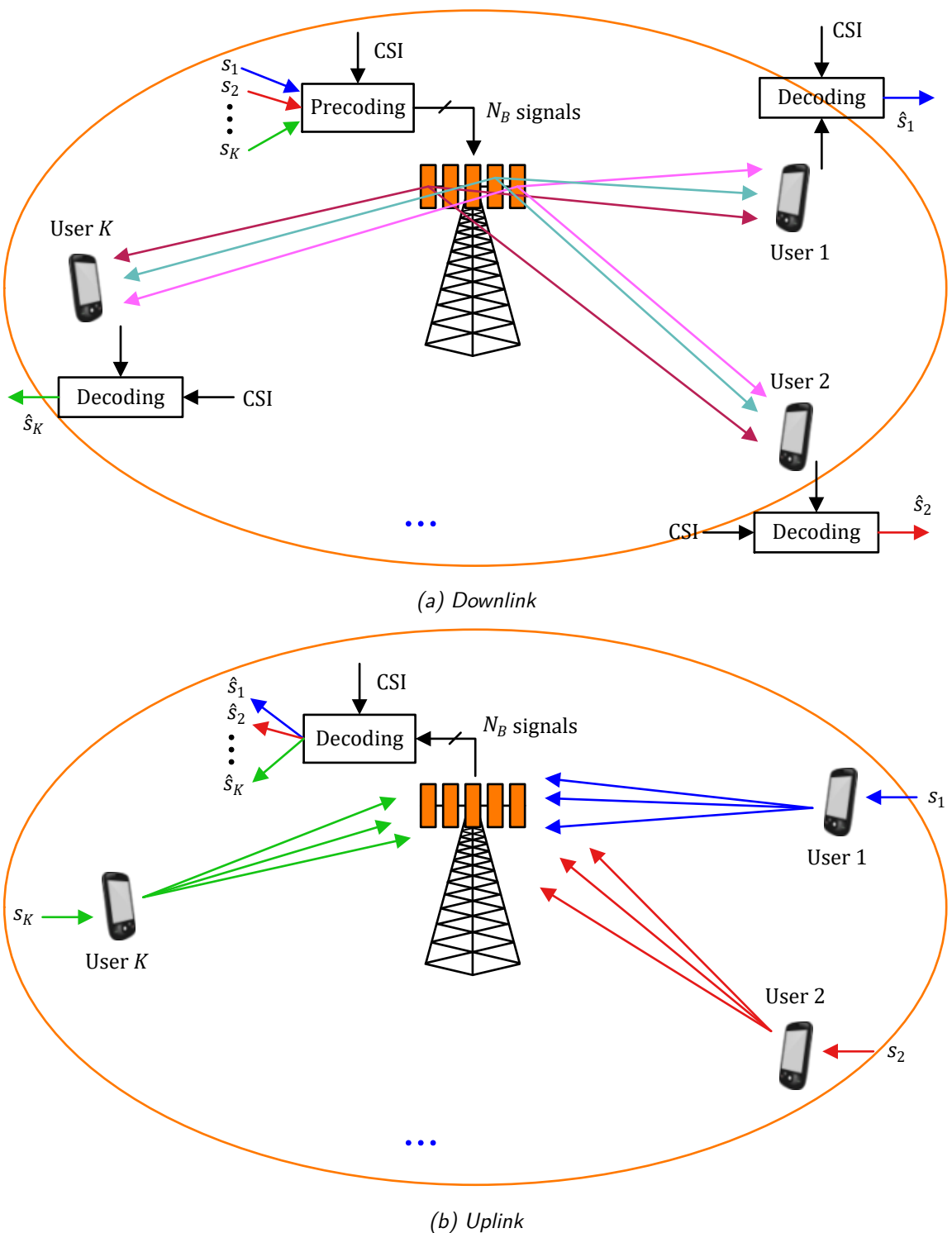


Figure 4.1: Downlink and uplink for a multi-user MIMO system; CSI = Channel State Information

4.2 Massive MIMO

The limitations of multi-user MIMO can be overcome in a massive MIMO setup. A base station with a large number of antennas N_B serves a large number of terminals K , each of which has at most a few antennas. In his original paper Ref. [7], Thomas Marzetta considered a base station with an unlimited number of antennas with single antenna user terminals. Nevertheless, mobile devices can also have multiple antennas but this number depends on the frequency of operation. In sub-6 GHz band, the wavelengths are large (on the order of several centimeters) and since antenna spacing is a function of the wavelength, there is a limit to which antennas can be packed in the small form factor of mobile devices. On the other hand, mmWave frequencies covered in Chapter 6 allow a relatively large number of antennas in the handsets as well.

The block diagram for such massive MIMO systems is shown in Figure 4.2a and Figure 4.2b for downlink and uplink scenarios, respectively. On both uplink and downlink, every transmission utilizes all the available time and frequency resources. However, base station with its large number of antennas is responsible for extracting the user information on the uplink while directing the intended signal towards them on the downlink either through physical or virtual beamforming. This is accomplished with the help of available Channel State Information (CSI) as described before. This possession of CSI at the base station, along with the large number of antennas, enables it to run signal processing algorithms for multiplexing and demultiplexing purposes.

While a massive MIMO system shares many of the features with a multi-user MIMO system described before, there are a few distinguishing features as follows.

- Observe from the block diagrams that the number of base station antennas N_B is much larger than the number of users K .
- The asymmetry between N_B and K facilitates simple linear processing at both the downlink and the uplink, as opposed to complex signal processing algorithms required for data detection in multi-user MIMO systems.
- Ideally, the user terminals do not have to learn about the channel coefficients to decode their data streams. It is sufficient for the CSI to be available at the base station only. Later in Section 4.4, we will describe in detail the available modes of operation.
- While the idea was originally conceived for sub-6 GHz range, massive MIMO is even more important for mmWave systems discussed in Chapter 6 where the frequency span is from 30 to 300 GHz. This is because a smaller wavelength enables a large number of antennas to be integrated with the radio that provide significant Tx/Rx gains to help close the link.

Having covered the main reasons behind adoption of massive MIMO in 5G systems, we explore how such an asymmetric arrangement provides the above mentioned solutions for signal detection.

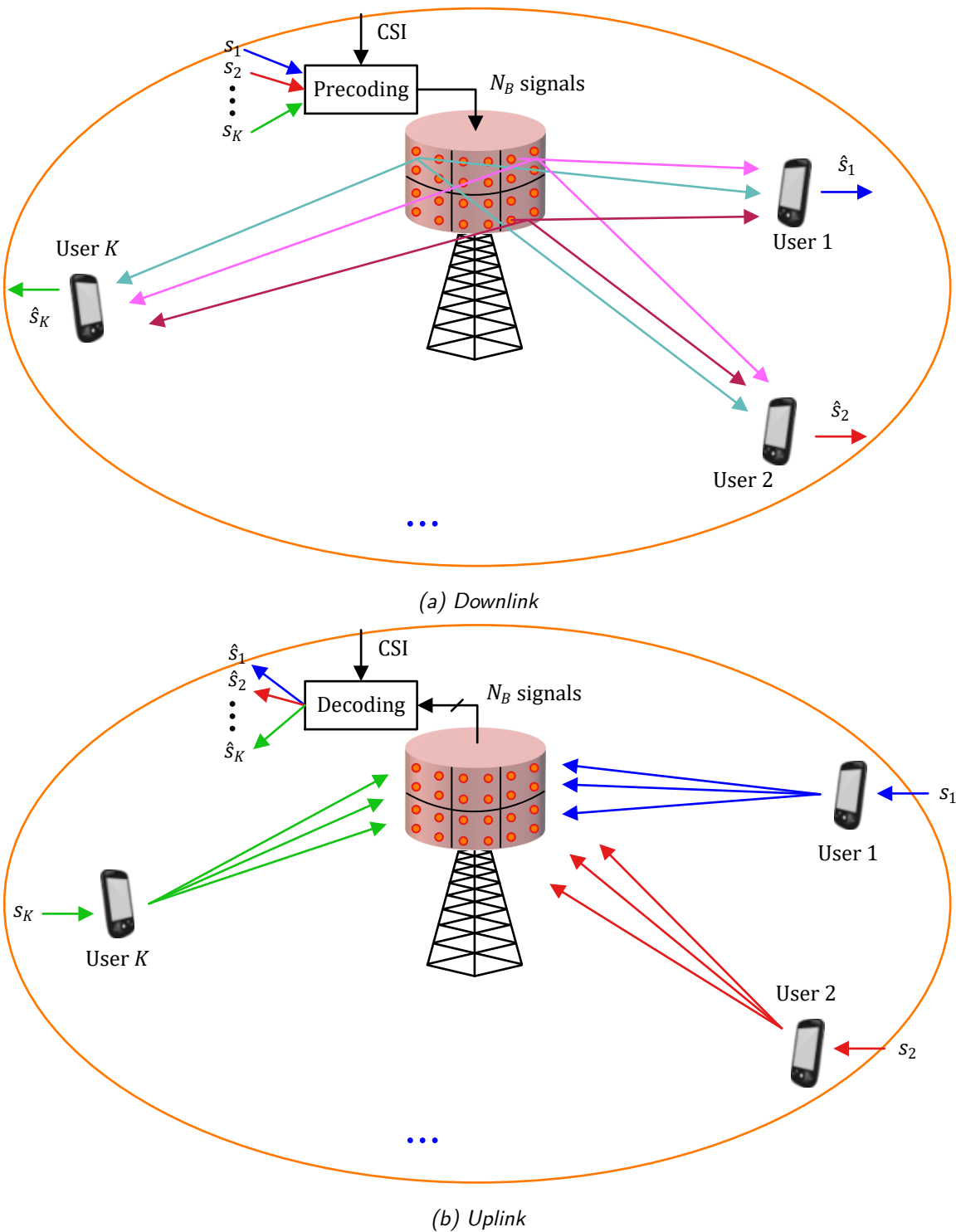


Figure 4.2: Downlink and uplink for a massive MIMO system; CSI = Channel State Information

4.3 Detection Algorithms

One of the most attractive features of massive MIMO is that simple linear algorithms can be employed for detecting the transmitted signal that translates into a significant reduction of computational load at the base station. This is what we pointed out earlier as well: a tendency to spend more upfront in terms of hardware and components instead of incurring repeated costs of computationally complex signal processing algorithms. Let us see how this can be accomplished.

Consider again Figure 4.2b that depicts an uplink massive MIMO setup. It is evident that the cumulative signal at each base station antenna j is a summation of signals arriving from each user terminal i . These signals are composed of individual modulation symbols s_1, s_2, \dots, s_K .

$$r_j = h_{(1 \rightarrow j)} \cdot s_1 + h_{(2 \rightarrow j)} \cdot s_2 + \dots + h_{(K \rightarrow j)} \cdot s_K + \text{noise}, \quad j = 1, 2, \dots, N_B \quad (4.1)$$

where the flat fading channel gain between i -th user terminal ($i = 1, 2, \dots, K$) and j -th base station antenna ($j = 1, 2, \dots, N_B$) is denoted by $h_{(i \rightarrow j)}$. As in Chapter 3, power control is ignored here for simplicity. The reader should keep in mind that power control is important in cellular systems to prevent signals from users with strong channels drowning the signals coming from users with weak channels. However, power control coefficients depend on large-scaling fading that renders them independent of both frequency and fast update rates.

The main task of the detection algorithms here is to free each modulation symbol s_i sent by a user terminal i from the interference of the other modulation symbols sent by rest of the mobile users. We explore these ideas next.

4.3.1 Spatial Matched Filtering (Maximum Ratio)

The simplest of linear processing techniques is spatial matched filtering, also known as conjugate beam-forming, which are other terms used for maximum ratio combining or transmission covered in Chapter 3. To understand the idea, let us consider the detection process through the perspective of mobile user 1. Eq (4.1) tells us that the original signal received at the base station is not coming from terminal 1 alone! Instead, all user terminals transmit simultaneously on the uplink and hence the cumulative signal r_j at each antenna j is a superposition of signals from K terminals. As a result, interference from $K - 1$ users is added to the desired signal.

Detection Process

Due to the large number of antennas, Figure 4.3 is drawn to avoid any confusion between the input to the detection algorithm and the desired output. We have the received signals r_j at N_B antennas as the input and an estimate of its modulation symbol \hat{s}_1 as the desired output for user 1.

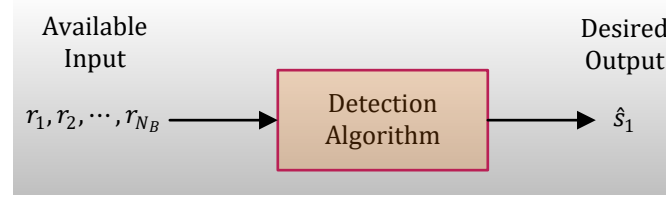


Figure 4.3: Available inputs r_1, r_2, \dots, r_{N_B} and desired output \hat{s}_1 at the base station from the perspective of user 1

Assume that perfect channel estimates $h_{(i \rightarrow j)}$ are available at the base station. Also, the decoding vector for a specific terminal, say user 1, consists of weights $w_{1,j}$ that are complex conjugates of $h_{(1 \rightarrow j)}$ (the channel gain from the single antenna of terminal 1 to the base station antenna j).

$$w_{1,j} = h_{(1 \rightarrow j)}^*, \quad j = 1, 2, \dots, N_B$$

What happens when we apply these weights $w_{1,j}$ to the available inputs r_1, r_2, \dots, r_{N_B} ? Let us explore this scenario for the signal at the first base station antenna given by r_1 as illustrated in Figure 4.4 which only shows the signal r_1 received at the first base station antenna. Similar receptions for other antennas are not plotted to keep the figure clear.

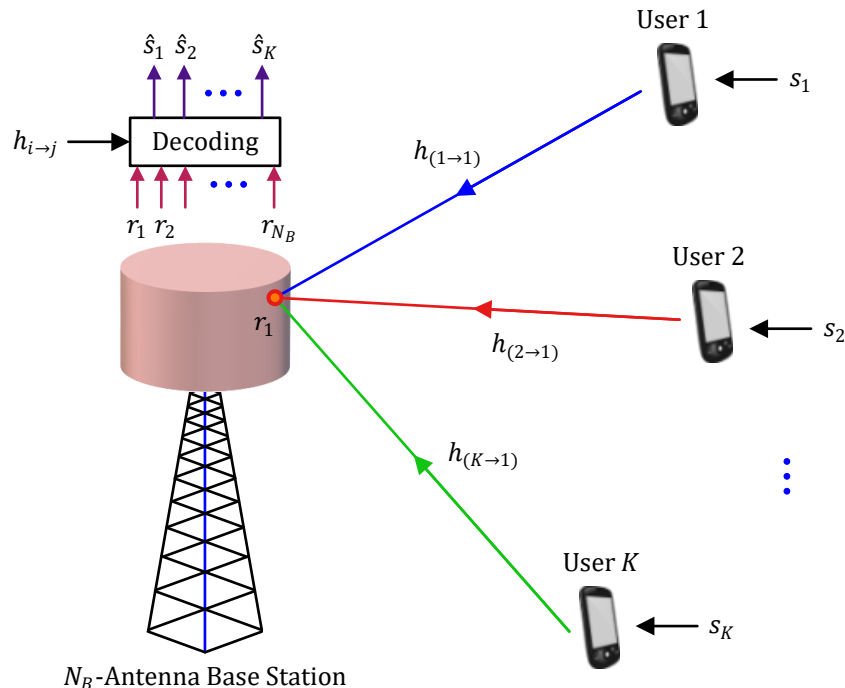


Figure 4.4: Uplink of a massive MIMO cell where received signal is shown at only first base station antenna for clarity

From Eq (4.1),

$$r_1 = h_{(1 \rightarrow 1)} \cdot s_1 + h_{(2 \rightarrow 1)} \cdot s_2 + \cdots + h_{(K \rightarrow 1)} \cdot s_K + \text{noise}$$

After multiplying this with $w_{1,1} = h_{(1 \rightarrow 1)}^*$, we get

$$\begin{aligned} h_{(1 \rightarrow 1)}^* \cdot r_1 &= h_{(1 \rightarrow 1)}^* \cdot h_{(1 \rightarrow 1)} \cdot s_1 + h_{(1 \rightarrow 1)}^* \cdot h_{(2 \rightarrow 1)} \cdot s_2 + \cdots + h_{(1 \rightarrow 1)}^* \cdot h_{(K \rightarrow 1)} \cdot s_K + \text{noise} \\ &= \underbrace{|h_{(1 \rightarrow 1)}|^2 \cdot s_1}_{\text{Desired Signal}} + \underbrace{\sum_{i=2}^K h_{(1 \rightarrow 1)}^* \cdot h_{(i \rightarrow 1)} \cdot s_i}_{\text{Interference}} + \text{noise} \end{aligned} \quad (4.2)$$

Notice that the above summation in the interference part is with respect to user terminals i , not base station antennas j . Also keep in mind that r_1 is simply the first antenna at the base station which has no relation to user 1. Instead, we eventually take the outputs from all N_B antennas. For instance, a similar equation at antenna $j = 2$ can be written as

$$\begin{aligned} h_{(1 \rightarrow 2)}^* \cdot r_2 &= h_{(1 \rightarrow 2)}^* \cdot h_{(1 \rightarrow 2)} \cdot s_1 + h_{(1 \rightarrow 2)}^* \cdot h_{(2 \rightarrow 2)} \cdot s_2 + \cdots + h_{(1 \rightarrow 2)}^* \cdot h_{(K \rightarrow 2)} \cdot s_K + \text{noise} \\ &= \underbrace{|h_{(1 \rightarrow 2)}|^2 \cdot s_1}_{\text{Desired Signal}} + \underbrace{\sum_{i=2}^K h_{(1 \rightarrow 2)}^* \cdot h_{(i \rightarrow 2)} \cdot s_i}_{\text{Interference}} + \text{noise} \end{aligned} \quad (4.3)$$

What happens when we average the weighted outputs from all N_B antennas?

- Imagine a vertical summation on the left side of Eq (4.2) and Eq (4.3). The average operation on these terms yields

$$\begin{aligned} \text{L.H.S.} &= \frac{1}{N_B} \left\{ h_{(1 \rightarrow 1)}^* \cdot r_1 + h_{(1 \rightarrow 2)}^* \cdot r_2 + \cdots + h_{(1 \rightarrow N_B)}^* \cdot r_{N_B} \right\} \\ &= \frac{1}{N_B} \sum_{j=1}^{N_B} h_{(1 \rightarrow j)}^* \cdot r_j \end{aligned} \quad (4.4)$$

- Imagine a vertical summation on the right side of Eq (4.2) and Eq (4.3). The average operation then gives the desired signal and interference[†] as

$$\text{R.H.S.} = \frac{1}{N_B} \sum_{j=1}^{N_B} \left\{ \underbrace{|h_{(1 \rightarrow j)}|^2 s_1}_{\text{Desired Signal}} + \underbrace{\sum_{i=2}^K h_{(1 \rightarrow j)}^* \cdot h_{(i \rightarrow j)} s_i}_{\text{Interference}} \right\} \quad (4.5)$$

These operations are illustrated in Figure 4.5. While the figure looks complicated, you can follow the expressions above to understand this block diagram.

Next, the impact of this combination on the desired signal and the interference part can now be investigated as follows.

[†]The interference part from Eq (4.2) and Eq (4.3) is

$$\begin{aligned} \text{Interference} &= \frac{1}{N_B} \left\{ \sum_{i=2}^K h_{(1 \rightarrow 1)}^* \cdot h_{(i \rightarrow 1)} \cdot s_i + \sum_{i=2}^K h_{(1 \rightarrow 2)}^* \cdot h_{(i \rightarrow 2)} \cdot s_i + \cdots + \sum_{i=2}^K h_{(1 \rightarrow N_B)}^* \cdot h_{(i \rightarrow N_B)} \cdot s_i \right\} \\ &= \frac{1}{N_B} \sum_{j=1}^{N_B} \sum_{i=2}^K h_{(1 \rightarrow j)}^* \cdot h_{(i \rightarrow j)} s_i \end{aligned}$$

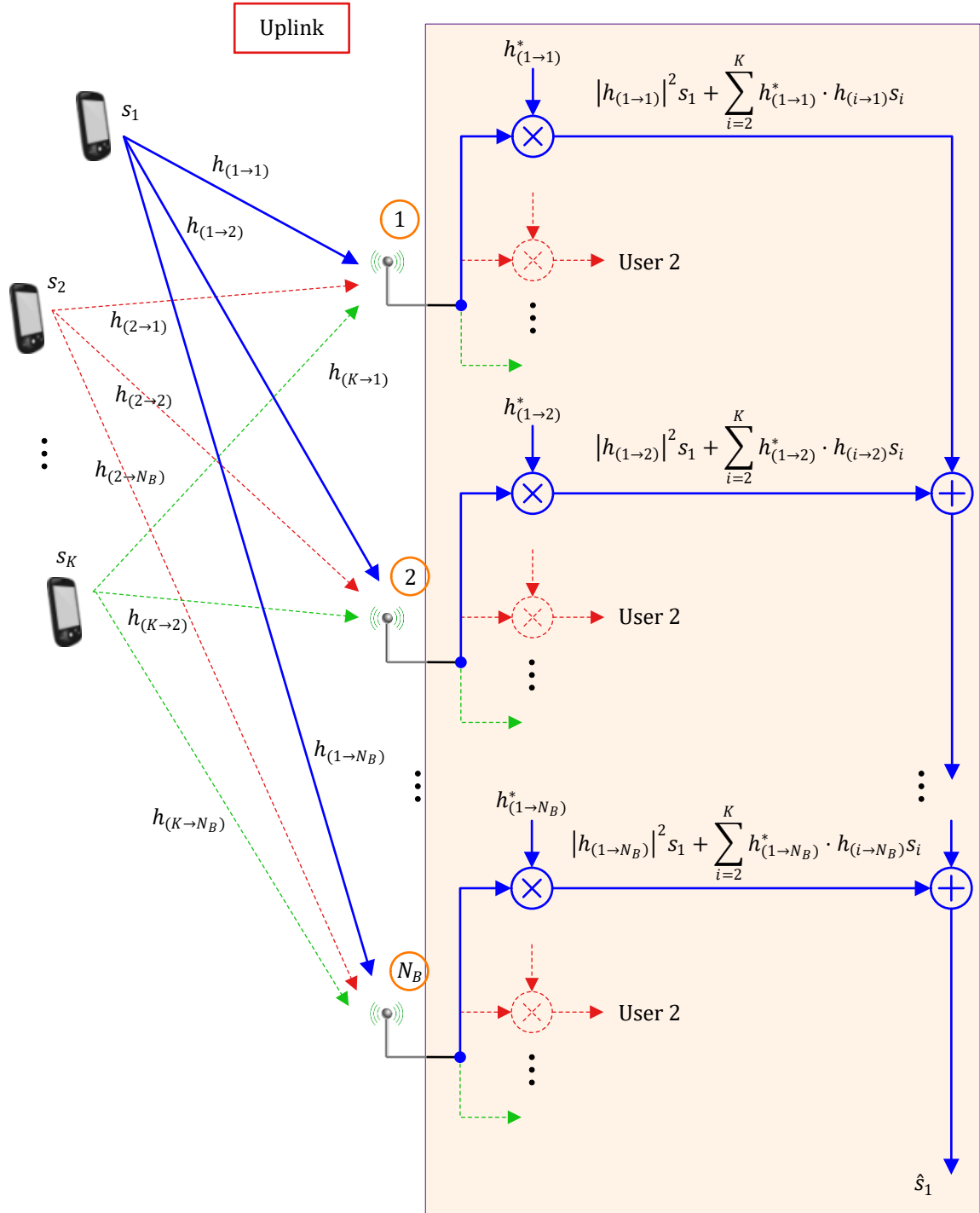


Figure 4.5: Signal processing for desired output \hat{s}_1 at the base station from the perspective of user 1

Channel Hardening

From Eq (4.5), the sum of the weighted outputs from all antennas yields the desired signal part in the first term as

$$\text{Desired Signal} = \frac{1}{N_B} \sum_{j=1}^{N_B} |h_{(1 \rightarrow j)}|^2 \cdot s_1 \quad (4.6)$$

$$\approx s_1 \quad \text{for large } N_B \quad (4.7)$$

Both of the above two steps require some explanation.

- Eq (4.6): With proper weighting, notice that the effective channel from terminal 1 at the output of the decoder becomes $\sum_{j=1}^{N_B} |h_{(1 \rightarrow j)}|^2$. As found in Section 3.4.1, the above expression is the Maximum Ratio Combining (MRC) or virtual beamforming towards all N_B antennas from the intended user 1 that aligns the phases and grades the magnitudes for each channel. This gain and phase matching according to the channel gains from user 1 maximizes the signal power accumulated from that particular transmission. And that is why it is also known as *spatial matched filtering* in the context of massive MIMO detection.
- Eq (4.7): When the base station has a large number of antennas N_B , we get

$$\frac{1}{N_B} \sum_{j=1}^{N_B} |h_{(1 \rightarrow j)}|^2 \rightarrow \text{Avg} \left\{ |h_{(1 \rightarrow j)}|^2 \right\} \rightarrow 1 \quad (4.8)$$

where we have assumed normalized channel gains, see Eq (3.3). By virtue of the law of large numbers, summing a large number of channel gains on the left side generates the arithmetic mean or average value over those gains that is a constant number. This is exactly what we saw in Eq (3.55) before in the context of maximum diversity gain. This phenomenon is known as *channel hardening*.

Massive MIMO benefits from channel hardening because it simplifies the signal processing and resource allocation at the base station. Looking back at Eq (4.8), observe that there is very little fluctuation in the cumulative channel from each terminal at the base station as this expression mostly converges towards a constant value (while this is shown as 1 here, the actual value depends on large-scale fading). The channel hardening idea is illustrated in Figure 4.6. The signal received at each antenna undergoes small-scale fading and fluctuates rapidly over a short time interval. This is due to the multipath nature of the channel described in detail in Chapter 2. However, the combined signal starts to smooth out when inputs at multiple antennas are taken into account. In MU-MIMO case at the top of this figure, the channel variations, though reduced, are still visible. On the other hand, the massive MIMO setup at the bottom of this figure plots the combined signal from a large number of antennas and shows no signs of rapid fluctuations.

The benefits achieved through channel hardening in a massive MIMO system are as follows.

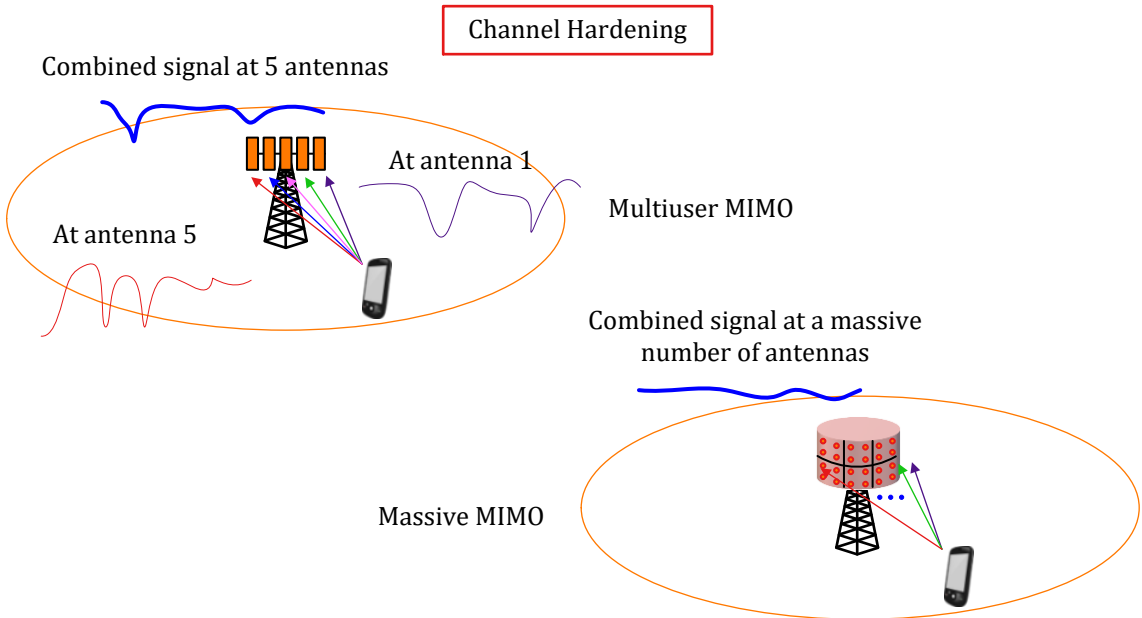


Figure 4.6: Channel hardening implies the channel fluctuations due to small-scale fading smooth out

Fading Vanishes

A constant output or the absence of channel fluctuations in time implies that the small-scale fading practically disappears! In other words, such an ideal system provides average SNR all the time as instantaneous SNR. It comes from an extreme case of the Inverse Anna Karenina Principle of Section 2.3.2 in Eq (2.18).

$$P(\text{success}) = 1 - P(\text{failure}) = 1 - p^L \rightarrow 1$$

With a large L , the probability of success goes to 1 since $0 < p < 1$. As a consequence, a Rayleigh fading channel is transformed into more like an AWGN one and several tens of dB more SNR theoretically required to cover the BER performance gap between AWGN and fading channels is reclaimed. In addition, this phenomenon enables a significant reduction of latency on the air interface because fading is the major bottleneck in building low-latency wireless networks.

Frequency Independence

Since the effective channel reduces to a constant value, there is no more frequency dependence for the channel gains. To understand this idea, recall from Eq (2.9) that channel delay spread is determined by the last and first most significant paths. Considering the downlink case, the precoding weights compensate for the time delays for narrowband signals (an idea we covered in Chapter 3). Consequently, the delay spread is compensated for by the base station through precoding before the transmission and the effective channel impulse response reduces to a single tap. In frequency domain, a small delay spared gives rise to a large coherence bandwidth and the

flat channel becomes deterministic with respect to small variations. A similar effect is observed through combining after the reception on the uplink.

Uniformly Good Service

In 4G (and previous generations of cellular networks), resource allocation was not a straightforward task since different users face different channel conditions as a function of frequency and a suitable modulation and coding scheme is selected accordingly (e.g., for each subcarrier in OFDM case). This is shown in Figure 4.7 where each subcarrier in an OFDM system encounters a different level of channel fade.

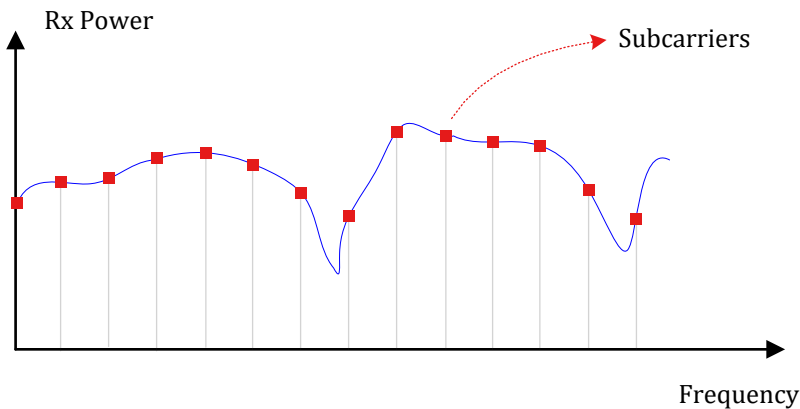


Figure 4.7: Channel conditions vary with frequency

A huge implication of the frequency independence in massive MIMO is the simplification of the multiple access strategy. It becomes possible for the base station to provide uniformly good service to all users in a simultaneous manner through large-scale fading power control. A uniformly good service simplifies not only resource allocation but also the signal processing complexity which we describe in the next section.

Channel Code

The role of a channel code in digital communication systems is to protect the data against noise and interference at the Rx with the purpose of avoiding retransmissions of the same information. Different strategies are applied for designing a channel code for a wireless channel as compared to a simple AWGN channel. One consequence of the above channel transformation is that standard modulation and coding schemes designed for AWGN also work well with the fading channels. We explore one such scheme, known as Low Density Parity Check (LDPC) codes, in Chapter 7.

Channel Estimation

From a theoretical viewpoint, due to channel hardening, channel estimation at the terminals is mostly not required for signal detection because the receiver only needs the statistical knowledge of the channel gains (instead of their instantaneous values) from large-scale fading. This eliminates

the need for downlink pilots transmission and saves power and training duration otherwise needed for channel estimation. Later, we will see that this is an oversimplification that does not hold in many circumstances.

Interference

From Eq (4.5), the interference part that comes from the sum of weighted outputs from all antennas yields

$$\text{Interference} = \sum_{i=2}^K \underbrace{\frac{1}{N_B} \sum_{j=1}^{N_B} h_{(1 \rightarrow j)}^* \cdot h_{(i \rightarrow j)} \cdot s_i}_{\rightarrow 0 \text{ for large } N_B} \quad (4.9)$$

$$\rightarrow 0 \quad (4.10)$$

The last expression $\frac{1}{N_B} \sum_{j=1}^{N_B} h_{(1 \rightarrow j)}^* \cdot h_{(i \rightarrow j)}$ goes to zero[†] because

- each factor $h_{(i \rightarrow j)}$ including $h_{(1 \rightarrow j)}$ is a complex random variable with a zero mean, and
- averaging the product of a large number of such random variables makes the numerator grow slower ($\sqrt{N_B}$ for Gaussian distribution) than the denominator N_B and hence the expression converges towards zero.

This is known as *asymptotic favorable propagation* exhibited by real wireless channels in which such a sum of products goes to zero when normalized with the number of base station antennas N_B . That then holds true even when the fading channel coefficients assume any non-Gaussian distribution as well. In academic works, however, using *strictly favorable propagation* without any normalization with N_B is more common due to its analytical tractability. In any case, favorable propagation is how massive MIMO achieves user separation in a cell through identifying their different spatial signatures

Favorable Propagation

Eq (4.8) and Eq (4.9) can now be combined into a single expression for a user i' as

$$\frac{1}{N_B} \sum_{j=1}^{N_B} h_{i' \rightarrow j}^* \cdot h_{(i \rightarrow j)} \rightarrow \begin{cases} 1, & i' = i \\ 0, & \text{otherwise} \end{cases} \quad (4.11)$$

where we have used the fact that $h_{(i \rightarrow j)}^* \cdot h_{(i \rightarrow j)} = |h_{(i \rightarrow j)}|^2$ which was normalized to 1 in Eq (3.3) before. In words, favorable propagation means

[†]Keep in mind that while the above expressions are written for user 1, this is true for all other users as well.

that user transmissions in the presence of decoding and precoding vectors virtually act as if each terminal is communicating alone with the base station, an idea known as orthogonality. This helps separating the users in spatial domain despite the fact that they share all the available time and frequency resources.

Finally, combining the left and right hand expressions in Eq (4.4) and Eq (4.5), the estimate at the base station with respect to user 1 data generates the output

$$\hat{s}_1 = \frac{1}{N_B} \sum_{j=1}^{N_B} h_{(1 \rightarrow j)}^* \cdot r_j$$

which is a simple linear expression! This is largely due to channel hardening and favorable propagation. This is why simple linear processing on signals can (ideally) achieve nearly optimal performance in a massive MIMO system.

On the uplink, a simple matched filter or maximum ratio combining (in the form of proper decoding vectors as described above) can overcome noise and interference for signal detection. Here, the signal model becomes multi-dimensional as

$$\mathbf{r} = \mathbf{H} \cdot \mathbf{s} + \text{noise}$$

where \mathbf{r} is a vector of received samples r_j , \mathbf{H} is a matrix whose entries $h_{(i \rightarrow j)}$ are channel gains from user i to antenna j and \mathbf{s} is the vector of modulation symbols s_1, s_2, \dots, s_K . Just like we multiplied the samples r_j with $h_{(1 \rightarrow j)}$ for user 1, the decoding vectors for all K users can be combined into an $N_B \times K$ matrix \mathbf{H} . The matched filter detector can thus be written as

$$\hat{\mathbf{s}} = \mathbf{H}^* \mathbf{r} \quad (4.12)$$

where \mathbf{H}^* here represents both a transpose and a conjugate operation[†] on channel matrix \mathbf{H} .

As far as the downlink is concerned, a similar *precoding* vector for each user enables the base station to beamform multiple data streams to all user terminals without causing significant mutual interference among them. Instead of deriving the relations, a block diagram from a signal processing perspective is drawn in Figure 4.8. The mobile terminal does not have to carry out the decoding part as the summation in the term \hat{s}_1 is automatically done by nature at the Rx antenna. This is very important in a multiuser system since the individual users do not have any information about channel gains of others and hence cannot suppress their interference.

In summary, with the help of channel hardening and favorable propagation, massive MIMO effectively creates dedicated virtual pipes between a base station and its terminals where the frequency independent channel can be simply determined through large scale fading and power control.

[†]Technically, both transpose and conjugate are incorporated as \mathbf{H}^H known as the Hermitian of a matrix but I preferred to avoid including another mathematical operation.

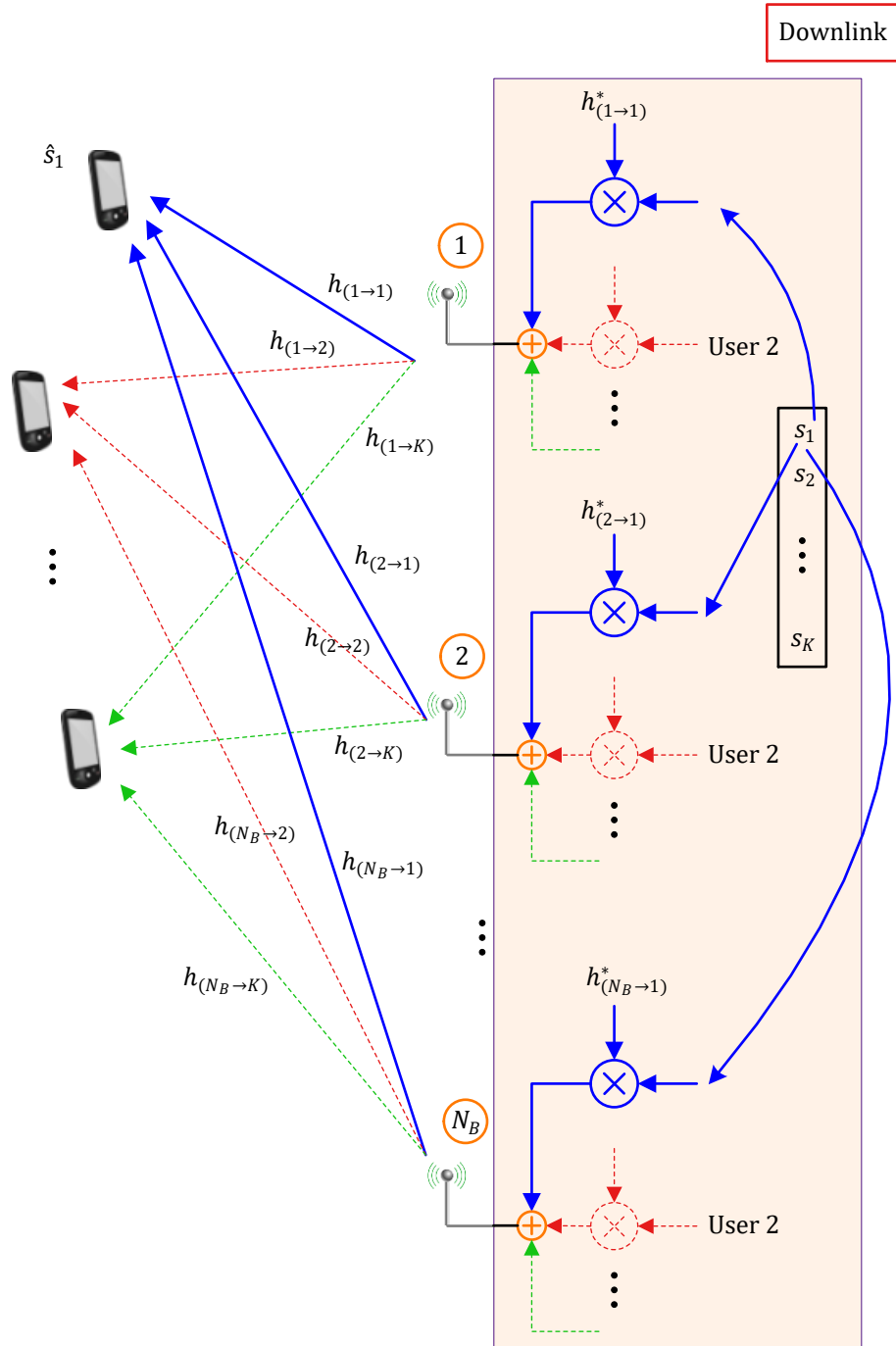


Figure 4.8: Signal processing for desired output \hat{s}_1 at the base station from the perspective of user 1

4.3.2 Zero-Forcing (ZF)

Notice that the favorable propagation scenario described in Eq (4.11) is approximately true and the relation is not exact. Hence, low amounts of interference from other terminals can still leak into the desired signal causing a degradation in performance. Our goal here is to make up for that performance loss without incurring significant computational complexity. Zero-Forcing (ZF) algorithm provides that solution which is slightly more complex than matched filtering but compensates for the performance loss at the same time.

A proper derivation of Zero-Forcing solution requires dealing with matrices since K user terminals communicate with N_B base station antennas on the uplink. All that data combined results in an $N_B \times K$ matrix of channel gains. However, I will present a simpler scalar derivation that illustrates the basic concept.

A Single Antenna System

As a graduate student in United States, one imperfect trick I often employed was to see the results from a single parameter viewpoint and simply generalize the result into a matrix formulation. Let us apply this trick to understand the general Zero-Forcing philosophy.

For a system with a single antenna *both* at the Tx and the Rx, we can write the received signal as

$$r = h \cdot s + \text{noise} \quad (4.13)$$

where s is the modulation symbol sent and h is the flat fading channel gain. As we learned in Section 3.4.1 during the derivation of MRC, the optimal strategy at the Rx is to multiply the incoming signal with a weight $w = h^*$ that has the same magnitude but an opposite phase to the channel gain. Moreover, a scaling factor in proportion to the gain magnitude $|h|^2$ is included to normalize the results. The final expression turns out to be $h^*/|h|^2$. This was the essence of virtual beamforming. Since $|h|^2 = h^* \cdot h$, we have

$$\frac{h^*}{h^* \cdot h} \cdot r = \frac{h^*}{h^* \cdot h} (h \cdot s + \text{noise}) = s + \frac{h^*}{|h|^2} \cdot \text{noise} \quad (4.14)$$

Thus, the symbol estimate \hat{s} can be expressed from left side as

$$\hat{s} = \frac{h^*}{h^* \cdot h} \cdot r = (h^* \cdot h)^{-1} h^* \cdot r \quad (4.15)$$

This relation will help lead us towards a general solution. Before that, we address the problem of estimation with multiple observations.

Computing the Slope of a Straight Line

Consider what should have been a straight line $y_j = m \cdot x_j$ where y_j are the set of received data points and x_j is the unknown parameter to be estimated. In the presence of noise, the received points y are

scattered around as shown in Figure 4.9. There are several lines with slopes m that can be fit through the points y_j but one of them is the best in some sense. Our task is to find a line through this set of points y_j that forms the best fit. Some of the candidates are also drawn in the same figure.

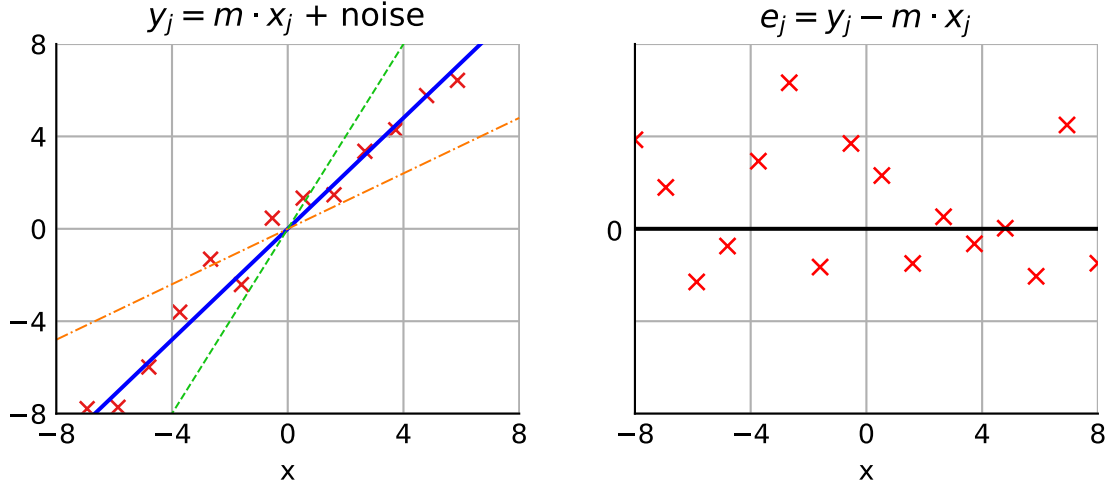


Figure 4.9: A graph of a straight line $y_j = m \cdot x_j$ along with the error samples in the presence of noise

We start with plotting the error $e_j = y_j - m \cdot x_j$ on the right side of Figure 4.9. Since the noise is Gaussian, the error samples e_j assume both positive and negative values. Owing to this bipolarity, one criterion to find the best fit line is by minimizing the total absolute value squared of the error samples $\sum_j |e_j|^2$. This criterion is known as the *Least Squares (LS)* solution. Let us find out where it leads.

$$\min \sum_j |e_j|^2 = \min \sum_j (y_j - m \cdot x_j)^2$$

The above function forms a parabola which has a unique minimum. This function can be minimized by taking the first derivative and equating it to zero. This first derivative is given by

$$\sum_j \frac{d}{dm} (y_j - m \cdot x_j)^2 = \sum_j 2(y_j - m \cdot x_j)(-x_j) = -2 \sum_j x_j \cdot y_j + 2m \sum_j x_j^2$$

Equating it to zero to find the minimum gives

$$-2 \sum_j x_j \cdot y_j + 2m \sum_j x_j^2 = 0 \quad \Rightarrow \quad \hat{m} = \frac{1}{\sum_j x_j^2} \sum_j x_j \cdot y_j \quad (4.16)$$

This is known as the linear least squares solution because it minimizes the sum of squared absolute values of the error terms.

A Single User in a Cell

Turning to our problem, assume that there was only a single terminal in the cell that communicates with all the base station antennas (i.e., there is no interference) such that the channel gains from that

user, say 1, to receive antenna j is $h_{(1 \rightarrow j)}$. With its modulation symbol denoted by s_1 , the received signal r_j at antenna j can be written as

$$r_j = s_1 \cdot h_{(1 \rightarrow j)} + \text{noise}, \quad j = 1, 2, \dots, N_B$$

Comparing with the linear equation $y_j = m \cdot x_j$, we have the following corresponding parameters.

$$\begin{aligned} y_j &\longrightarrow r_j \\ m &\longrightarrow s_1 \\ x_j &\longrightarrow h_{(1 \rightarrow j)} \end{aligned}$$

From Eq (4.16), the solution \hat{s}_1 can be correspondingly written as

$$\hat{s}_1 = \frac{1}{\sum_j |h_{(1 \rightarrow j)}|^2} \sum_j h_{(1 \rightarrow j)}^* \cdot r_j$$

The two differences from the straight line solution, i.e., the absolute value squared and conjugate operation, appear because $h_{(1 \rightarrow j)}$ is a complex number (the fading channel coefficient). Since $|h_{(1 \rightarrow j)}|^2 = h_{(1 \rightarrow j)}^* \cdot h_{(1 \rightarrow j)}$, we can write

$$\hat{s}_1 = \left(\sum_j h_{(1 \rightarrow j)}^* \cdot h_{(1 \rightarrow j)} \right)^{-1} \sum_j h_{(1 \rightarrow j)}^* \cdot r_j \quad (4.17)$$

that is analogous to Eq (4.15). With this result in hand, it is straightforward to understand the Zero-Forcing algorithm for a multi-user scenario.

Multiple Users in a Cell

Now in reality, there is not a single user but multiple users in a cell which communicate with the base station at the same time and frequency thanks to favorable propagation scenario discussed in the last section. In such a case, hidden in the received data samples r_j are not simply the modulation symbols s_1 from terminal 1 but also the modulation symbols s_2, \dots, s_K from all K users. Therefore, the signal model $r_j = s_1 \cdot h_{(1 \rightarrow j)}$ becomes multi-dimensional as

$$\mathbf{r} = \mathbf{H} \cdot \mathbf{s} + \text{noise} \quad (4.18)$$

where \mathbf{r} is a vector of received samples, \mathbf{H} is a matrix whose entries $h_{(i \rightarrow j)}$ are channel gains from user i to antenna j and \mathbf{s} is the vector of modulation symbols s_1, s_2, \dots, s_K . Just like a single user where $\sum_j (y_j - m \cdot x_j)^2$ or $\sum_j (r_j - h_{(1 \rightarrow j)} \cdot s_1)^2$ was minimized, the least squares solution now focuses on minimizing $\|\mathbf{r} - \mathbf{H} \cdot \mathbf{s}\|^2$. Then, the solution can be straightforwardly written just like Eq (4.17) or Eq (4.15) as

$$\hat{\mathbf{s}} = (\mathbf{H}^* \mathbf{H})^{-1} \mathbf{H}^* \mathbf{r} \quad (4.19)$$

where the term before \mathbf{r} is known as a pseudo-inverse of a matrix and \mathbf{H}^* implies both a transpose and a conjugate operation on channel matrix \mathbf{H} . This is the expression you would have seen in most research papers and books on 5G physical layer algorithms. While this matrix result seems difficult to understand at first, I believe the derivation of a single user as in Eq (4.17) helps in grasping the underlying basic idea. The enhancement of gains and nullifying the interference in the directions of other users with a *massive* number of antennas results in a system that is quite different from a simple multi-user system. This is illustrated in Figure 4.10 where the cost of additional antennas simplifies the system design in other aspects. Keep in mind that although physical beams are drawn in this figure, the idea stays the same for virtual beamforming scenario. A few comments are in order here.

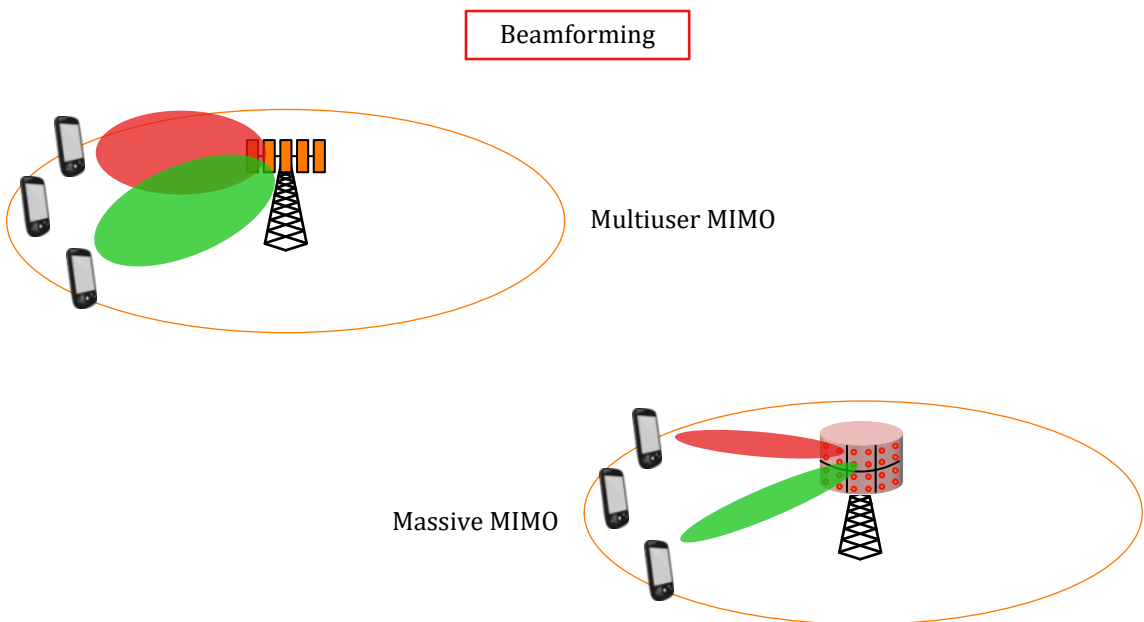


Figure 4.10: Beamforming in multi-user vs massive MIMO systems

Why Zero-Forcing?

In the case of matched filter detector, we relied only on favorable propagation conditions summarized in Eq (4.11) to nullify the interference coming from $K - 1$ users. We also mentioned that this only approximately holds true for a large number of antennas N_B . In the present instance, the algorithm is known as Zero-Forcing because the decoding vectors are structured in a way to nullify interference among the users, i.e., force zeros on the off-diagonal terms of the matrix. Let us find out how.

Plug in the value of the received samples \mathbf{r} from Eq (4.18) into the Zero-Forcing solution of

Eq (4.19), we get

$$\begin{aligned}\hat{\mathbf{s}} &= (\mathbf{H}^* \mathbf{H})^{-1} \mathbf{H}^* (\mathbf{H} \cdot \mathbf{s} + \mathbf{noise}) \\ &= \mathbf{s} + \text{modified noise}\end{aligned}\quad (4.20)$$

The operation $(\mathbf{H}^* \mathbf{H})^{-1} \mathbf{H}^* \mathbf{H}$ equals \mathbf{I} in the first term, where \mathbf{I} is an identity matrix with ones along the main diagonal and zeros everywhere else. As a result, the signal part in the first term now contains only a vector with each user's modulation symbol free of influence from the other symbols.

Noise Enhancement

One drawback of a Zero-Forcing solution is noise enhancement. Refer back to Eq (4.20) and focus on the effective noise part now. The problem with the multiplicative factor appearing with noise is that it is an inverse of a matrix, much like the expression $(\sum_j h_{(1 \rightarrow j)}^* \cdot h_{(1 \rightarrow j)})^{-1}$ for a single user in Eq (4.17) before. With these channel gains in the denominator, the effective noise can be enhanced at frequencies where channel gains assume low values. This enhanced noise then dominates the signal part and deteriorates the estimation performance.

Regularization Factor

From the above description, a balance between SNR enhancement and interference mitigation is required. One solution is to introduce an additional factor in Eq (4.19) that limits the extent of inversion.

$$\hat{\mathbf{s}} = (\mathbf{H}^* \mathbf{H} + \delta \mathbf{I})^{-1} \mathbf{H}^* \mathbf{r}$$

where δ is a positive number known as a *regularization factor* that can be tuned to strike a tradeoff between the two techniques covered before.

- When $\delta \rightarrow 0$, the effect of channel dominates and this is clearly the Zero-Forcing solution of Eq (4.19), i.e., $\hat{\mathbf{s}} = (\mathbf{H}^* \mathbf{H})^{-1} \mathbf{H}^* \mathbf{r}$.
- When $\delta \rightarrow \infty$, the identity matrix dominates the channel matrix and the inverse of \mathbf{I} is close to identity \mathbf{I} as well. This is clearly maximum ratio or matching filtering of Eq (4.12), i.e., $\hat{\mathbf{s}} = \mathbf{H}^* \mathbf{r}$.

Regularized Zero-Forcing has proved to be a good candidate between complexity and tradeoff in implementation of massive MIMO in commercial networks.

Finally, on the downlink, a *precoding* matrix similar to Eq (4.19) before data transmission enables the base station to beamform multiple data streams to all user terminals without causing any mutual interference among them. Due to a large number of base station antennas N_B , linear processing

algorithms described above such as matched filtering and Zero-Forcing are nearly optimal in massive MIMO systems and computationally complex signal processing algorithms such as those discussed in Chapter 5 are not required.

It must be mentioned that there is a performance gap that exists between all the schemes. Optimal detection is better than Zero-Forcing that in turn performs better than maximum ratio or matched filtering. This makes sense because Zero-Forcing nullifies the interference layers beforehand that results in a significant improvement in SINR.

4.4 Acquiring Channel State Information (CSI)

You would have noticed that in deriving all the above results, we have assumed the availability of Channel State Information (CSI) at the base station, i.e., some resources must be allocated to estimate the channel gains $h_{(i \rightarrow j)}$ from terminal i to antenna j . This can be accomplished in the following manner. Keep in mind that the channel is changing over time and frequency and perfect estimates can never be attained.

Conventional Channel Estimation

There are three participants in wireless transmission under a flat fading scenario, namely the Tx signal s , the channel gain h and the Rx signal r .

$$r = h \cdot s + \text{noise} \quad (4.21)$$

In the simplest of settings, knowledge of the h and r at the Rx lead to the detection of the Tx signal s as

$$\hat{s} = \frac{r}{h}$$

The question is how to estimate h . Clearly, if h is unknown in Eq (4.21), then knowledge of s can help us determine the value of h .

$$\hat{h} = \frac{r}{s}$$

Where does this knowledge of s come from? In infrastructure based wireless networks, it is a common practice for the base station to embed reference signals, known as a *training sequence* or *pilot symbols*, in the transmitted message. A training sequence is drawn in Figure 4.11a for the case of a series of +1s and -1s that is prepended before the actual data. On the other hand, pilot symbols are illustrated in Figure 4.11b that are embedded periodically within the data symbols. The channel can be determined at each time or frequency (subcarrier in an OFDM system) and there are CSI smoothing techniques that can be applied to learn the complete channel in time-frequency grid. This is a highly simplified description but enough for our purpose.

In summary, when the Tx signal is known, channel gains can be estimated and when the Tx signal is unknown, the computed channel estimate can be utilized to estimate the data symbols. We now

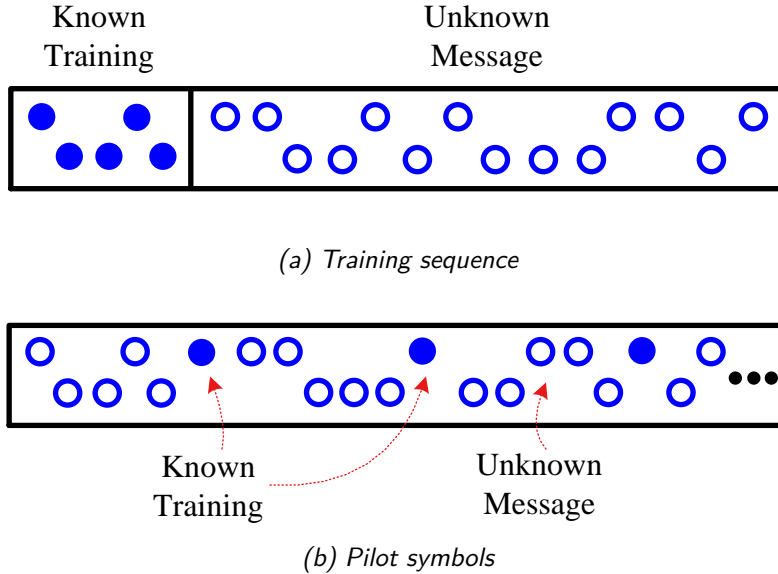


Figure 4.11: CSI acquisition at the Rx side is done through known reference signals

explain how the channel information is obtained at the base station in massive MIMO systems. In the discussion that follows, we imply the base station as the Tx and the user terminal as the Rx.

Massive MIMO in Time Division Duplex (TDD) Mode

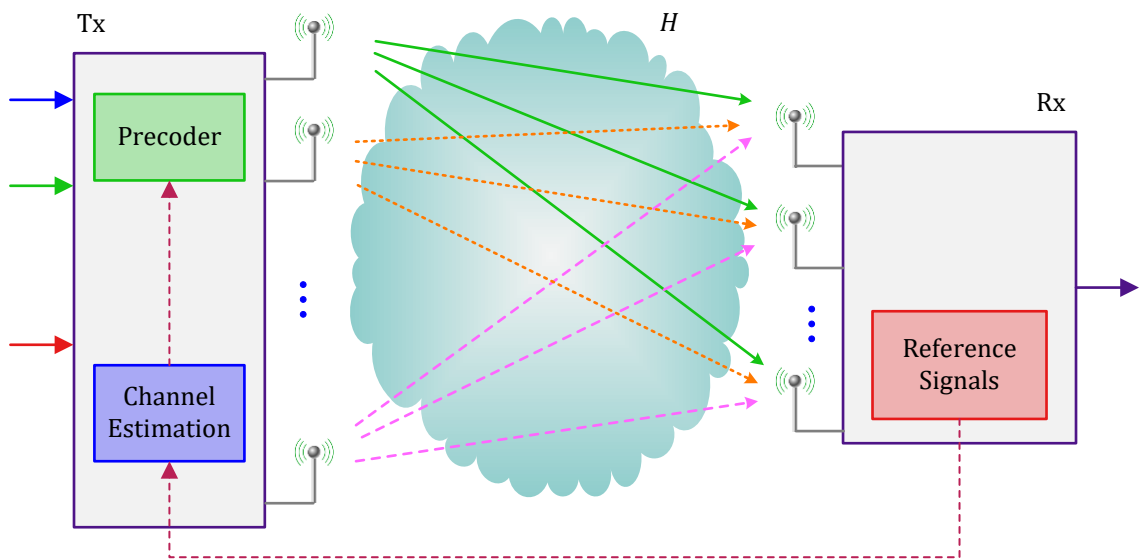
In Time Division Duplex (TDD) mode, the base station and user terminals use the same frequency on a time sharing basis[†]. The main advantage in TDD mode is *channel reciprocity*: the channel response in the downlink is the same as that in the uplink. The mobile can transmit reference signals that can help the base station measure the channel response that it can subsequently use to form precoding vectors in the downlink as illustrated in Figure 4.12a. While all the Rx antennas are shown on one station to simplify the block diagram, the Rx part can easily be broken down into a number of terminals each with a few antennas. In NR, this channel sounding is done by Sounding Reference Signals (SRS).

The issue of duplex mode is sensitive in the context of massive MIMO systems and there are some advantages in adopting the TDD mode.

Scalability

The number of base stations antennas N_B is significantly higher than the users K . If the base station can learn the channel through uplink pilots, only K pilots are required where K is the number of user terminals that is much less than N_B . This configuration also makes the system

[†]In NR standard, dynamic TDD is also possible which allows for a more flexible sharing of resources between the uplink and downlink.



(a) *The base station can learn the channel from uplink reference signals*



(b) *The fireworks can be independently observed by each child (image credit: New Line Cinema)*

Figure 4.12: Time Division Duplex (TDD) mode

more scalable with respect to N_B . For example, one can double the number N_B without any extra overhead of double the number of pilots; the same number will theoretically suffice.

Gandalf and the Fireworks

To understand this idea, look at Figure 4.12b and observe that when Gandalf sets off the fireworks, all the children – irrespective of how many they are – can observe them and enjoy the show. This is analogous to how each antenna at the base station can learn the channel from one transmission of a reference signal by a user. On the other hand, if Gandalf were to observe the fireworks expertise of each child and give them feedback according to a scale, then he has to observe their performance one by one, thus significantly increasing the number of fireworks required and the duration of the show. This is what happens in FDD mode discussed shortly.

Processing Load

Both the channel estimation and precoding/combining operations are done at the base station instead of the user equipment that is constrained by limited power. In a conventional system, there are four slots needed for uplink and downlink message exchange, one each for pilots and the other for data. In a massive MIMO system working in a TDD mode, this can be done in three slots. As shown in Figure 4.13, the base station estimates the channels from uplink pilots and then use the estimates to combine the data in the uplink from different users. Then, it can send the downlink data after precoding that uses the same channel estimates because this complete cycle happens in one coherence interval, i.e., within the coherence time T_C and the coherence bandwidth B_C .

Update Rate

Recall from Chapter 2 that the channel only stays approximately constant within a coherence interval. Therefore, a higher update rate is required in mobile users which can be smoothly accommodated in TDD mode measurements.

What we have learned so far is the following: if the base station and the users separate their transmissions in time, then they can use the *same frequency band* leading towards the idea of reciprocity: the same channel estimates acquired at the uplink can be utilized in the downlink. Such a TDD setup forms a natural partnership with massive MIMO system.

For a wireless network with small bandwidths and symmetric traffic, the actual performance of a TDD

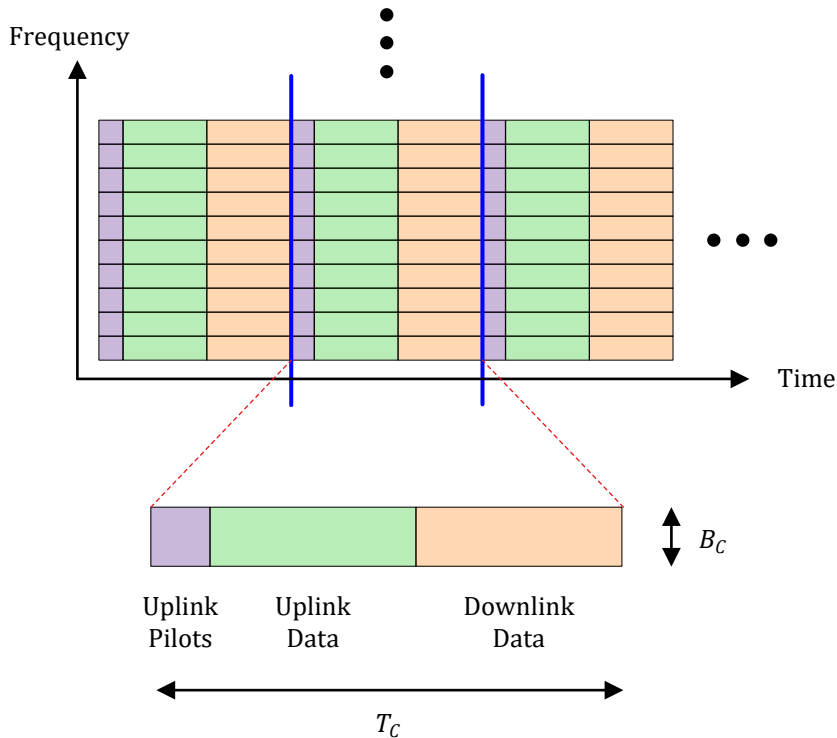


Figure 4.13: Massive MIMO operation in TDD mode

massive MIMO system is not far from what is expected. However, when such a system is implemented in a commercial network like 5G, new challenges arise some of which are described below [20].

Radio Alignment

While the propagation channel is reciprocal in a TDD setup, the Tx/Rx frontend and the antennas exhibit different characteristics. For an end to end transmission, they are indeed a part of the wireless channel that gives rise to alignment errors between the uplink and downlink channels. Consequently, the forward channel can be quite different than the reverse channel. This problem affects virtual or generalized beamforming more than physical or classical beamforming because the former relies on weighting by appropriate channel gain values instead of a simple angle. This can be solved through calibration of the hardware between the Tx and Rx.

Bandwidth

A base station measures the channel coefficients through uplink transmissions of pilots. It needs to scan the whole bandwidth for this purpose. However, each pilot occupies a certain part of the bandwidth. On the other hand, signal bandwidths have been increasing throughout the evolution of cellular networks. As we see in Chapter 6, NR standard defines up to 400 MHz of bandwidth

for single carriers in mmWave band and even 100 MHz in lower frequency ranges. Since the Tx power at the mobile is fixed, the same power is distributed over a wider bandwidth for wideband transmissions, i.e., for each part of the bandwidth (e.g., a subcarrier in OFDM), the received power at the base station decreases with frequency thus reducing the Signal to Interference plus Noise Ratio (SINR). It is evident from the example in Figure 4.14 that the Tx power/Hz spreads out with 3 MHz of bandwidth as compared to 1 MHz case because

$$\text{Tx Power} = \frac{\text{Tx Power}}{\text{Hz}} \times \text{Bandwidth}$$

This affects the quality of the channel estimated by the base station at each frequency and subsequently the formation of appropriate precoding vectors in the downlink. The cell edge users suffer more from this problem as compared to the terminals close to the base station.

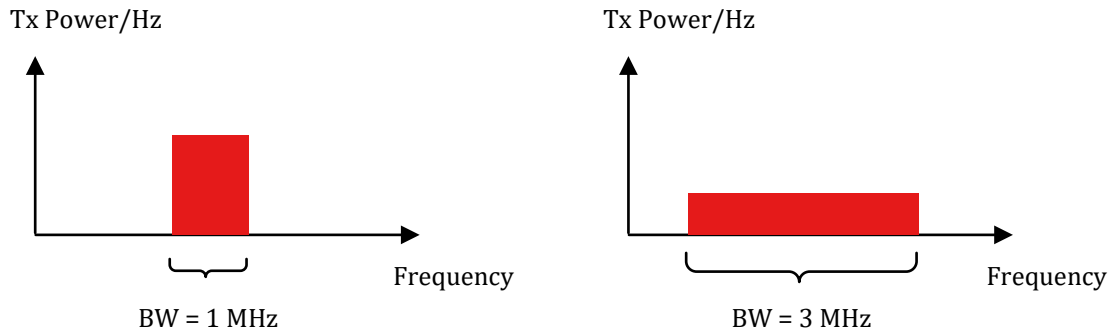


Figure 4.14: Effect of bandwidth on received power

Tx/Rx Mode in User Antennas

The trend towards increasing the number of antennas continues not only with the base station but also with the user equipment. Cell phones supporting NR are expected to have four antennas, a number that can increase later. Their main purpose (at least initially) is to increase the user side diversity in Rx mode because the number of Tx radio chains at user terminal is usually limited. This implies that reference signals cannot be simultaneously sent from all the available antennas. As a consequence of partial antenna sounding at the user side, the base station cannot learn the whole channel using the reciprocity principle, i.e., from each Tx antenna to each Rx antenna. This is known as *partial channel reciprocity problem* that reduces the potential performance of massive MIMO beamforming due to the missing channel gains. While antenna switching can enable all those antennas to transmit pilots on the uplink utilizing the same Tx chain, it takes more time to complete one round of sounding and that time is already limited due to the coherence interval.

Carrier Aggregation

Cellular networks have to deal with fragmented spectrum due to regulations and legacy systems. As we saw earlier, one way to increase the data transmission is to increase the signal bandwidth.

When the bandwidth at a certain frequency is limited by the standard, the goal can still be achieved by aggregating the bandwidths from different carrier frequencies. For obvious reasons, the amount of bandwidth and the number of carriers are different in uplink than in the downlink. As shown in Figure 4.15, there are parts of spectrum for which no information can be obtained from the uplink transmissions. Consequently, the channel cannot be learned by the base station and this limits the opportunity to form precoding or combining vectors in TDD mode.

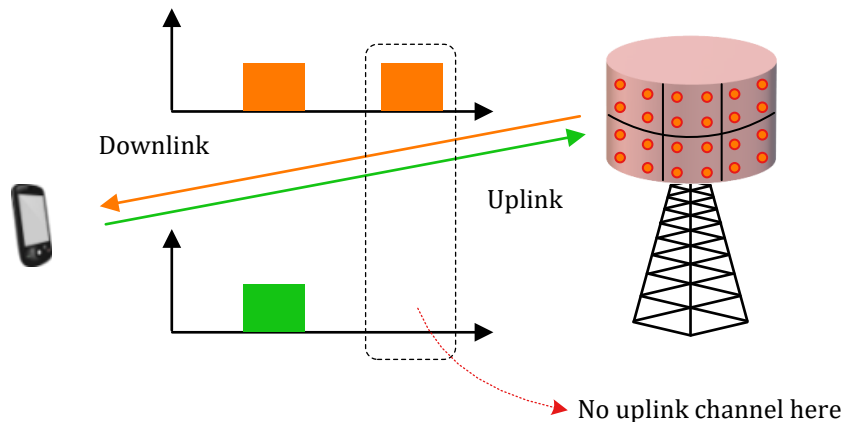


Figure 4.15: Carrier aggregation results in asymmetry between uplink and downlink transmissions

Massive MIMO in Frequency Division Duplex (FDD) Mode

In Frequency Division Duplex (FDD) mode, the allocated bandwidth is split into two separate parts, one for the uplink and the other for the downlink. Due to frequency selectivity, channels in these spectra are not the same and training or pilots are transmitted in both directions. Recall that massive MIMO systems shift most of the signal processing burden on the base station. While the base station can measure the channel in uplink transmissions, how does it know the channel coefficients in the downlink? For this purpose, each user terminal measures the channel coefficient during downlink transmission by utilizing pilot symbols embedded in its data stream. This channel information can then be fed back to the base station for subsequent computation of the precoding vector as illustrated in Figure 4.16.

Clearly, in a Frequency Division Duplexed (FDD) system, a large number of channel estimates plus their feedback are naturally required within each coherence interval that depends on both the number of base station antennas N_B (one reference signal for each antenna) as well as the users K (one feedback transmission from each user). This overhead puts constraints on limited time and frequency resources and hence an upper limit on the number of antennas and/or users participating in the network. Some of the few techniques that have been employed to solve this problem are as follows.

- Channel estimation is generally performed through orthogonal pilots, i.e., reference signals that are separated in time or frequency. To reduce the number of pilot sequences from N_B to a

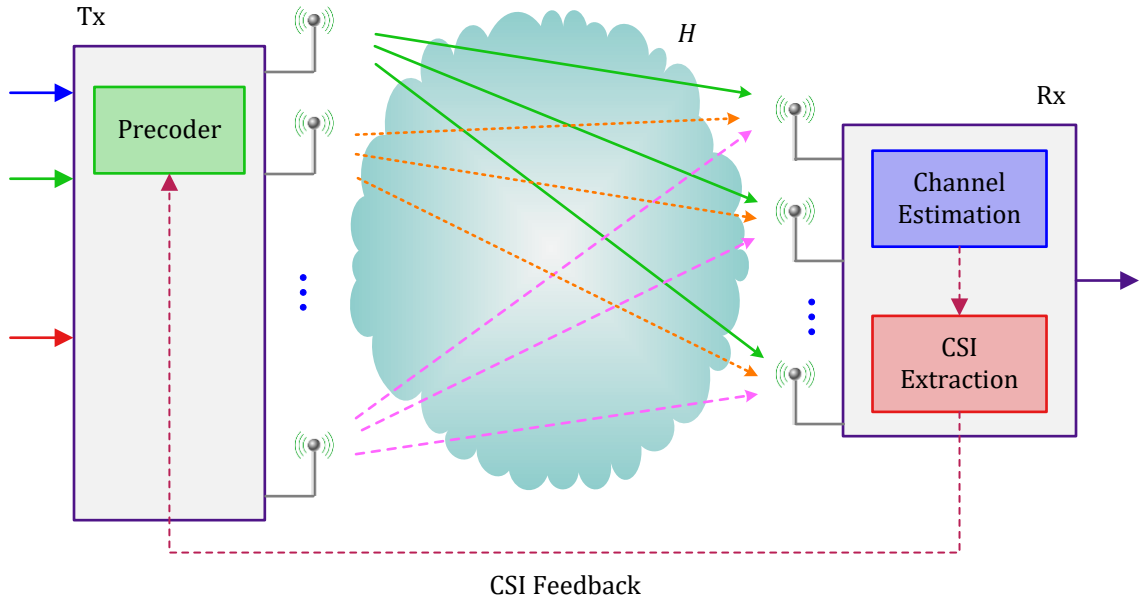


Figure 4.16: In FDD mode, the base station can learn the channel from the feedback sent by the user terminals

lesser value, non-orthogonal pilot sequences with low cross-correlation can be utilized that can be transmitted at the same time or frequency. The cost is degraded channel estimates that seem inadequate in practice for the purpose of demodulation.

- To reduce the amount of feedback, the channel state information can be compressed into a few bits (e.g., quantizing the channel coefficients) before sending to the base station.
- Remember that the fundamental problem is not to accurately estimate the channel but instead build an efficient precoder at the base station that can maximize the downlink SINR. For this purpose, a finite number of precoder matrices can be stored in a *codebook* and one of them is chosen for downlink transmission at a time. To accomplish this goal, spatial correlation feedback received on the uplink can be exploited to select the most suitable precoder from the codebook.
- A more practical approach involves the user equipment in the process. The receiver estimates some channel properties based on which it selects a precoder out of the codebook and finally reports that recommendation to the base station. The amount of feedback in this case, known as *Precoder Matrix Indicator (PMI)*, is simply a pointer index for the matrix position in that codebook. Keep in mind that it is not mandatory for the same precoder to be used; it can simply fit as a parameter into a more complicated algorithm at the base station that determines the actual precoder for transmission.
- A product precoder scheme can also be employed in which the precoder matrix is seen as a product

of two matrices; the first one takes care of the large scale channel correlation properties while the other, which is now reduced in dimensionality, can come from actual channel tracking. This division considerably reduces the amount of feedback involved. In such a scheme, the size of the second precoder becomes small enough to allow quantization of individual matrix coefficients. This is known as advanced CSI feedback and supported by NR standard.

4.5 Pilot Contamination

NR supports both FDD and TDD mode described above. For a reasonably pure estimate, it is necessary to make sure that each pilot transmission occurs in a vacuum, i.e., free from the interference of other pilots in the same time or frequency. This is achieved through orthogonality or separation of training signals in time or frequency slots. As we see now, simple orthogonality is not enough and new problems emerge due to the interaction among different cells in a network.

- A set of orthogonal pilots in one cell can also reach the base station antennas of a neighboring cell and interfere with the pilots of that base station. This is the *pilot contamination problem* where the signal arriving at a base station is a linear combination of pilots from one user in the same cell and another user in a neighboring cell. This is illustrated in Figure 4.17.

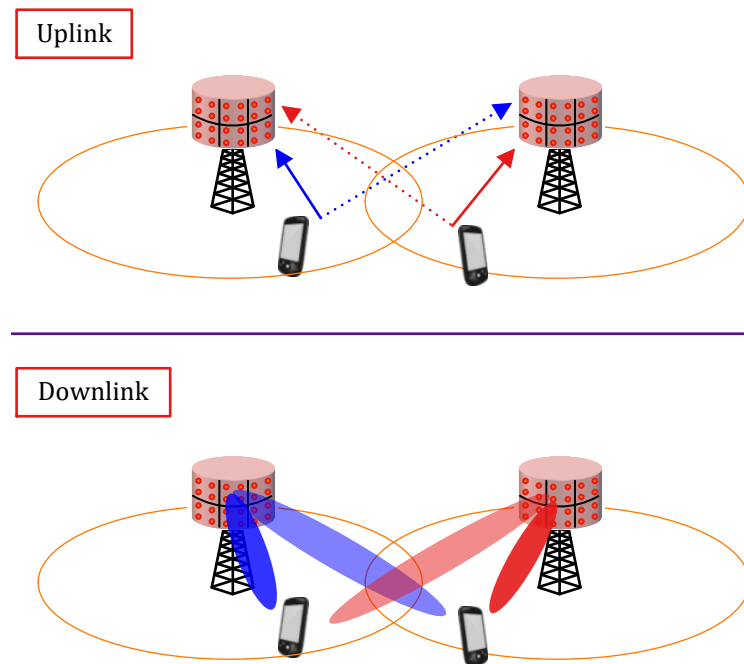


Figure 4.17: The pilot contamination problem arises by reusing the same set of pilots in different cells

Note that it is not necessary that the other user sends the same pilot signal to the base station as the desired user. All the other pilots that are not completely orthogonal to the other pilot will

also create additional interference in the uplink during training stage and in the downlink during the data transmission stage as described below.

- During downlink operation, the base station will beamform a signal intended for the original user but it will also unintentionally interfere with the undesired user in the other cell. In the left cell of Figure 4.17, for example, the blue beam is directed towards its cell user but a shadowed blue beam is also arriving at the terminal in the right cell, thus interfering with its original red beam transmission.

Can the pilots be separated in neighboring cells? Yes it is possible but at a huge cost to throughput and efficiency, both of which require as few pilots as possible. Recall the description of a coherence interval in Chapter 2 which is a time-frequency resource defined by the product of coherence bandwidth B_C and coherence interval T_C . The pilots need to be repeated after every coherence interval due to a change in channel conditions. This puts an upper limit on the number of orthogonal pilot sequences. The following remedies for pilot contamination problem can be implemented.

Reuse Factor

A reuse factor determines which cells are assigned the same set of pilots. For example, Figure 4.18 shows a reuse factor of 1 at the top. This means that the same set of orthogonal pilots are being used in every cell of the network. This creates problems of interference as demonstrated before. On the other hand, the bottom part of the figure shows a reuse factor of 3 where only the cells of the same color employ the same set of pilots. Clearly, by creating separation between transmissions at the same time-frequency resource, the pilot contamination can be reduced (but cannot be completely eliminated). An even higher reuse factor (e.g., 7) can separate the interfering signals thus creating a larger buffer between cells.

Blind Estimation

There has been a lot of research on blind channel estimation techniques for the past several decades. Blind algorithms estimate the parameter from the signal statistics without any pilot or training from the Tx side. Applications of these techniques can enable a higher throughput network with no transmission tax paid in the form of known training. The drawbacks are the worse quality of the estimate and a longer time to acquire them. Moreover, a common theme in infrastructure based networks, including 5G, is to insert training at regular intervals/subcarriers for continuous channel estimation and tracking. At this time, this trend seems to continue except in some special circumstances.

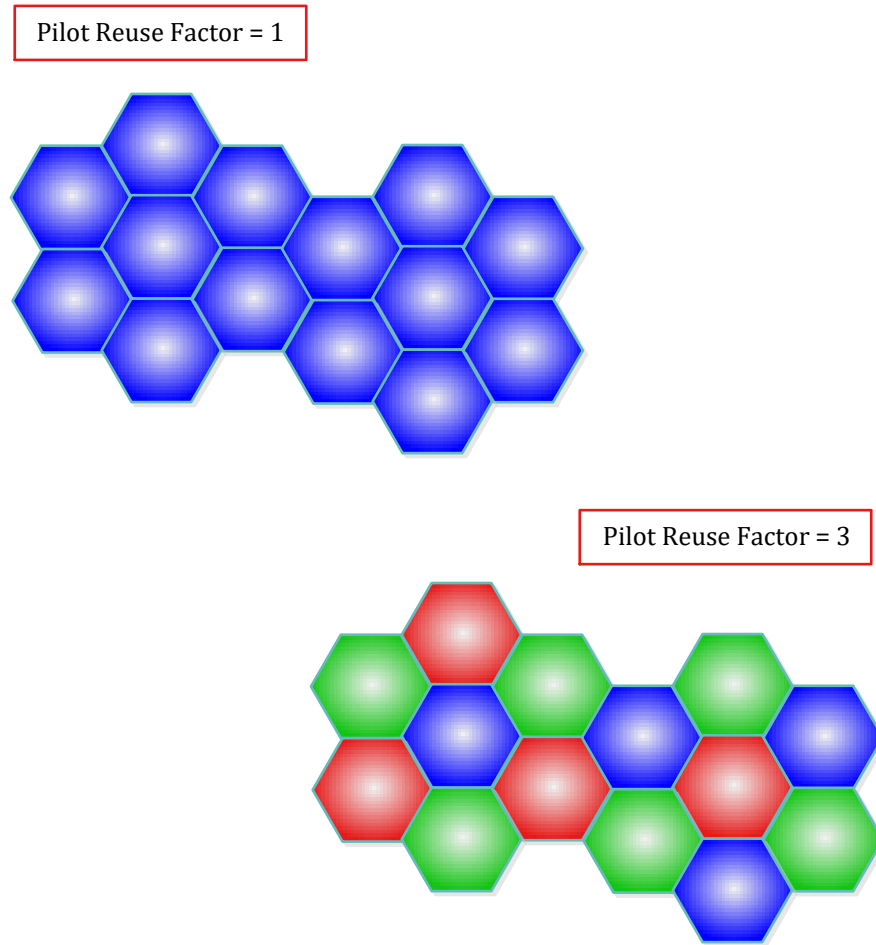


Figure 4.18: A reuse factor of 1 vs 3

4.6 The Small Picture

Substantially increasing the number of antennas with respect to the served users simplifies the system design in many aspects.

- Channel hardening eliminates the effects of fading and frequency dependence.
- Favorable propagation reduces the amount of interference between transmissions of different users in a cell.
- A large number of antennas makes linear signal processing nearly optimal in performance.

The direction of future is now only an increase in the number of elements (whether active or passive). The effect on wireless communication is similar to digital revolution in the field of electronics. Once the benefits of collecting samples in time, or collecting samples in space, are established, it is impossible to go back to analog processing whether in time or in space.

Chapter 5

Spatial Multiplexing



In the past 100 years, scientists have imagined new ways of boosting the capacity of wireless channels. Around the middle of 20th century, we began to truly understand the role of fundamental players in this equation, namely power and bandwidth. It was realized that the capacity of a wireless channel increases logarithmically with SNR and hence quickly approaches the region of diminishing returns. Nevertheless, with a few exceptions, almost all the research was exclusively focused on single antenna systems. It was only in mid 1990s that the power of using multiple antennas at both ends of the link was discovered. It turned out that the capacity increases *linearly* with the number of antennas (minimum of Tx and Rx antennas to be exact), even on a single device! This came as a remarkable result at that time. We can now recognize this trend from nature: Working in a team was the major factor that put the humble homo sapiens at the top of the food chain. Even in the modern world, when a single person hits the ceiling of individual skill acquisition or productivity, they need to transform from an organism to an organization. Entrepreneurs, investors, politicians and social workers utilize this route and leverage the best minds available in a team formation. Teams have often pulled off feats that individuals can only dream of.



Figure 5.1: Working in a team is a route to more achievement

In a similar spirit, multiple antennas have become the key technology for high rate wireless systems in which an input data stream can be split into multiple parallel streams in space domain. These systems are termed as Multiple Input Multiple Output (MIMO) systems. This defining feature kickstarted a new era of cellular networks which continues with 5G NR incorporating a large number of antennas (massive MIMO). To emphasize the trend of parallelism in wireless industry, we will learn in Chapter 8 that from a waveform viewpoint, Orthogonal Frequency Division Multiplexing (OFDM) is nothing but a set of parallel virtual wires in the air.

Before the advent of spatial multiplexing, multipath from a wireless channel was considered as an enemy and systems were designed to remove its effects from the signal. Instead of utilizing this phenomenon to our advantage, the focus was to make the communication systems resilient to this fading. The opposite to resilient is fragile in common dictionaries. According to Nassim Nicholas Taleb,

Antifragile

"Some things benefit from shocks; they thrive and grow when exposed to volatility, randomness, disorder, and stressors and love adventure, risk, and uncertainty. Yet, in spite of the ubiquity of the phenomenon, there is no word for the exact opposite of fragile. Let us call it antifragile. Antifragility is beyond resilience or robustness. The resilient resists shocks and stays the same; the antifragile gets better."

Nassim Nicholas Taleb - Antifragile: Things That Gain From Disorder

If you know about equalizers in a wireless communication system, notice that an equalizer makes a wireless communication system robust against multipath fading by exploiting the sum of multiple copies (thus providing frequency diversity). The presence of multipath, however, does not make such a system better.

On the other hand, spatial multiplexing can exploit a rich multipath fading environment to create independent spatial streams between a Tx and a Rx. We can say that such a framework makes the wireless systems antifragile by gaining (in terms of data rate) from the multipath disorder.

5.1 From Multi-User MIMO to Single-User MIMO

Multiple antenna systems have a long and rich history. Beamforming is perhaps the first known technique utilizing an array of antennas. Diversity on the Rx side has also played a major role in designing reliable communication systems in harsh fading channels. However, it was the discovery of throughput increase between two users, i.e., spatial multiplexing, in the 1990s that became the killer application for multiple antenna systems and lead to their widespread adoption. In fact, the terminology MIMO itself is still used by many scientists all over the world to refer to a spatial multiplexing system. This technology became the cornerstone of 4G cellular systems as well as WiFi standards starting from IEEE 802.11n. And this worked well for point-to-point systems. Nevertheless, the problem faced by cellular system designers is more complex: they need to increase the throughput while simultaneously decreasing the interference generated from one user towards the remaining users in a cell. Moreover, the mobile terminals should be kept simple for longer battery usage. While spatial multiplexing is still part of NR standard, beamforming has played a more dominant role in 5G systems. We have come full circle in a sense, a trend often seen in many other technological advancements.

In Section 3.4.4, we introduced the idea of spatial multiplexing in the context of Multi-User MIMO

(MU-MIMO), i.e., the base station with multiple antennas communicates with several well-separated users utilizing the same time and frequency resources. In this chapter, we will discuss how spatial multiplexing can also be performed between two devices, each of which is equipped with an antenna array, i.e., geographical separation is not necessary if the multipath channel is rich enough. This is known as Single-User MIMO (SU-MIMO). Figure 5.2 shows MU-MIMO at the bottom where the base station sends multiple independent streams to several single antenna terminals. This is what we saw in Chapter 3. These multiple terminals can be thought of coming together and combining in a single terminal with multiple antennas as shown at the top. Just like MU-MIMO, we explore how multiple streams can *still* be sent on separate antennas (up to a limit) and correctly decoded at the Rx.

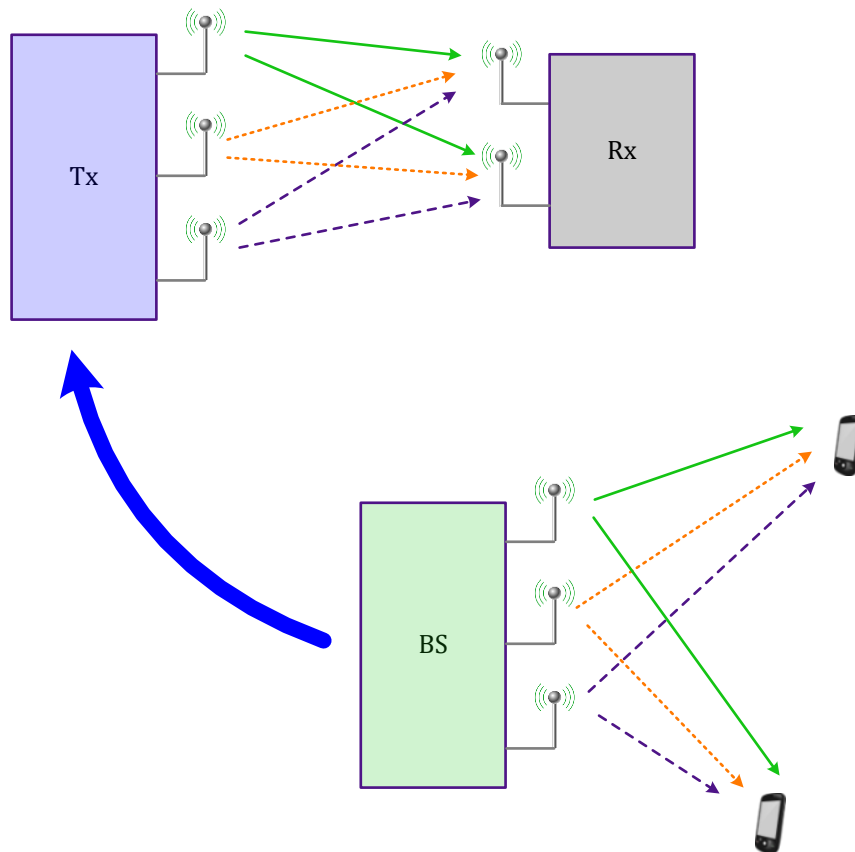


Figure 5.2: Multi-User vs Single-User MIMO

There are two modes of operation in this regard.

- When the Tx knows the channel gains, spatial multiplexing in SU-MIMO operates on roughly similar principles as spatial multiplexing in MU-MIMO, i.e., precoding and combining matrices are derived according to the channel conditions.
- When the Tx has no knowledge of multipath channel, then this is known as open-loop spatial

multiplexing. The task of the Rx is to first estimate the channel using reference signals and then run suitable detection algorithms to separate the individual streams.

As you can see in Figure 5.2, all Tx signals arrive at each Rx antenna and it is not straightforward to separate them through signal processing techniques. Consequently, we start the description with a simple example where the same modulation symbol s is sent from all Tx antennas. Clearly, this is beamforming and not spatial multiplexing but it will help us understand the ideas coming next.

5.2 Detection with Tx Channel Knowledge

During the discussion on physical and virtual beamforming in Chapter 3, we usually considered either 1 Tx antenna and N_R Rx antennas as in Maximum Ratio Combining (MRC) or N_T Tx antennas and 1 Rx antenna as in Maximum Ratio Transmission (MRT). What happens when we employ multiple antennas at *both* the Tx and the Rx? This is where things get more interesting.

Why Simple Combining Does Not Work?

A block diagram of a MIMO system with N_T Tx antennas and N_R Rx antennas is drawn in Figure 5.3. In the current context, a single data symbol s is sent from all N_T antennas (i.e., beamforming). Later we will expand to the general spatial multiplexing scenario where separate symbols are sent from different Tx antennas.

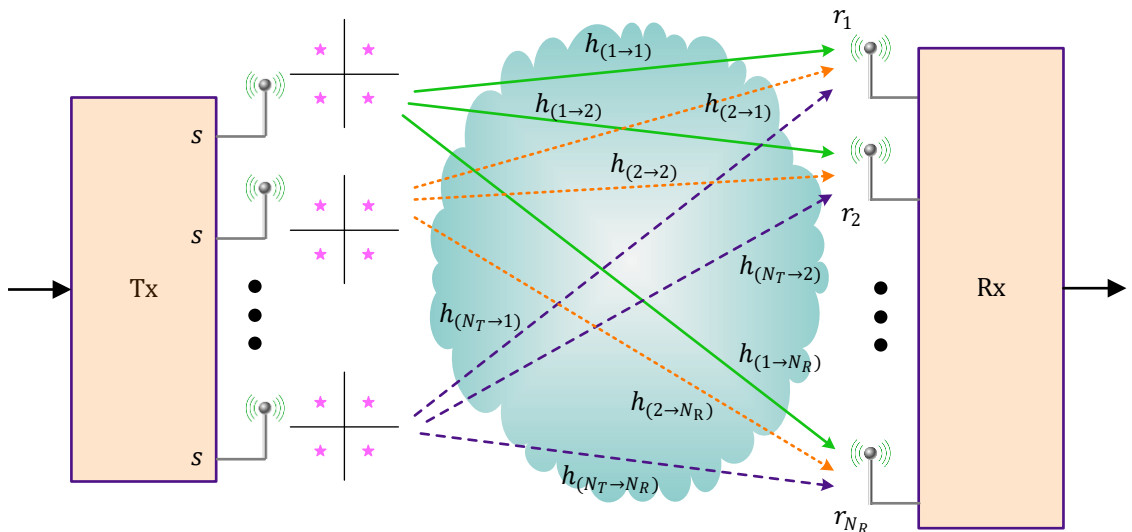


Figure 5.3: A MIMO system $N_T \times N_R$ antennas

The first idea that comes to mind in this setup is to apply the MRT technique at the Tx and MRC at the Rx. However, if the gains are already aligned at the Tx during the departure of waves, why do

they need to be aligned again through MRC at the Rx? To understand the answer to this question, look at Figure 5.3 again where the flat fading channel gain between i -th Tx antenna and j -th Rx antenna is denoted by $h_{(i \rightarrow j)}$. Here, i goes from 1 to N_T and j is from 1 to N_R . All the channel gains from Tx antennas to Rx antennas come together to form what I like to call a *channel cloud*. Observe on the Rx side of Figure 5.3 that the cumulative signal r_1 at the first antenna is a summation of signals arriving from all Tx antennas.

$$\begin{aligned} r_1 &= h_{(1 \rightarrow 1)} \cdot s + h_{(2 \rightarrow 1)} \cdot s + \cdots + h_{(N_T \rightarrow 1)} \cdot s + \text{noise} \\ &= (h_{(1 \rightarrow 1)} + h_{(2 \rightarrow 1)} + \cdots + h_{(N_T \rightarrow 1)}) \cdot s + \text{noise} \end{aligned} \quad (5.1)$$

where the term in the bracket here is the cumulative channel at the first antenna. A similar expression can be written as r_j for j^{th} antenna where $j = 1, 2, \dots, N_R$. Now we can see the problem here. If transmit weights w_i are chosen as the conjugates of $h_{(1 \rightarrow 1)}$, $h_{(2 \rightarrow 1)}$, and so on, they will form a beamforming vector with phase cancellation and magnitude scaling all right but that will be possible for *one* such destination only, namely the first antenna. The remaining $N_R - 1$ antennas will suffer from fading as a result of failing to beamform the Tx signal according to their own channel gains. For example, if Tx weights w_i are chosen as

$$w_1 = h_{(1 \rightarrow 1)}^*, \quad w_2 = h_{(2 \rightarrow 1)}^*, \quad \dots$$

then after scaling by w_i at the Tx and encountering the channel gains along the way to the Rx, we have their summation appearing at the Rx antenna 1.

$$\begin{aligned} \sum_{i=1}^{N_T} w_i \cdot h_{(i \rightarrow 1)} &= h_{(1 \rightarrow 1)}^* \cdot h_{(1 \rightarrow 1)} + h_{(2 \rightarrow 1)}^* \cdot h_{(2 \rightarrow 1)} + \cdots + h_{(N_T \rightarrow 1)}^* \cdot h_{(N_T \rightarrow 1)} \\ &= |h_{(1 \rightarrow 1)}|^2 + |h_{(2 \rightarrow 1)}|^2 + \cdots + |h_{(N_T \rightarrow 1)}|^2 \end{aligned}$$

This is clearly virtual beamforming directed towards the Rx antenna 1. But at another Rx antenna, say 2, we will have

$$\sum_{i=1}^{N_T} w_i \cdot h_{(i \rightarrow 2)} = h_{(1 \rightarrow 1)}^* \cdot h_{(1 \rightarrow 2)} + h_{(2 \rightarrow 1)}^* \cdot h_{(2 \rightarrow 2)} + \cdots + h_{(N_T \rightarrow 1)}^* \cdot h_{(N_T \rightarrow 2)}$$

which neither aligns the phases nor grades the magnitudes. If such technique cannot be adopted for beamforming a single modulation symbol s , clearly it is not applicable to the spatial multiplexing scenario where separate streams s_1, s_2, \dots , are sent from different Tx antennas. This failure of precoding at the Tx and combining at the Rx requires a more generalized framework.

MIMO Signal Model

A block diagram for a MIMO system with N_T antennas and N_R antennas is drawn in Figure 5.4. In spatial multiplexing mode, separate modulation symbols s_1, s_2, \dots, s_{N_T} , are simultaneously sent

through their respective Tx antennas. For example, for $N_T = 2$, the first antenna sends s_1, s_3, s_5, \dots while the second antenna transmits s_2, s_4, s_6, \dots . These are known as *spatial streams* or *layers* in MIMO jargon.

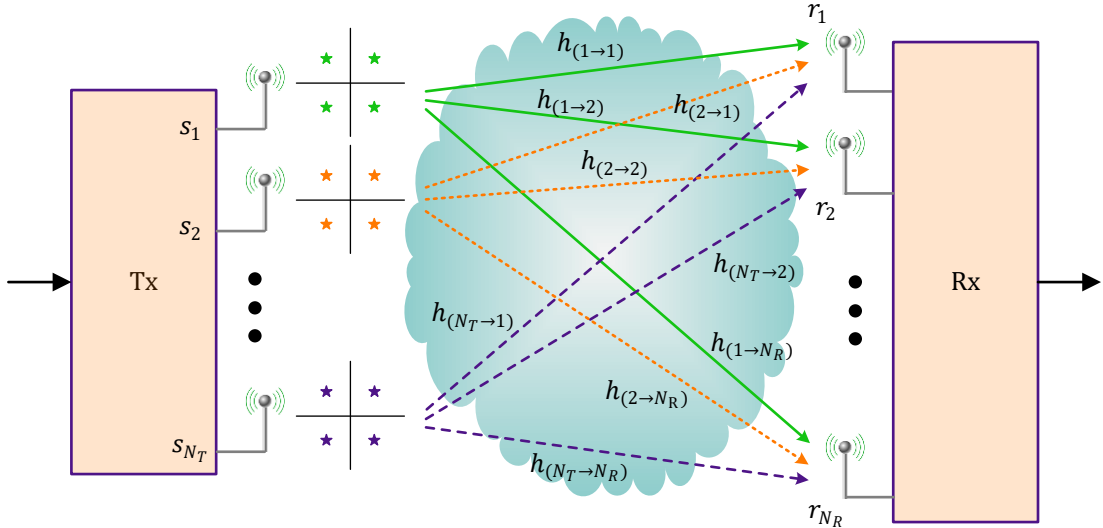


Figure 5.4: A MIMO system with spatial multiplexing

The flat fading channel gain between i -th Tx antenna and j -th Rx antenna is denoted by $h_{(i \rightarrow j)}$ where i is from 1 to N_T and j is from 1 to N_R in this case. Observe on the Rx side of Figure 5.4 that the cumulative signal at each antenna is a summation of signals arriving from all Tx antennas.

$$r_j = h_{(1 \rightarrow j)} \cdot s_1 + h_{(2 \rightarrow j)} \cdot s_2 + \dots + h_{(N_T \rightarrow j)} \cdot s_{N_T} + \text{noise}, \quad (5.2)$$

$$j = 1, 2, \dots, N_R$$

While this expression looks complicated, you can put $j = 1$ like before and follow the signals in Figure 5.4 to understand the participating signals. The main feature of this expression is that all of the modulation symbols s_1, s_2, \dots, s_{N_T} , are different in each time slot (only one time slot is shown here). They are also sharing the same frequency resources and the only separation is in space (i.e., antennas). That is what maximizes the data rate.

Since the signals from all Tx antennas arrive at each Rx antenna, the main task of the detection algorithms here is to free each modulation symbol sent by one Tx antenna from the interference of the other modulation symbols sent by rest of the Tx antennas. How to accomplish that is where we go next.

What is Orthogonality and Why Do We Like It?

Until now, I have deliberately avoided the dreadful 'o' word here: *orthogonality*, because this is a concept that comes with heavy mathematical details. However, in accordance to the general theme of this text,

I will explain it in a simple and non-rigorous manner. Look at the soda dispenser in Figure 5.5 and observe that when you press the lever with the label Fanta, only Fanta comes out without mixing with Sprite or Coca-Cola. This is orthogonality in a nutshell. Imagine what would happen if the beverage machine delivers non-orthogonal output and you have to separate Fanta each time from a mixture of Fanta, Sprite and Coca-Cola in your glass.



Figure 5.5: Orthogonality implies that the soda from each outlet does not mix with the soda from any other outlet

In a similar manner, assume that our purpose is to transmit several modulation symbols s_1, s_2, s_3, \dots , in parallel with each other such that none of them interferes with the other at the Rx. We like this orthogonality because it helps in a simple receiver design with no signal processing algorithms required to separate the modulation symbol s_1 from the influence of symbols s_2, s_3, \dots , at each transmission interval. We could have achieved an orthogonality similar to the soda machine if a wire was running from every Tx antenna to a Rx antenna. But this is not possible. Furthermore, what should we do if the number of antennas at the Tx and the Rx are different?

The fundamental idea behind DSP can be of help here. Remember that the whole purpose of DSP is to transform variations of a real-world phenomenon into a signal that can then be converted into a sequence of numbers. Once in numbers form, simple and neat tricks from the language of mathematics can be applied that are beyond the wildest imaginations of those lingering in the old world from a scientific viewpoint. For instance, we can represent each of those numbers as a vector in an N -dimensional space at 90° to each other.

- The good thing about vectors at 90° is that there is no interference among them, just like the

beverages from the soda machine above. This is orthogonality in terms of numbers and it is quite similar to motion tracking in our 3D world. For any position coordinates given by (x, y, z) , no matter how far I travel in x -direction, there is absolutely no change in y and z coordinates. For this reason, we like to design the signals that are orthogonal to each other *at the Rx*.

- The problem is that when the modulation symbols arrive at the Rx *after being acted upon by the wireless channel*, they are spread out all over that N -dimensional space because the signal at each Rx antenna contains the contributions from *all* Tx antennas, thus providing us with a mixture (i.e., summation) of all the transmissions. Shown to the left of Figure 5.6 are the vectors that are orthogonal at the Tx side as 90° vectors in different directions[†]. After passing through the wireless channel, each of the components in x , y and z directions has a contribution from all of s_1 , s_2 , s_3 , etc., as shown to the right of Figure 5.6. Novel algorithms are needed to individually extract them from the mixture.
- Given this situation, we use our mathematical tricks to come up with some weights at the Tx and the Rx such that they do fall at 90° to each other in the end result.



Figure 5.6: Left: Signals at the Tx are at 90° to each other. Right: Orthogonality is destroyed at the Rx as they are spread in all directions

This understanding leads us to the concept of the Singular Value Decomposition (SVD).

Stretching and Rotation

One drawback in a purely mathematical approach such as the Singular Value Decomposition (SVD) is the difficulty to explain it without covering some matrix theory and linear algebra. However, I shall describe the basic idea from an intuitive viewpoint which should help the readers without a mathematical background grasp the main concept. To keep the big picture clear, we are heading towards creating independent parallel pipes in the air by performing simple operations at the Tx and Rx sides.

[†]Since the language of mathematics exists in our heads and not in reality, we can extend the concept of orthogonality beyond 3 dimensions to any number N .

Refer back to the block diagram in Figure 5.4 and assume for a moment that the number of Tx and Rx antennas is the same, i.e., $N_T = N_R$. Also assume that different modulation symbols are being sent from different Tx antennas, i.e., s_1 from Tx antenna 1, s_2 from Tx antenna 2, and so on. The flat fading channel gain between i -th Tx antenna and j -th Rx antenna is denoted by $h_{(i \rightarrow j)}$. Observe on the Rx side that the cumulative signal at each antenna is a summation of signals arriving from all Tx antennas as

$$\begin{aligned} r_1 &= h_{(1 \rightarrow 1)} \cdot s_1 + h_{(2 \rightarrow 1)} \cdot s_2 + \cdots + h_{(N_T \rightarrow 1)} \cdot s_{N_T} + \text{noise} \\ r_2 &= h_{(1 \rightarrow 2)} \cdot s_1 + h_{(2 \rightarrow 2)} \cdot s_2 + \cdots + h_{(N_T \rightarrow 2)} \cdot s_{N_T} + \text{noise} \\ &\vdots \\ r_{N_R} &= h_{(1 \rightarrow N_R)} \cdot s_1 + h_{(2 \rightarrow N_R)} \cdot s_2 + \cdots + h_{(N_T \rightarrow N_R)} \cdot s_{N_T} + \text{noise} \end{aligned} \quad (5.3)$$

We could write the above set of equations as

$$\mathbf{r} = \mathbf{H} \cdot \mathbf{s} + \text{noise} \quad (5.4)$$

where

- \mathbf{r} is a vector consisting of elements r_j , i.e., the signals arriving at Rx antennas
- \mathbf{s} is a vector consisting of the modulation symbols s_i
- \mathbf{H} is a matrix of channel coefficients $h_{(1 \rightarrow 1)}$, $h_{(2 \rightarrow 1)}$, and so on.

What is the effect of such multiplication between a matrix and a vector in Eq (5.4)? For this purpose, consider a single modulation symbol s sent over a flat fading channel h that is received as

$$r = h \cdot s + \text{noise}$$

We know that a product between two complex numbers multiplies the magnitudes and adds the phases. For two numbers h and s , we have[†]

$$\begin{aligned} |h \cdot s| &= |h| \cdot |s| \\ \angle(h \cdot s) &= \angle h + \angle s \end{aligned}$$

As an example, the left side of Figure 5.7 illustrates a vector with magnitude 1 and angle 60° in the complex plane which is multiplied with a complex number with magnitude 1.5 and an angle of 70° . After the multiplication, the vector magnitude on the right side of the figure increases to 1.5 and the angle goes to $60^\circ + 70^\circ = 130^\circ$. In other words, the original vector is rotated by the angle of the complex number and stretched by the magnitude of the complex number (here, the word 'stretch' includes the

[†]In complex notation, we have for $h = ae^{j\theta_1}$ and $s = be^{j\theta_2}$,

$$h \cdot s = ae^{j\theta_1} \cdot be^{j\theta_2} = (a \cdot b)e^{j(\theta_1+\theta_2)}$$

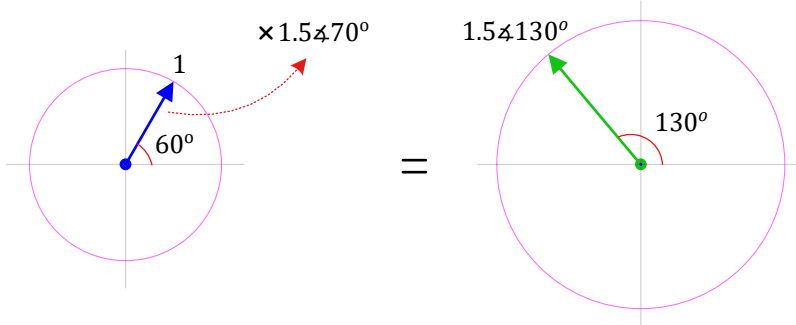


Figure 5.7: A complex multiplication stretches a vector and rotates it

case of compression where the magnitude of the multiplier is less than 1). *Rotation* and *stretching* thus define the multiplication operation. In a similar manner, the matrix \mathbf{H} rotates and stretches the symbol vector \mathbf{s} in Eq (5.4)!

Singular Value Decomposition (SVD)

This rotation and stretching by the matrix \mathbf{H} depends on the channel coefficients $h_{(i \rightarrow j)}$. In general, such an operation results in the input vectors spreading out in all directions, just like what we saw on the right side of Figure 5.6. However, it turns out that for each \mathbf{H} , there is a special set of vectors denoted by \mathbf{V} that are at 90° to each other and when acted upon by the matrix \mathbf{H} (our wireless channel in this case), the resulting set of vectors is, even after rotation and stretching, also at 90° to each other! In other words, an input set of orthogonal vectors \mathbf{V} when multiplied with the channel matrix \mathbf{H} produces an output set of orthogonal vectors denoted by \mathbf{U} , which is then stretched by different scaling factors combined in a diagonal matrix Σ . Such an operation is drawn in Figure 5.8 for two vectors for illustration purpose. Here, two vectors v_1 and v_2 that are 90° apart are multiplied with the channel matrix which results in their rotation to form vectors u_1 and u_2 that are also 90° apart. These u_1 and u_2 are then scaled by σ_1 and σ_2 , respectively, to produce the final output. Such sets of input and output vectors exist for every \mathbf{H} and this property proves very useful to our system design.

In summary, we can write the SVD expression for one vector as

$$\mathbf{H} \cdot \mathbf{v}_i = \sigma_j \cdot \mathbf{u}_j \quad (5.5)$$

where i and j , or the number of input and output vectors, can be different to each other. In 2D geometry, a circle on the left of Figure 5.8 is transformed into an ellipse. The orientation of the axes are dictated by the vectors u_j and the lengths of the major and minor axes by σ_j . These values σ_j are known as *singular values*. The vectors \mathbf{v}_i and \mathbf{u}_j in Eq (5.5) can then be combined into matrices \mathbf{V} and \mathbf{U} , respectively, to produce the final SVD expression[†].

[†]Just for the interested reader, since Σ is a diagonal matrix with singular values σ_j on the diagonals and zero elements

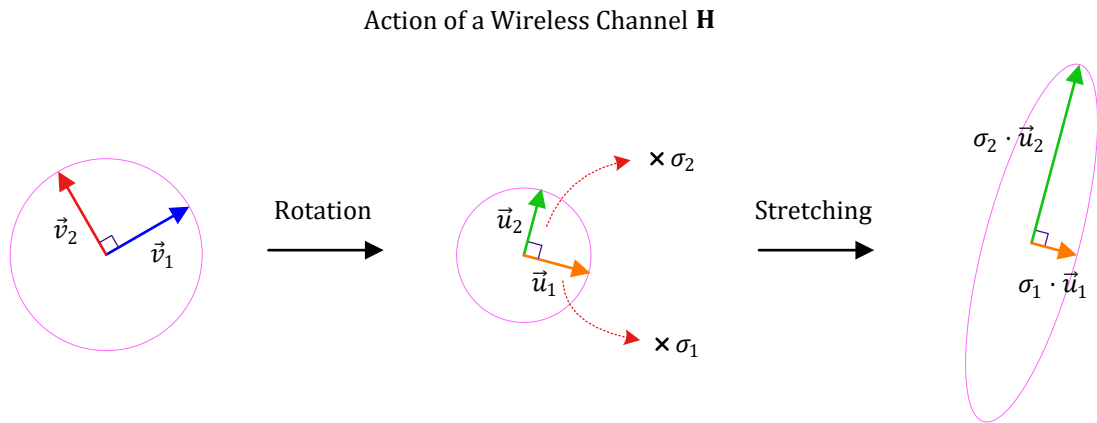


Figure 5.8: A wireless channel matrix \mathbf{H} rotates an orthogonal set of vectors \mathbf{V} to produce another set of orthogonal set of vectors \mathbf{U} that are stretched by scaling factors σ_i

Creating Independent Pipes

The question is how we can utilize this knowledge about the channel matrix \mathbf{H} to design a system in which final vectors at the Rx are at 90° or orthogonal to each other. This can be accomplished as follows with the help of Figure 5.9.

- Imagine the wireless channel represented by the matrix \mathbf{H} as a black box. We just learned that vectors in the direction of orthogonal vectors \mathbf{v}_i will still be orthogonal at the output of this black box (albeit at a different orientation defined by \mathbf{u}_j and scaled by σ_i).
- At the input of this black box, i.e., the Tx side, we rotate our modulation symbols s_1, s_2, \dots , in the direction of orthogonal vectors \mathbf{v}_i . This is done by multiplying the modulation vector \mathbf{s} with the matrix \mathbf{V} that consists of all \mathbf{v}_i , as illustrated in Figure 5.9. This is virtual beamforming at the Tx side, also known as *linear precoding*.
- At the output of this black box, i.e., the Rx side, we de-rotate the received vectors in the opposite direction from \mathbf{u}_j so that the modulation symbols become interference-free again. This is accomplished through multiplying the Rx vector with the matrix \mathbf{U}^* that consists of conjugates of all \mathbf{u}_j . Recall that a conjugate operation keeps the magnitude the same but inverts the phases which cancels the channel effect here. This is virtual beamforming at the Rx side, also known as *linear postcoding*.

In this way, each modulation symbol becomes independent of all the other modulation symbols: *we have forged virtually parallel pipes in the air!* No complicated signal processing is required to remove everywhere else, we have

$$\mathbf{H} \cdot \mathbf{V} = \mathbf{U} \cdot \Sigma \quad \mathbf{H} = \mathbf{U} \cdot \Sigma \cdot \mathbf{V}^* \quad (5.6)$$

where actually $\mathbf{V}^{-1} = \mathbf{V}^*$ due to its special structure as a unitary matrix.

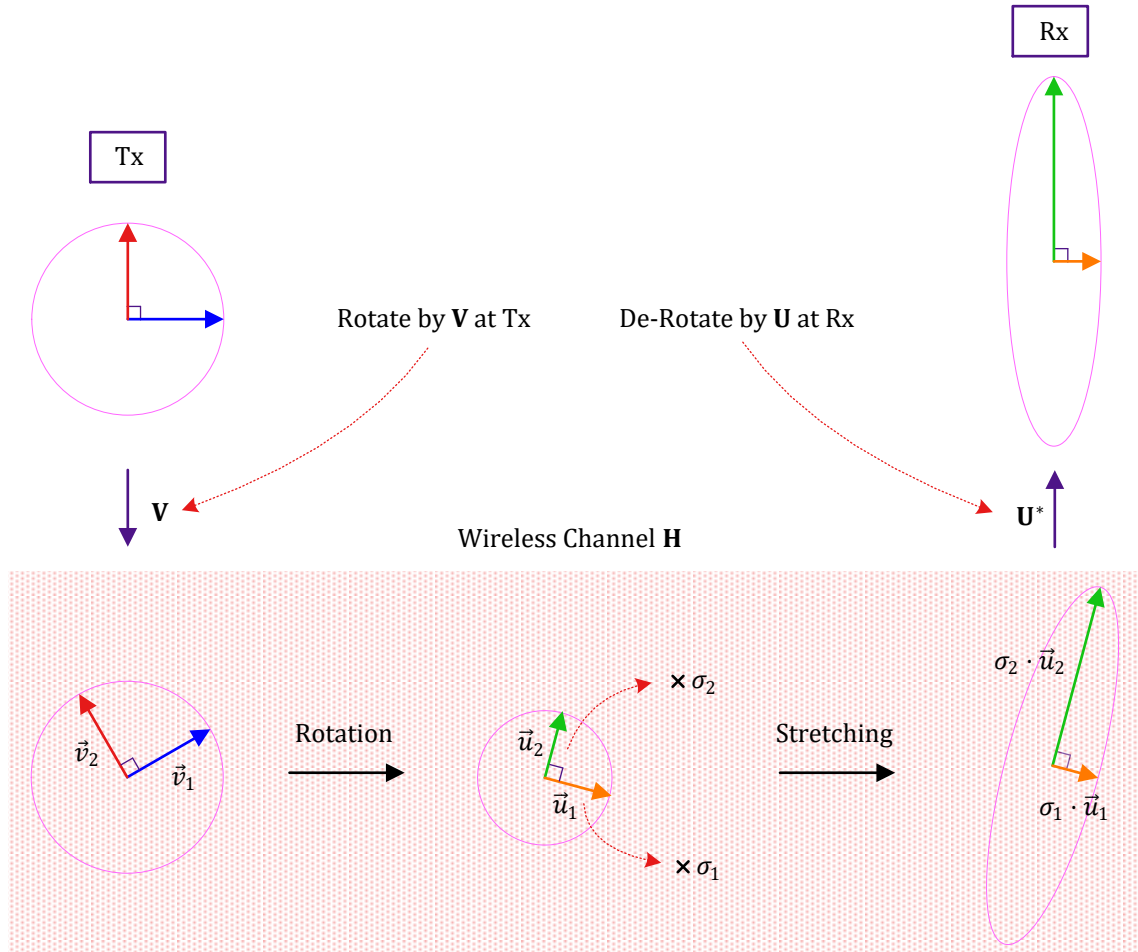


Figure 5.9: A generalized view of beamforming

their effect from each other. In Figure 5.10, I have metaphorically shown this wireless channel as consisting of pipes at different orientations and thicknesses from each other that represent the vectors 90° apart. Since the flow of fluid in any pipe does not affect the fluid in the other, this framework is now similar to the soda machine analogy encountered in Figure 5.5.

- The pipes orientations at the left of the channel represent the directions of \mathbf{v}_i towards which the Tx weights should focus the energy.
- The thickness of the pipes represents the singular values σ_i that signify how much fluid each pipe can carry.
- The pipes orientations at the right of the channel represent the directions of \mathbf{u}_j from which Rx should virtually collect the energy.

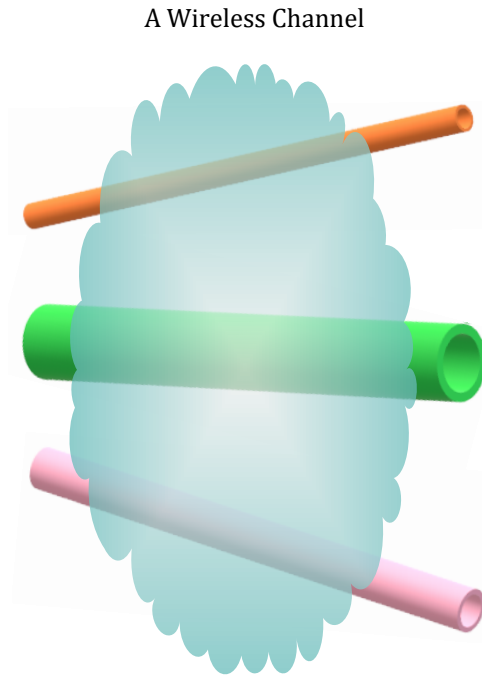


Figure 5.10: A metaphorical depiction of the Singular Value Decomposition (SVD) of a wireless channel

Randomly Spraying Energy

We earlier assumed that the number of Tx antennas N_T is the same as the number of Rx antennas N_R and each Tx antenna is transmitting an independent modulation symbol s_i . This is why we represented the singular values σ_i with index i , otherwise the number of singular values depends on the minimum of i and j . Let us now break free from these assumptions and any number of modulation symbols can be chosen before beamforming at the Tx that determines the number of virtual pipes utilized. Notice that in each of the expressions in Eq (5.3), various linear combinations of modulations symbols are being constructed at each Rx antenna while passing through the wireless channel.

- If we do not exploit the channel knowledge at the Tx which implies an absence of weighting coefficients from \mathbf{V} , it is like randomly emitting the energy in various directions without really caring about the constructive summation (virtually) pointed towards the Rx.
- If we do not exploit the channel knowledge at the Rx which implies an absence of weighting coefficients from \mathbf{U}^* , it is like randomly collecting the energy from various directions without really caring about the constructive summation (virtually) pointed towards the orientation of pipes.

Such a scenario is depicted in Figure 5.11. With no weighting at the Tx, this random spray of energy

from the Tx does not allow an optimal injection of the fluid into the target pipes. Similarly, no weights at the Rx implies randomly collecting energy from all directions instead of the channel pipes from which the actual fluid is arriving. We have three options here.

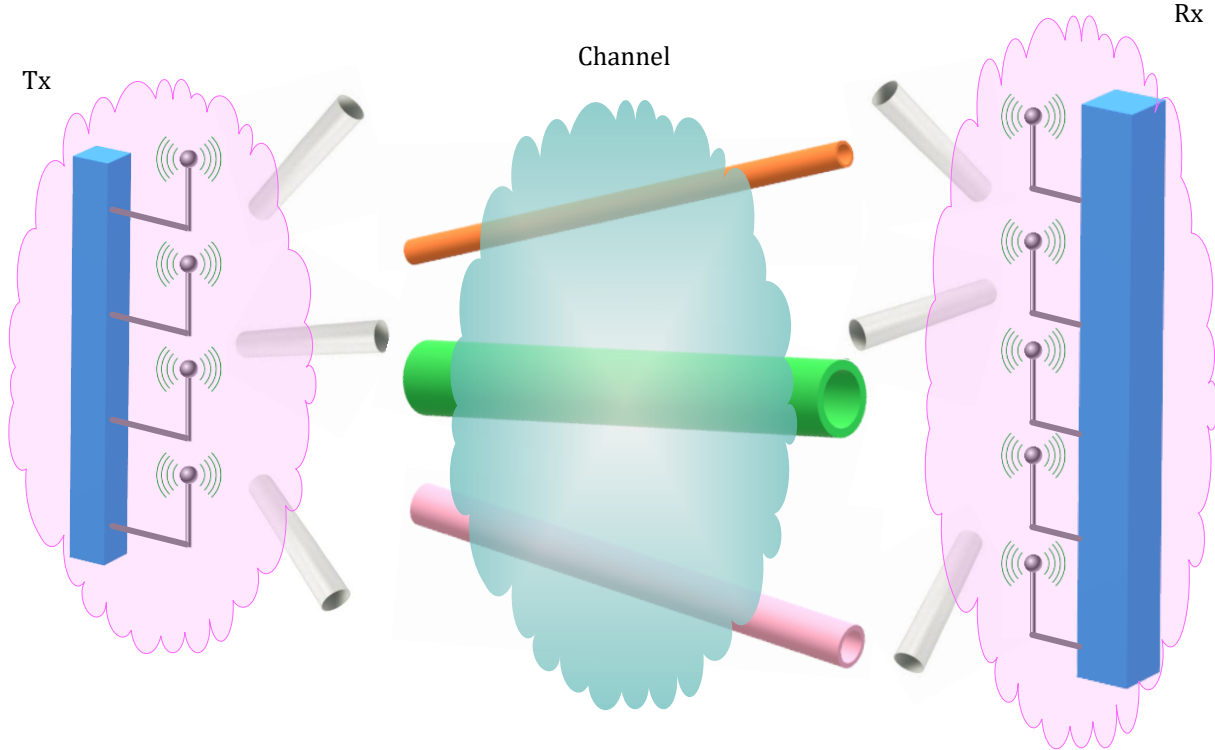


Figure 5.11: Not exploiting the channel knowledge implies that signal energy is uniformly distributed to and collected from all directions

1. Mark the fattest pipe in the channel and inject all the Tx energy into that pipe. This scheme is known as *diversity precoding* which maximizes the data reliability. Sometimes this scheme is also known as *maximum ratio transmission*. While transmitting one modulation symbol s , this is what we can do to focus the energy from *all* N_T Tx antennas towards *all* N_R Rx antennas.
2. Direct the energy in proportion to the thickness of each pipe while transmitting independent data in each of them. This scheme is known as *spatial multiplexing* which maximizes the data rate. In the context of Multi-User MIMO, remember that if the terminals are sufficiently well separated then the singular vectors described above can be approximated by directional array response vectors encountered in physical beamforming.
3. Strike a balance between reliability and data rate by choosing only a few thickest pipes.

In all of these cases, linear precoding at the Tx and postcoding at the Rx needs to be implemented.

Diversity Precoding

Diversity precoding is a special case of linear precoding in which the only target is to improve reliability and a single modulation symbol is transmitted. The precoder is one of the vectors v_i we saw before in the SVD of the wireless channel. Specifically, the Tx weights are v_i where the index i here refers to the vector corresponding to the largest singular value σ_{\max} . As shown in Figure 5.12, it is like pointing the whole fire hose towards the fattest pipe in the wireless channel. In a corresponding manner, the Rx chooses the vector u_j as its beamforming weights where j also corresponds to the index of the largest singular value σ_{\max} . As shown in Figure 5.12, this is like collecting all the energy from one fattest pipe only and discarding everything coming from elsewhere. This is similar to MRC at the Tx and MRC at the Rx in a simultaneous manner for a single symbol.

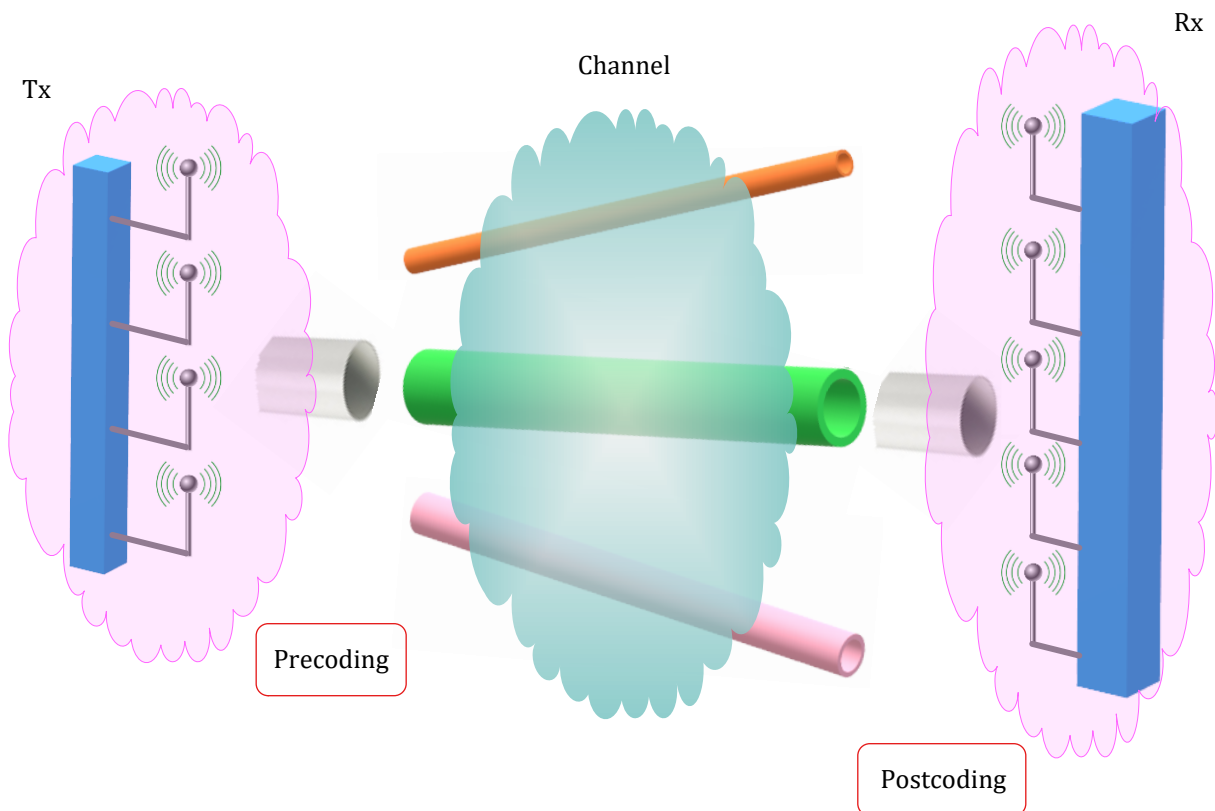


Figure 5.12: A visualization of diversity precoding technique

In this scenario, the equivalent model after precoding and postcoding is given by

$$r = \sigma_{\max} \cdot s + \text{noise}$$

With the assumption of the modulation symbol energy normalized to 1 and noise variance given by σ^2 , the SNR at the Rx can be written as

$$\text{SNR} = \frac{\sigma_{\max}^2}{\sigma^2}$$

Keep in mind that in a practical implementation of this idea, it is common to take interfering signals into account as well. Then, the precoding and postcoding weights are computed according to the desired user and interfering users which maximizes the Signal to Interference plus Noise Ratio (SINR).

Closed-Loop Spatial Multiplexing

Diversity precoding ensures reliability but not throughput. Let us now simultaneously transmit N modulation symbols where N is equal to the minimum of N_T and N_R . This choice maximizes the throughput with a sacrifice in data reliability.

- For the discussion here, channel coefficients need to be known at the Tx side which can take advantage of this information to beamform the signal in the right directions. The terminology closed-loop implies that the base station sends reference signals to the mobile terminals which then feed the channel state information back to the base station, thus ‘closing’ the loop.
- As discussed in Section 4.4, this closed-loop procedure implies a Frequency-Division Duplex (FDD) system where the Tx and the Rx occupy different frequency bands for communication. Such feedback is not required in Time Division Duplex (TDD) systems in which the Tx and Rx utilize the same frequency band but different time slots. There, the base station can estimate the channel coefficients matrix due to the principle of reciprocity: the channel at the uplink is the same as the channel in the downlink.
- We will discuss in Section 5.3 the algorithms required for open-loop spatial multiplexing, i.e., in which the Tx has no information about the channel.

Recalling the idea behind the SVD of the channel matrix in Eq (5.6), the modulation symbols are now precoded with the matrix \mathbf{V} at the Tx while the received signal samples in space are postcoded with the matrix \mathbf{U}^* . Both of these matrices come from the SVD of the channel matrix. A symbolic representation of such a setup is drawn in Figure 5.13 where the Tx injects its energy into specific virtual pipes while the Rx collects energy from specific virtual orientations. This then becomes practically similar to point-to-point microwave links from each Tx entity to each Rx entity.

Choosing the precoding and postcoding weights according to the channel matrix SVD is like simultaneously implementing MRT at the Tx and MRC at the Rx for all modulation symbols. In these techniques, we either send the signal from Tx antennas or collect the signal energy at Rx antennas in an optimal manner that depends on the channel coefficients. Here, we are meeting at a middle ground: we focus the Tx energy in some particular directions (vectors \mathbf{v}_i) and gather the Rx energy from some specific directions (vectors \mathbf{u}_j).[†]

Two comments are in order now.

[†]To complement the introduction to SVD given in Eq (5.6) for an interested reader, the channel knowledge at both the Tx and the Rx can be exploited by precoding the Tx symbols \mathbf{s} by the matrix \mathbf{V} yielding $\mathbf{V} \cdot \mathbf{s}$ while postcoding the

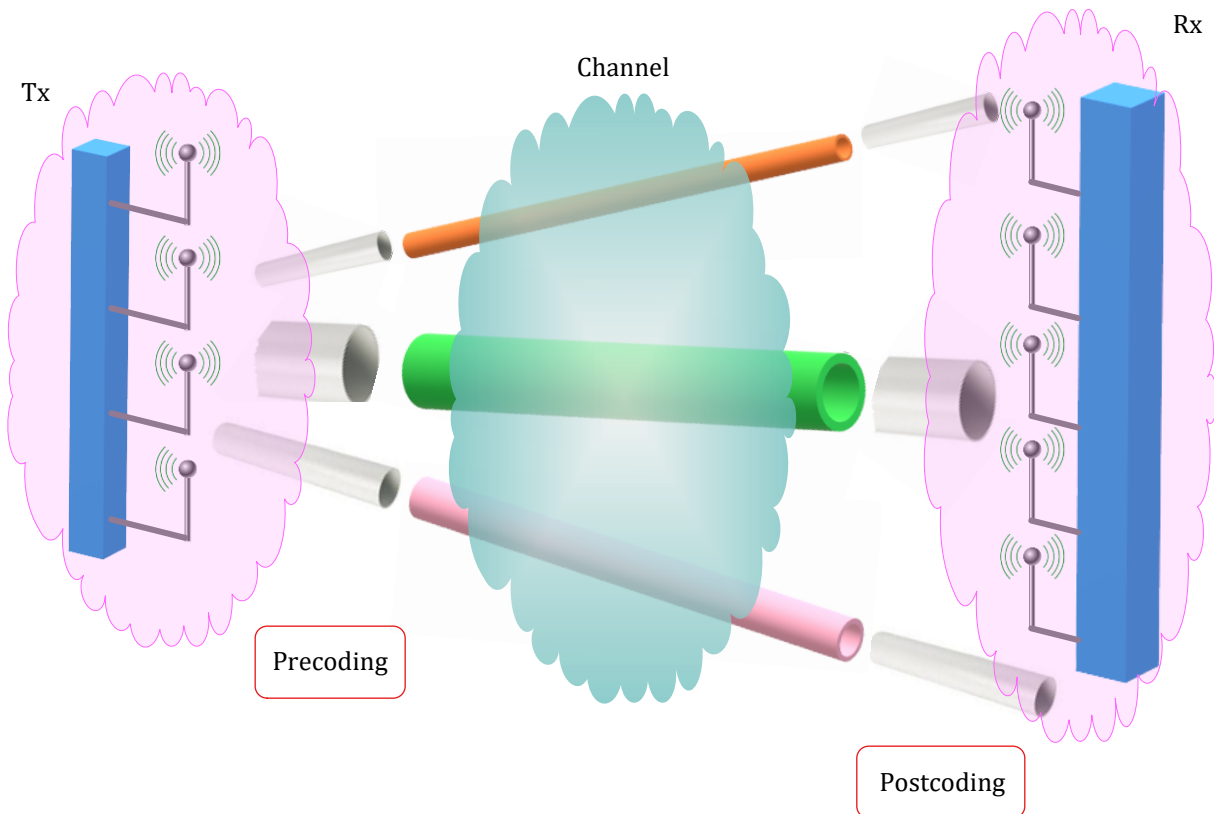


Figure 5.13: A symbolic representation of aligning the Tx weights and Rx weights according to the channel conditions for maximum throughput

- The number of independent pipes is not the same as the number of Tx or Rx antennas. The actual number of pipes depends on something known as channel rank, i.e., the number of independent columns in the channel matrix or physically speaking the number of angular bins that can support uncorrelated entries. To emphasize this point, I have shown 4 Tx antennas, 5 Rx antennas and 3 pipes in Figure 5.13. For a rich multipath channel with signal energy arriving from all angles, this number is equal to the minimum of the Tx and Rx antennas.
- The orientations of channel pipes on the Tx side and Rx side as well as their thicknesses are different for each channel and depend on that instantaneous realization of the channel.

Next, we move towards the scenario where the Tx has no knowledge about the wireless channel.

received vector $\mathbf{r} = \mathbf{H} \cdot \mathbf{V} \cdot \mathbf{s}$ as

$$\mathbf{U}^* \cdot \mathbf{r} = \mathbf{U}^* \cdot \mathbf{H} \cdot (\mathbf{V} \cdot \mathbf{s}) = \mathbf{U}^* \cdot (\mathbf{U} \cdot \Sigma \cdot \mathbf{V}^*) \cdot \mathbf{V} \cdot \mathbf{s} = \Sigma \cdot \mathbf{s}$$

because $\mathbf{U}^* \cdot \mathbf{U} = \mathbf{I}$ and $\mathbf{V}^* \cdot \mathbf{V} = \mathbf{I}$ as they are unitary matrices. Since Σ is a diagonal matrix, it acts like independent pipes with varying thicknesses as shown in Figure 5.13.

5.3 Detection with no Tx Channel Knowledge

Many wireless engineers automatically visualize the MIMO systems in spatial multiplexing mode as a transformation of the channel cloud into virtual parallel channels, similar to the independent pipes in the air shown in Figure 5.13 before. That is a misleading interpretation.

- As described before in Section 5.2, creation of independent spatial pipes demands channel knowledge at *both* the Tx and the Rx. With channel information absent at the Tx, we talk about the open-loop mode in which no feedback is received from the Rx indicating the channel condition.
- The number of such pipes is not equal to the Tx or Rx antennas. Instead, it depends on the path richness of the wireless channel reflected in a number known as rank of the channel matrix. Physically speaking, this is the number of angular bins that can support uncorrelated entries. As we will see in Chapter 6 for the mmWave bands, signal blockage and narrow beamwidths limit the number of waves arriving in all angular bins thus limiting the spatial multiplexing gains.

Let us now discuss some practical detection schemes for a transmission of symbol layers between two multiple antenna devices when Tx has no channel knowledge.

5.3.1 Linear Detection

Linear detectors, as the name says, perform linear operations on incoming signals r_j in Eq (5.2). Since computationally complex algorithms lead to faster battery drainage, linear detectors are attractive due to their simplicity in terms of algorithmic computations. There are two main kinds of linear detectors:

- Zero-Forcing (ZF), and
- Minimum Mean Square Error (MMSE)

In this investigation, we will mainly focus on the Zero-Forcing detector, not only because it is the simpler of the two but also MMSE detection demands a background knowledge of probability theory which is outside the scope of this text. Nevertheless, we will touch upon the modification required to transform a Zero-Forcing solution into an MMSE one.

General Solution

Recall Section 4.3.2 where we derived the Zero-Forcing solution for multiple users in a cell. For a system with a single antenna both at the Tx and the Rx, we can write the received signal as

$$r = h \cdot s + \text{noise} \quad (5.7)$$

where s is the modulation symbol sent and h is the flat fading channel gain. In a similar manner, a matrix equation for the received signal in the presence of multiple antennas can be written as

$$\mathbf{r} = \mathbf{H} \cdot \mathbf{s} + \text{noise}$$

where \mathbf{r} is the received signal vector at all N_R antennas, \mathbf{H} is the channel matrix composed of coefficients $h_{(i \rightarrow j)}$ while \mathbf{s} is the vector of modulation symbols. The Zero-Forcing solution was derived in Eq (4.19) as

$$\hat{\mathbf{s}} = (\mathbf{H}^* \mathbf{H})^{-1} \mathbf{H}^* \cdot \mathbf{r} \quad (5.8)$$

Since the above matrix expression could look complicated, we explain the separation procedure of two spatial streams using Zero-Forcing solution. To start, refer to the example from a grade 6 algebra lesson below.

Example from Grade 6 Algebra

You can understand the working of the Zero-Forcing algorithm easily if you can solve the following set of equations for two numbers s_1 and s_2 .

$$2 \cdot s_1 + 7 \cdot s_2 = -1$$

$$4 \cdot s_1 - 5 \cdot s_2 = 17$$

Multiply the first equation with 2 and subtract the second equation.

$$19 \cdot s_2 = -19$$

The result is $s_2 = -1$ and $s_1 = 3$. This example will now help you in decoding of two spatial streams next.

Now let us see how this can be applied to the individual detection of modulation symbols in spatial multiplexing mode.

Two Layers

As a first step, Figure 5.14 illustrates the block diagram of a MIMO system with $N_T = 2$ and $N_R = 2$ antennas. Both Tx antennas send separate modulation symbols s_1 and s_2 , respectively. From Eq (5.2), we can write the expressions for the two signals at the Rx antennas as

$$\begin{aligned} r_1 &= h_{(1 \rightarrow 1)} \cdot s_1 + h_{(2 \rightarrow 1)} \cdot s_2 + \text{noise} \\ r_2 &= h_{(1 \rightarrow 2)} \cdot s_1 + h_{(2 \rightarrow 2)} \cdot s_2 + \text{noise} \end{aligned} \quad (5.9)$$

This system of equations can be solved like any two equations in algebra. Multiplying the first equation above with $h_{(2 \rightarrow 2)}$ and the second equation with $h_{(2 \rightarrow 1)}$, we get

$$\begin{aligned} h_{(2 \rightarrow 2)} \cdot r_1 &= h_{(2 \rightarrow 2)} \cdot h_{(1 \rightarrow 1)} \cdot s_1 + \cancel{h_{(2 \rightarrow 2)} \cdot h_{(2 \rightarrow 1)} \cdot s_2} + \text{noise} \\ h_{(2 \rightarrow 1)} \cdot r_2 &= h_{(2 \rightarrow 1)} \cdot h_{(1 \rightarrow 2)} \cdot s_1 + \cancel{h_{(2 \rightarrow 1)} \cdot h_{(2 \rightarrow 2)} \cdot s_2} + \text{noise} \end{aligned}$$

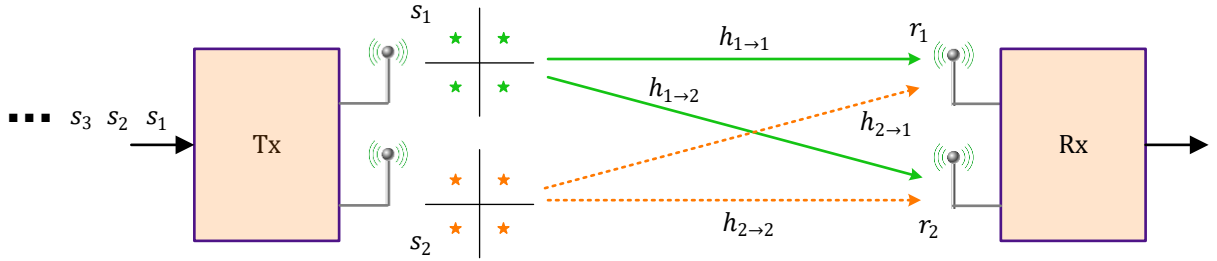


Figure 5.14: A 2×2 MIMO spatial multiplexing system, i.e., $N_T = 2$ and $N_R = 2$

where the cross-terms are canceled through subtraction. We can thus write

$$h_{(2 \rightarrow 2)} \cdot r_1 - h_{(2 \rightarrow 1)} \cdot r_2 = \{h_{(2 \rightarrow 2)} \cdot h_{(1 \rightarrow 1)} - h_{(2 \rightarrow 1)} \cdot h_{(1 \rightarrow 2)}\} \cdot s_1 + \text{noise}$$

which yields the estimate of s_1 – denoted as \hat{s}_1 – as

$$\hat{s}_1 = \frac{h_{(2 \rightarrow 2)} \cdot r_1 - h_{(2 \rightarrow 1)} \cdot r_2}{h_{(2 \rightarrow 2)} \cdot h_{(1 \rightarrow 1)} - h_{(2 \rightarrow 1)} \cdot h_{(1 \rightarrow 2)}} \quad \longrightarrow \quad \begin{array}{|c|c|c|c|} \hline \star & \star & \star & \star \\ \hline \star & \star & \star & \star \\ \hline \star & \star & \star & \color{purple}{\star} \\ \hline \star & \star & \color{blue}{\star} & \star \\ \hline \end{array} \quad (5.10)$$

For known normalized channel gains and a zero noise scenario, this estimate \hat{s}_1 maps exactly on one of the modulation symbols. When noise or other distortions are present, a 16-QAM example is also shown above where the blue point \hat{s} gets pulled to the nearest star for a decision. This is due to Gaussian nature of noise distribution.

To find \hat{s}_2 (the estimate of s_2), multiply the first equation in Eq (5.9) with $h_{(1 \rightarrow 2)}$ and the second equation with $h_{(1 \rightarrow 1)}$. After subtracting the first equation from the second, \hat{s}_2 is given as

$$\hat{s}_2 = \frac{-h_{(1 \rightarrow 2)} \cdot r_1 + h_{(1 \rightarrow 1)} \cdot r_2}{h_{(2 \rightarrow 2)} \cdot h_{(1 \rightarrow 1)} - h_{(2 \rightarrow 1)} \cdot h_{(1 \rightarrow 2)}}$$

Since both \hat{s}_1 and \hat{s}_2 are found through elimination of the other symbol, we conclude that a Zero-Forcing detector fully eliminates spatial interference from the Tx signal. The result can be generalized to any number of Tx and Rx antennas in a MIMO system where the number of Tx antennas N_T does not necessarily have to be equal to the number of Rx antennas N_R .

Some relevant comments are in order now.

Channel Estimation

The channel estimates $h_{(1 \rightarrow 1)}$, $h_{(1 \rightarrow 2)}$, $h_{(2 \rightarrow 1)}$ and $h_{(2 \rightarrow 2)}$ are initially not known at the Rx which

in practice need to be obtained through a known training sequence or pilot symbols embedded in the sent message.

Diversity Order

Recall from Eq (3.50) that diversity order refers to the negative slope of the BER curve on a logarithmic plot. Consequently, the higher the diversity order, the lower the BER curve. In Zero-Forcing algorithm, from the viewpoint of one stream (e.g., for s_1 above), the energy from the other modulation symbols (e.g., from s_2 above) is treated as an interference nulling problem. This null forcing implies that the diversity order of the Zero-Forcing solution is 1 in the current scenario. For a general MIMO system with N_T Tx antennas and N_R Rx antennas where $N_R > N_T$, the Zero-Forcing algorithm has a diversity order of $N_R - N_T + 1$. This is because $N_T - 1$ dimensions at the Rx are employed for removal of spatial interference while the rest $N_R - N_T + 1$ provide the diversity gain.

Noise Enhancement

Notice that we ignored the role of noise in the above calculations. Looking back at Eq (5.10), the denominator $h_{(2 \rightarrow 2)} \cdot h_{(1 \rightarrow 1)} - h_{(2 \rightarrow 1)} \cdot h_{(1 \rightarrow 2)}$ appears with the noise terms too. It is also evident in Eq (4.14) with the channel gain $|h|^2$ in the denominator. Consequently, the channel gains with low values in this denominator severely amplify the noise, a phenomenon known as *noise enhancement* creating bad spatial sub-channels. Results in trial experiments have shown poor performance by the Zero-Forcing solution, particularly in previous generations of cellular networks where there is abundant interference present from other users. This, however, changes with a very large number of antennas at the base station or massive MIMO systems, the driving technology behind 5G standard and described in Chapter 4. In that setup, Zero-Forcing is the dominant technique for interference cancellation.

Due to the noise enhancement problem, a Minimum Mean Squared Error (MMSE) solution is often preferred in which noise variance is also taken into account before the matrix inversion[†]. This is a compromise between noise enhancement and spatial interference suppression.

5.3.2 Successive Interference Cancellation

As we saw above, the performance of linear detectors is unsatisfactory for actual implementations of conventional MIMO systems. On the other hand, they are also very attractive due to their low computational complexity. A nice balance between performance and complexity can be achieved through

[†]Compared with the Zero-Forcing solution in Eq (5.8), an MMSE solution is given by

$$\hat{s} = (\mathbf{H}^* \mathbf{H} + \sigma^2 \mathbf{I})^{-1} \mathbf{H}^* \cdot \mathbf{r} \quad (5.11)$$

where σ^2 represents noise power and \mathbf{I} is an identity matrix. Non-zero noise power prevents very low values in the inversion process.

a neat trick employed by successive interference cancellation. The concept was devised by Gerard Foschini from Bell Labs, although it was not a new idea. Successive interference cancellation was already proposed for the detection algorithms in CDMA systems. Again, the fundamental idea was borrowed from decision feedback equalization schemes in single-carrier systems. Owing to the analogy between interference among different CDMA users and multiple Tx antenna streams, the same algorithm was tweaked in the context of MIMO detection.

On the Tx side, the mapping architecture was named as V-BLAST which stands for Vertical-Bell Laboratories Layered Space-Time architecture (the term layer originates from the spatial streams in Tx antennas). The term V-BLAST stems from the fact that modulation symbols s_1, s_2, \dots , are presented to the Tx antennas in order from 1 to N_T . An example for $N_T = 4$ antennas is illustrated in Figure 5.15 where the binary data is coded and modulated first and then a demultiplexer maps successive symbols to respective antennas. In the figure, for instance, symbol s_1 is mapped to the first antenna, s_2 to the second antenna and so on. This cycle continues forming data layers in space until the symbol s_5 comes back to Tx antenna 1. V-BLAST is a different architecture as compared to Diagonal or D-BLAST in which coded modulation symbols are presented to Tx antennas in a cyclical manner. This makes each stream or layer being sent in a diagonal of space and time thus increasing the reliability.

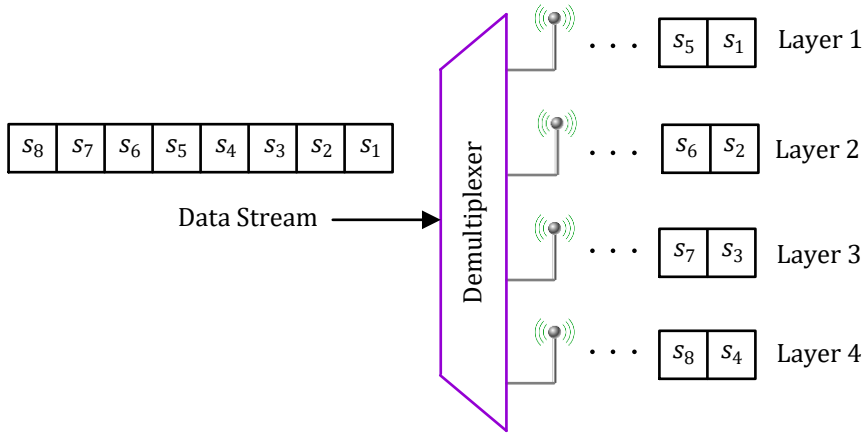


Figure 5.15: A V-BLAST architecture for 4 Tx antennas

On the Rx side, a Successive Interference Cancellation (SIC) algorithm is employed. Despite this fancy name, the underlying concept is quite easy. Let us first explain an intuitive sense of its operation.

- First, multiple spatial streams or layers are put in a descending ordered based on some chosen criterion (e.g., highest SNR stream first).
- Next, a linear detection algorithm like Zero-Forcing or MMSE that have been discussed before is applied to detect the modulation symbols of the first stream.
- Since the channel gains are known at the Rx, the full impact of this stream or layer can then be removed by subtraction from the received signal! In case the decisions were correct, the new

signal now contains contributions from $N_T - 1$ spatial streams but not from the first one. This again allows the detection of the second layer in order through a linear algorithm.

- The process is continued until the last spatial stream is estimated.

Now we turn towards the actual implementation details with an example of a 2×2 MIMO system, i.e., $N_T = 2$ and $N_R = 2$ as shown in Figure 5.14. The system model is reproduced here from Eq (5.9).

$$\begin{aligned} r_1 &= h_{(1 \rightarrow 1)} \cdot s_1 + h_{(2 \rightarrow 1)} \cdot s_2 + \text{noise} \\ r_2 &= h_{(1 \rightarrow 2)} \cdot s_1 + h_{(2 \rightarrow 2)} \cdot s_2 + \text{noise} \end{aligned} \quad (5.12)$$

Refer to the flowchart in Figure 5.16 showing the ordered successive interference cancellation algorithm to understand what follows.

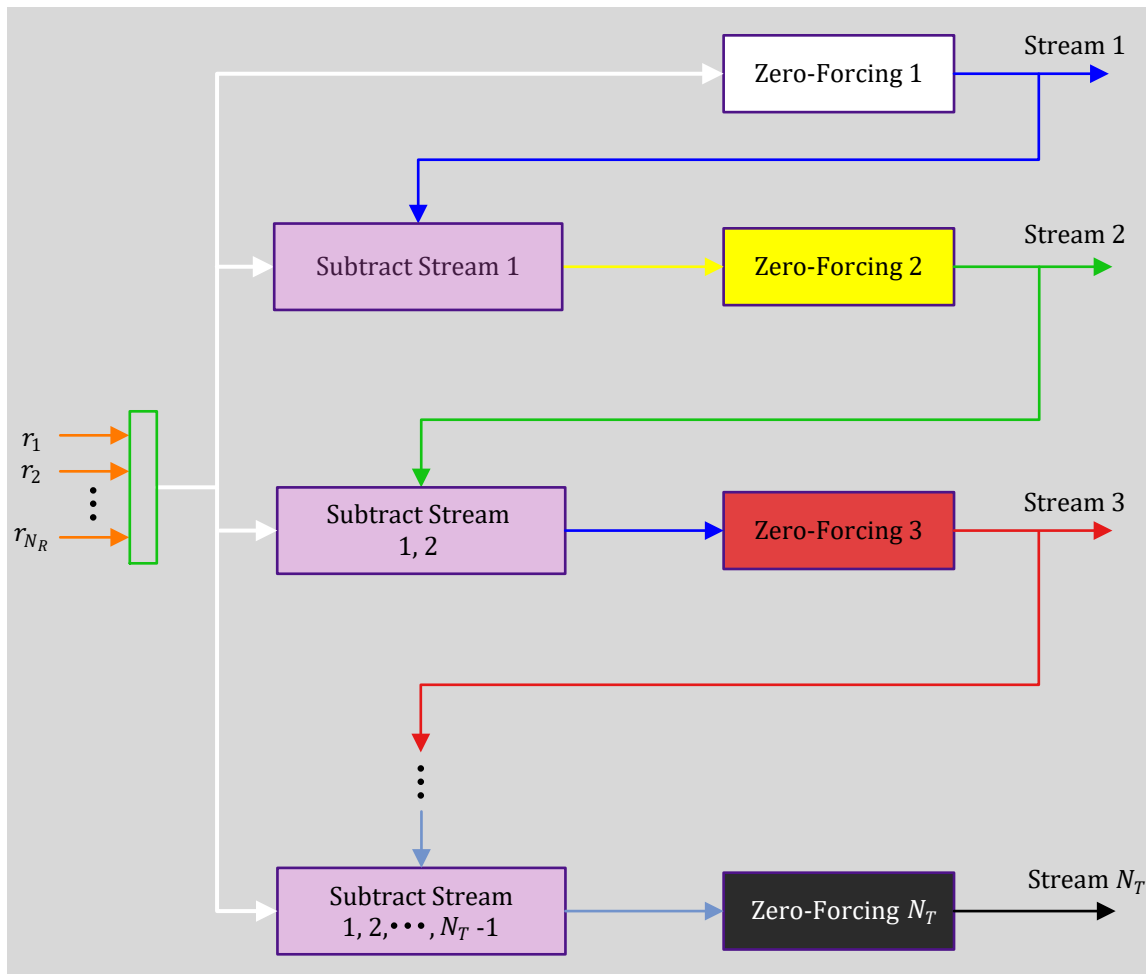


Figure 5.16: A flowchart for ordered successive interference cancellation algorithm with N_T Tx antennas and N_R Rx antennas

Ordering and First Stream Detection

This method starts with the ordering of the two streams according to some chosen criterion (e.g., SNR). Then, a linear detection algorithm (e.g., Zero-Forcing or MMSE) can be applied to detect the modulation symbols from the first stream as derived in Eq (5.10) above.

$$\hat{s}_1 = \frac{h_{(2 \rightarrow 2)} \cdot r_1 - h_{(2 \rightarrow 1)} \cdot r_2}{h_{(2 \rightarrow 2)} \cdot h_{(1 \rightarrow 1)} - h_{(2 \rightarrow 1)} \cdot h_{(1 \rightarrow 2)}}$$

This brings us to the next stage.

Removal of Interference

Having known the first stream and assuming the decisions were correct, its impact can be removed from *all* the Rx signals through subtraction. Assuming that \hat{s}_1 was detected, Eq (5.12) is modified as

$$\begin{aligned} \tilde{r}_1 &= r_1 - h_{(1 \rightarrow 1)} \cdot \hat{s}_1 = \cancel{h_{(1 \rightarrow 1)} \cdot \{s_1 - \hat{s}_1\}}^0 + h_{(2 \rightarrow 1)} \cdot s_2 + \text{noise} \\ \tilde{r}_2 &= r_2 - h_{(1 \rightarrow 2)} \cdot \hat{s}_1 = \cancel{h_{(1 \rightarrow 2)} \cdot \{s_1 - \hat{s}_1\}}^0 + h_{(2 \rightarrow 2)} \cdot s_2 + \text{noise} \end{aligned} \quad (5.13)$$

If there are no errors, i.e., $\hat{s}_1 = s_1$, the contribution from s_1 cancels out at both Rx antennas! In case there are more than 2 spatial streams, then the linear algorithm can be applied again to detect s_2 . Subsequently, the interference contribution from s_2 can be removed by subtraction in a similar manner as shown above for s_1 .

Detection of Last Stream

Observe that the signals \tilde{r}_1 and \tilde{r}_2 above have become functions of modulation symbol s_2 only. We have two independent equations and one unknown. In case of a single layer or a single antenna system, there is no difference between Maximal Ratio Combining (MRC) and a Zero-Forcing solution. So the same algorithm can be applied to estimate \hat{s}_2 which looks like MRC technique. This incorporates the SNR from all the Rx antennas and hence the weights w_i should be conjugates of complex channel gains involved with s_2 in Eq (5.13).

$$h_{(2 \rightarrow 1)}^* \cdot \tilde{r}_1 + h_{(2 \rightarrow 2)}^* \cdot \tilde{r}_2 = \left\{ |h_{(2 \rightarrow 1)}|^2 + |h_{(2 \rightarrow 2)}|^2 \right\} \cdot s_2 + \text{noise}$$

The decision on s_2 can now be taken as the constellation point closest to the value from the left hand side above.

$$\hat{s}_2 = \frac{h_{(2 \rightarrow 1)}^* \cdot \tilde{r}_1 + h_{(2 \rightarrow 2)}^* \cdot \tilde{r}_2}{|h_{(2 \rightarrow 1)}|^2 + |h_{(2 \rightarrow 2)}|^2}$$

Coloring Scheme

To help the reader understand the idea, observe that Figure 5.16 is drawn with a hidden RGB (Red, Green, Blue) coloring scheme. Since white color contains an equal contribution from all of them, the signal input to the algorithm is shown as white in color. After the blue stream is detected, the arrows are shown as blue while the Zero-Forcing is applied now to a combination of Red and Green, i.e., yellow. After the detection of Green layer, the arrows are green and the final Red stream is detected in the end. The last box for stream N_T is drawn black since black color means absence of all colors.

A few comments regarding this scheme are in order.

Diversity order

A linear algorithm is applied for the detection of the first spatial stream (s_1 in our example above). Consequently, the diversity order is similar to what we found for linear detection of the previous section: $N_R - N_T + 1$. However, as compared to the detection of s_1 , one spatial stream s_2 next is detected through two Rx antennas, see Eq (5.13). This is similar to the scenario of 1 Tx antenna and 2 Rx antennas. Therefore, the diversity order for s_2 is 2.

The advantage of this scheme is now clear. The modulation symbols that are detected successively at later stages benefit from a progressively higher diversity order. Consequently, the diversity order is equal to N_R for the last stream because that is virtually detected with N_R antennas at the Rx.

Error Propagation

Notice from Eq (5.13) that the terms involving $s_1 - \hat{s}_1$ only go to zero if $\hat{s}_1 = s_1$. Otherwise, instead of removing the interference, such an operation actually *injects* more interference into the output streams thus making it more difficult to detect the modulation symbols down the subsequent stages. This is known as *error propagation*.

Ordering

Due to error propagation, the order in which streams are chosen for estimation and subsequent interference removal significantly impacts the overall performance. There are different methods for this purpose such as SNR based ordering, Signal to Interference plus Noise (SINR) based ordering and ordering based on channel gains of each particular stream (e.g., $h_{(1 \rightarrow 1)}$, $h_{(2 \rightarrow 1)}$, \dots , $h_{N_T \rightarrow 1}$ all belong to symbol s_1).

Until now, we have found that linear detection is computationally simple with the trade-off being a worse performance. On the other hand, SIC strikes a balance between computational complexity and performance through iterative interference removal. Next, we turn our attention towards the optimal signal detection strategy against which the performance of other schemes are benchmarked. This is known as the Maximum Likelihood (ML) detection and it works according to the principle first displayed in Figure 5.17.

5.3.3 The Algorithm from a Clever Horse

Without channel knowledge and hence no independent parallel pipes in the air, the detection algorithms exploit the fact that each modulation symbol (e.g., s_1 from Tx antenna 1) arrives not only at Rx antenna 1 but also at all the other Rx antennas. Hence, an ideal detection algorithm in open-loop mode should combine energy from each Rx antenna related to the modulation symbol s_1 for decision purpose. A similar argument holds for the symbols s_2 to s_{N_T} . Such an interpretation is drawn in Figure 5.17 and in practice it is not necessarily employed by all MIMO detection algorithms.

Maximum Likelihood (ML) detection is a statistical signal processing technique which aims to find the best decision (e.g., a modulation symbol estimate) under a given probability distribution model. Since expressions involving probability are outside the scope of this text, I will describe an intuitive view of how this technique works as a MIMO detection algorithm in spatial multiplexing mode. Let us understand this concept with a short story of Clever Hans, a German horse, taken from Wikipedia.

The Story of Clever Hans

Hans was a horse that lived in Germany in the early 20th century (shown on the left in Figure 5.18). He belonged to a man called Herr Wilhelm von Osten. Von Osten was a teacher who taught math at a local school. He was an amateur horse trainer too.

Inspired by Charles Darwin, this was a time when people were becoming interested in measuring the intelligence of animals. Von Osten taught Hans to add, subtract, multiply, divide, work with fractions, tell the time and date, read and spell and to understand German. If he asked the horse a question such as: "What is 12 plus 12?", the horse would tap its hoof 24 times. Von Osten traveled around the country with Hans, showing off his clever horse to the public.

Later an investigation into his intelligence found that the horse did not know any of the mathematics and was instead picking slight facial cues from the owner or the person asking the question to know where to stop.

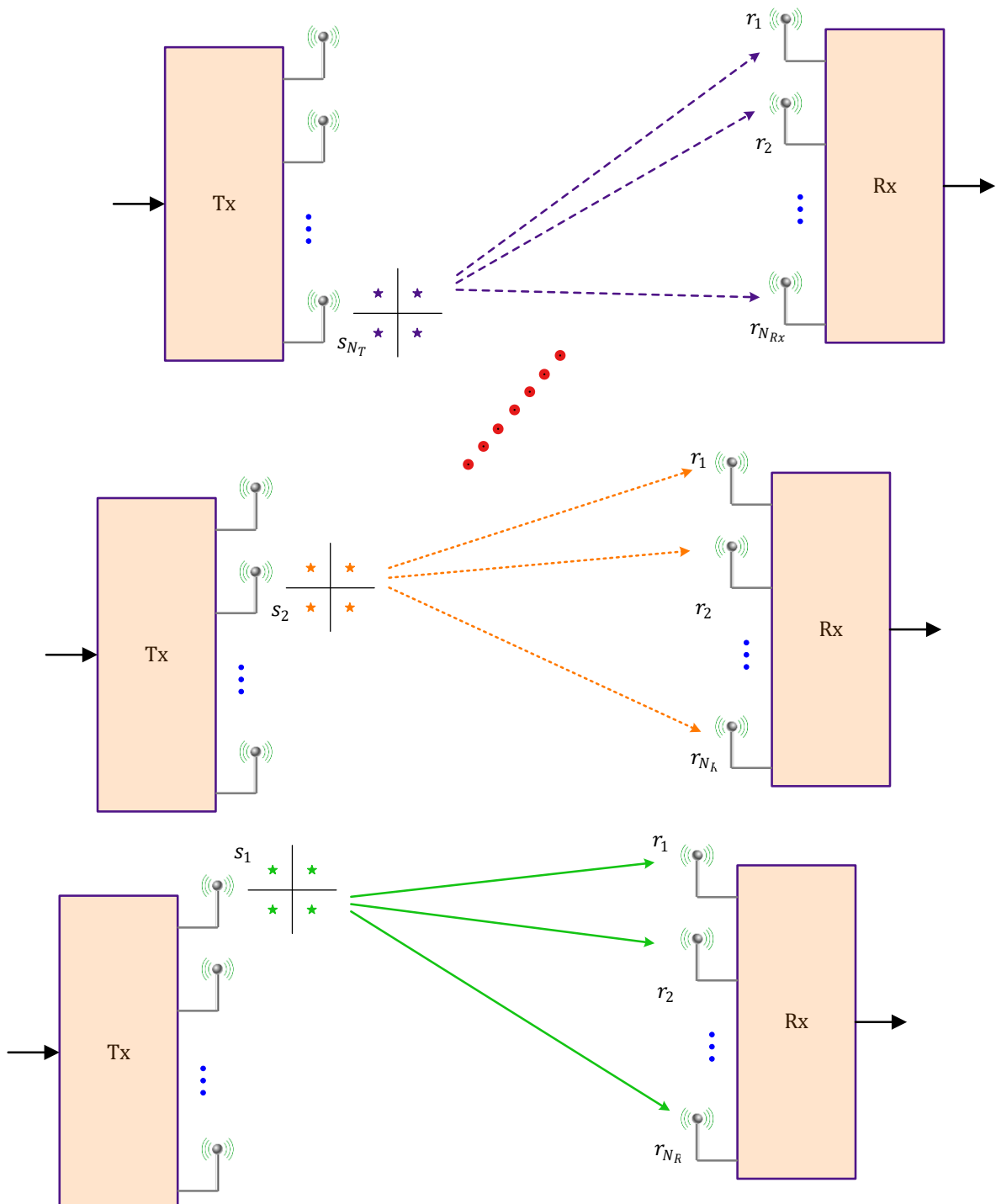


Figure 5.17: Energy from each Tx antenna is collected at all Rx antennas

Imagine that you have two game controllers as shown on the right in Figure 5.18 and you know that only one particular combination will save the player's virtual life, i.e., a correct button (red, green, blue



Figure 5.18: The horse Clever Hans performing his mathematical magic (Image credit: Wikipedia)

or yellow) from game controller 1 and another from game controller 2 need to be found out. Suppose that Clever Hans is given the task of guessing the correct combination. What would he do? He would tap its hoof on all the possible combinations (shown below) and stop on the correct answer based on your facial expressions. In this example, the correct answer is (B, G): the blue button on controller 1 and green button on controller 2.

		Red	Blue	Green	Yellow
		(R, R)	(R, B)	(R, G)	(R, Y)
Game Controller 1	Red	(R, R)	(R, B)	(R, G)	(R, Y)
	Blue	(B, R)	(B, B)	(B, G)	(B, Y)
	Green	(G, R)	(G, B)	(G, G)	(G, Y)
		Yellow	(Y, R)	(Y, B)	(Y, G)
					(Y, Y)

The principle of ML detection is exactly the same. While the terminology is fancy, the algorithm is not smarter than a clever horse. As we saw before, decisions on modulation symbols are made according to their minimum Euclidean distance from a constellation point[†]. In ML detection, this distance from

[†]This is because noise is modeled as Gaussian which implies that its probability distribution function is

$$f(x) = \frac{1}{\sigma\sqrt{2\pi}} e^{-\frac{1}{2\sigma^2}(x-\mu)^2}$$

where μ is the mean, σ is the standard deviation and σ^2 is the variance. Maximizing this probability implies minimizing the argument of the exponential function $(x - \mu)^2$. Due to this squared quantity, you see so many algorithms in detection and estimation theory targeting to minimize the Euclidean distance through L2 norm ($|\cdot|^2$) of a vector or Frobenius norm of a matrix ($\|\cdot\|^2$)

the Rx vector r_i is computed from *all sets of candidate constellation points* and then the one with the smallest distance is chosen as the most probable decision. Let us explore the details with the help of a MIMO system example in which there are $N_T = 2$ antennas at the Tx and $N_R = 2$ antennas at the Rx.

For such a system, the Rx signal at the two antennas was stated in Eq (5.9) and reproduced below.

$$\begin{aligned} r_1 &= h_{(1 \rightarrow 1)} \cdot s_1 + h_{(2 \rightarrow 1)} \cdot s_2 + \text{noise} \\ r_2 &= h_{(1 \rightarrow 2)} \cdot s_1 + h_{(2 \rightarrow 2)} \cdot s_2 + \text{noise} \end{aligned}$$

For one Rx antenna, say 1, this minimum distance part can be written as

$$\min \left| r_1 - h_{(1 \rightarrow 1)} \cdot s_1 - h_{(2 \rightarrow 1)} \cdot s_2 \right|^2$$

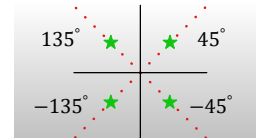
When signals from all Rx antennas from 1 to 2 are taken into account, the best decisions are based on total minimum distance. This is similar to navigating your way to a destination with the help of GPS. The optimal distance is the one that minimizes the *sum total* of distance (or time), not just one segment along the way.

$$\min \left[\left| r_1 - h_{(1 \rightarrow 1)} \cdot s_1 - h_{(2 \rightarrow 1)} \cdot s_2 \right|^2 + \left| r_2 - h_{(1 \rightarrow 2)} \cdot s_1 - h_{(2 \rightarrow 2)} \cdot s_2 \right|^2 \right] \quad (5.14)$$

To find the solution for the above expression, consider that the signal r_i at each Rx antenna i is known. Also, the channel gains $h_{(i \rightarrow j)}$ have already been estimated through training or pilot symbols. Here is the trick behind the algorithm. While modulation symbols are unknown, there are only certain values they can acquire. These are the candidates for the possible solutions. For example, a 4-QAM signal can have one of the four values shown below (the I and Q amplitudes are not shown in the figure to avoid any confusion). Both \hat{s}_1 from Tx antenna 1 and \hat{s}_2 from Tx antenna 2 can take any one of these four values.

$$45^\circ, \quad 135^\circ, \quad -45^\circ, \quad -135^\circ$$

→



Let us take an example of a 2x2 MIMO system with QPSK symbols. Just like Clever Hans case, a table for possible solutions of \hat{s}_1 and \hat{s}_2 can be built as follows.

	45°	135°	-45°	-135°
\hat{s}_2	($45^\circ, 45^\circ$)	($45^\circ, 135^\circ$)	($45^\circ, -45^\circ$)	($45^\circ, -135^\circ$)
\hat{s}_1	($135^\circ, 45^\circ$)	($135^\circ, 135^\circ$)	($135^\circ, -45^\circ$)	($135^\circ, -135^\circ$)
\hat{s}_1	($-45^\circ, 45^\circ$)	($-45^\circ, 135^\circ$)	($-45^\circ, -45^\circ$)	($-45^\circ, -135^\circ$)
\hat{s}_1	($-135^\circ, 45^\circ$)	($-135^\circ, 135^\circ$)	($-135^\circ, -45^\circ$)	($-135^\circ, -135^\circ$)

These fixed values can be plugged into the above metric in Eq (5.14) *one by one* to come up with several candidate pairs. The one with the smallest metric is the correct solution. Here, a sample answer ($135^\circ, -45^\circ$) is highlighted in orange as the correct solution. A few remarks are in order now.

Diversity Order

Since this algorithm jointly optimizes the target metric for all Tx modulation symbols, the diversity order obtained is the number of Rx antennas N_R *for all symbols*. In other words, ML algorithm achieves the best detection performance in the absence of channel knowledge at the Tx as described before in Figure 5.17.

Complexity

Due to the excellent performance, one would think that ML detection should be implemented in real wireless networks as the method of choice. This is not true because the algorithm complexity increases exponentially with the constellation size and number of Tx antennas N_T . For example, in the QPSK example above, the constellation size was 4 and the number of Tx antennas was 2. Therefore, the number of possible candidates was $4^2 = 16$ shown in the table above. Let us see how this number comes up.

For this purpose, consider a 16-QAM modulation and 2 Tx antennas where we have two symbols s_1 and s_2 , each of which can acquire 16 possible values. *For each such value of s_1* , the algorithm has to search for 16 possible candidates for s_2 , as shown in Figure 5.19. Since this procedure has to be repeated 16 times in total (once for each s_1), the total number of candidates comes out to be $16 \times 16 = 16^2 = 256$.

If you think this is still not a very large number, the actual transmissions in high rate wireless networks use a much higher constellation size as well as the number of Tx antennas. For a good channel condition case of 256-QAM with 8 Tx antennas, this number grows to

$$256^8 \approx 1.85 \times 10^{19}$$

Alternatives

Many alternatives to ML detection with less complexity have been devised such as sphere decoding algorithm and various lattice reduction techniques. Furthermore, while the computation complexity of ML detection algorithm is prohibitive in most cases, its performance serves as a benchmark against which the performance of other practical algorithms such as Zero-Forcing or SIC can be gauged.

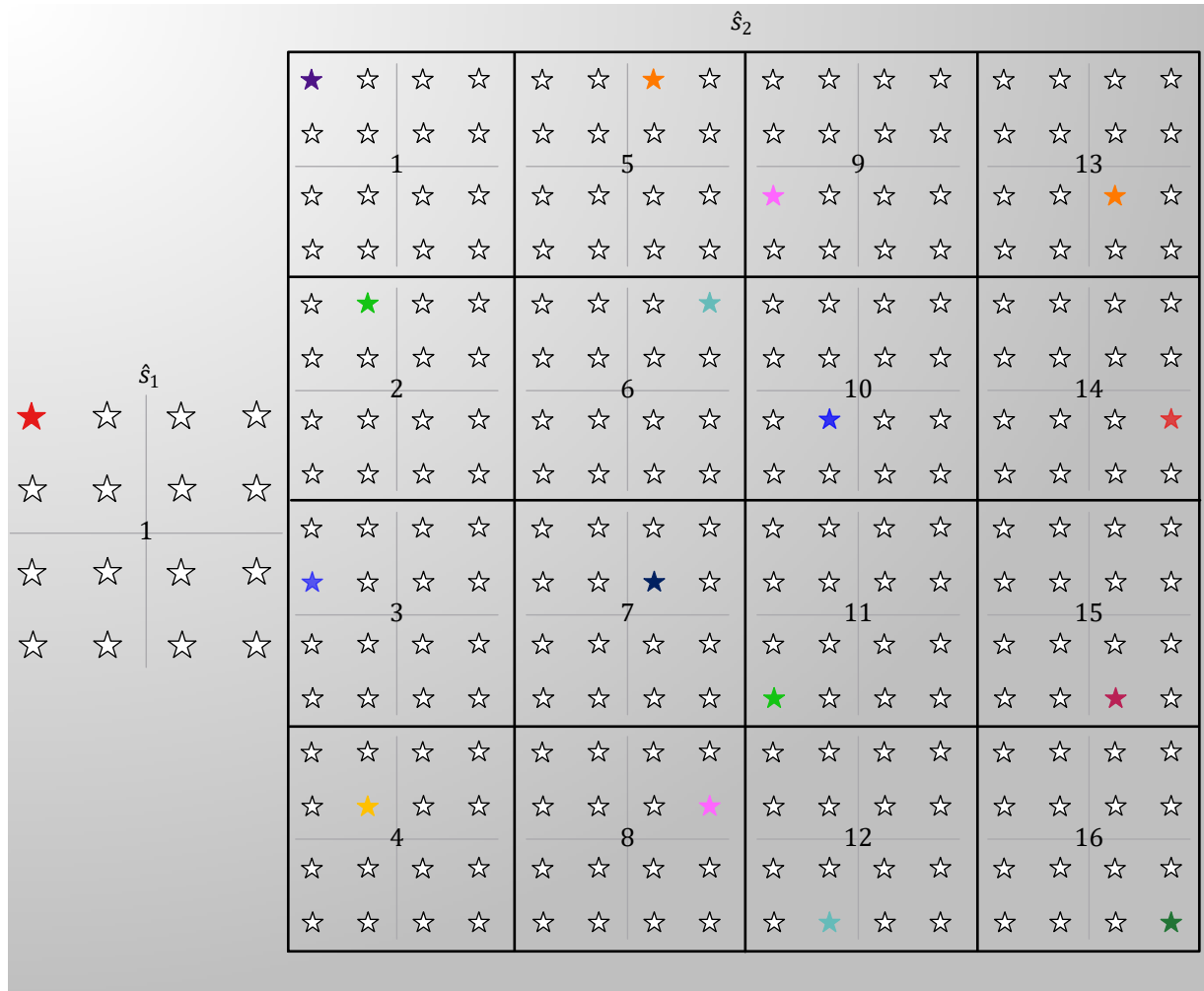
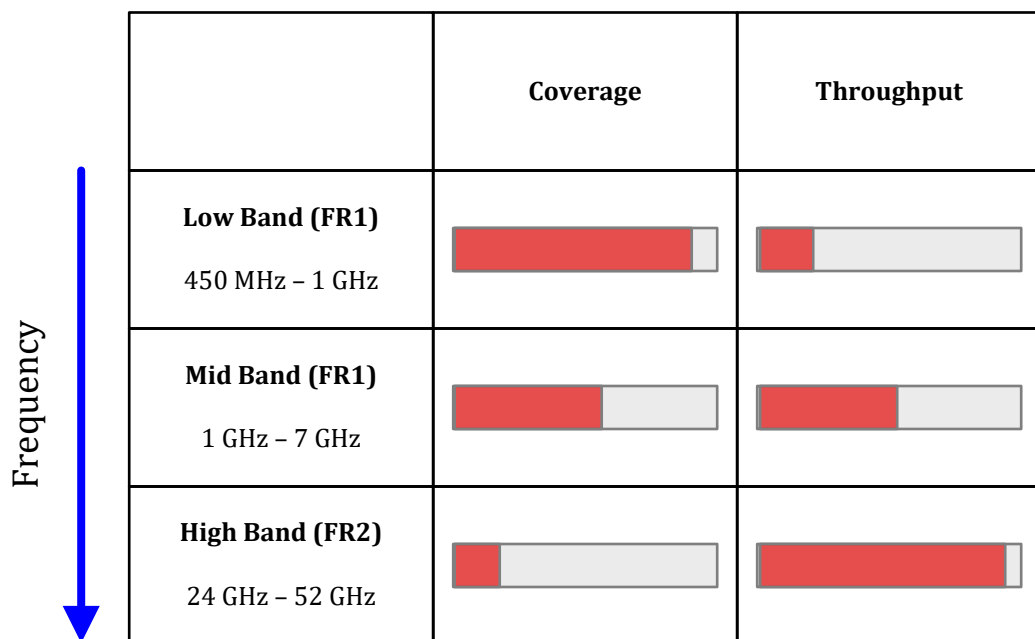


Figure 5.19: A case of 16-QAM modulation with 2 Tx antennas. For each s_1 candidate, there are 16 possible candidates for s_2

Chapter 6

Millimeter Wave (mmWave) Communication



Rising wireless traffic demands a continuous improvement in aggregate data rates delivered within a geographical area that requires fundamentally different design decisions as compared to a point-to-point system. We saw in Chapter 1 that the area throughput can be broken as

$$\text{Area throughput (bits/s/km}^2\text{)} = \underbrace{\text{Spectral efficiency (bits/s/Hz/cell)}}_1 \times \underbrace{\text{Cell density (cells/km}^2\text{)}}_2 \times \underbrace{\text{Bandwidth (Hz)}}_3$$

We also saw that a wider bandwidth directly translates into higher throughput, just like increasing the number of lanes on a road directly impacts the traffic handled at peak times. This is the original reason for opening up the higher GHz and THz bands where vast amounts of empty spectrum is available.

A bird's eye view of the history of wireless transmission reveals that the wireless throughput increase during the past century has relied far more on bandwidth expansion than smart physical layer techniques. At the same time, currently used spectrum at microwave frequencies spans only several hundreds of MHz. This puts a limit on the gain that can be extracted through bandwidth expansion. Past efforts to increase this scarce spectrum have mostly been made in the following two directions.

- Reallocate the existing microwave spectrum is one strategy that can create spaces for new applications. However, this has not been a successful approach due to reasons such as having a limited spectrum to start with and high costs of moving the existing allottees. One such redistribution from terrestrial TV portion generated only about 80 MHz of extra spectrum.
- Intelligent sharing of spectrum through cognitive radio received large amounts of research funding as a potential solution. Nevertheless, two factors significantly hindered its widespread adoption. One is the reluctance on part of licensed spectrum holders to share it with secondary opportunistic users. The second is that the march of current 5G and later standards is towards an ever-present wireless connectivity. Intelligence costs money and rather than continuously sensing the environment for simply a permission to transmit, signal processing energy budget can be allocated to more useful applications arising from such vast networks.

Due to these obstacles, the trend of spectrum expansion has looked towards other directions. At the time of this writing, 3.5 GHz range (3.3 GHz to 4.2 GHz) has become very attractive for 5G deployments around the world due to spectrum availability and good coverage at low frequencies. Nevertheless, this spectrum is still limited and mmWave band has become the most significant contributing factor behind astronomically high data rates in 5G systems. Strictly speaking, millimeter wave (mmWave) spectrum is considered as occupying the wavelengths between 1 mm to 10 mm. Let us denote the wavelength by λ and use the relation $c = F_C \cdot \lambda$ where c is the speed of an electromagnetic wave and F_C is the carrier frequency. Then, $\lambda = 1 \text{ mm}$ implies

$$F_C = \frac{c}{\lambda} = \frac{3 \times 10^8}{1 \cdot 10^{-3}} = 300 \text{ GHz}$$

In a similar manner, a wavelength of 10 mm corresponds to

$$F_C = \frac{c}{\lambda} = \frac{3 \times 10^8}{10 \cdot 10^{-3}} = 30 \text{ GHz}$$

Therefore, the mmWave spectrum span lies between 30 GHz and 300 GHz, although the term is commonly associated with the band between 10 GHz and 100 GHz in the wireless community. The remaining 100 GHz to 300 GHz spectrum is loosely defined as 'sub-TeraHz' as illustrated at a logarithmic scale in Figure 6.1. Most providers are focusing on the spectrum between 24 GHz and 100 GHz for 5G cellular systems although trials in sub-TeraHz bands are already on their way for possible inclusion in 6G standard.

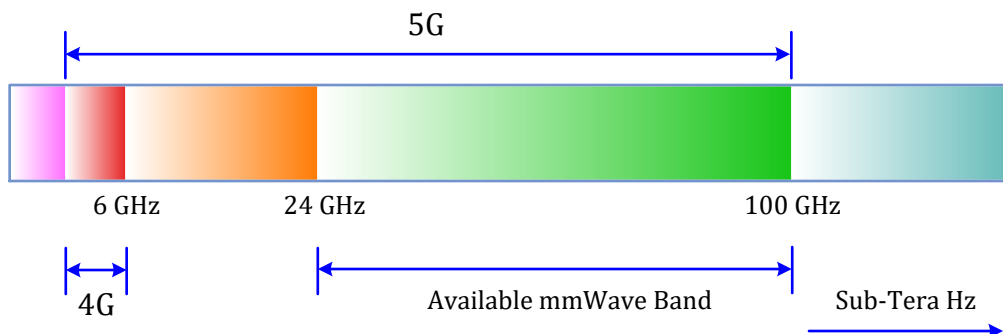


Figure 6.1: Spectrum for sub-6 and mmWave bands. Compare the 4G allocations with (potential) 5G ranges

Communications in mmWave band has an interesting history. In fact, one of the very first demonstrations of information transmission through wireless medium was at mmWave frequencies! In 1895 at Calcutta, India, the polymath Jagadish Chandra Bose demonstrated the transmission and reception of electromagnetic waves at 60 GHz over a distance of 23 meters through two walls by remotely ringing a bell and detonating some gunpowder. This higher part of the spectrum was not pursued later for mass wireless applications due to the challenges faced in signal transmission and device design at high frequencies. But this changed with the 5G standard when designers looked for higher transmission rates and found that a steady rise in the number of transistors packed in a given area eventually enabled circuit designs with the ability to process GHz of bandwidth for data transmission.

What impact could the carrier frequency have on the design of wireless networks? As far as the physical layer is concerned, a common practice in communication system designs is to rely on baseband level simulations operating on complex signals and systems, making them independent of the carrier frequency employed. This framework assumes a linear wireless channel, the impulse response of which is characterized through extensive measurement campaigns. The responsibility of maintaining a sufficient level of linearity in the hardware is then passed on to the analog and RF engineers. This works well for the conventional systems operating in microwave spectrum where the carrier frequencies as well as the

bandwidths are not very large. On the other hand, high carrier frequencies in mmWave spectrum, large bandwidths and the use of directional antenna arrays impact many aspects of physical layer design. This is even true for higher layers of the network. Here, we limit our discussion to some of these issues with an understanding that the rest are outside the scope of this text.

6.1 Channel Propagation

As far as the radio waves in a wireless channel is concerned, we distinguish between the free space path loss and realistic propagation conditions.

Free Space

Recall Eq (2.1) and assume that a Tx transmits P_{Tx} watts of power uniformly radiating in all spatial directions. Taking the Tx as a point source, the power radiates outwards in every dimension, i.e., in a sphere, which is known as isotropic radiation. Then, the power density at a distance d from the Tx point source is the ratio of the Tx power P_{Tx} to the surface area of the sphere $4\pi d^2$.

$$\text{Power density} = \frac{P_{\text{Tx}}}{4\pi d^2}$$

This is for an ideal isotropic antenna. Now if the gain of the real Tx antenna towards the Rx is given by G_{Tx} , the above expression becomes

$$\text{Power density} = \frac{P_{\text{Tx}}}{4\pi d^2} \cdot G_{\text{Tx}}$$

This gain factor accounts for the losses from a real antenna as well as its directionality: it is the ratio of the radiation intensity in a given direction to the radiation intensity that would be obtained for an isotropic antenna emitting equal power in all directions.

Next, assume that the Rx antenna has an effective aperture given by A_E which determines the amount of incident power collected at the Rx side. Therefore, P_{Rx} can be written as the product between the power density and effective aperture.

$$P_{\text{Rx}} = \text{Power density} \times A_E = \frac{P_{\text{Tx}}}{4\pi d^2} \cdot G_{\text{Tx}} \cdot A_E \quad (6.1)$$

From antenna theory, this effective aperture is given by the expression below, the derivation of which is outside the scope of this text.

$$A_E = G_{\text{Rx}} \cdot \frac{\lambda^2}{4\pi} \quad (6.2)$$

where λ is the carrier wavelength and G_{Rx} is the Rx antenna gain. Therefore, we have

$$P_{\text{Rx}} = \frac{P_{\text{Tx}}}{4\pi d^2} \cdot G_{\text{Tx}} \cdot G_{\text{Rx}} \cdot \frac{\lambda^2}{4\pi} = \frac{P_{\text{Tx}}}{(4\pi d)^2} \cdot G_{\text{Tx}} \cdot G_{\text{Rx}} \cdot \lambda^2 \quad (6.3)$$

There are two opposing factors at interplay in the above expressions.

Scenario I

From Eq (6.3), we observe that the Rx power in free space increases with λ^2 , the squared wavelength. Since wavelength has an inverse relation to frequency, or $\lambda = c/F_C$, another way of saying this is that the signal power decreases in proportion to F_C^2 , the squared carrier frequency. To understand this idea intuitively, consider two antenna arrays, one operating at low or mid band FR1 and the other at high band FR2. For the same number of antenna elements and antenna spacing with respect to the wavelength (e.g., $\lambda/2$), the antenna array at high band will be significantly smaller than the antenna array at low or mid bands. This is drawn in Figure 6.2 where two antenna arrays, both of which have a similar gain, are shown. This is similar to a window in your room: the larger the window size, the higher the amount of sunshine captured.

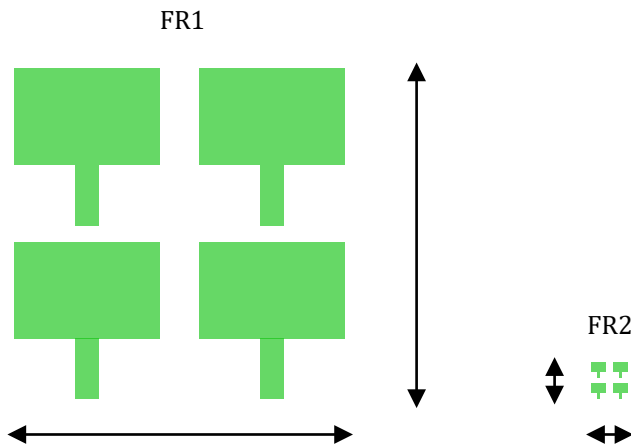


Figure 6.2: For the same number of antennas and their spacing (with respect to the wavelength), the area of the array at high band is smaller thus capturing a reduced amount of power

Let us compare this path loss at a distance $d = 50$ meters in a representative set of frequencies for equal Tx power, omnidirectional antennas and, most importantly, unit Tx and Rx gains $G_{Tx} = G_{Rx} = 1$.

$F_C = 900 \text{ MHz}$	\rightarrow	-65 dB
$F_C = 2.4 \text{ GHz}$	\rightarrow	-74 dB
$F_C = 5.8 \text{ GHz}$	\rightarrow	-82 dB
$F_C = 60 \text{ GHz}$	\rightarrow	-102 dB

In words, operating in mmWave band requires the designer to compensate for around 20-40 dB of Rx power loss in comparison to the lower microwave frequencies. Fortunately, this is possible if we note that this frequency dependence is a pure [antenna effect](#). Otherwise, a high frequency electromagnetic wave itself suffers no [extra](#) attenuation while propagating from the Tx to a Rx in the far field region.

Scenario II

The increased attenuation at higher frequencies is largely due to the *assumption* of constant gains G_{Tx} and G_{Rx} above that is a result of reducing the antenna size with the decreasing wavelength at high band. Now if the area of the antenna array is kept constant regardless of the wavelength and the element spacing is again fixed at, say $\lambda/2$, then more number of antenna elements are required to cover the same physical space. This is drawn in Figure 6.3 where the array now consists of a significantly larger number of elements. An increase in the array elements thus increases the Tx and Rx gains.

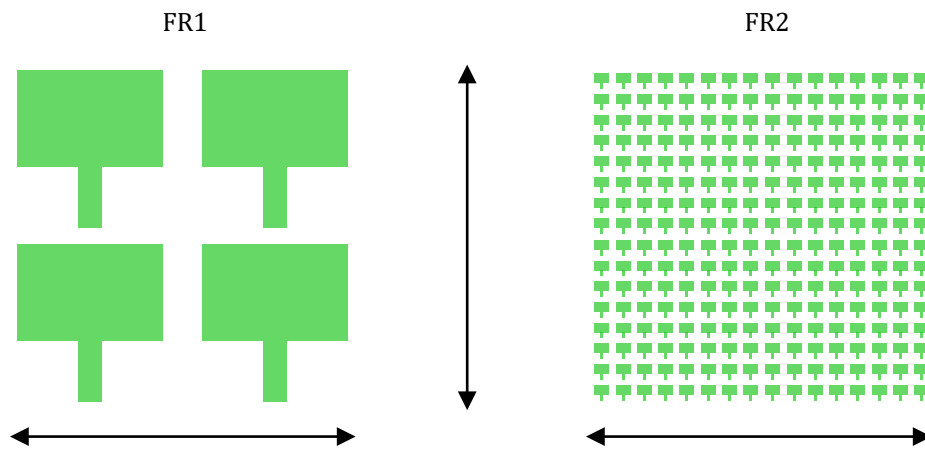


Figure 6.3: For the same area and their spacing (with respect to the wavelength), the number of elements in the array at high band is larger thus capturing a similar or increased amount of power

What is the effect of final received power P_{Rx} ? From Eq (6.2), the gain is inversely proportional to λ^2 .

$$G_{Rx} \propto \frac{1}{\lambda^2}$$

Plugging this in Eq (6.3), we get

$$P_{Rx} \propto \frac{P_{Tx}}{(4\pi d)^2} \cdot G_{Tx} \cdot \frac{1}{\lambda^2} \cdot \lambda^2 = \frac{P_{Tx}}{(4\pi d)^2} \cdot G_{Tx}$$

The effect of wavelength or frequency is thus completely eliminated! In fact, if similar antenna arrays are used at *both* sides of the link, i.e., at the Tx side too thus changing G_{Tx} , then the received power can be *increased* at high band! The coverage at mmWave frequencies can in fact become better in free space than sub-6 GHz frequencies.

To consider the effect of gain in terms of actual numbers, a system with 1000 Watts of Tx power along with a gain of 10 (10 dB) provides the power equal to

$$1000 \times 10 = 10000$$

This number is the same as 100 Watts of Tx power along with a gain of 100 (20 dB).

$$100 \times 100 = 10000$$

In reality, while a higher gain is achieved through a large number of antennas at mmWave frequencies that adequately provide the coverage, the allowed output power is still limited and the coverage area is usually smaller than sub-6 GHz frequencies.

To summarize, higher attenuation at mmWave frequencies can be compensated for, and even surpassed, through highly directional antennas as it is easier to increase the Tx and Rx antenna gains than the Tx power in mmWave systems. This is the principle on which mmWave communication is based where increased directivity is provided by massive MIMO and beamforming in 5G systems. The interesting point to note is that antenna array in a massive MIMO system requires a reasonably small form factor due to the dependence of antenna spacing on very short wavelengths. As a consequence, it forms a natural partnership with mmWave frequencies for transmissions at Gbps.

Atmospheric Effects

Coming to the realistic channels, the mmWave path loss increases *over and above the free space attenuation* due to several frequency-dependent factors [12].

Water Vapors and Oxygen

At lower microwave frequencies, the effects of water vapors and oxygen molecules in the air can be safely ignored. This is not true for mmWave spectrum. For a reference, Figure 6.4 indicates the excess attenuation across the mmWave and sub-TeraHz spectrum at 60 GHz, 120 GHz, 180 GHz, 320 GHz and 380 GHz caused by atmospheric absorption. In particular, electromagnetic waves around 60 GHz are severely attenuated due to oxygen absorption, a phenomenon that results in more than 15 dB/km loss in Rx power. Therefore, these frequencies are suited for indoor networks with short coverage range. The remaining frequencies, e.g., around 50 GHz, 100 GHz or 150 GHz, there is very little attenuation beyond the normal free space propagation loss.

Rain

In addition to the atmospheric absorption, the weather also impacts the mmWave propagation such as rain and snow. This is because the physical size of the raindrops, hail stones and snowflakes is on the order of the propagating wavelength causing non-negligible scattering. As a consequence, the link budget needs to account for approximately 15 dB/km extra attenuation during heavy rains and is usually closed with the help of additional beamforming gains.

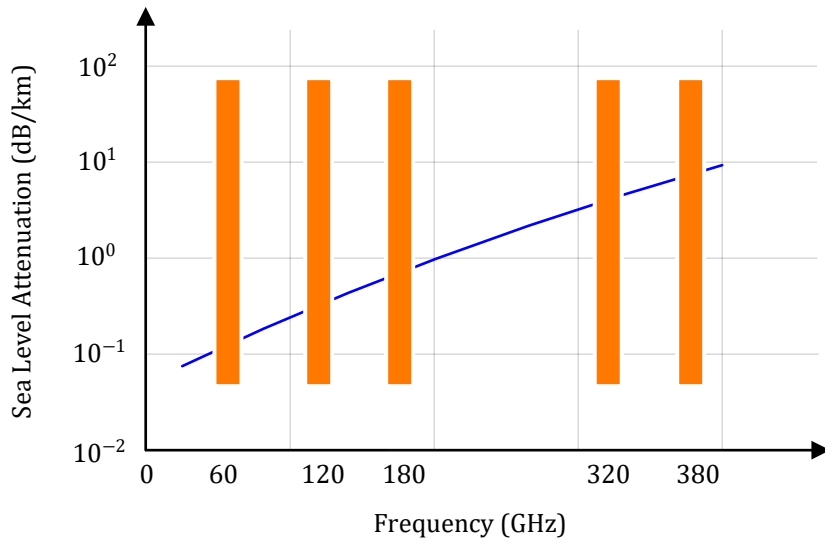


Figure 6.4: Excess attenuation (dB/km) over free space propagation due to atmospheric absorption as a function of carrier frequency or wavelength

Penetration

Several measurement campaigns have shown that penetration into outdoor building material also suffers from losses amounting to several tens of dBs over free space loss. Therefore, it is difficult for mmWave signals to penetrate into the buildings from outside and vice versa.

There are three main mechanisms for wave propagation in a wireless channel: diffraction, scattering and reflection. Diffraction is the bending of waves around corners of the obstacles. That object or aperture effectively becomes a secondary source of the propagating wave. From the perspective of a wireless signal at microwave frequencies, waves coming from diffracting objects keep the communication link operational even when there is no line of sight between the user terminal and the base station. On the other hand, diffraction mechanism suffers from heavy losses in mmWave band as compared to other phenomena like reflections and scattering. Therefore, mmWave systems do not rely on diffraction for wave propagation and instead resort to virtual beamforming described in Section 3.4 in which the Tx and Rx look for reflected and scattered paths to maximize the Rx power through array gain.

Delay Spread

As explained in Section 2.2, the delay spread of a wireless channel is a measure of the time difference between the first and the last arriving multipath. In general, it is characterized by the symbol time of the system, i.e., the same delay spread of, say, $2 \mu\text{s}$ can extend to 1 symbol or 100 symbols, depending on whether the symbol rate is 0.5 MHz or 50 MHz. This implies that for smaller symbol rates (i.e., larger

symbol times), there is less Inter-Symbol Interference (ISI) which determines the amount of bandwidth over which the spectrum is relatively constant. This is known as a frequency flat channel. On the other hand, for larger symbol rates (i.e., lower symbol times), the multipath extends over several tens of symbols thus introducing ISI and dips in the signal spectrum. This is known as a frequency selective channel.

It turns out that there are three effects governing this behavior in mmWave channels.

- The main attraction of mmWave bands is to exploit vast unused spectrum where even several GHz of bandwidth can be committed to a single user. Since the symbol rate is directly proportional to the bandwidth, we have significantly large symbol rates or reduced symbol times in mmWave systems as compared to lower frequency bands. Such a large bandwidth (i.e., short symbol time) necessitates long delays if the multipath at mmWave frequencies follow the same pattern as the lower bands.
- As we found above, free space path loss, atmospheric absorption and penetration losses result in substantial attenuation before the signal reaches the Rx. Therefore, even within the same environment, propagation characteristics are different and multiple copies die down relatively much quicker thus reducing the delay spread.
- 4G and the previous generations of cellular systems relied on omnidirectional radiation patterns, thus opening the possibility of multiple copies arriving after reflection, scattering and diffraction from any objects around the Tx or Rx. Such a scenario naturally increases the delay spread because a multipath can arrive from any direction. In contrast, mmWave Tx and Rx in 5G systems employ highly directional antenna arrays that either ‘look’ into particular directions (physical beamforming) or bouncing the multipath signals off various objects for a coherent summation at the Rx (virtual beamforming). As a result of these smaller number of paths, the delay spread is further reduced. One consequence of a pointed beam as in physical beamforming and subsequent reduction in multipath spread is that the extent of equalization needed at the Rx also gets simplified.

In conclusion, the overall effect of the above phenomena is that mmWave systems suffer from smaller delay spreads and hence less frequency selective fading. In fact, frequency dependence can be significantly reduced with a massive MIMO setup since the effective channel reduces to a constant value as described in Section 4.3.1.

Doppler Spread

In Chapter 2, we learned that there is a shift in frequency, known as **Doppler shift**, that arises from movement in the channel and given by Eq (2.4).

$$F_D = -\frac{\nu}{c} F_C$$

From the above expression, the Doppler shift depends on the carrier frequency F_C and the velocity of the Rx antenna ν . The relevance here is clear: the higher the frequency, the higher the Doppler shift and vice versa.

Now let us run some quick numbers for mmWave frequencies. If the user is moving at a normal walking speed of 5 km/hr (around 1.4 m/s) exactly in a line away from the Tx (so $\phi = \pi$) and the transmission is taking place at a carrier frequency of $F_C = 60$ GHz, then the Doppler frequency turns out to be

$$F_D = -\frac{1.4}{3 \cdot 10^8} \cdot 60 \cdot 10^9 \approx -280 \text{ Hz}$$

This number will be far greater at vehicular speeds. As explained in detail in Ref. [2], when multiple paths undergo different Doppler shifts, the result is a phenomenon known as *Doppler spread* that is the frequency domain counterpart of delay spread in time domain. Just like the delay spread determines the frequency selective nature of the channel, the Doppler spread governs the time selective nature of the channel, i.e., the rate of change of the channel gains (which are assumed constant for a frame duration) depends on the Doppler spread. The exact time varying characteristics depend on the velocity, carrier frequency and the bandwidth as well as the beamwidth.

There are a few factors that help achieve a balance for this time varying effect at mmWave frequencies.

- For coherent demodulation in 5G systems as we have seen before in MIMO detection algorithms, channel gains need to be estimated at the base station. These estimates need to be updated according to how fast the channel varies with time, say, by moving 1/8th of the wavelength. As the mmWave carrier frequencies increase with a corresponding decrease in the wavelength, a significant channel variation occurs for even small movements. For the same speed, the channel varies 15 times faster at 52 GHz as compared to 3.5 GHz. Consequently, a faster rate of update is needed that demands more pilots at a cost of actual data rate penalty.
- As we saw before, the reason to move to higher carrier frequencies is to exploit vast bandwidths that translate into higher symbol rates and consequently shorter symbol times! This implies that there is no substantial change in the number of symbols that fit into a coherence interval.
- With narrow beams resulting in a reduced angular spread, remember that mmWave base stations serve a small number of low mobility users in a limited geographical area. This eases the stringent requirements that could have arisen with rapid channel variations.

In summary, the size of a frame with a given percentage of pilot symbols can still be kept the same. If the channel changes more rapidly, say 5 times faster, then the frame also gets transmitted in a shorter time while maintaining the same number of pilot symbols. This strategy, along with higher cell density with small low mobility users, aligns with the goals of 5G systems that aim for a *lower communication latency* as compared to 4G systems.

A final summary of coverage and throughput in different frequency bands is shown in Figure 6.5. While the throughput rises with increasing frequency, the coverage shrinks due to the propagation effects discussed above. The decision on the frequency band of choice then depends on the actual deployment scenario.

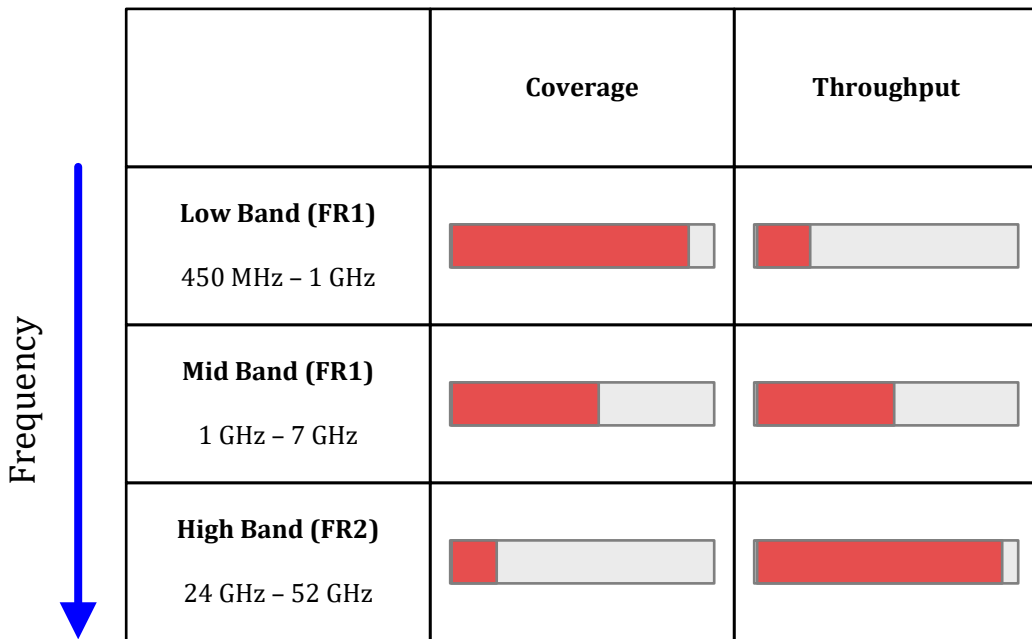


Figure 6.5: Coverage and throughput in different bands

6.2 Analog, Digital and Hybrid Beamforming

Beamforming is one of the most practical solutions to overcome higher path loss and atmospheric attenuation in mmWave bands. How it is implemented is a matter of great interest to RF industry due to the conflicting requirements of efficiency and flexibility. In a tradeoff between cost, size and complexity, analog beamforming is combined with digital beamforming to give rise to a hybrid solution, an architecture of choice in current 5G mmWave systems. Nevertheless, digital beamforming is inevitably the direction of future and it is only a matter of time before it will be used in 5G networks in high bands too [15].

Analog Beamforming

Like most other technologies, beamforming in early years started as a humble analog solution that was improved gradually in multiple stages. It began with fixed phase shifters for generating beam at a single frequency. Flexibility was later incorporated through a switching architecture with several phase

shifters, each for a different beam pattern. Finally, adjustable phase shifters at each antenna element were introduced to enable flexible and adaptive beams that could look into any direction.

A simplified analog beamforming framework is shown in Figure 6.6 where I have prioritized a clear explanation of underlying functionality over an illustration of actual RF design. The weights are adaptively computed in digital domain and updated in analog domain using specific DSP algorithms for a target criterion.

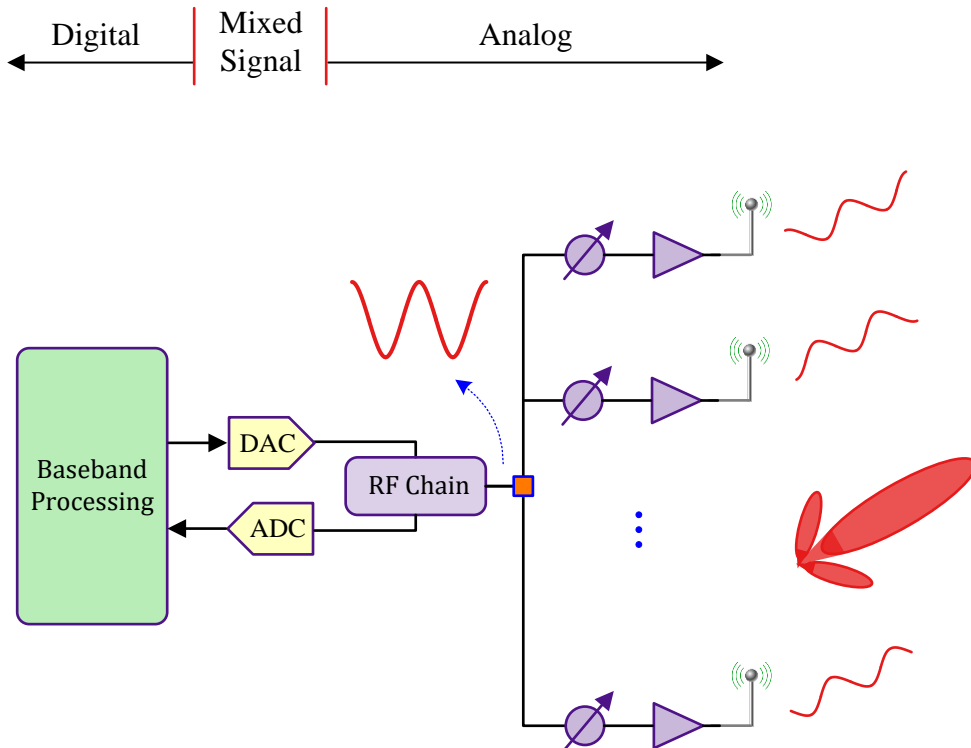


Figure 6.6: Analog beamforming

On the Tx side, the baseband signal is generated in the digital domain that is converted into an analog signal through a Digital-to-Analog Converter (DAC), up-converted to a higher carrier frequency (e.g., 28 GHz) and then fed to an analog beamforming network through a splitter. Here, the weights are applied through several digitally controlled phase shifters, one per antenna element. Generating complicated beam patterns, e.g., in a multiuser environment, is not easy to implement through analog components. On the Rx side, the arriving signal is phase shifted at each element before combined, filtered and downconverted to baseband or intermediate frequency. Digital samples are then produced through the ADC. Since the signal has already been beamformed in the analog domain before, the sampled signal is a superposition of various waves which cannot be manipulated in digital domain.

Analog beamforming is power and cost efficient as it has only one pair of ADC, DAC and a single RF chain, see Figure 6.6. However, it comes at a cost of following drawbacks.

- It is difficult to implement advanced beamforming techniques such as creating nulls in specific directions during transmit or receive. This can create significant interference among undesired directions.
- Fine tuning of the beams is limited due to the low resolution of quantized phase shifts.
- From Figure 6.6, it is difficult to support multiple streams for multiuser MIMO. In general, a phase shifted version of the same signal is sent from all the antennas into a particular direction.
- RF phase shifters suffer from performance degradations due to losses and distortions.

All these challenges are easier to overcome through a digital beamformer.

Digital Beamforming

A simplified digital beamforming architecture is illustrated in Figure 6.7. In this case, each antenna element has its own dedicated RF chain as well as individual DACs and ADCs. Recalling the sampling analogy, this implies that the gain and phase of each spatial sample is adjusted in an individual manner along with baseband processing before upconversion at Tx or after downconversion at Rx. This enables a true implementation of mathematical algorithms with maximum flexibility, most of which treat each antenna output as an accessible sample. For example, this flexibility is evident in the following scenarios.

- Along with maximizing the signal strength in a desired direction, nulls can also be created in undesired directions to suppress the interference.
- Multiple spatial streams can be simultaneously created for spatial multiplexing discussed in Chapter 5. More complicated precoders can be implemented for this purpose to generate multiple beams and enable multiuser communications. This is done by matrix multiplication in digital domain similar to the SVD decomposition.
- The beamforming weights, discussed in both physical and virtual scenarios, were for narrowband signals. A digital architecture allows for catering large bandwidths by selecting the weights for a frequency selective scenario. Wideband signal transmission and reception improves the spectral efficiency of the system by operating over a large signal bandwidth without beam squint (change in beam pattern as a function of operating frequency).

To obtain all these benefits, all spatial samples need to be individually processed. Here, each antenna element having its own frontend comes at a cost. ADCs and DACs operating at Multi-GHz clock frequencies are complex and power consuming. Consequently, fully digital beamforming is utilized in commercial multi-antenna systems in the lower frequency range while initial mmWave systems mostly utilize hybrid beamforming architectures as described next.

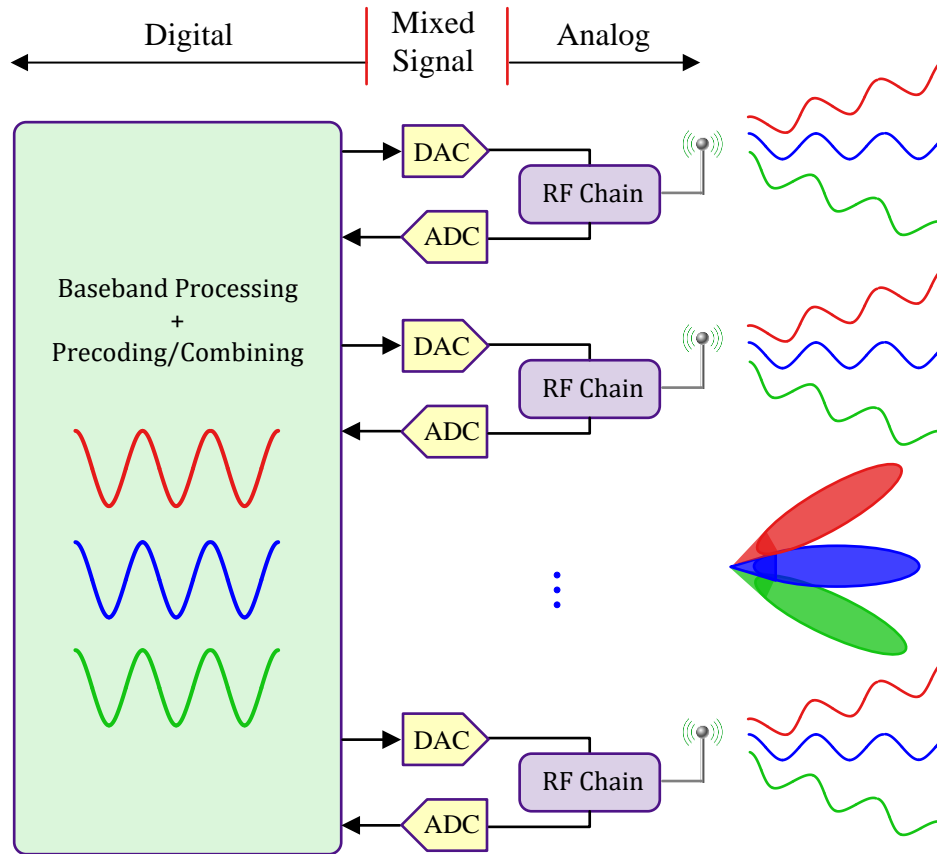


Figure 6.7: Digital beamforming

Hybrid Beamforming

Hybrid beamforming is a compromise between low power but less flexible analog beamforming and power hungry but fully flexible digital beamforming solutions. This two-stage architecture is drawn in Figure 6.8 where precoding or combining is done first in the analog part and later in the digital domain. While the antenna elements are still driven by analog phase shifters, the number of RF chains and ADC/DAC are lesser than the number of antennas. Precoding is then performed in the digital domain at the level of radio chains. This reduction in the number of data converters and corresponding chains results in less cost, computational load and power consumption. Multiple spatial streams can also be supported, albeit only upto the number of RF chains and hence less than what pure digital beamforming has to offer. In summary, both the digital and analog beamforming work together in this case to improve the coverage or to provide multiple beams to spatially separated users.

Analog or RF precoding/combining in Figure 6.8 can be implemented through two different schemes.

- An antenna array is divided into several subarrays, each forming an analog beamforming network and connected to its own RF chain. Since the subarrays operate more or less in an indepen-

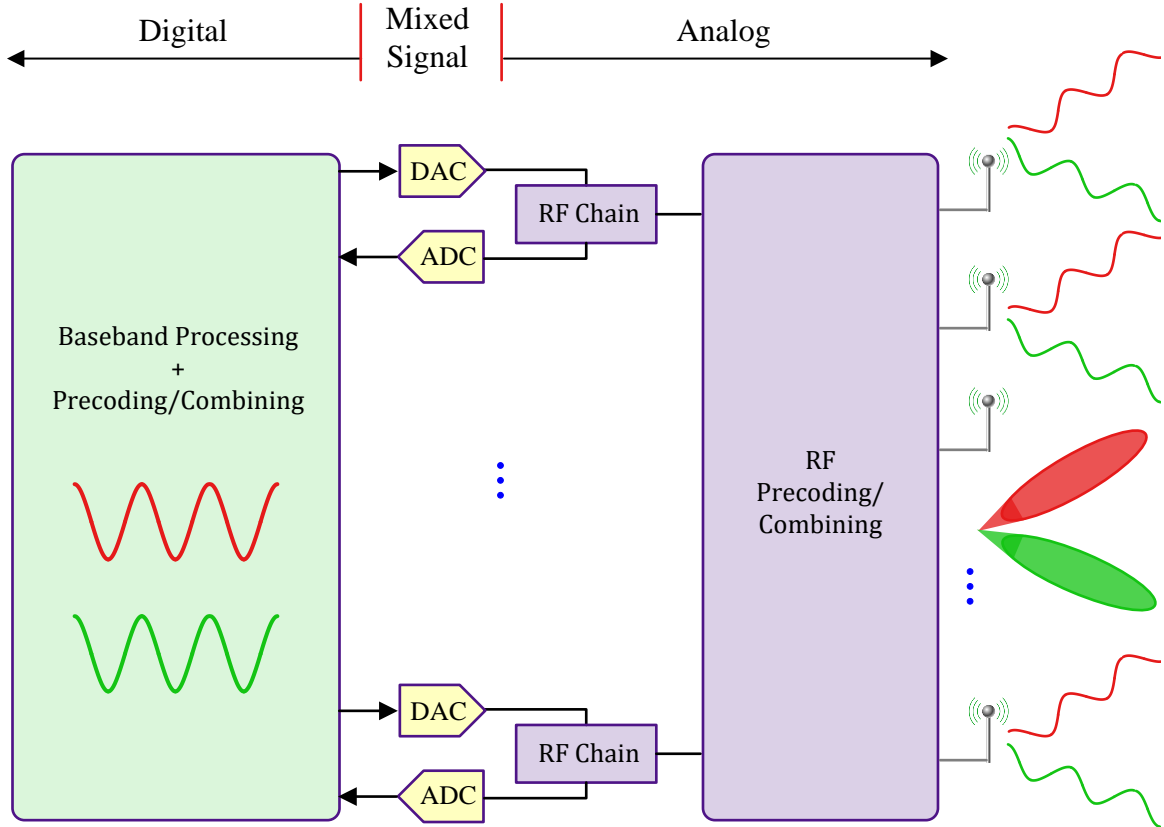


Figure 6.8: Hybrid beamforming

dent manner, the overall framework reduces complexity and power consumption at a cost of less flexibility. This is drawn in Figure 6.9a.

- Each antenna is connected to all RF chains and the digitally controlled phase shifters are computed based on some jointly optimal criteria. This provides maximum flexibility in directing and manipulating multiple beams at a cost of complexity. Such an architecture is shown in Figure 6.9b.

The weights in digital and analog domains are chosen to closely approximate the optimal solution that results in minimum interference among the streams. The optimal solution is not trivial due to the number of antennas and subarrays involved as well as additional constraints that come with choosing imprecise analog weights. A trade-off needs to be made between performance and complexity.

To see why hybrid beamforming strikes a good balance between complexity and flexibility, remember that the spatial selectivity implemented by a beamformer comes from a combination of signals generated from or arriving at individual antenna elements, each of which radiates or receives according to its own radiation pattern, irrespective of the array factor. Since each element has its own RF chain from the element down to the baseband in a digital beamformer, each of them has to accommodate both the desired and undesired signals and thus suffers from a high dynamic range (the ratio between maximum

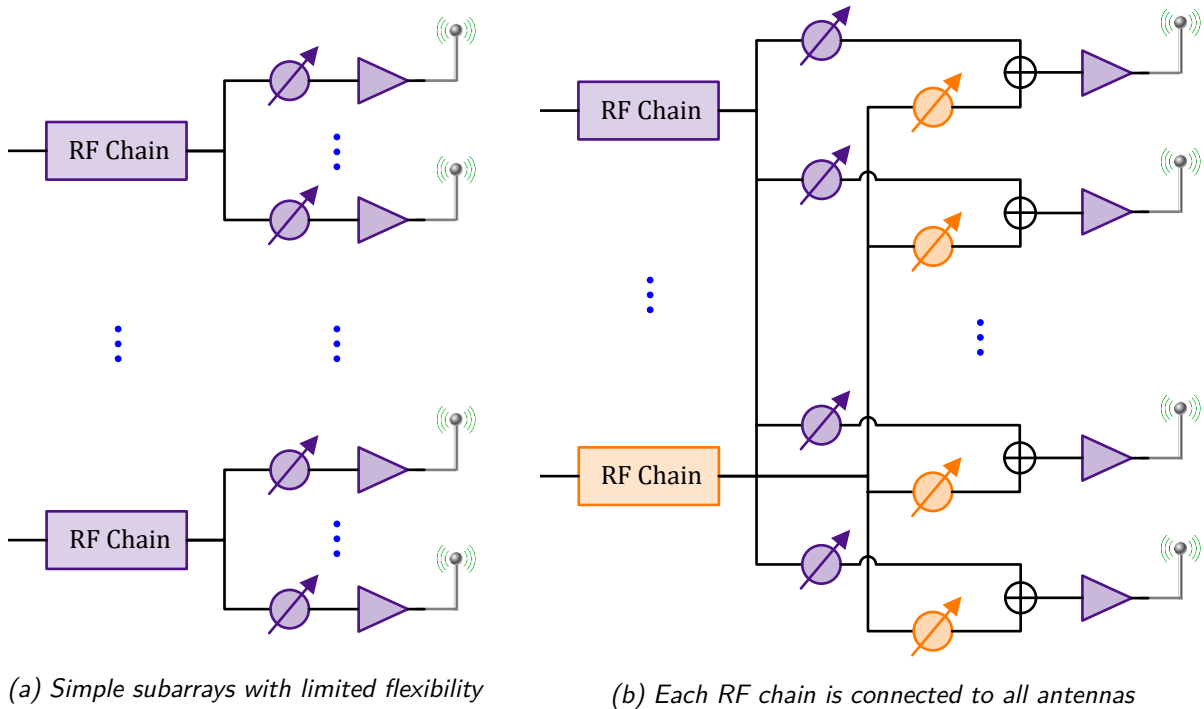


Figure 6.9: Two techniques to implement analog beamforming part

and minimum signal level). This leads to high power consumption. Now notice from Figure 6.8 that it is not being done for all antennas in the array in the hybrid solution. Instead, a set of antennas already implement analog beamforming before the signal is presented to the digital path.

As described before, things are changing fast though in this area. With advancement in data conversion technology (e.g., RF sampling ADCs and DACs) and increased level of on-chip integration, the era of an all-digital beamforming in mmWave bands is on the horizon.

Time Domain vs Frequency Domain Beamforming

In the last section, we covered how beamforming can be done in analog domain after the DAC at Tx side and before the ADC at Rx side. This is shown within the Analog Signal Processing (ASP) block in Figure 6.10 which obviously implements other tasks related to the frontend too in addition to the phase shifting operations. In a similar manner, beamforming can also be performed in digital domain before the DAC on the Tx side or after the ADC on the Rx side, as drawn in the same figure. In practice, the case for digital beamforming gives more choices in this regard.

We will learn in Chapter 8 how in an OFDM system, the modulation symbols are considered to be in frequency domain and an inverse Fast Fourier Transform (iFFT) generates the actual time domain waveform. Therefore, there are two possible options to execute digital beamforming: frequency domain and time domain. This is illustrated in Figure 6.10 where the beamforming operations before the iFFT

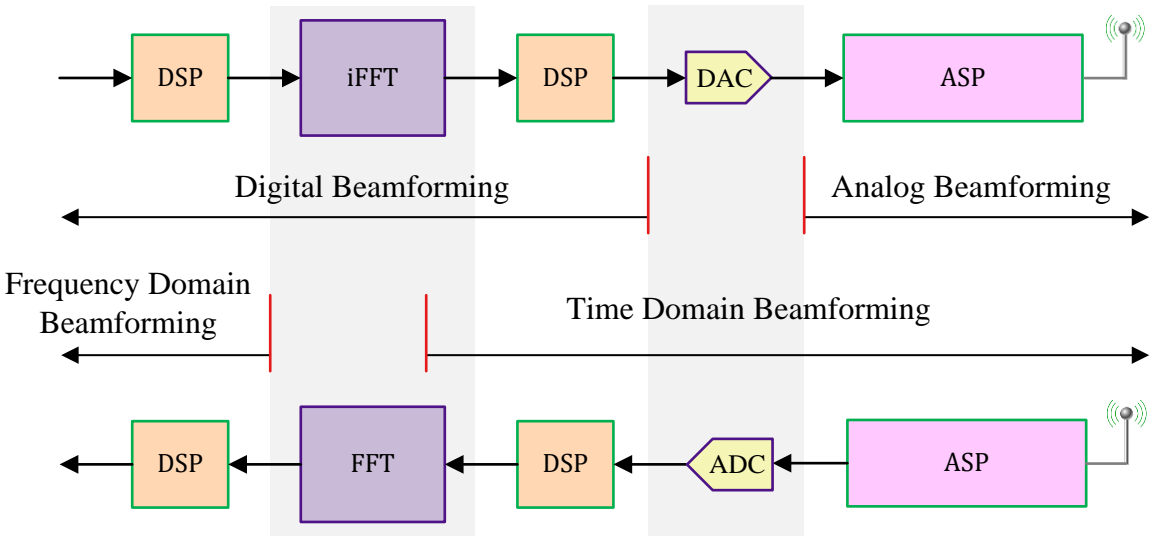


Figure 6.10: Different types of beamforming options

fall in the frequency domain while the operations after the iFFT belong to time domain beamforming. The importance of frequency domain beamforming comes from the implementation of the process in a frequency selective manner, i.e., different precoding weights can be associated with separate subcarriers, thus providing maximum flexibility in *both* time and frequency domains. The whole beamforming operation can also be broken down into different subsets which can then be individually executed at different stages.

6.3 mmWave Massive MIMO

We have described before that higher attenuation at mmWave frequencies poses communication challenges that can be overcome either through increased Tx power, or a directional antenna with a large gain or a massive antenna array. The array option is the best due to both performance and cost advantages. By selecting appropriate gains and phases, the beams can be steered to Tx or Rx from any direction. Furthermore, interference can be suppressed through assigning null response at appropriate places. There are a few fundamental differences between massive MIMO at sub-6 GHz and mmWave frequencies as outlined below.

Array Size

As discussed earlier in Chapter 4, the concept of massive MIMO originated with an assumption of single antenna user terminals. Mobile devices in 5G can also have multiple antennas but this number depends on the frequency of operation. In sub-6 GHz band, the wavelengths are large

(on the order of several centimeters) and since antenna spacing is a function of the wavelength, there is a limit to which antennas can be packed in the small form factor of those mobiles. There are two observations in this regard.

- Assume a modern smartphone with dimensions of 130x70 mm and antenna spacing of $\lambda/2$. Using the relation $c = F_C\lambda$, we can find out how many antennas can *ideally* fit into the device for two frequencies, 5 GHz and 60 GHz.

$$\begin{aligned} 5 \text{ GHz} &\Rightarrow \frac{\lambda}{2} = 30 \text{ mm} & \text{Antennas} &\approx \frac{130}{30} \times \frac{70}{30} \approx 10 \\ 60 \text{ GHz} &\Rightarrow \frac{\lambda}{2} = 2.5 \text{ mm} & \text{Antennas} &\approx \frac{130}{2.5} \times \frac{70}{2.5} \approx 1400 \end{aligned}$$

Serious power consumption, hardware complexity, ADC and other practical constraints are all obstacles in this path but the direction of future is clear. The number of antennas in the mobile terminals will grow with time.

- Let us reproduce Eq (6.3) from the start of this chapter.

$$P_{Rx} = \frac{P_{Tx}}{(4\pi d)^2} \cdot G_{Tx} \cdot G_{Rx} \cdot \lambda^2$$

It is evident that the Tx and Rx gains appear as a product in forming the cumulative gain of the link. Now instead of a massive array of N_B antennas at the base station side, the same beamforming gain can be attained through factorizing N_B into a product as

$$N_B = N_{B,new} \cdot N_{Mobile}$$

For instance, 512 antennas in total provide the same performance as 64 base station antennas and 8 mobile antennas. This leads to a smaller array at the base station and relatively larger but still small array at the user equipment.

Far or Near Field

Despite the fact that electromagnetic waves propagate as a spherical wavefront, we saw in Figure 3.9 that all the paths can be considered parallel for a sufficiently large distance between the Tx and Rx. This is known as far field assumption. Far field region is a reasonable assumption if the following condition is satisfied [9].

$$d > \frac{2L^2}{\lambda}$$

where L is the array length given by $(N - 1)d$. For a large array length or high frequency (small wavelength), the far field region can be much farther away than a reasonably small cell size. With dense cells and higher mmWave bands, this might lead to designing new signal processing algorithms that deal with signals in near field region.

Pilot Contamination

We discussed the pilot contamination problem in Chapter 4 in the context of sub-6 GHz frequencies. Since communication needs to be done within a finite coherence block, there is a finite amount of resources that can be devoted to learning the channel response. All pilots in all the cells cannot be orthogonal to each other and there is a correlation between pilots in different cells either due to pilot reuse or correlation in semi-orthogonal pilots. We concluded that the base station learns about not only the channel of the user within its own cell but also the channel from an interfering user of a neighboring cell.

This problem is less severe at mmWave frequencies due to additional blockage and small cells [16]. A small cell serves a few users at maximum at short range and orthogonal pilots can be assigned in neighboring cells. This can be visualized in the limiting case where each user occupies their own individual cell.

6.4 The Small Picture

We can now list the major benefits of moving upwards in mmWave bands as follows.

Higher Data Rate

Large bandwidths directly translate into higher data rates both for individual users and for slicing the spectrum among a number of users in a cellular network.

Cell Density

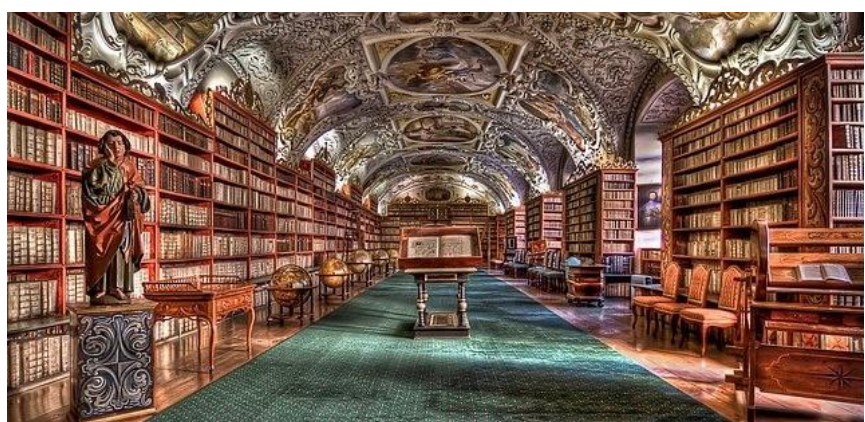
Larger attenuation and penetration losses naturally limit the propagation of waves at mmWave frequencies. Due to these shorter distances, cell density can be increased within the same geographical area to serve a higher number of users through frequency reuse.

Array Size

A higher frequency implies a shorter wavelength. It is now possible to integrate large antenna arrays with the rest of the RF circuitry in a small form factor that fits our mobile phones.

Chapter 7

Low Density Parity Check (LDPC) Codes



Imagine the top sprinters of the world (say, Usain Bolt, Tyson Gay and Yohan Blake) meeting at a place, the fastest of whom is Usain Bolt with a 100m record of 9.58 seconds. Imagine the buzz it would create if a swimmer entered the gathering with a claim of running a 100m sprint in under 7 seconds. This is exactly what happened in 1993 in Geneva, Switzerland, at the IEEE International Conference on Communications (ICC) when Claude Berrou et al. (who were complete outsiders in the coding community) introduced turbo codes that came very close to achieving Shannon limit with reasonable decoding complexity (the Shannon limit along with the coding gain was shown in Figure 1.1 at the start of this text). There was a widespread disbelief according to MIT News, “People almost laughed them out of the room, especially because they were not coming from the coding side; they were coming from the electronics side”. In words of [17]:

“The invention of turbo codes began with Alain Glavieux’s suggestion to his colleague Claude Berrou, a professor of VLSI circuit design, that it would be interesting to implement the SOVA (Soft Output Viterbi Algorithm) decoder in silicon. While studying the principles underlying the SOVA decoder, Berrou was struck by Hagenauer’s statement that a SISO decoder is a kind of SNR amplifier. As a physicist, Berrou wondered whether the SNR could be further improved by repeated decoding, using some sort of “turbo-type” iterative feedback. As they say, the rest is history.”

“Turbo type” implies the use of an iterative decoding procedure where extra information is extracted from the output of a decoder and exchanged with the output of another decoder as prior information. The decoding process converges after a few such iterations of extrinsic information exchange. This is the essence of the *turbo principle* which was later utilized in many other communication applications as well, including the decoding of LDPC codes.

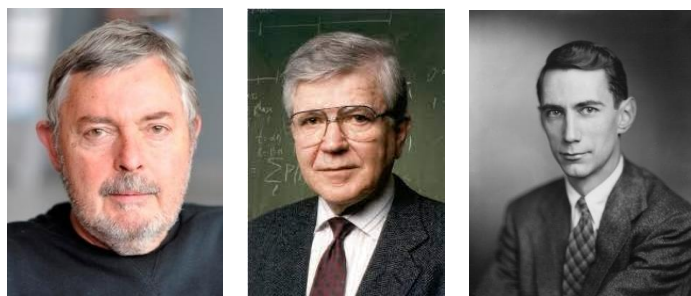


Figure 7.1: From left to right: Claude Berrou, Robert Gallager, Claude Shannon

The turbo principle is one piece out of three in this story. The other two are provided by Claude Shannon and Robert Gallager.

To understand the idea of coding, recall that communication channels suffer from noise that corrupts the digital data sent from the Tx to the Rx, a phenomenon that is particularly striking in wireless channels. Error correction coding, also known as Forward Error Correction (FEC), is a process of correcting these bit errors through addition of redundant bits to the Tx stream. Subsequent utilization of this redundancy at the Rx attempts to correct the errors and recover the original data.

Since the early ages of information revolution, communication engineers wondered about what could be the fundamental limits on sending data over any channel such as an optical fiber, telephone line or a wireless medium. The answer was provided by Claude Shannon in 1948 in a landmark paper *A Mathematical Theory of Communication* that actually changed the history of information and communication technologies. People knew then that redundancy needs to be added to protect data from corruption due to noise (e.g., by repeating the same bit a certain number of times). However, it was a common belief that the number of errors can only go to zero with infinite repetition because noise, a tax on communicating information imposed by nature, cannot be completely defeated. Shannon showed the surprisingly remarkable result that the error rate can be made zero for a *finite* amount of redundant bits as long as the transmission rate is below a certain threshold, now known as Shannon limit. This perfection is not found in most natural phenomena.

To realize its true significance, here is a passage from Ref. [17] on a history of channel coding.

Claude Shannon

... the extraordinary efforts that were required to achieve this objective may not be fully appreciated by future historians. McEliece imagined a biographical note in the 166th edition of the *Encyclopedie Galactica* along the following lines.

Claude Shannon: Born on the planet Earth (Sol III) in the year 1916 A.D. Generally regarded as the father of the Information Age, he formulated the notion of channel capacity in 1948 A.D. Within several decades, mathematicians and engineers had devised practical ways to communicate reliably at data rates within 1% of the Shannon limit ...

This feat, approaching the Shannon limit, has been accomplished most closely by Low Density Parity Check (LDPC) codes. They were first discovered by MIT student Robert Gallager in 1960 as part of his PhD dissertation. However, they were seen as another manifestation of linear block codes requiring substantial computational effort and hence were conveniently forgotten as a purely theoretical idea. For around 30 years since then, the LDPC codes remained dormant underneath all the push by the coding community to close the remaining gap. Then came the turbo decoding principle that changed everything.

Having found the turbo hammer, everyone started looking for more nails. It was then that Spielman and MacKay independently rediscovered LDPC codes in 1996 that could be decoded through the application of turbo or iterative decoding principle. With time, LDPC codes have emerged as the leading candidate in the error correction race, surpassing even the Turbo codes and thus making their way into the 5G standard for data channels (the control channels in 5G use a different type of codes known as polar codes). The LDPC description here is largely based on a simple example. If the overall concept

seems straightforward to you, keep in mind that the simplest (and not the most efficient) algorithm is explained here and many of the details are skipped for ease of exposition.

7.1 Encoding

An LDPC encoder is built on a straightforward and perhaps one of the earliest error detection scheme, known as a *parity bit*.

Parity Bit for Error Detection

A parity bit, also known as a check bit, is one redundant bit added at the end of a binary string of 1s and 0s. It works on the principle of modulo-2 addition denoted by \oplus .

$$\begin{array}{lll} 0 \oplus 0 = 0 & & \\ 0 \oplus 1 = 1 & 1 \oplus 1 = 0 & (7.1) \\ 1 \oplus 0 = 1 & & \end{array}$$

where the three expressions are shown on the left as they produce the same result as in decimal addition. The expression on the right rolls back from 2 to 0 due to modulo-2 arithmetic. Such a scheme is particularly helpful in high speed hardware applications where bit errors are rare and detecting such an error is considered enough for most purposes. For instance, a common format in serial data transmission is 7 data bits, one parity bit and one or two stop bits generated and processed by the interface hardware.

The purpose of a parity bit is to guarantee that the total number of 1s in a bit stream is either even (even parity) or odd (odd parity). For example, the 7-bit sequence 1011100 has a total number of 4 1s. With an even parity, the 8-bit output is 1011100 **0** because the number of 1s is already even. Mathematically, we write

$$1 \oplus 0 \oplus 1 \oplus 1 \oplus 1 \oplus 0 \oplus 0 = 0$$

If the number of 1s in this sequence was odd, then an extra 1 would have been added in place of the last 0, i.e., for an odd parity, the 8-bit output is 1011100**1** thus ensuring that the total number of 1s is 5, an odd number. If there is an error in any one Rx bit, the total number of 1s will change from even to odd in the former case while from odd to even in the latter case. Thus, a single bit error will be successfully detected.

Parity Bits for Error Correction

Observe in the previous description that we are able to detect an error but not correct it because any one of those 7 bits – whether it was the second or the sixth bit – could be in error and disturb the parity. For the purpose of an error correction procedure that can locate the erroneous bit, more redundancy in the form of extra parity bits is needed. For this purpose, we can have a whole set of parity bits that can

provide additional segments of protection. These checks can be arranged in a matrix form known as a *Low Density Parity Check (LDPC)* matrix \mathbf{H} , one example of which is given below.

$$\begin{matrix} 1 & 1 & 0 & 1 & 0 & 0 & 0 \\ 0 & 0 & 1 & 1 & 1 & 0 & 0 \\ 0 & 0 & 0 & 1 & 0 & 1 & 1 \end{matrix}$$

The reason behind the term LDPC is as follows.

Parity Check

The LDPC matrix has several parity check equations, one corresponding to each row. Our example matrix and the one shown in Figure 7.2 have 3 and 15 parity check equations, respectively. The ones in each row indicate which bits are involved in that parity check.

Low Density

The matrix shown above is not a typical LDPC matrix and it is only chosen for ease understanding. A normal LDPC matrix is very large and has a low density of 1s compared to the total size. Another example described by Gallagher himself is given in Figure 7.2. The codes used in practical applications have a much larger LDPC matrix with rows and columns numbering in thousands. Observe a low proportion of ones as compared to zeros.

1	1	1	1	1	0	0	0	0	0	0	0	0	0	0	0	0	0	0	0
0	0	0	0	1	1	1	1	0	0	0	0	0	0	0	0	0	0	0	0
0	0	0	0	0	0	0	0	1	1	1	1	0	0	0	0	0	0	0	0
0	0	0	0	0	0	0	0	0	0	0	0	0	1	1	1	1	0	0	0
0	0	0	0	0	0	0	0	0	0	0	0	0	0	0	0	0	1	1	1
1	0	0	0	1	0	0	0	1	0	0	0	1	0	0	0	0	0	0	0
0	1	0	0	0	1	0	0	0	1	0	0	0	0	0	0	0	1	0	0
0	0	1	0	0	0	1	0	0	0	0	0	0	1	0	0	0	0	1	0
0	0	0	1	0	0	0	0	0	0	1	0	0	0	1	0	0	0	0	1
0	0	0	0	0	0	0	1	0	0	0	1	0	0	0	0	1	0	0	1
1	0	0	0	0	1	0	0	0	0	0	1	0	0	0	0	0	0	1	0
0	1	0	0	0	0	1	0	0	0	1	0	0	0	0	0	1	0	0	0
0	0	1	0	0	0	0	1	0	0	0	0	1	0	0	0	0	0	0	1
0	0	0	1	0	0	0	0	0	1	0	0	0	1	0	0	0	0	0	1
0	0	0	0	1	0	0	0	0	0	1	0	0	0	0	1	0	0	0	1

Figure 7.2: An LDPC matrix described by Gallagher

We have discussed so far the making of a parity check matrix. However, remember that the parities

are checked at the Rx side, not the Tx side! Therefore, we need another matrix at the Tx side for encoding purpose, known as a *Generator Matrix* \mathbf{G} . Naturally, this generator matrix is derived from the parity check matrix \mathbf{H} through a defined procedure that involves operations from linear algebra. We will not go into the details of the procedure. Interested readers can easily find the conversion from \mathbf{H} to \mathbf{G} in any textbook or online resource. The final codeword is produced through multiplication of a block of bits with the generator matrix.

The Rx can utilize these redundant parity bits to correct upto a certain number of errors in the received sequence. We explore this decoding process next.

7.2 Decoding

To understand the decoding process, let us first refer back to Eq (1.5) where we discussed transformation of bits into symbols, a process known as modulation.

Binary Modulation

Binary modulation implies that a binary 0 can be mapped to signal level $s = +1$ (or $s = -1$) and a binary 1 can be mapped to signal level $s = -1$ (or $s = +1$). For i^{th} bit, we have

$$s_i = 1 - 2b_i \quad (7.2)$$

This expression maps bit 0 to $s_i = +1$ and bit 1 to $s_i = -1$. The received signal r_i is corrupted by the addition of random noise and given as

$$r_i = s_i + \text{noise}$$

where the modulation symbol s_i is either $+1$ or -1 depending on the data bit 0 and 1, respectively. As a consequence of noise addition, the received symbols are scattered around the actual symbol values. For the Rx to perform an inverse mapping from voltage levels or symbols back to bits, common sense dictates that bit decisions \hat{s}_i should be taken according to the minimum distance rule:

$$\hat{s}_i = \begin{cases} +1, & r > 0 \\ -1, & r < 0 \end{cases} \quad \hat{b}_i = \begin{cases} 0 & \\ 1 & \end{cases}$$

This is known as *hard decision decoding*. When there is no error in the message, all hard decisions map to the original levels and their *signs* are enough to find corresponding bits, as shown in the above expression. On realistic wireless channels, however, the actual magic lies in soft decision decoding as we explore through an example.

Parity Check on Channel Outputs

For the purpose of explanation, assume that the coded sequence takes the following values.

$$b_0 \ b_1 \ b_2 \ b_3 \ b_4 \ b_5 \ b_6 = 1 \ 0 \ 1 \ 1 \ 0 \ 0 \ 1$$

Assuming the same parity check matrix as before,

$$\begin{array}{ccccccc} 1 & 1 & 0 & 1 & 0 & 0 & 0 \\ 0 & 0 & 1 & 1 & 1 & 0 & 0 \\ 0 & 0 & 0 & 1 & 0 & 1 & 1 \end{array} \quad (7.3)$$

the corresponding parity check expressions from the product of the above matrix and the coded sequence are all satisfied. For example, for the first row with the coded sequence above, we have

$$1 \cdot 1 \oplus 1 \cdot 0 \oplus 0 \cdot 1 \oplus 1 \cdot 1 \oplus 0 \cdot 0 \oplus 0 \cdot 0 \oplus 0 \cdot 1 = 0$$

These parity checks are also satisfied for the other two rows, thus verifying the codeword as correct.

Now after binary modulation described before in Eq (7.2), we have the symbols s_i as

$$s_0 \ s_1 \ s_2 \ s_3 \ s_4 \ s_5 \ s_6 = -1 \ +1 \ -1 \ -1 \ +1 \ +1 \ -1$$

In the presence of additive white Gaussian noise, the receive values r_i might take the following example values during signal transmission from Ref. [19].

$$-9 \ -7 \ -12 \ -4 \ +7 \ +10 \ -11 \quad (7.4)$$

If hard decisions are taken at this stage on the basis of each sign (i.e., making decisions on bits based on the above values), then inverse mapping is performed from Eq (7.2) to generate our decisions according to

$$\hat{b}_i = \frac{1}{2}(1 - \hat{s}_i)$$

Such an inverse mapping outputs a bit 0 for $\hat{s}_i = +1$ and bit 1 for $\hat{s}_i = -1$. Applying this to the above AWGN channel output, our bit decisions are given as

$$b_0 \ b_1 \ b_2 \ b_3 \ b_4 \ b_5 \ b_6 = 1 \ \textcircled{1} \ 1 \ 1 \ 0 \ 0 \ 1$$

with an error at circled bit position that will fail the parity check. Let us now move towards the idea of iterative decoding where we will use this example.

The Bayesian Approach

Let us start by reproducing the relation between the observed channel outputs r and symbols s .

$$r = s + \text{noise}$$

We have omitted the subscripts i for simplifying the forthcoming discussion. There are two possible approaches here.

1. We simply focus on the probability of the observation, given that it originated from a certain candidate. Mathematically,

Compute for each candidate: $p(\text{observation} \dots \text{given} \dots \text{the candidate})$ (7.5)

Then, we can compare all possible candidates and choose the one with the highest such probability. This is known as a maximum likelihood approach, an idea we saw before in Section 5.3.3.

In the context of signal in noise problem, we apply this principle by computing the probability of an observation r , *given that the sent symbol s was -1 or $+1$* as follows.

- Let the probability of the observation r , given the sent symbol s was -1 , be $p(r \text{ given } s = -1)$.
- Let the probability of the observation r , given the sent symbol s was $+1$, be $p(r \text{ given } s = +1)$.

Now a decision can be made by choosing the maximum of these two probabilities. In general, there is less ambiguity regarding very large negative or very large positive values. The former decode back to symbols -1 and the latter to $+1$ with a high probability (or bits 1 and 0, respectively). However, this approach fails us when the observations r have a small magnitude, the scenario where most frequent errors occur.

2. A better approach[†] then is to compute the probability of a given candidate *given the new observations*. Reversing Eq (7.5), we get

Compute for each candidate: $p(\text{candidate} \dots \text{given} \dots \text{the observation})$ (7.6)

That turns the first approach around and places things in a natural order because the question is posed as updating our belief about a possibility after the availability of information. This approach brings us to the celebrated Bayes' Theorem.

Thomas Bayes was an English statistician and Presbyterian minister who came up with this theorem in 18th century during his investigation on how to update the understanding of a phenomenon *as more evidence becomes available*. At that time, he did not deem it worthy of publication and never submitted it to any journal. It was discovered in his notes after his death and published by his friend Richard Price. To understand the Bayesian approach, let us take a well known puzzle described by Daniel Kahneman in his book "Thinking Fast and Slow".

[†]To put things into context, the science here is opinion based and historically there have been heated arguments between what the statisticians call the frequentist and Bayesian camps.

The Librarian or Farmer Puzzle

An individual has been described by a neighbor as follows: "Steve is very shy and withdrawn, invariably helpful but with little interest in people or in the world of reality. A meek and tidy soul, he has a need for order and structure, and a passion for detail." Is Steve more likely to be a librarian or a farmer? According to Kahneman, most people assume Steve is a librarian, thus illustrating the inability of our minds to think in probabilistic terms. "Did it occur to you that there are more than 20 male farmers for each male librarian in the United States? Because there are so many more farmers, it is almost certain that more 'meek and tidy' souls will be found on tractors than at library information desks." In other words, we hardly take into account the *prior probability* in real world problems!



Figure 7.3: The concept of prior probability

The prior probability of an uncertain quantity expresses one's belief about it *before* some evidence shows up. Then, we fuse this prior probability with the likelihood in the light of new information and update our belief. Mathematically, we can write this update process as

$$p(\text{candidate} \dots \text{ given } \dots \text{ the observation}) \propto \underbrace{p(\text{candidate})}_{\text{prior belief}} \cdot \underbrace{p(\text{observation} \dots \text{ given } \dots \text{ the candidate})}_{\text{likelihood of that candidate}} \quad (7.7)$$

where a proportional sign instead of an equality indicates the absence of a normalizing constant. In the context of the above puzzle, we can write

$$p(\text{librarian} \dots \text{ given } \dots \text{ a meek and tidy soul}) \propto \underbrace{p(\text{librarian})}_{\text{prior probability}} \cdot \underbrace{p(\text{a meek and tidy soul} \dots \text{ given } \dots \text{ librarian})}_{\text{likelihood of that candidate}}$$

Even when the likelihood of a meek and tidy soul being a librarian is high, the prior probability $p(\text{Librarian})$ is very low as compared to $p(\text{Farmer})$ in the United States (around 1 : 20). Consequently, the product of the above two probabilities on the right hand side is relatively small. This clarifies the confusion in correctly answering this puzzle.

The Log Likelihood Ratios (LLR)

In the context of signal in noise problem, we decide whether each bit is a 0 or a 1 *after* the observations are presented to us.

- Let the probability of $s = -1$, given the observation r , be $p(s = -1 \text{ given } r)$
- Let the probability of $s = +1$, given the observation r , be $p(s = +1 \text{ given } r)$.

Here, prior probabilities appear in the form of $p(s = +1)$ and $p(s = -1)$. We decide in favor of the larger probability after the update, e.g., if $p(s = +1 \text{ given } r)$ is greater than $p(s = -1 \text{ given } r)$, then $s = +1$ is a better candidate for symbol decision.

$$p(s = +1 \text{ given } r) \geq p(s = -1 \text{ given } r) \Rightarrow \frac{p(s = +1 \text{ given } r)}{p(s = -1 \text{ given } r)} \geq 1$$

Taking logarithms on both sides, we get

$$\underbrace{\log \left\{ \frac{p(s = +1 \text{ given } r)}{p(s = -1 \text{ given } r)} \right\}}_{L(s \dots \text{ given } \dots r)} \geq 0 \quad (7.8)$$

This expression is known as the Log Likelihood Ratio (LLR). We decide in favor of $s = +1$ (i.e., bit $\hat{b} = 0$) if the above LLR is positive and vice versa. Applying Eq (7.7) to this term, we get

$$\begin{aligned} L(s \dots \text{given} \dots r) &= \log \left\{ \frac{p(s = +1 \text{ given } r)}{p(s = -1 \text{ given } r)} \right\} \\ &= \log \left\{ \frac{p(r \text{ given } s = +1) \cdot p(s = +1)}{p(r \text{ given } s = -1) \cdot p(s = -1)} \right\} \end{aligned}$$

Using the property $\log(A \cdot B) = \log A + \log B$, we have

$$L(s \dots \text{given} \dots r) = \underbrace{\log \left\{ \frac{p(r \text{ given } s = +1)}{p(r \text{ given } s = -1)} \right\}}_{\text{Channel reliability}} + \underbrace{\log \left\{ \frac{p(s = +1)}{p(s = -1)} \right\}}_{L(s)} \quad (7.9)$$

Let us discuss the two terms on the right hand side one by one.

Channel Reliability

This is the likelihood part of the expression above. To simplify this first term, the question is to find $p(r \text{ given } s = +1)$ and $p(r \text{ given } s = -1)$. In our simple BPSK model where the modulation symbol $s = \pm 1$, the received signal r becomes

$$r = s + \text{noise} \quad \Rightarrow \quad r = \pm 1 + \text{noise}$$

In Eq (7.18) of Appendix 7.3, we have simplified the first term in Eq (7.9) as

$$\log \left\{ \frac{p(r \text{ given } s = +1)}{p(r \text{ given } s = -1)} \right\} = L_c \cdot r \quad (7.10)$$

where L_c is called the *channel reliability value*, sometimes also known as the channel Log Likelihood Ratio (LLR). It is derived in Appendix 7.3 as $L_c = 2/\sigma^2$ for AWGN that changes into $2h_i/\sigma^2$ for a fading channel with gain h_i . It can be inferred that this term is a constant in AWGN case and time-varying for a fading channel.

A Priori Information

Let us denote the second term in Eq (7.9) by $L(s)$ which is seen to be a Log Likelihood Ratio (LLR) of the two possibilities.

$$L(s) = \log \left\{ \frac{p(s = +1)}{p(s = -1)} \right\}$$

It is not immediately clear where can we get these values from. In the answer to this question lies the secret of iterative decoding that lead the modern codes to approach capacity. We shortly see that these a priori values are obtained from other sources.

Combining the above two in Eq (7.9) yields the following expression.

$$L(s \dots \text{given} \dots r) = L_c \cdot r + L(s)$$

(7.11)

Next, we explore the last part of the puzzle, i.e., how to handle the parity checks in which multiple bits are involved.

Obtaining Parity Checks

Note that the information about each bit in either decoder is conveyed through multiple routes. For example, the information about the first bit comes not only from the channel output r_1 (i.e., $s_1 + \text{noise}$) but also from the horizontal parity check in the first row of the parity check matrix in Eq (7.3). How should the above information be incorporated in the decoder structure? Similar to individual LLRs, we need to find out the LLRs for *sums of bits* having the same value versus having different values. For instance, for a sum of two statistically independent bits b_0 and b_1 forming symbols s_1 and s_2 ,

$$p(b_0 \oplus b_1 = 0) = p(s_1 = +1) \cdot p(s_2 = +1) + p(s_1 = -1) \cdot p(s_2 = -1) \quad (7.12)$$

This is because on a bit level, the modulo-2 sum of two bits, $b_0 \oplus b_1$, is 0 when they are the same, see Eq (7.1). That is why the above two products are for the same symbol $+1$ or -1 . Naturally, this xor sum is 1 when the two bits are different, the probability of which can be given by

$$\begin{aligned} p(b_0 \oplus b_1 = 1) &= 1 - p(b_0 \oplus b_1 = 0) \\ &= 1 - p(s_1 = +1) \cdot p(s_2 = +1) - p(s_1 = -1) \cdot p(s_2 = -1) \end{aligned} \quad (7.13)$$

From here, the LLR form is derived in Eq (7.21) of Appendix 7.3 as

$$L(b_0 \oplus b_1) \approx \text{sign}\{L(s_1)\} \cdot \text{sign}\{L(s_2)\} \cdot \min\{|L(s_1)|, |L(s_2)|\}$$

In words, this value can be computed simply by the product of their signs and the minimum of the two magnitudes. This expression can be generalized for more than two bits as a product of all LLR signs with the magnitude given by the minimum.

$$L\left(\bigoplus_i b_i\right) \approx \prod_i \text{sign}\{L(s_i)\} \cdot \min\{|L(s_i)|\} \quad (7.14)$$

With all the pieces in place, we can now move towards the iterative decoding process.

Iterative Decoding

We start with describing the parity check matrix as a *bipartite graph* that presents a graphical view of codeword connected with their corresponding parity checks. For instance, for our example matrix \mathbf{H} , the bipartite graph is drawn in Figure 7.4a. There are two sets of nodes in this figure.

- Bit nodes represent the codeword bits that have been transmitted. We have length 7 codeword in our continuing example and hence 7 bit nodes, each of which corresponds to a column of the parity check matrix.
- Check nodes represent the sum of bits for which a particular parity check equation should be true. Three check nodes in Figure 7.4a correspond to three parity check equations, one for each row. Verify from this figure that for every 1 in the parity check matrix, a connection exists between that bit node and the check node.

The decoding philosophy for LDPC codes can now be summarized as follows.

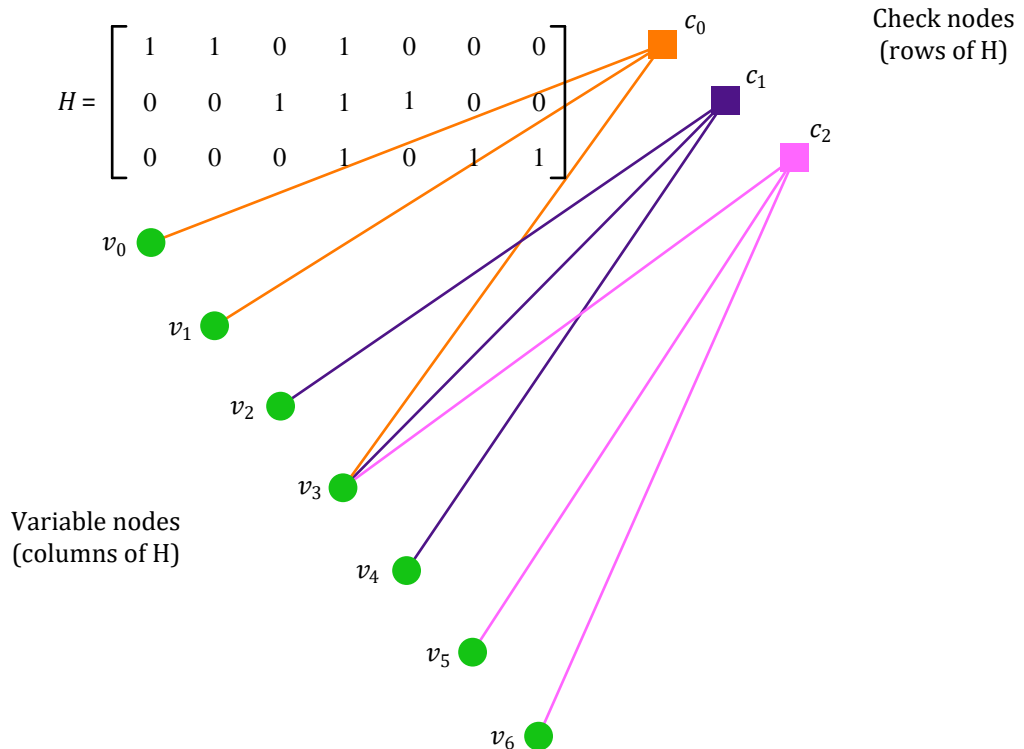
LDPC Decoding Philosophy

- Each parity check operates on multiple bits to produce its output.
- But each bit is also involved in *multiple* parity checks!
- Information can be repeatedly exchanged between these two entities to update our beliefs about each bit.

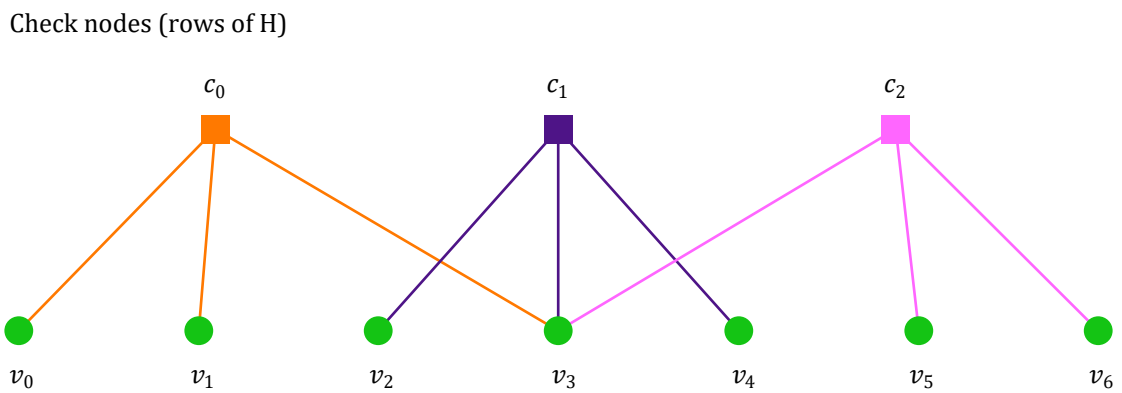
Here we will describe a message passing algorithm on a graph shown in Figure 7.4b which is a redrawn version of Figure 7.4a. Based on the philosophy described above, the messages are passed along the edges of the graph from the bit nodes to the check nodes (how these messages are constructed will be discussed shortly). After the check node process the incoming information from all the branches, it sends the constructed message back to the bit nodes. In this regard, there are three types of messages that are passed along the edges. These are illustrated in Figure 7.5.

- The channel output that becomes the input to a bit node. It is denoted by $L_i = L_c \cdot r_i$ for the i -th bit.
- The message from a bit node i to a check node j . It is denoted by $V_{(i \rightarrow j)}$.
- The message from a check node j to a bit node i . It is denoted by $C_{(j \rightarrow i)}$.

The final question is now how to construct these messages and then utilize them for decoding. This procedure is explained below.



(a) Forming of bit nodes and check nodes from the parity check matrix \mathbf{H} . Observe a connection between each bit node and check node at locations where there is a 1 in \mathbf{H}



(b) A redrawn version of the above graph

Figure 7.4: Bipartite graph for the example parity check matrix

From Bit Node to Check Node $V_{(i \rightarrow j)}$

Figure 7.5 also shows the procedure to construct the message $V_{(i \rightarrow j)}$ with bit node 3 as an example.

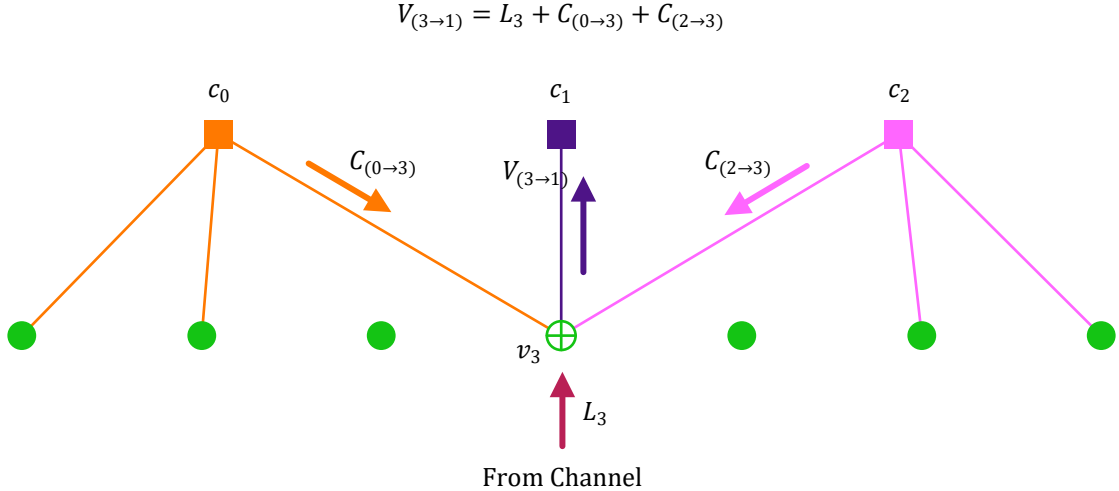


Figure 7.5: 3 message types that participate in the decoding process

This is done by ignoring the connection between i and j (bit node 3 and check node 1 in this case) and sum the messages coming along all the other routes, including the channel output L_i .

$$V_{(3 \rightarrow 1)} = L_3 + C_{(0 \rightarrow 3)} + C_{(2 \rightarrow 3)}$$

The general expression is then

$$V_{(i \rightarrow j)} = L_i + \sum_k C_{(k \rightarrow i)} \quad \text{excluding } k = j \quad (7.15)$$

From Check Node to Bit Node $C_{(j \rightarrow i)}$

Recall from the definition of parity check matrix that the check on each bit is provided by the *remaining bits* in the same row. Therefore, the check for b_0 in the first row is computed by running the above operation on those remaining bits. Generalizing for a bit i , we get from Eq (7.14)

$$L(s_i) \approx \prod_k \text{sign}\{L(s_k)\} \cdot \min \left\{ |L(s_k)| \right\} \quad \text{excluding } k = i \quad (7.16)$$

In words, the magnitude of the message $C_{(j \rightarrow i)}$ is determined by the least magnitude component while the sign is governed by the product of the individual signs.

Reliability Metric

At the end of each iteration, the cumulative reliability metric is computed in a manner similar to $V_{(i \rightarrow j)}$ with the difference that all incoming messages, *including those from check node j* contribute towards the final summation.

$$R_i = L_i + \sum_j C_{(j \rightarrow i)} \quad (7.17)$$

This process is then repeated for several iterations until all the parity check equations are satisfied or a certain maximum number of iterations have already been done. Let us now see go through this process with the help of an example in Ref [19] where the actual codeword is given by

$$b_0 \ b_1 \ b_2 \ b_3 \ b_4 \ b_5 \ b_6 = 1 \ 0 \ 1 \ 1 \ 0 \ 0 \ 1$$

Iteration 1

Channel Output L_i

The channel output L_i is given by Eq (7.4).

$$L_i = -8, -5, -10, -3, +4, +7, -9$$

Comparing with the actual codeword above, bit 1 is in error and hence encircled in Figure 7.6.

From Bit Nodes to Check Nodes $V_{(i \rightarrow j)}$

The messages coming into the bit nodes, i.e. $C_{(j \rightarrow i)}$, are initialized to zero. Therefore, according to Eq (7.15), the bit nodes simply reproduce the channel output L_i on all their connected edges. This is illustrated in Figure 7.6

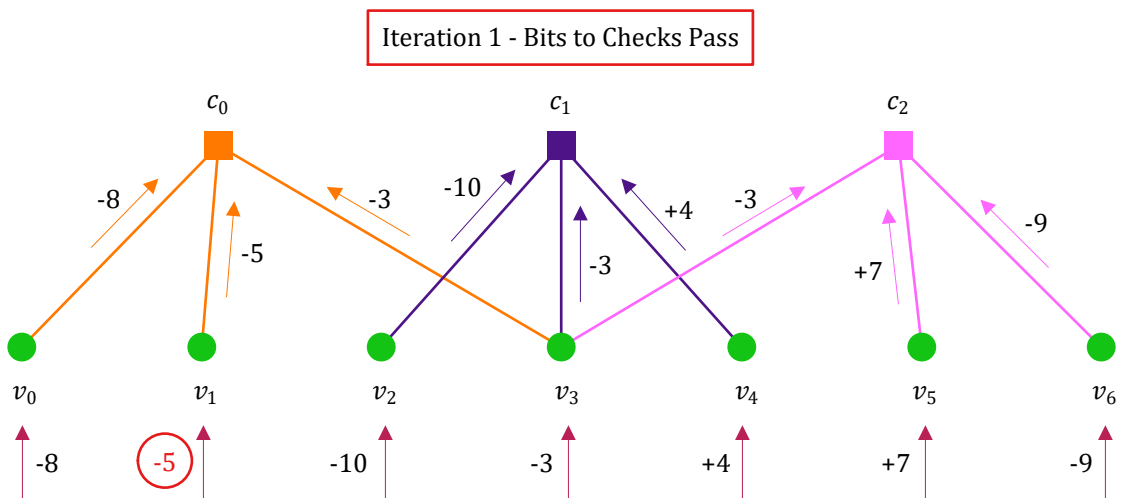


Figure 7.6: Iteration 1: From bit nodes to check nodes

From Check Nodes to Bit Nodes $C_{(j \rightarrow i)}$

The output from each check $C_{(j \rightarrow i)}$ is illustrated in Figure 7.7. For instance, the message $C_{(0 \rightarrow 0)}$ is computed by referring to Eq (7.16) as

$$C_{(0 \rightarrow 0)} = \text{sign}\{-5\} \cdot \text{sign}\{-3\} \cdot \min\{5, 3\} = +3$$

This value +3 can be seen passing from check node 0 to bit node 0 of Figure 7.7. The remaining messages along the graph are also computed in a similar manner.

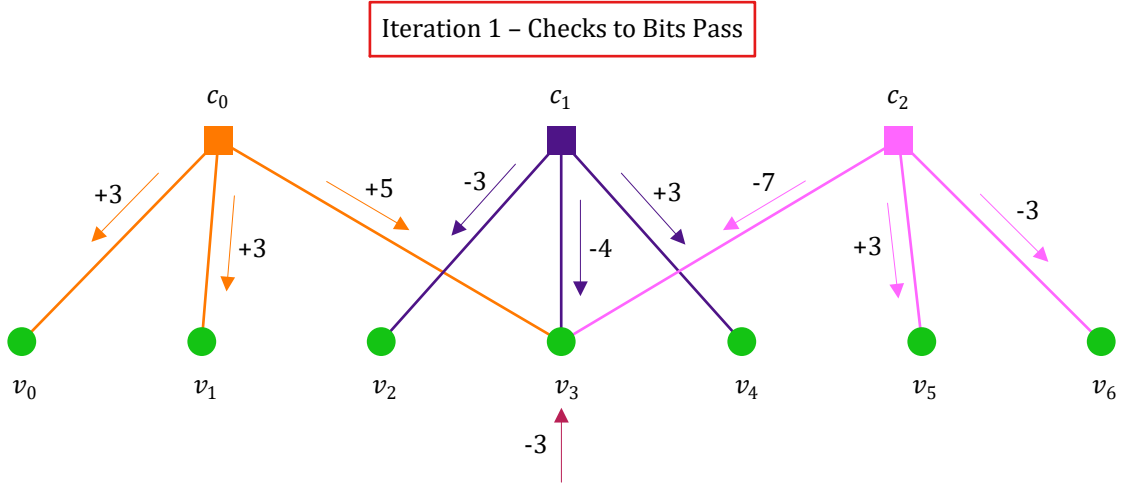


Figure 7.7: Iteration 1: From check nodes to bit nodes

Reliability Metric

The reliability metric R_i is now computed from Eq (7.17). For instance, R_3 can be calculated from Figure 7.7 as

$$R_3 = \underbrace{-3}_{L_3} + \left(\underbrace{+5}_{c_0} + \underbrace{-4}_{c_1} + \underbrace{-7}_{c_2} \right) = -9$$

On a similar note, these values for all bits are given by

$$R_i = -5, -2, -13, -9, +7, +10, -12$$

Applying the decoding rule

$$\hat{s}_i = \begin{cases} +1, & r > 0 \\ -1, & r < 0 \end{cases} \quad \hat{b}_i = \begin{cases} 0 \\ 1 \end{cases}$$

we can deduce that the decoded codeword should be

$$1 \quad \textcircled{1} \quad 1 \quad 1 \quad 0 \quad 0 \quad 1$$

Here, the circled bit position is still in error if we compare it to the actual codeword. Therefore, we run another iteration to refine the results.

Iteration 2

The following steps are performed in iteration 2.

Channel Output L_i

The channel output L_i is obviously the same.

$$L_i = -8, -5, -10, -3, +4, +7, -9$$

From Bit Nodes to Check Nodes $V_{(i \rightarrow j)}$

The messages coming into the bit nodes, i.e. $C_{(j \rightarrow i)}$, are now available. Therefore, the bit nodes prepare their messages according to Eq (7.15). Instead of solving this exercise for all bit and check nodes, we can focus on bit node 3 which connects to all three parity check nodes in Figure 7.7.

$$V_{(3 \rightarrow 0)} = -3 + (-4 - 7) = -14$$

$$V_{(3 \rightarrow 1)} = -3 + (+5 - 7) = -5$$

$$V_{(3 \rightarrow 2)} = -3 + (+5 - 4) = -2$$

You can see these and all other values going from bit nodes to check nodes in Figure 7.8.

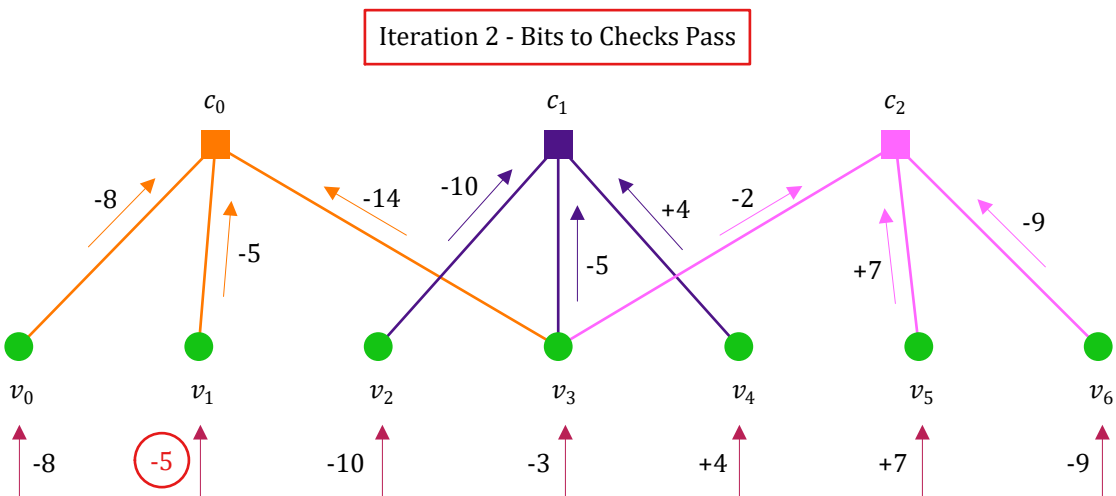


Figure 7.8: Iteration 2: From bit nodes to check nodes

From Check Nodes to Bit Nodes $C_{(j \rightarrow i)}$

The output from each check $C_{(j \rightarrow i)}$ is now illustrated in Figure 7.9. For instance, the message $C_{(0 \rightarrow 1)}$ is computed by referring to Eq (7.16) as

$$C_{(0 \rightarrow 1)} = \text{sign}\{-8\} \cdot \text{sign}\{-14\} \cdot \min\{8, 14\} = +8$$

This value +8 can be seen passing from check node 0 to bit node 1 of Figure 7.9. Recall that this was the bit in error and we will see next how this bit is corrected. The remaining messages along the graph are also computed in a similar manner.

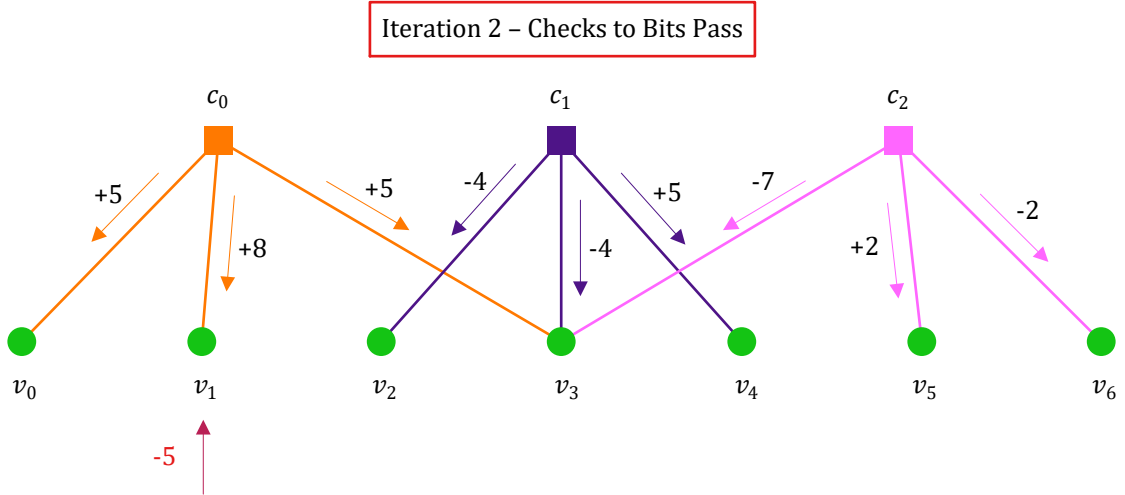


Figure 7.9: Iteration 2: From check nodes to bit nodes

Reliability Metric

The reliability metric R_i is again computed from Eq (7.17). For instance, R_1 can be calculated from Figure 7.7 as

$$R_1 = -5 + (+8) = +3$$

where the sign is now correctly inverted. On a similar note, these values for all bits are given by

$$R_i = -3, \quad +3, \quad -14, \quad -9, \quad +9, \quad +9, \quad -11$$

Applying the decoding rule, we correctly decode the bits as

1 0 1 1 0 0 1

Since all bits are correct now, there is no need to run more iterations and the decoding can be terminated.

Performance

The interested reader can easily find online the programs that can be used for LDPC encoding and decoding procedures (e.g., software from Radford Neal who was a co-author with David MacKay on rediscovery of LDPC codes). Figure 7.10 plots the BER of an LDPC code with block length 4096 with 2048 information bits. It is evident that the performance of the LDPC code substantially reduces the BER and bends the curve inwards towards the Shannon limit. At a fixed BER, this provides the *coding gain* that was introduced at the start of this text in Figure 1.1.

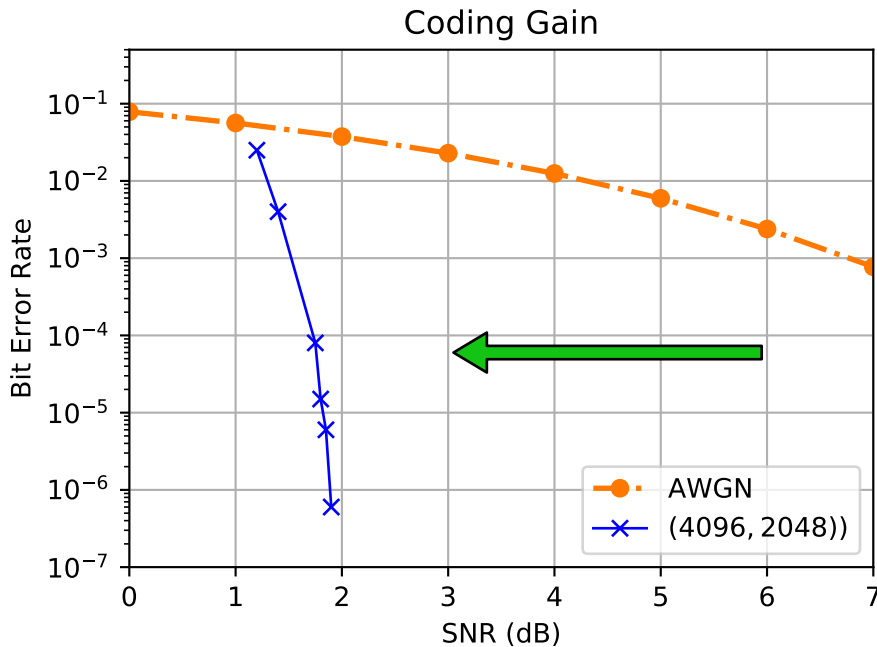


Figure 7.10: BER comparison of an LDPC code with AWGN and the huge coding gain

General Themes

There are three general themes that can be found in the iterative decoding procedure.

Use the Association Machine

Iterative decoding works in an associative manner where bits with high reliability pull the ones with low reliability out of noise through associations they develop during the encoding process. This is not much different than a human mind which works through assigning links to new concepts from previously stored knowledge. For example, if I show you a number 1202, you will forget it in a few minutes. But with extra information that this number is the year 2021 in reverse, you will remember it for a long time. The link between 1202 and 2021 will function as the message passed between bit and check nodes and keep the memory alive and correct.

Get Help from Outside the Box

The decoding attempts before the discovery of turbo principle tried to extract the maximum juice from within the decoder. It is only with the help of a second decoder that new information arrives and lifts the decoding performance. In the context of LDPC codes, this is accomplished by looking at the rows and columns as separate decoders, one providing the bit node processing and the other check sum processing. In conclusion, by looking outside the fixed box of any problem, one can bring fresh information as well as insights to generate ingenious solutions.

Explore the Missing Elements

What intrigued Claude Berrou about conventional decoding attempts was an absence of repeated feedback, one of the most fundamental ideas in electronic design. For example, phase locked loops, amplifiers, control systems, and countless other electronic products are built on this principle. Incorporating such a feedback mechanism in a turbo hypothesis just proved to be the missing element in the grand scheme of coding world.

7.3 Appendix

We start with computation of channel reliability value.

Channel Reliability

Recall that a Gaussian random variable with mean μ and variance σ^2 has a pdf given by

$$f(x) = \frac{1}{\sigma\sqrt{2\pi}} \exp\left[-\frac{1}{2\sigma^2}(x-\mu)^2\right]$$

Ignoring the constant $\sigma\sqrt{2\pi}$ as it cancels out in the numerator and the denominator, we can write the first term in Eq (7.9) as

$$\begin{aligned} \log \left\{ \frac{p(r \text{ given } s = +1)}{p(r \text{ given } s = -1)} \right\} &= \log \frac{\exp\left\{-\frac{1}{2\sigma^2}(r-1)^2\right\}}{\exp\left\{-\frac{1}{2\sigma^2}(r+1)^2\right\}} \\ &= \log \left\{ \exp\left[-\frac{1}{2\sigma^2}(r-1)^2 + \frac{1}{2\sigma^2}(r+1)^2\right] \right\} \\ &= -\frac{1}{2\sigma^2}(r-1)^2 + \frac{1}{2\sigma^2}(r+1)^2 = \frac{1}{2\sigma^2} \cdot 4r \\ &= \frac{2}{\sigma^2} \cdot r = L_c \cdot r \end{aligned} \tag{7.18}$$

Bit Probabilities

This can be done by using the fact that $p(s = +1) + p(s = -1) = 1$. These are the only two possibilities which must add up to 1.

$$L(s) = \log \frac{p(s = +1)}{p(s = -1)} = \log \frac{p(s = +1)}{1 - p(s = +1)}$$

Rearranging the above expression,

$$\begin{aligned} e^{L(s)} &= \frac{p(s = +1)}{1 - p(s = +1)} \\ e^{L(s)} - e^{L(s)} \cdot p(s = +1) &= p(s = +1) \\ e^{L(s)} &= p(s = +1) \cdot (1 + e^{L(s)}) \end{aligned}$$

which leads to

$$p(s = +1) = \frac{e^{L(s)}}{1 + e^{L(s)}} \quad (7.19)$$

In an analogous manner,

$$\begin{aligned} p(s = -1) &= 1 - p(s = +1) = 1 - \frac{e^{L(s)}}{1 + e^{L(s)}} \\ &= \frac{1}{1 + e^{L(s)}} \end{aligned} \quad (7.20)$$

Parity Check

Let us start with loosely defining the LLR here as

$$L(b_0 \oplus b_1) = \log \frac{p(b_0 \oplus b_1 = 0)}{p(b_0 \oplus b_1 = 1)} = \log \frac{p(b_0 \oplus b_1 = 0)}{1 - p(b_0 \oplus b_1 = 0)}$$

Plugging the expressions from Eq (7.12) and Eq (7.13), we get

$$L(b_0 \oplus b_1) = \log \frac{p(s_1 = +1) \cdot p(s_2 = +1) + p(s_1 = -1) \cdot p(s_2 = -1)}{1 - p(s_1 = +1) \cdot p(s_2 = +1) - p(s_1 = -1) \cdot p(s_2 = -1)}$$

Using Eq (7.19) and Eq (7.20),

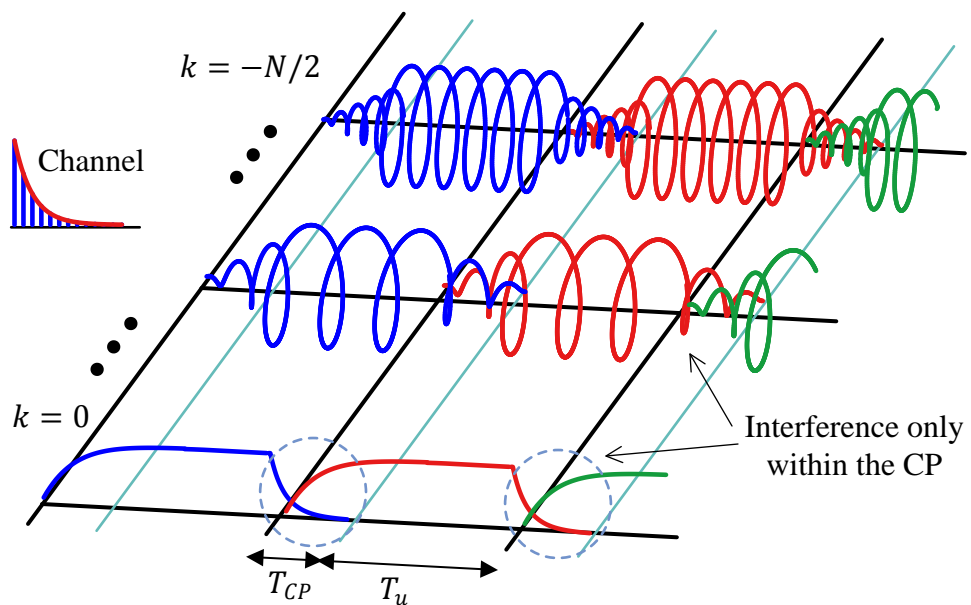
$$\begin{aligned} L(b_0 \oplus b_1) &= \log \left[\frac{\frac{e^{L(s_1)}}{1 + e^{L(s_1)}} \cdot \frac{e^{L(s_2)}}{1 + e^{L(s_2)}} + \frac{1}{1 + e^{L(s_1)}} \cdot \frac{1}{1 + e^{L(s_2)}}}{1 - \frac{e^{L(s_1)}}{1 + e^{L(s_1)}} \cdot \frac{e^{L(s_2)}}{1 + e^{L(s_2)}} - \frac{1}{1 + e^{L(s_1)}} \cdot \frac{1}{1 + e^{L(s_2)}}} \right] \\ &= \log \left[\frac{\frac{e^{L(s_1)} e^{L(s_2)} + 1}{\{1 + e^{L(s_1)}\} \{1 + e^{L(s_2)}\}}}{1 - \frac{e^{L(s_1)} e^{L(s_2)} + 1}{\{1 + e^{L(s_1)}\} \{1 + e^{L(s_2)}\}}} \right] \\ &= \log \left[\frac{\frac{e^{L(s_1)} e^{L(s_2)} + 1}{\{1 + e^{L(s_1)}\} \{1 + e^{L(s_2)}\}}}{\frac{e^{L(s_1)} e^{L(s_2)} + 1 + e^{L(s_1)} + e^{L(s_2)} - e^{L(s_1)} e^{L(s_2)} - 1}{\{1 + e^{L(s_1)}\} \{1 + e^{L(s_2)}\}}} \right] \\ &= \log \left[\frac{e^{L(s_1)} \cdot e^{L(s_2)} + 1}{e^{L(s_1)} + e^{L(s_2)}} \right] \end{aligned}$$

From Ref. [18], the above expression can approximated as

$$L(b_0 \oplus b_1) \approx \text{sign}\{L(s_1)\} \cdot \text{sign}\{L(s_2)\} \cdot \min \left\{ |L(s_1)|, |L(s_2)| \right\} \quad (7.21)$$

Chapter 8

Orthogonal Frequency Division Multiplexing (OFDM)



1G cellular standard, although it was not called 1G at that time, was based on analog communication. A shift towards digital communication occurred in 2G systems, e.g., GSM was based on a single carrier waveform with time domain equalization. Next, 3G systems were based on Code Division Multiple Access (CDMA) scheme while 4G standard adopted Orthogonal Frequency Division Multiplexing (OFDM) as the underlying waveform. What is the common pattern in all these developments? That no technology from one generation survived the aggressive onslaught of new candidates in this fast paced industry. It was only a Multi-Carrier (MC) waveform, namely OFDM, that successfully kept its place intact from 4G to 5G standard and there is hardly any visible contestant to replace the general multi-carrier waveform in the near future. What is so special about this technology? Why is high data rate wireless communication being realized through a multi-carrier waveform these days? Why is OFDM adopted in both downlink and uplink in NR standard? These are the questions we uncover in this chapter.

As a brief overview, some of the benefits of a multi-carrier waveform are as follows.

- It provides flexible resource allocation in frequency domain, something that is accomplished through a natural slicing of the spectrum.
- Signal processing complexity of an equalizer, the major bottleneck in implementing high rate systems, is significantly reduced.
- OFDM can easily integrate with multiple antenna techniques in what we call MIMO-OFDM systems. Along with the Inter-Symbol Interference (ISI), it handles inter-antenna interference that is difficult to handle in single-carrier systems.

One of the disadvantages of OFDM is its high Peak to Average Power Ratio (PAPR). For this purpose, single-carrier systems having low PAPR values are more desirable that make the user terminal power efficient leading to a longer battery life. One version of this scheme, known as DFT-precoded OFDM, is also adopted along with OFDM for uplink transmissions in NR standard. This topic is explained in Section 8.5.

8.1 From the Printer Port

We start this topic with an analogy that can help us better visualize the transmission and interference processes. First, consider the following two opposing constraints.

Short Symbol Time

Recall from Chapter 2 that the major problem with high speed wireless communication is that the multipath components arriving at the Rx cause different attenuations plus phase shifts and consequently constructive and destructive interference throughout the signal span. This multipath depends on the physical environment around the Tx and Rx. For low data rates, the multipath

arrive very close in time to each other with respect to the symbol time T_M . However, as we increase the data rate, each symbol starts interfering with dozens of symbols in the future, a phenomenon known as Inter-Symbol Interference (ISI).

Long Symbol Time

Since this physical environment cannot be changed, a safe method to avoid this long reaching effect of ISI is to reduce our symbol rate, i.e., elongate the symbol time T_M . The reduction of symbol rate is then insufficient for meeting our growing needs for faster data rates. What to do in this situation?

Assume that like a printer (parallel) port, the system designer has access to an array of parallel wires in the air that do not interfere with each other during their flight. We will see later how these parallel wires can be elegantly created. It is evident that if N such parallel wires are included in the design, the symbol time T_M can be simply increased by a factor of N , i.e., the new symbol time (actually, the block time) can be NT_M without compromising on the overall throughput of the system. This is shown in Figure 8.1 where the block duration $NT_M = 6T_M$ is indicated at the bottom.

- In Figure 8.1a, a serial data stream with symbol duration T_M is shown.
- It is segmented into blocks of $N = 6$ symbols and a guard interval is inserted within each such block as plotted in Figure 8.1b. Take this guard interval as a shield for saving the next block from the multipath interference of the previous block.
- Finally, each symbol in a block of $N = 6$ symbols is sent on a set of $N = 6$ parallel wires shown in Figure 8.1c where each wire is $N = 6$ times longer than the symbol duration T_M . Due to parallelism of our fictitious wires, there is no interference within the data symbols on one set. Moreover, the guard interval prevents the multipath of one block smearing into the next as long as the channel length is lesser than the guard interval.

The main theme to focus in Figure 8.1 is how the serial symbol stream of +1s and -1s are mapped on parallel symbol streams and sent on separate wires in the air. For example, verify that the first six symbols $-1, +1, -1, -1, +1, -1$ are all sent to the first block starting from top to bottom. A simple example demonstrates what we gain from such a serial to parallel conversion of the data symbols.

Fooling the Channel

Assume that the wireless channel in which such a communication system is deployed has a maximum delay spread of about a symbol time $1T_M$, i.e., *it interferes with only one next symbol*.

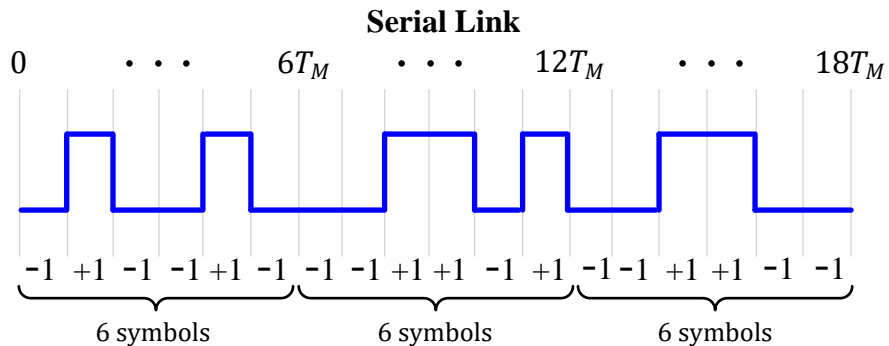
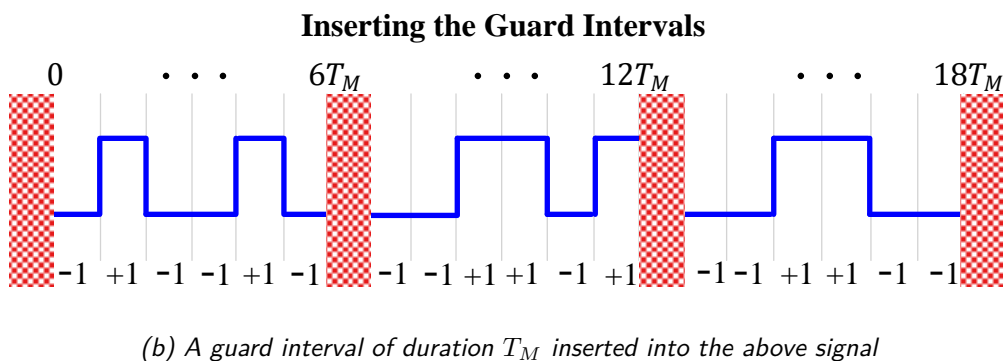
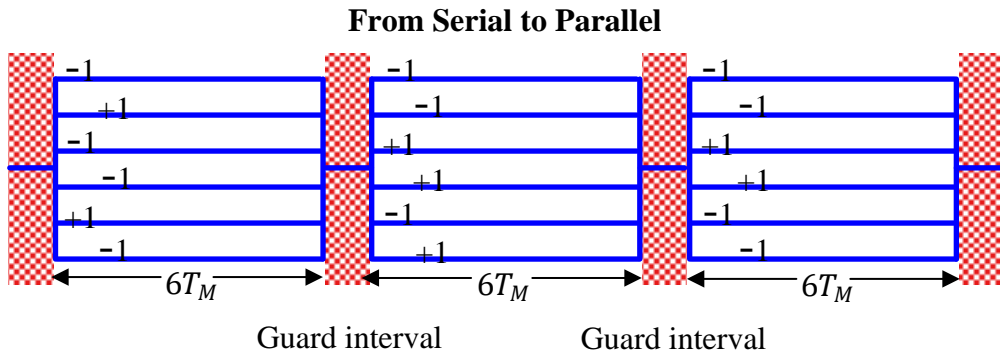
(a) A serial symbol stream with symbol duration T_M (b) A guard interval of duration T_M inserted into the above signal(c) $N = 6$ symbols collected into one block and sent on N parallel wires

Figure 8.1: A serial data stream is segmented into blocks of $N = 6$ parallel wires where the length of each wire is $N = 6$ times that of the original symbol T_M

- The multipath copies of the serial link will arrive T_M seconds later. Temporarily neglecting the impact of carrier wave, each symbol copy will overlap with the next symbol, thus completely randomizing the Rx

sequence (since the source generates an independent stream of +1s and -1s). The resultant signal is drawn in the upper part of Figure 8.2 before their addition.

- For the parallel mode, a copy of the elongated symbol of duration $6T_M$ will also be delivered after a delay of T_M , since the multipath channel is the same. However, as opposed to a complete overlap of one symbol into the next, we will have a relatively short overlap of just $1T_M$ which is $1/6$ or 16.7% of the parallel symbol duration $6T_M$! This is shown in the lower part of Figure 8.2 where by rearranging the symbols from serial to parallel, symbols in one elongated block do not interfere with the next elongated block. The small delay spread of duration T_M is catered for by the guard interval.

“By introducing parallelism, we have fooled a channel with a significant delay spread into behaving as a channel with a negligible delay spread!”

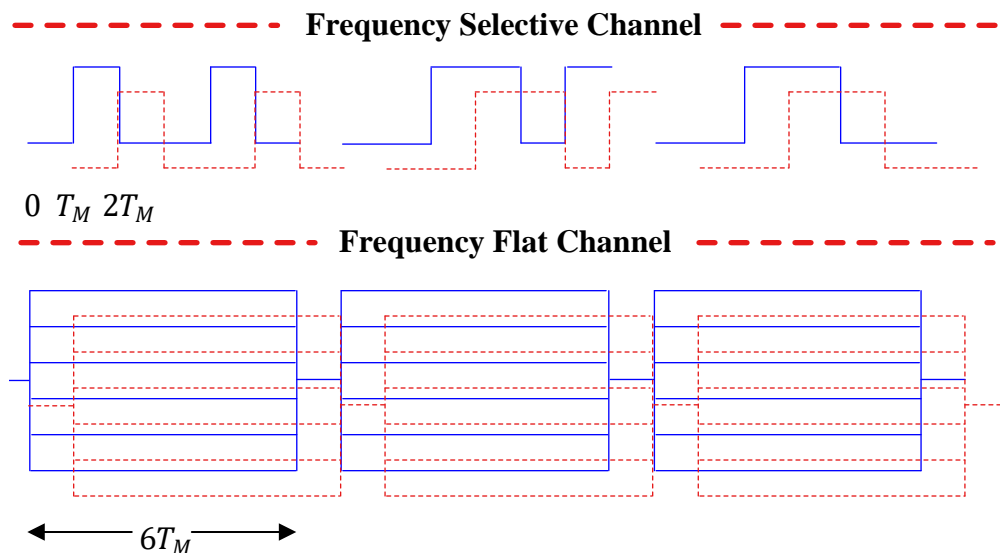


Figure 8.2: By rearranging the symbols from serial to parallel, a frequency selective channel (for symbols of duration T_M) has been converted into a frequency flat channel (for elongated symbols of duration $6T_M$)

By increasing N significantly larger than 6, a severe (much longer) channel can be tamed into behaving as a flat channel as well. Let us now see how these parallel wires are created in a virtual manner.

Parallel Wires in the Air

To avoid using the confusing terms of a symbol and an elongated symbol, we will call this elongated version **an OFDM symbol** from now onwards. By definition, the duration of an OFDM symbol is NT_M , i.e., N times longer than a conventional symbol duration T_M (later, we will see that its duration increases after inserting the guard interval). Now, the question is how to create these parallel wires in the air.

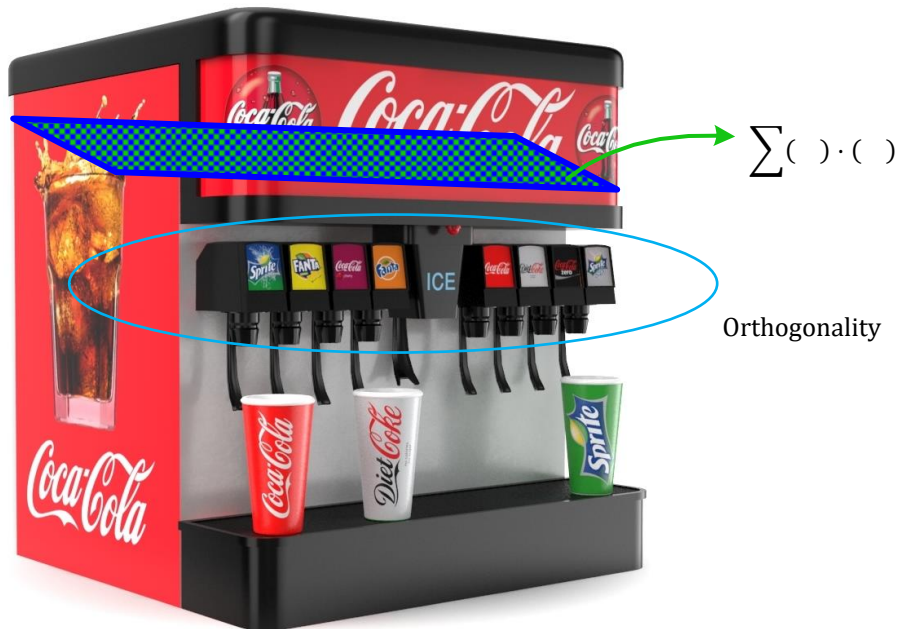


Figure 8.3: Orthogonality implies that the soda from each outlet does not mix with the soda from any other outlet. This is achieved here through a correlation operation

Recall the soda dispenser in Figure 5.5 which is now reproduced in Figure 8.3 along with a filter. Orthogonality implies that when you press the lever with the label Fanta, only Fanta comes out without any contribution from Sprite or Coca-Cola. Imagine a situation where the beverage machine is given a non-orthogonal input, i.e., a mixture of Fanta, Sprite and Coca-Cola is present at the top. If you want to drink Fanta, you have to separate it from the mixture by using a filter. This filter is a signal processing operation known as **correlation** which essentially is a summation of sample-by-sample product of the two signals. For this purpose, we focus on N samples that form an OFDM symbol and use length- N complex sinusoids introduced in Section 1.2. Since OFDM does not (theoretically) need to oversample

a signal, the symbol time T_M here is the same as the sample time T_S that is the inverse of the system sample rate F_S .

The lowest frequency that can be represented by these N samples is the one by a sinusoid that completes one full cycle – and no more – during this interval of NT_S seconds. Being an inverse of time period, such a frequency is given by $1/(NT_S)$ Hz and is known as the fundamental frequency F_1 .

$$\begin{array}{ll} I \rightarrow & V_I(t) = \cos 2\pi \frac{1}{NT_S} t = \cos 2\pi F_1 t \\ Q \uparrow & V_Q(t) = \sin 2\pi \frac{1}{NT_S} t = \sin 2\pi F_1 t \end{array}$$

Let us sample this complex sinusoid at a rate of $F_S = 1/T_S$.

$$\begin{array}{ll} I \rightarrow & V_I[n] = \cos 2\pi \frac{1}{NT_S} t \Big|_{t=nT_S} = \cos 2\pi \frac{1}{NT_S} nT_S = \cos 2\pi \frac{1}{N} n \\ Q \uparrow & V_Q[n] = \sin 2\pi \frac{1}{NT_S} t \Big|_{t=nT_S} = \sin 2\pi \frac{1}{NT_S} nT_S = \sin 2\pi \frac{1}{N} n \end{array}$$

where the discrete frequency can be seen as $1/N$. We now see how it is orthogonal to another sinusoid with frequency $2/N$ when a sum of products $\sum (\cdot) \cdot (\cdot)$, shown as a filter in Figure 8.3, is utilized. For simplicity, consider a real sine wave drawn in Figure 8.4.

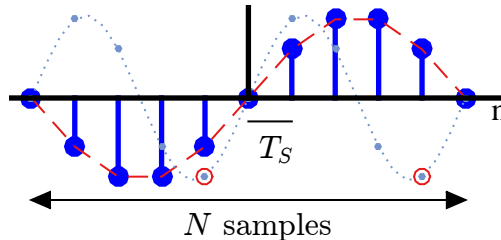


Figure 8.4: Two discrete-time sine waves with N samples, one with discrete frequency $1/N$ and the other with $2/N$

- It is evident that the sum of all samples in one period of the sine wave with frequency $1/N$ is zero because one half of the wave is positive while the other half is negative with the same amplitudes.

$$\sum_{n=0}^{N-1} \sin 2\pi \frac{1}{N} n = 0$$

- Now observe that the sine with frequency $2/N$ has 2 periods within N samples. In its first period, the products of its samples are taken with negative samples of the sine with frequency $1/N$. In its second period, the same products are taken with positive samples of the sine with frequency $1/N$ with exactly the same magnitude. In this way, this sum turns out to be zero as well!

$$\sum (\cdot) \cdot (\cdot) = \sum_{n=0}^{N-1} \left(\sin 2\pi \frac{1}{N} n \right) \cdot \left(\sin 2\pi \frac{2}{N} n \right) = 0 \quad (8.1)$$

This is evident from circles drawn around two of its samples in Figure 8.4. Verify that the corresponding samples of the sinusoid with frequency $1/N$ have opposite signs.

Now some real sinusoids for $N = 6$ are illustrated in Figure 8.5 where $k = 0, 1, \dots, N-1$. Although cosines are drawn here instead of sines, the sum of one or more periods is still zero because a cosine is simply a shifted version of a sine. To verify their orthogonality between different frequencies, take for example $k = 0$ and $k = 1$. The sinusoid with $k = 0$ are all ones, so its sample-by-sample product with $k = 1$ sinusoid yields the same sinusoid back. So for $k = 1$, notice that the sum of all samples are zero. The same holds true for $k = 2, 3, \dots, N-1$, thus proving the orthogonality.

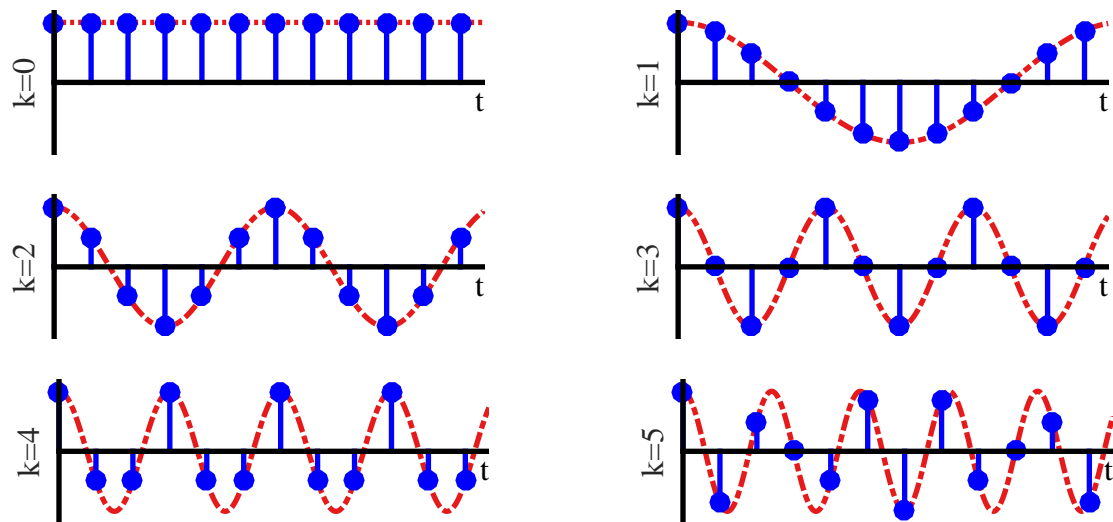


Figure 8.5: Real sinusoids act as a set of parallel waves in the air

You can repeat this computation for $k \neq 0$ by simulating in software; the sum of sample-by-sample product between any two sinusoids over an integer number of cycles is zero as long as their frequencies are a multiple of a fundamental frequency ($k = 1$ in this example).

In conclusion, orthogonality in DSP terms assumes one extra step, i.e., $\sum (\cdot) \cdot (\cdot)$, as opposed to orthogonal vectors which are inherently 90° apart. The idea can be extended to any sinusoid with an integer multiple of $1/N$. As a reminder, this orthogonality only holds for an integer number of cycles within a time duration. For non-integer number of cycles (e.g., three and a half periods), the orthogonality is destroyed due to the contribution from partial cycles. We have proved the following result.

All complex sinusoids having frequencies as integer multiples of a fundamental frequency $1/N$ are orthogonal to each other.

There we have a set of N parallel wires or waves that do not interfere with each other when correlated over a duration of N samples. **This set of sinusoids acts as our invisible parallel wires in the air!** This is similar to a parallel port used in personal computers between 1970s to 2000s and shown in Figure 8.6 that sends multiple bits of data at once through multiple parallel wires in its cable and port connector. It was gradually replaced with a serial USB standard.

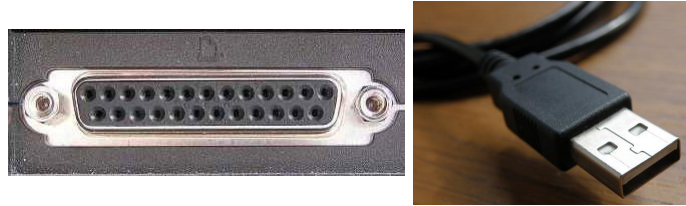


Figure 8.6: A parallel port (image from Wikipedia) has gradually been replaced by a serial port (USB) while the trend is opposite in wireless systems

Modulation and Demodulation

To benefit from this orthogonality, as the data symbols $a[k]$ are produced, we modulate each such sinusoid with one data symbol. For a real sinusoid with frequency k/N , modulation is performed as

$$a[k] \cdot \cos 2\pi \frac{k}{N} n, \quad k = 0, 1, \dots, N-1$$

With N modulation symbols, all such waveforms are added together to form the cumulative signal as drawn in Figure 8.7. This summation does not destroy individuality of each sinusoid within the whole as we shortly see during the demodulation process.

At the Rx side, a correlation of the above signal is performed with each such sinusoid of frequency k'/N . Orthogonality implies that

$$\sum_{n=0}^{N-1} \left\{ a[k] \cos 2\pi \frac{k}{N} n \right\} \cdot \cos 2\pi \frac{k'}{N} n = \begin{cases} a[k] & k = k' \\ 0 & k \neq k' \end{cases} \quad (8.2)$$

where a constant scaling factor of 2 has been ignored. This can be proved as follows.

- For $k \neq k'$, the orthogonality condition in Eq (8.1) simply makes the expression zero, as a sine and a cosine yield a similar result.

$$a[k] \sum_{n=0}^{N-1} \cos 2\pi \frac{k}{N} n \cdot \cos 2\pi \frac{k'}{N} n = 0$$

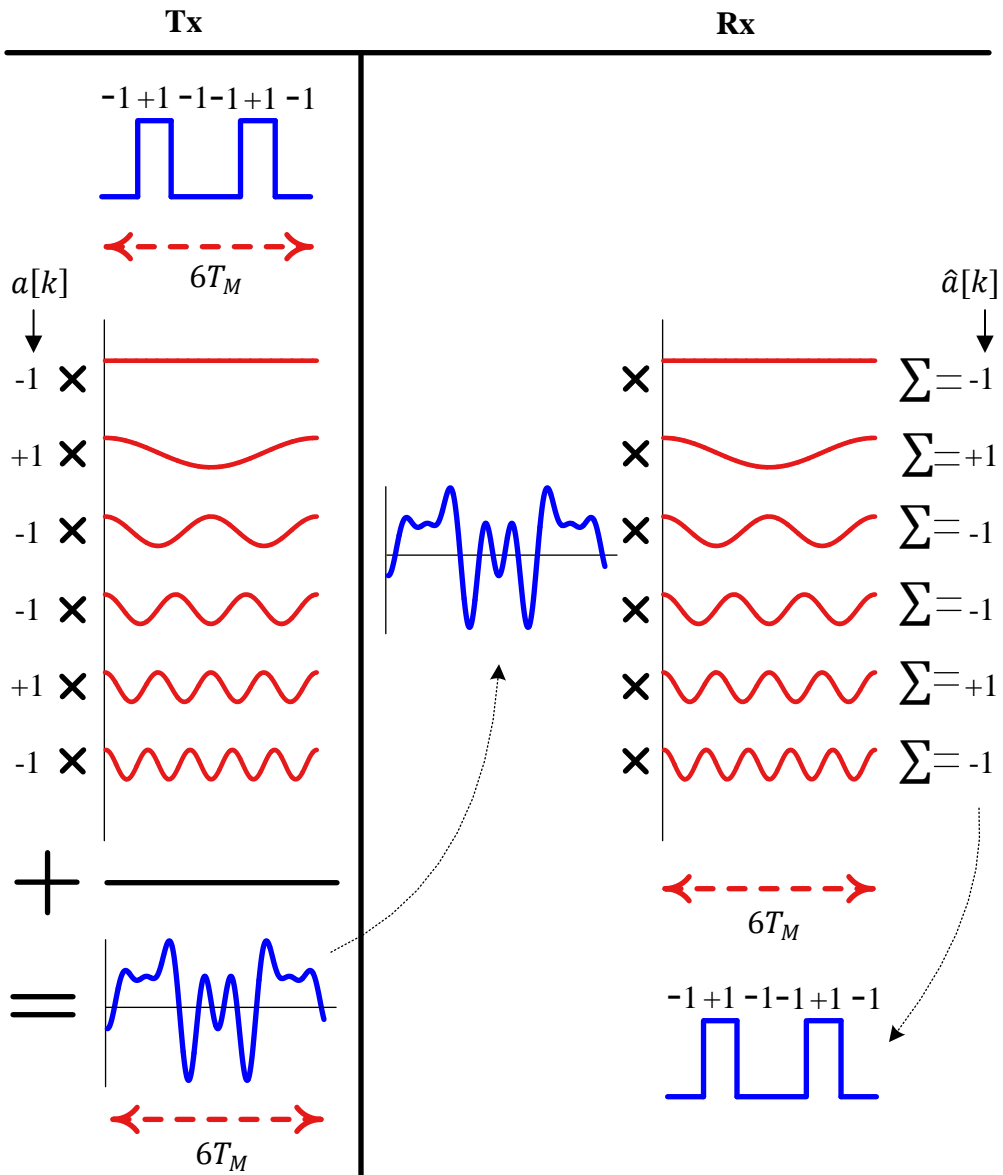


Figure 8.7: Data symbols modulated onto orthogonal sinusoids and added together to form the Tx signal. At the Rx, it is correlated with orthogonal sinusoids to generate symbol decisions

- For $k = k'$, use the double angle identity of a cosine $\cos^2 \theta = \frac{1}{2}(1 + \cos 2\theta)$ in Eq (8.2).

$$a[k] \sum_{n=0}^{N-1} \left(\cos^2 2\pi \frac{k}{N} n \right) = \frac{a[k]}{2} \sum_{n=0}^{N-1} \left(1 + \cos 2 \cdot 2\pi \frac{k}{N} n \right)$$

The first term is a constant and produces $a[k]$ at the output (ignoring the scaling factor of 2), while the second term is a cosine whose summation over a whole period (or a set of periods) for $n = 0$ to $N - 1$ is zero.

Consequently, if each such sinusoid of frequency k/N was modulated with a different data symbol $a[k]$ and added to all the others, each data symbol would have come out at the Rx side undistorted from the presence of other $N - 1$ symbols in parallel. This is illustrated in Figure 8.7 on the Rx side and can be verified as follows.

Let us form a cumulative signal by adding all N symbols modulated with their respective sinusoids.

$$\begin{aligned} v[n] &= a[0] \cos 2\pi \frac{0}{N} n + a[1] \cos 2\pi \frac{1}{N} n + \cdots + a[N-1] \cos 2\pi \frac{N-1}{N} n \\ &= \sum_{k=0}^{N-1} a[k] \cos 2\pi \frac{k}{N} n \end{aligned}$$

A correlation with $2 \cos 2\pi(k'/N)n$ at the Rx would yield

$$\sum_{n=0}^{N-1} \left\{ \sum_{k=0}^{N-1} a[k] \cos 2\pi \frac{k}{N} n \right\} \cdot 2 \cos 2\pi \frac{k'}{N} n = a[k]$$

This can be seen by taking an example of $k' = 1$.

$$\begin{aligned} &\sum_{n=0}^{N-1} \left\{ a[0] \cos 2\pi \frac{0}{N} n \right\} \cdot 2 \cos 2\pi \frac{1}{N} n + \sum_{n=0}^{N-1} \left\{ a[1] \cos 2\pi \frac{1}{N} n \right\} \cdot 2 \cos 2\pi \frac{1}{N} n + \\ &\quad \cdots + \sum_{n=0}^{N-1} \left\{ a[N-1] \cos 2\pi \frac{N-1}{N} n \right\} \cdot 2 \cos 2\pi \frac{1}{N} n \\ &= 0 + a[1] + \cdots + 0 = a[1] \end{aligned}$$

The right side of Figure 8.7 shows this process in action where the cumulative waveform is multiplied with each orthogonal sinusoid that generates the estimate for each data symbol $\hat{a}[k]$ independent of the other data symbols. Since these sinusoids carry the data symbols $a[k]$ in an independent fashion, these are known as **subcarriers**. A subcarrier is the word you would hear a lot during any discussion on OFDM.

From Real to Complex Sinusoids or Subcarriers

Having clarified the simple case of real sinusoids, we can show the realistic scenario of complex sinusoids known as subcarriers in the context of OFDM. A set of subcarriers for $k = -N/2, \dots, N/2 - 1$ is drawn in a 3D plane in Figure 8.8. Since some people are more comfortable with 2D figures, a set of subcarriers in terms of I and Q components is also illustrated in Figure 8.9 for $N = 4$.

The modulation and demodulation in terms of complex signals is performed as follows. For a subcarrier with frequency k/N and a modulation scheme with no Q component (such as BPSK), we can write

$$\begin{array}{ll} I & \rightarrow a[k] \cos 2\pi \frac{k}{N} n \\ Q & \uparrow a[k] \sin 2\pi \frac{k}{N} n \end{array}$$

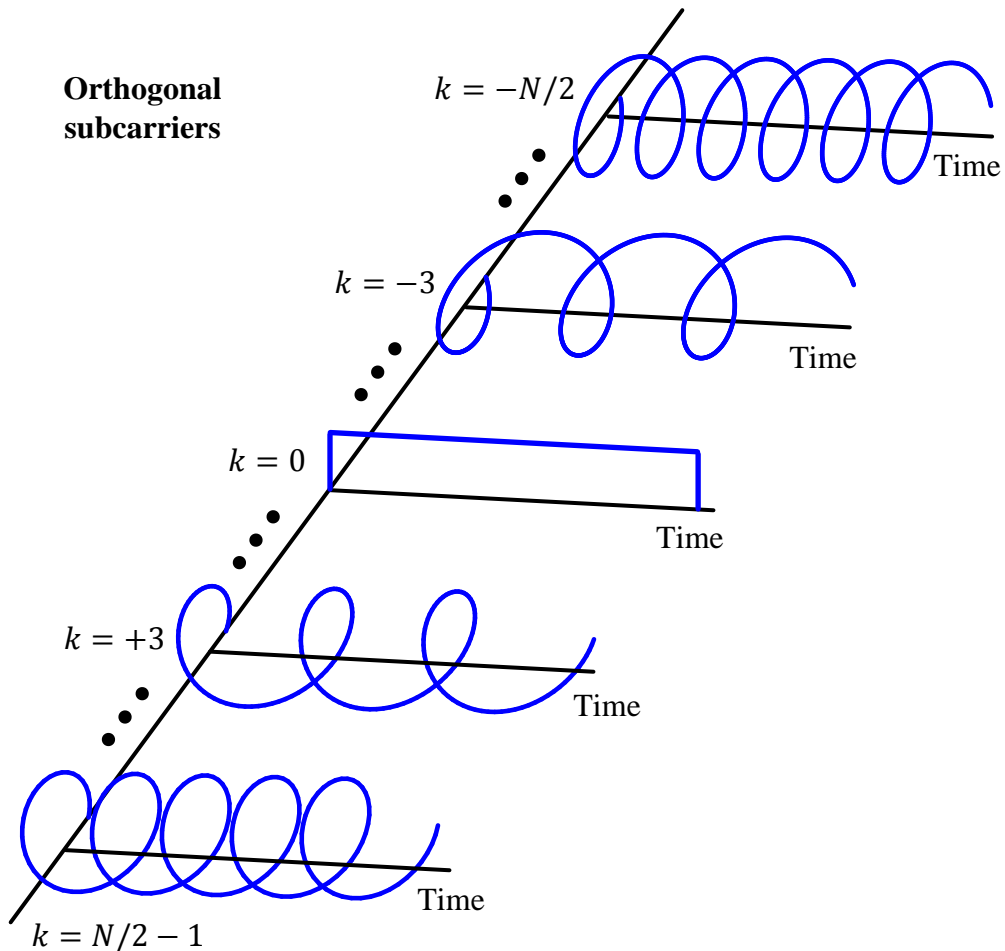


Figure 8.8: Complex subcarriers (which are nothing but complex sinusoids) act as a set of parallel waves in the air. Notice that these are the same sinusoids used in the computation of the DFT

More generally, for a QAM scheme with $a_I[k]$ and $a_Q[k]$ as I and Q parts, respectively, we can multiply them with a subcarrier of frequency k/N as follows.

$$\begin{array}{ll} I & \rightarrow \\ & a_I[k] \cos 2\pi \frac{k}{N} n - a_Q[k] \sin 2\pi \frac{k}{N} n \\ Q & \uparrow \\ & a_Q[k] \cos 2\pi \frac{k}{N} n + a_I[k] \sin 2\pi \frac{k}{N} n \end{array}$$

With the concept of subcarriers in place, we can clearly see how this modulation process can be very efficiently implemented: comparing the above expression with the definition of an inverse Discrete Fourier Transform (iDFT), *the subcarriers themselves are the DFT sinusoids* and the data symbol modulation process is exactly taking the iDFT of the symbol sequence $a[k]$. Consequently, OFDM can

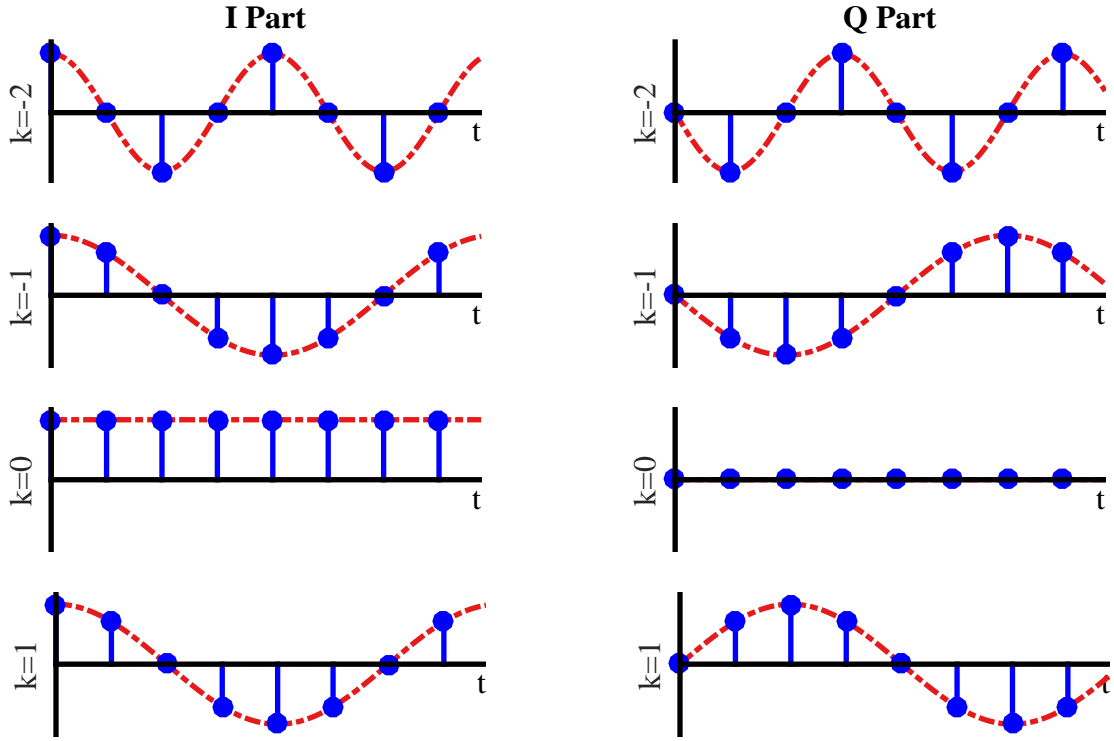


Figure 8.9: *I* and *Q* components of the subcarriers (which are nothing but complex sinusoids)

be implemented through iDFT as[†]

$$\begin{aligned} I \rightarrow \quad v_I[n] &= \frac{1}{N} \sum_{k=-N/2}^{N/2-1} \left[a_I[k] \cos 2\pi \frac{k}{N} n - a_Q[k] \sin 2\pi \frac{k}{N} n \right] \\ Q \uparrow \quad v_Q[n] &= \frac{1}{N} \sum_{k=-N/2}^{N/2-1} \left[a_Q[k] \cos 2\pi \frac{k}{N} n + a_I[k] \sin 2\pi \frac{k}{N} n \right] \end{aligned} \quad (8.3)$$

Since the iDFT is used to transform a signal from frequency domain to time domain, we can see why the terminology ‘frequency domain symbols’ is used for data symbols $a[k]$. This has nothing to do with some frequency domain property of data symbols but simply because the Tx signal is naturally considered to be in time domain and any signal before the iDFT block is then considered to be present in frequency domain.

Logically, the reverse operation, i.e., a DFT, is performed at the Rx side to transform the Rx signal into frequency domain for both equalization and detection purpose. The data symbol estimates are

[†]In terms of complex exponentials, you will often see the equivalent expression below.

$$v[n] = \frac{1}{N} \sum_{k=-N/2}^{N/2-1} a[k] \cdot \exp \left(j2\pi \frac{k}{N} n \right)$$

given as

$$\begin{aligned} I \rightarrow \hat{a}_I[k] &= \sum_{n=0}^{N-1} \left[v_I[n] \cos 2\pi \frac{k}{N} n + v_Q[n] \sin 2\pi \frac{k}{N} n \right] \\ Q \uparrow \hat{a}_Q[k] &= \sum_{n=0}^{N-1} \left[v_Q[n] \cos 2\pi \frac{k}{N} n - v_I[n] \sin 2\pi \frac{k}{N} n \right] \end{aligned} \quad (8.4)$$

Although a mathematical proof can be constructed by utilizing the subcarriers orthogonality, suffice it to say that the iDFT operation and DFT operation are inverse of each other and hence the data symbols appearing in Eq (8.3) can be perfectly recovered by applying Eq (8.4). It should also be remembered that both the iDFT and the DFT are implemented through the iFFT (inverse Fast Fourier Transform) and FFT (Fast Fourier Transform) procedures, which are efficient algorithms to compute their respective transforms. From here onwards, we will refer to going to and coming back from frequency domain through FFT operations interchangeably for the DFT.

Let us now see how a portion of an OFDM symbol - known as a Cyclic Prefix (CP) - is prepended back to combat the wireless channel.

Inserting the Cyclic Prefix (CP)

Let us call the expression NT_S that represents one block of N samples as T_u where u stands for the useful part of the symbol. We will shortly see what useful means in this context.

$$T_u = NT_S \quad (8.5)$$

This also implies that the frequency of the first subcarrier $F_1 = 1/T_u$ and the remaining frequencies are integer multiples of this fundamental frequency. A Cyclic Prefix (CP) consists of the last N_{CP} samples of the Tx sequence where N_{CP} is determined by the maximum *expected* channel length. For an OFDM symbol of length N , the process to insert the CP is shown in Figure 8.10 and consists of

$$N_{OFDM} = N_{CP} + N$$

samples instead of N samples. The time duration of the complete OFDM symbol is therefore defined as

$$T_{OFDM} = N_{OFDM} T_S = (N_{CP} + N) T_S = T_{CP} + T_u$$

where

$$T_{CP} = N_{CP} T_S$$

The question is why we need a CP in the first place. It turns out that the job of the CP is threefold in an OFDM system.

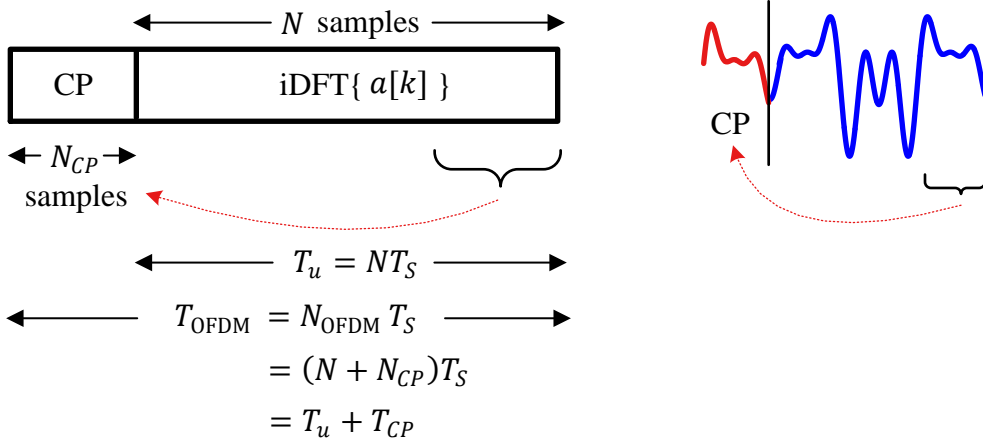


Figure 8.10: A Cyclic Prefix (CP) in the context of an OFDM symbol

Inter-Symbol Interference (ISI)

To provide a guard interval for the channel such that no interference from the previous OFDM symbol enters the next OFDM symbol. This happens when the length of the CP is chosen as the maximum expected channel length. The idea of a guard interval was explained before with the help of Figure 8.2. Here, Figure 8.11 depicts components of an OFDM symbol without any CP or guard interval, where **only the negative subcarriers are drawn** to keep the figure size small. The negative sign in the frequency of the last sinusoid, $-N/2$, appears due to its clockwise direction of rotation. These components are the subcarriers that are orthogonal to each other (earlier drawn in Figure 8.9 with I and Q parts separated) and scaled by data symbol $a[k]$ (all assumed +1 here). The actual OFDM signal is formed through summing all the corresponding samples in these subcarriers.

Notice that since the subcarriers are completing their full number of cycles within each OFDM symbol, they are all orthogonal to each other within that OFDM symbol and no ISI occurs. Next, Figure 8.12 draws the same OFDM signal without any CP but after it has passed through a wireless channel. In this figure, only $k = 0$ subcarrier is shown for all three intervals while the rest of the subcarriers are drawn for OFDM symbol 1 only for clarity. It is straightforward to identify the ISI due to the intruding of one OFDM symbol into the next. This problem is prevented through the insertion of CP.

Inter-Carrier Interference (ICI)

A detailed mathematical reasoning on the prevention of ICI through a CP is probably too cumbersome to include here. For the understanding of the basic mechanism, I take the familiar path and demonstrate this concept with the help of a few figures. For this purpose, recall from the discussion on orthogonality that it holds for signals with an integer number of cycles within a time frame. This is because the signals with frequencies other than the set k/N are not periodic in the

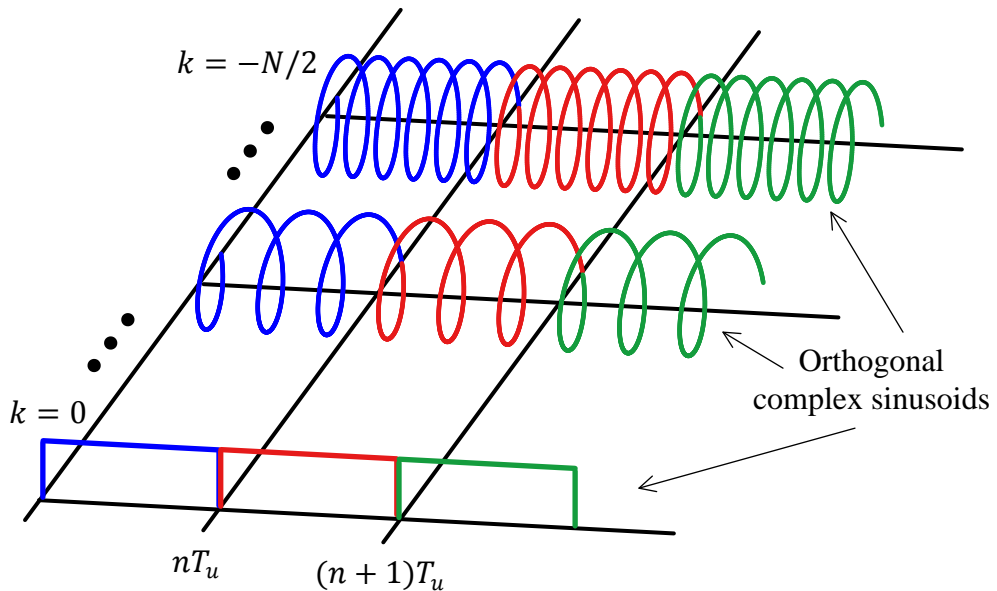


Figure 8.11: Orthogonal subcarriers (complex sinusoids) in an OFDM symbol without a Cyclic Prefix (CP) or guard interval

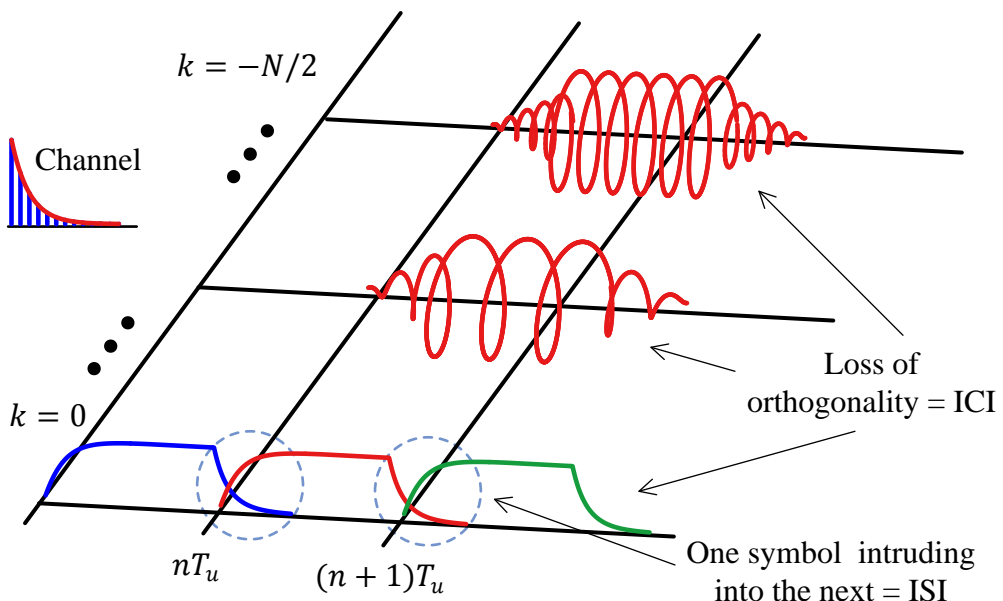


Figure 8.12: After passing through the wireless channel, Inter-Carrier Interference (ICI) arises due to the loss of orthogonality among subcarriers and Inter-Symbol Interference (ISI) arises due to one OFDM symbol intruding into the next

observation window and are suddenly terminated without completing the final cycle in full. This discontinuity violates the orthogonality relation yielding a non-zero result and becomes responsible for spectral contributions over the entire set of frequencies k/N . Due to the convolution with the wireless channel, a loss of exact complete periods within an OFDM symbol is evident in our current Figure 8.12 which gives rise to ICI among subcarriers. *The data symbols $a[k]$ are not traveling on independent parallel waves anymore!*

On the other hand, when a CP is inserted with a length greater than the maximum expected channel length, the effect of ISI remains limited to the CP duration. This is drawn in Figure 8.13a. The CP also acts as a buffer against introducing ICI in the system because the loss of orthogonality only happens within the CP duration. When it is removed, it not only helps in getting rid of the ISI in the system but the remaining parts of the subcarriers exhibit a completion of rotation within the useful period T_u , thus restoring the orthogonality among the subcarriers. The OFDM symbol is ICI-free and the data symbols $a[k]$ can then be independently detected. This is illustrated in Figure 8.13b.

Converting Linear Convolution into Circular Convolution

A CP converts linear convolution between the Tx signal and the wireless channel into circular convolution. This circular convolution enables the discrete frequency domain product between their respective transforms. The concept of convolution is outside the scope of this text but it is quite similar to correlation, i.e., a summation of sample-by-sample product between two signals. The only difference is that one of the signals is flipped around index 0 during a convolution.

Observe that the channel $h[m]$ – at any single output sample of convolution – cannot affect the incoming signal beyond its own length. Therefore, the best compromise is to only repeat a portion of the Tx sequence **from the end** with length equal to channel memory minus one. This last portion of the Tx sequence, prefixed at the start of the modified Tx sequence, is known as a **Cyclic Prefix (CP)**. Since the channel length is $N_{tap} + 1$ in our context, the length of the CP is N_{tap} .

In general, we say that the length of a cyclic prefix should be equal to the maximum expected channel length. We do not know the channel beforehand but important parameters like maximum delay spread D_S , coherence bandwidth, Doppler spread and coherence time are found through extensive channel measurement campaigns. Then, the maximum delay spread is converted into maximum expected channel length by dividing it through the sample time T_S and the result is chosen as the CP length N_{CP} .

$$N_{CP} = \frac{D_S}{T_S}$$

Since the Rx sequence starting from sample N_{CP} is a circular convolution between the Tx sequence and the channel impulse response, we can now easily take it into frequency domain by taking the N_D -point DFT $Z[k]$ of this sequence **after discarding the CP**. This DFT is now a legitimate product of

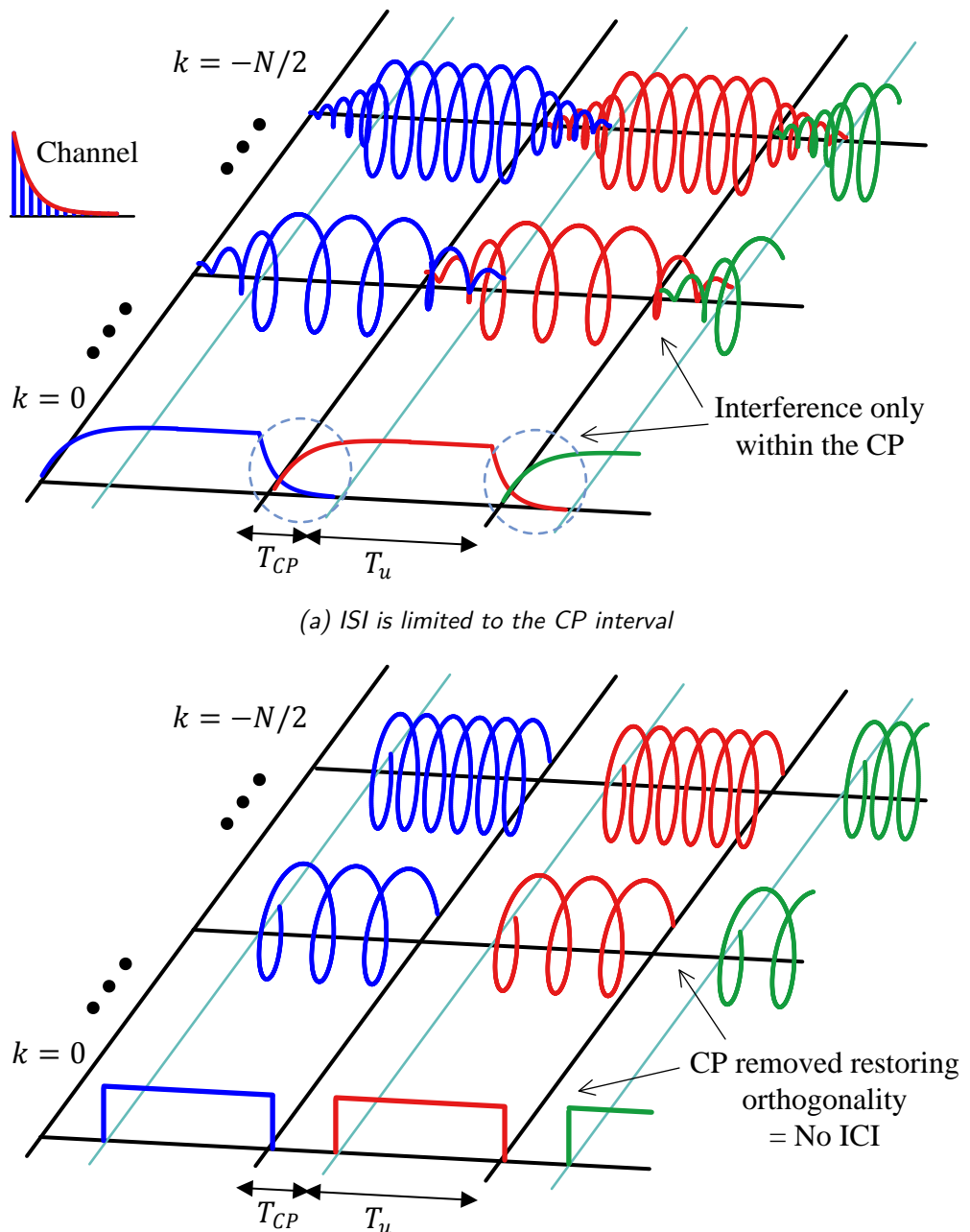


Figure 8.13: Effect of CP on ISI and ICI

the DFTs of the Tx sequence and the channel response.

$$Z[k] = A[k] \cdot H[k] \quad \text{for each } k = -N_D/2, \dots, N_D/2 - 1 \quad (8.6)$$

The CP is now useless as it just contains the transient response of the channel. Later, we will see that it also gets polluted with ISI from the previous symbol when used with block processing. Therefore, it is discarded right away at the Rx side. The CP is the price we pay for launching a high data rate signal (geared up for simpler frequency domain equalization) into the environment. This is similar to a rocket launching a shuttle into space and then it either falls off in the ocean, burns up or becomes space junk.

Now we discuss why the equalization becomes simpler in an OFDM system as compared to a single-carrier system.

Why Equalization Becomes Simpler

Complexity of equalization has been the bottleneck in successful implementation of high rate single-carrier systems. The introduction of subcarriers in OFDM simplifies this process to a considerable level and has been the major factor in its adoption in high speed wireless systems. Although this process of simple equalization is better explained in frequency domain later, we still have a look at the channel impact in time domain to get an idea.

For this purpose, we continue with $N = 6$ subcarriers shown earlier in Figure 8.7 as an example and see what happens in the presence of a multipath channel. This is drawn in Figure 8.14 where two observations are important.

1. We have explained before that as long as the delay spread of the channel remains less than 10 or so percent of the symbol duration, the channel is frequency flat fading and hence multiplies the signal with a single coefficient, instead of a complete convolution as in the case of a frequency selective fading channel. Now the channel example shown here is a frequency selective channel for the serial symbol stream because the multipath duration is equal or greater than a symbol time T_M . However, due to the elongated symbol length, i.e., NT_M here, it has been converted into a frequency flat fading channel *for each subcarrier*.
2. With the addition of a CP, the orthogonality of each subcarrier is ensured and the channel impacts each subcarrier in an individual manner. Notice in Figure 8.14 how each subcarrier will be deteriorated by the channel but discarding the CP gets rid of both ISI from one OFDM symbol to the next as well as ICI among different subcarriers. Then, for each subcarrier, the channel is just a summation of complex sinusoids *of the same frequency with different amplitudes and delays* which all add up to generate a resultant amplitude and phase without changing the frequency. Let us derive this resultant channel for a subcarrier k .

Referring to Figure 8.14, assume that the delay of the direct path $\tau_0 = 0$ and its amplitude $\rho_0 = 1$. With a single multipath with delay τ_1 (which is $n_1 = \tau_1/T_S$ in terms of samples) and amplitude ρ_1 , the I output can be expressed as below. Recalling that the subcarriers are complex sinusoids, *the actual amplitudes γ_i are complex* and given as a function of carrier frequency F_C in Eq (2.6). Nevertheless, for

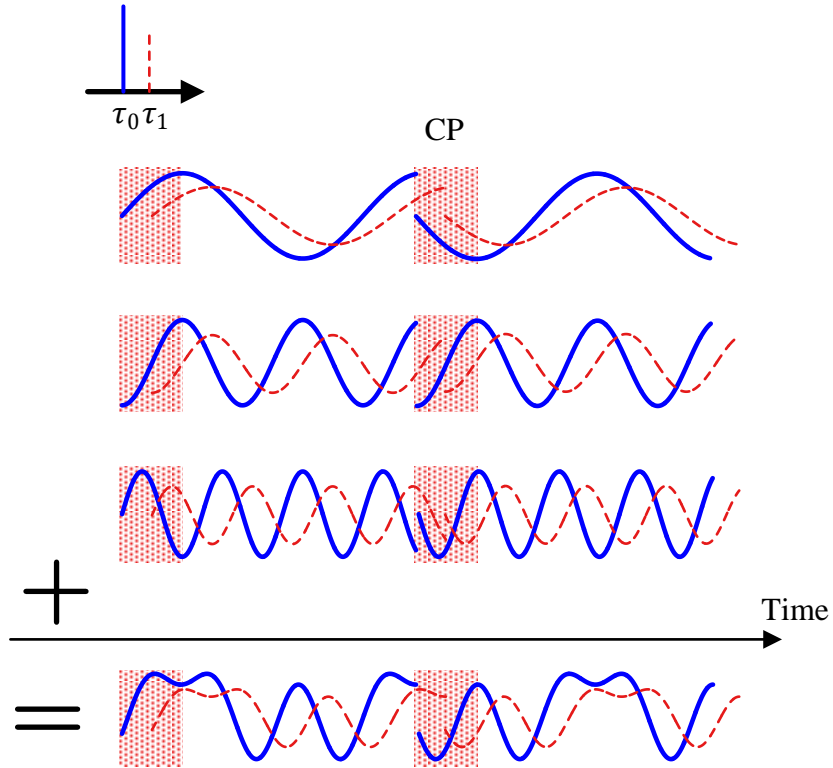


Figure 8.14: In the presence of a CP, multipath in time domain impact each subcarrier individually due to their orthogonality. Moreover, an elongated symbol implies flat fading for each individual subcarrier

removing clutter to simplify the derivation, here we take them as real and equal to ρ_i . Using $\cos(A - B) = \cos A \cos B + \sin A \sin B$, the sum of these two paths can be written as

$$\begin{aligned}
 & \cos 2\pi \frac{k}{N} n + \rho_1 \cos 2\pi \frac{k}{N} (n - n_1) = \cos 2\pi \frac{k}{N} n + \\
 I \rightarrow & \quad \rho_1 \cos 2\pi \frac{k}{N} n \cdot \cos 2\pi \frac{k}{N} n_1 + \rho_1 \sin 2\pi \frac{k}{N} n \cdot \sin 2\pi \frac{k}{N} n_1 \\
 & = \left(1 + \rho_1 \cos 2\pi \frac{k}{N} n_1\right) \cos 2\pi \frac{k}{N} n + \left(\rho_1 \sin 2\pi \frac{k}{N} n_1\right) \sin 2\pi \frac{k}{N} n
 \end{aligned}$$

On a similar note,

$$\begin{aligned}
 & \sin 2\pi \frac{k}{N} n + \rho_1 \sin 2\pi \frac{k}{N} (n - n_1) = \sin 2\pi \frac{k}{N} n + \\
 Q \uparrow & \quad \rho_1 \sin 2\pi \frac{k}{N} n \cdot \cos 2\pi \frac{k}{N} n_1 - \rho_1 \cos 2\pi \frac{k}{N} n \cdot \sin 2\pi \frac{k}{N} n_1 \\
 & = -\left(\rho_1 \sin 2\pi \frac{k}{N} n_1\right) \cos 2\pi \frac{k}{N} n + \left(1 + \rho_1 \cos 2\pi \frac{k}{N} n_1\right) \sin 2\pi \frac{k}{N} n
 \end{aligned}$$

where $\sin(A - B) = \sin A \cos B - \cos A \sin B$. From the multiplication rule of complex signals $I \cdot I - Q \cdot Q$ and $Q \cdot I + I \cdot Q$, we can see that the subcarrier k is being multiplied with a *single channel*

coefficient given by

$$\begin{array}{ll} I \rightarrow & H_I[k] = 1 + \rho_1 \cos 2\pi \frac{k}{N} n_1 \\ Q \uparrow & H_Q[k] = -\rho_1 \sin 2\pi \frac{k}{N} n_1 \end{array} \quad (8.7)$$

For each subcarrier, even when the number of multipath copies increases, the number of terms in the above expression increases but the frequency of their sum signal remains the same (equal to k/N). Subsequently, the important point to remember is that each such sum, for each subcarrier, remains orthogonal to all the other subcarriers $k' \neq k$. The orthogonality among subcarriers, each experiencing a flat fading channel, is the main reason behind simpler equalization required for an OFDM system.

In summary, OFDM increases the symbol duration from T_M to $T_u = NT_M$ such that the information is transmitted in many low rate parallel streams. After the CP, the multipath copies do not destroy the orthogonality where each sinusoid is multiplied by a complex constant. This eases the equalization part of the Rx processing to separate the subcarriers.

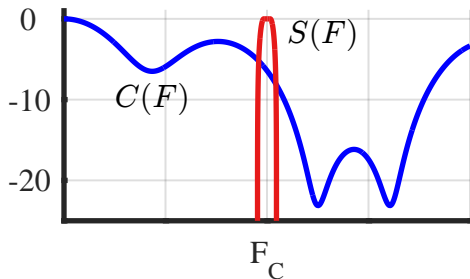
Having viewed the concept of OFDM in time domain, we look at its frequency domain interpretation.

8.2 To a Sliced Bread

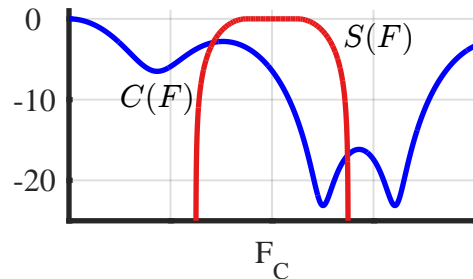
We start with the problem high rate single-carrier systems face in frequency domain and then explain how OFDM addresses that issue.

Increasing the Symbol Rate

The frequency response of the wireless channel from Chapter 2 is redrawn here in Figure 8.15a for a frequency flat fading channel and in Figure 8.15b for a frequency selective fading channel. Here, $C(F)$ and $S(F)$ are the frequency domain representations of the channel and Tx signal, respectively.



(a) A frequency flat fading channel



(b) A frequency selective fading channel

Figure 8.15: Our symbol rate determines the signal bandwidth and consequently whether the channel behaves as a frequency flat or selective fading channel

With respect to frequency domain, the signal at the Rx is a product of the spectra of the Tx signal and the wireless channel. The low data rate signal in Figure 8.15a needs less manipulation by the Rx to get the original data back. Essentially for this kind of signal, the channel acts just as a single multiplier that can be equalized through estimating that channel coefficient and dividing the Rx signal by the estimated value. Consequently, the equalization process reduces to a single division operation.

Coming to Figure 8.15b, it is evident that due to the high data rate and hence large signal bandwidth, the whole bandwidth extends beyond the coherence bandwidth of the channel and hence the Rx magnitude is distributed across a wide spectral region. The equalization across this wide spectrum needs a lot of Rx processing. Such a computationally complex equalizer is incompatible with a high rate symbol stream.

Subcarriers/Complex Sinusoids in Frequency Domain

To view this process in frequency domain, we need to know how the Fourier Transform of a complex sinusoid looks like.

- If we had infinitely long subcarriers, then their Fourier Transform would just have been an impulse at that frequency. This is shown at the top of Figure 8.16. Recalling the definition of frequency as cycles/second, the frequency of this impulse is $3/T_u$ because there are three complete cycles of the complex sinusoid in our measurement time T_u .
- However, the subcarriers are only T_u wide in time which is the same as multiplying them with a rectangular signal of length T_u . A rectangular signal has a sinc signal as its Fourier Transform shown in the middle of Figure 8.16.
- Finally, a multiplication in time induces a convolution in frequency. For this reason, the sinc signal in frequency gets shifted to the frequency of the subcarrier, $3/T_u$ in our example.

Now we want to inspect all the subcarriers together in frequency domain. For this purpose, the following two questions need to be answered.

Spacing Between any Two Subcarriers

First, remember from Eq (8.5) that the duration of each subcarrier, or complex sinusoid, is

$$T_u = NT_S, \quad \rightarrow \quad F_1 = \frac{1}{T_u} \quad (8.8)$$

and there are N such subcarriers forming the overall signal. The indices of these subcarriers range from $k = -N/2$ to $k = N/2 - 1$. From this information, we deduced the actual frequency F_k of each subcarrier as

$$F_k = \frac{k}{NT_S} = \frac{k}{T_u}$$

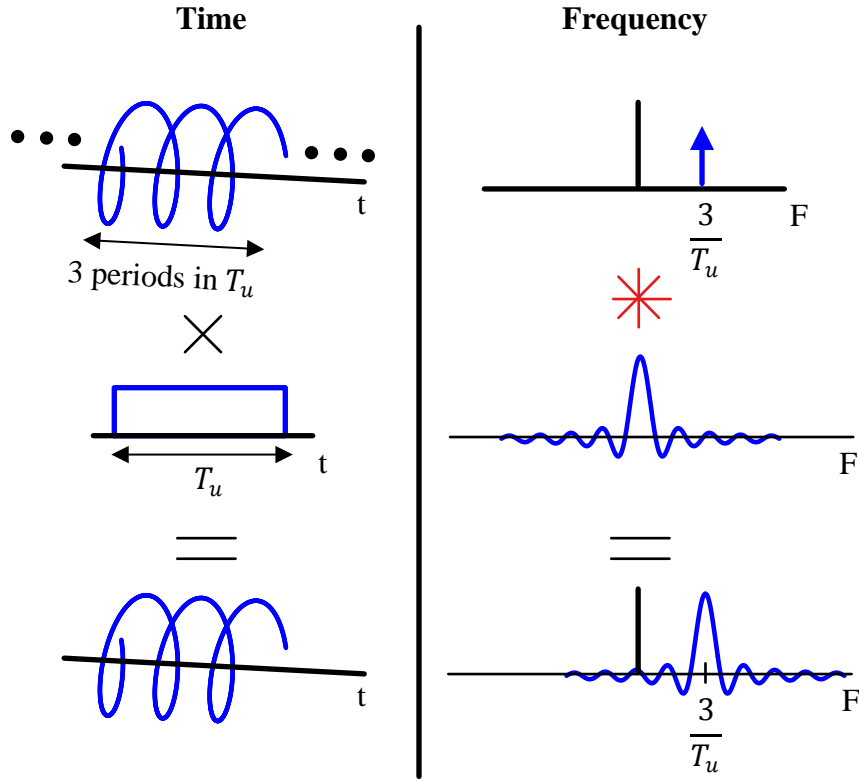


Figure 8.16: Limiting the complex sinusoid or subcarrier in time domain creates its spectrum as a sinc signal in frequency domain

From $k = 0$ and $k = 1$, we can find the spacing Δ_F between any two subcarriers.

$$\Delta_F = \frac{1}{T_u} - \frac{0}{T_u} = \frac{1}{T_u} \quad (8.9)$$

Location of Sinc Signal's First Zero Crossing

The first zero crossing in frequency domain is the same as the length of the rectangular signal in time domain. With N samples that cover the duration T_u , we get the first zero crossing frequency F_{zc} as

$$F_{zc} = \frac{1}{NT_S} = \frac{1}{T_u} \quad (8.10)$$

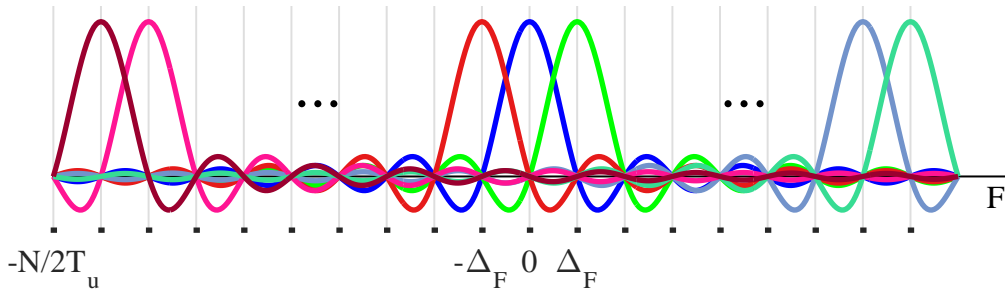
which interestingly is the same as Eq (8.9). It is not surprising that the spacing Δ_F between any two subcarriers and the first zero crossing of the sinc signal is the same, equal to $1/T_u$. *This is what orthogonality means in frequency domain!*

With this information at hand, we draw the subcarriers in frequency domain, all at the same time

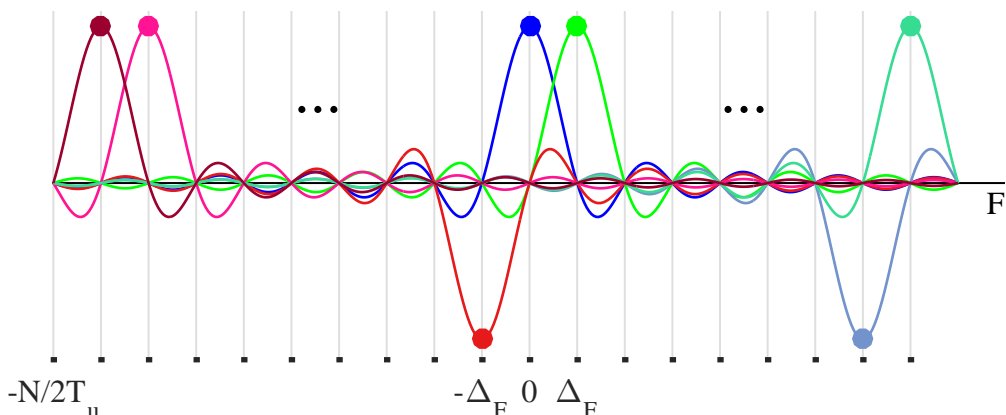
in Figure 8.17a. Notice the zero crossings of the 0^{th} subcarrier passing through

$$\pm\Delta_F = \pm\frac{1}{T_u}, \quad \pm 2\Delta_F = \pm\frac{2}{T_u}, \quad \dots$$

and so on, right at the peaks of the other subcarrier locations $k\Delta_F = k/T_u$.



(a) Unmodulated OFDM subcarriers in frequency domain. Notice the zero crossings of each subcarrier passing through other subcarrier frequencies $k\Delta_F = k/T_u$



(b) Modulated OFDM subcarriers in frequency domain. The Rx utilizes exactly the same frequencies $k\Delta_F = k/T_u$ for DFT that 'samples' the signal in frequency domain at ideal ICI-free instants

Figure 8.17: Unmodulated and modulated OFDM subcarriers in frequency domain spaced $\Delta_F = 1/T_u$ apart from each other

When a linear modulation scheme, such as BPSK, is utilized, the subcarrier amplitudes are modulated as $a[k] = +1$ or $a[k] = -1$. These $a[k]$ modulate the subcarriers in Figure 8.17b and an iDFT is taken to generate the time domain signal. The DFT at the Rx then needs to be taken at exactly the same set of frequencies k/T_u . In that way, the Rx 'samples' the OFDM waveform in frequency domain at exactly the peaks of subcarriers, exhibiting zero Inter-Carrier Interference (ICI): maximum contribution comes from the desired subcarrier and zero contribution from all the rest. However, the presence of a carrier frequency offset causes the 'sampling' in frequency domain at the wrong instants thus introducing ICI in the system.

Why Equalization Becomes Simpler

We saw the time domain picture of the multipath components of the orthogonal subcarriers in Figure 8.14 and claimed that the simpler equalization of OFDM systems is better explained in frequency domain. Let us explore this fact here.

First, denote the DFT of the channel impulse response as $H[k]$. To find the nature of these channel coefficients $H[k]$ in frequency domain, we first refer to Figure 8.14 where delayed copies of the Tx signal were drawn for each individual subcarrier k . Next, we use a property of Fourier Transform that was introduced in Eq (2.8): a delay t_0 in time domain induces a *frequency dependent phase shift* in frequency domain given by $-2\pi F t_0$. For the discrete frequency k/N case,

$$\text{Time shift } s[(n \pm n_0) \bmod N] \longrightarrow \pm 2\pi \frac{k}{N} n_0 \quad \text{Phase shift}$$

The delay τ_i in seconds becomes τ_i/T_S in samples. Consequently, while each multipath copy of a subcarrier k arrives with the same frequency k/N but an amplitude ρ_i , its phase is also changed by an amount $-2\pi(k/N)\tau_i/T_S$. For example, for a single multipath copy arriving with amplitude ρ_1 at τ_1 seconds after the direct path, this phase shift is illustrated in Figure 8.18 along with the direct path which is a graphical manifestation of what we got in Eq (8.7) during time domain description.

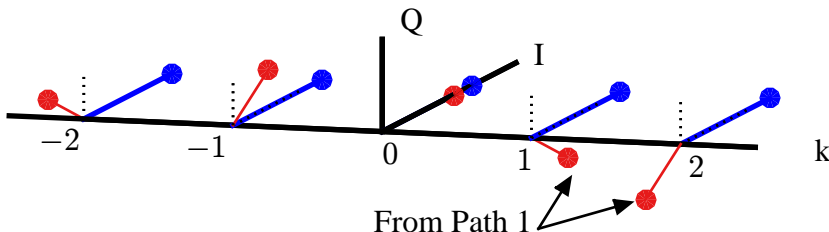


Figure 8.18: Multipath in frequency domain impact each subcarrier individually due to their orthogonality. Moreover, these narrow subcarriers induce flat fading for each k

The result for several multipath signals can be produced by extending the same concept, i.e., when many of these vectors are added for the same subcarrier frequency k/N , we get the channel coefficient $H[k]$ for each k as a vector sum of the channel taps.

In summary, the output of the channel – a product between the data symbols $a[k]$ and the channel frequency response $H(F)$ – is sampled at N locations in frequency domain by the subcarriers. The DFT output at the Rx is just the product between the Tx signal DFT $S[k]$ and $H[k]$.

$$Z[k] = S[k] \cdot H[k] \quad (8.11)$$

for each $k = -N/2, \dots, N/2 - 1$

Owing to the orthogonality of the subcarriers which manifests itself in the form of each subcarrier k/T_u passing through zero at other subcarrier frequencies k'/T_u (i.e., zero ICI), $S[k]$ for each k is nothing

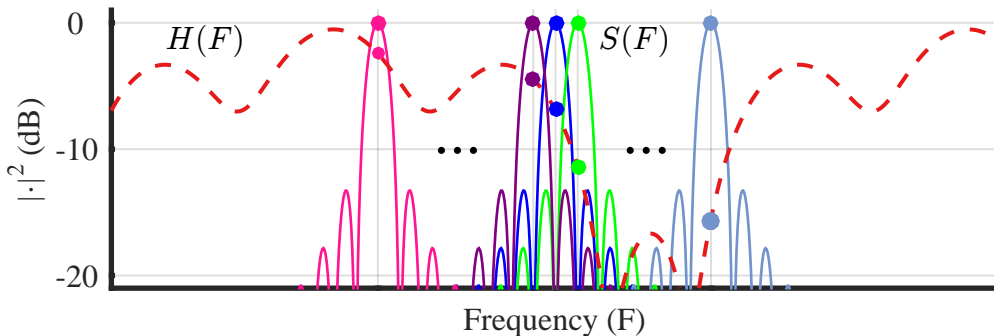


Figure 8.19: The DFT output at the Rx is the spectral product between the data symbol values $a[k]$ and channel frequency response $H[k]$ sampled at subcarrier frequencies $k\Delta_F = k/T_u$

but the data symbol value $a[k]$. Thus, we can write

$$\boxed{Z[k] = a[k] \cdot H[k]} \quad (8.12)$$

for each $k = -N/2, \dots, N/2 - 1$

Figure 8.19 illustrates this process for our example channel and an all-ones modulated OFDM symbol where the sinc sidelobes in dB are clearly visible. The channel frequency response $H(F)$ is sampled by the DFT at the subcarrier frequencies $k\Delta_F = k/T_u$ to yield $H[k]$. This is shown as the dashed red curve, the Δ_F -spaced samples of which are multiplying each subcarrier data individually. It is evident that such a wideband channel has been converted into many parallel *frequency flat subchannels* through using the subcarriers.

Therefore, to recover the data symbol value when a channel estimate $\hat{H}[k]$ is available, all we have to do is divide each DFT output $Z[k]$ from $k = -N/2$ to $N/2 - 1$ by its corresponding channel coefficient $\hat{H}[k]$.

$$\boxed{\hat{a}[k] = \frac{Z[k]}{\hat{H}[k]}} \quad (8.13)$$

This is the fundamental concept of equalization in an OFDM system. That comes out to be N divisions for N symbols, or **1 division/symbol**, a huge computational saving over a time domain equalizer for a similar frequency selective channel.

The sliced bread

The OFDM operation is very similar to processing a bread. Long ago, each time a person wanted to eat bread, they had to take a knife and cut a piece of bread for themselves. Then came sliced bread in July 1928 invented by

a jeweler Otto Frederick Rohwedder that changed everything. Processing each individual slice got much easier; you could put jam, butter or cheese on different slices, see Figure 8.20.

It was difficult to process the whole bread before that invention. Similarly, it is difficult to process the collective spectrum for communication purposes before OFDM came on the scene. By slicing the spectrum, OFDM not only made it easier to equalize the wireless channel but also made it possible to send different modulation signals on different subcarriers. It also made possible to assign different subcarriers to different users for transmission and reception.

On a lighter note, now we have a formal proof that OFDM is the best thing that happened since sliced bread.



Figure 8.20: Just like a whole bread needs to be sliced for eating convenience, OFDM slices the spectrum for communication convenience. Compare with Figure 8.19

In summary, what OFDM does in frequency domain is fairly simple. It just segments the available bandwidth of a frequency selective channel into *many parallel frequency flat channels* through utilizing those sinusoidal subcarriers. This is because the segmentation factor N is chosen such that the bandwidth of these frequency flat channels Δ_F is within the coherence bandwidth B_C of the channel. Hence, equalization for each narrow slice requires just a single division operation, rendering the computational load of the equalizer to a total of N divisions.

An OFDM Transceiver

After understanding the mechanism behind a multi-carrier waveform, we can draw a block diagram for an OFDM system as done at the top of Figure 8.21. The information bits are first coded through a channel encoder such as LDPC covered in Chapter 7. These coded bits are then mapped to the symbols in accordance with the chosen modulation scheme, e.g., 64-QAM. Next, the symbols are grouped in blocks of N by a serial-to-parallel converter and an N -point inverse Fast Fourier Transform (iFFT) – which is a very efficient implementation of Discrete Fourier Transform (DFT) – is taken to generate

the time domain waveform of the complex signal. The last N_{CP} samples of this time domain waveform are prepended back to the start of the sequence as a Cyclic Prefix (CP) for reasons mentioned earlier, i.e., to prevent ISI, ICI and converting linear convolution into a circular convolution. A parallel-to-serial converter then produces the serial sequence that is fed to a radio chain that includes a DAC, filters, upconversion to the carrier frequency and an amplifier. The output is the continuous-time OFDM waveform transmitted through the antenna.

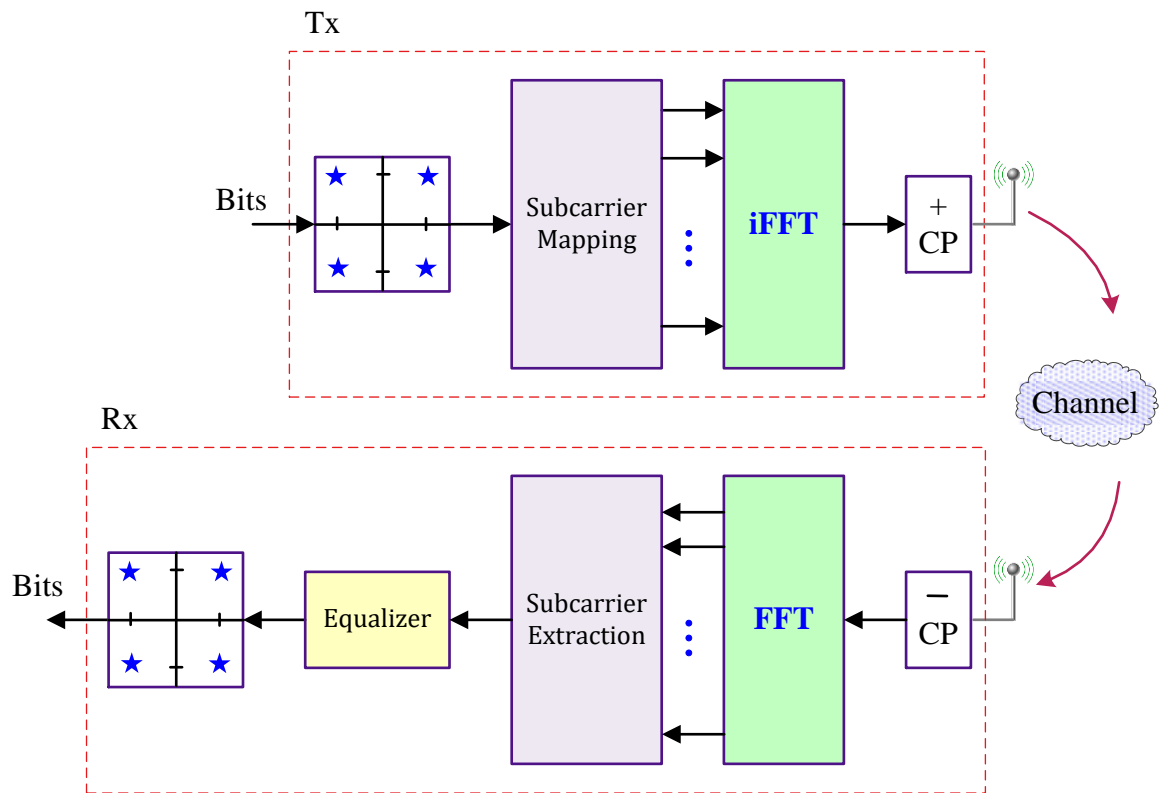


Figure 8.21: A block diagram of an OFDM system

A block diagram of a Rx is also drawn at the bottom of Figure 8.21. The OFDM Rx implements similar operations as the Tx but in reverse order. A continuous-time waveform is first bandpass filtered and downconverted with the help of a Local Oscillator (LO) where the choice of the ADC placement depends on the Rx architecture. This is lowpass filtered to reduce interference and noise as well as for sample rate conversion. Timing synchronization, carrier synchronization and channel estimation are performed at this stage. Then, a serial-to-parallel converter prepares the input for FFT computation. However, the first N_{CP} samples are first discarded since they are contaminated from the ISI of the previous block. Next, an N -point FFT is taken and multiplied with the channel inverse $1/\hat{H}[k]$ to equalize in frequency domain. Since the data symbols were produced in frequency domain (which is the same as saying that an iFFT has already been taken) at the Tx, the equalized signal is ready for symbol detection which is parallel-to-serial converted and input to the channel decoder.

Now we summarize the main benefits behind CP-OFDM as the choice of modulation.

8.3 Why CP-OFDM?

Having understood the fundamental ideas behind a CP-OFDM waveform, we are in a position to list its main benefits that became the reason behind its adoption for 5G cellular systems.

Tx/Rx Complexity

As explained in detail before, computational complexity of handling an OFDM waveform is much less than a single-carrier waveform with an equally high data rate. This is due to that one-tap equalizer for each subcarrier. Overcoming the Inter-Symbol Interference (ISI) through the cyclic prefix also helps but that can also be implemented into a single-carrier waveform by introducing a block structure.

Spectral Flexibility

The waveform lends itself to ease of manipulation through spectral slicing that is effectively an operation of spectral sampling. A relevant analogy is that of a train versus a fleet of trucks. While the train carriages might look quite similar, they are units in one complete set but the fleet of trucks comes with an independence of handling and manipulating each truck in an individual manner. For example, subcarriers experiencing a ‘good’ channel can be used to transmit a higher-order modulation signal (e.g., 64 or 256-QAM) that translates into more bits within the same time. Moreover, different subcarriers could be assigned to different users that forms the concept of Orthogonal Frequency Division Multiple Access (OFDMA). This kind of spectral slicing and manipulation helped in adoption of OFDM over many transmission schemes, even ahead of those with a slightly superior performance in some aspects.

MIMO Compatibility

In wireless channels, the ISI arises from multiple paths of the same signal arriving at the Rx antenna from different directions. MIMO systems suffer from additional interference where a signal sent by *each antenna at the Tx* is also received by *each antenna at the Rx*. If OFDM was not employed, the extent of both kinds of interference could hardly be manageable even with the best of equalizers. But with an underlying OFDM operation, each subcarrier stays independent of the others, thus producing frequency flat fading subcarriers even in the presence of multiple paths from the wireless channel as well as multiple signals coming from the Tx antennas. This is why MIMO-OFDM is the dominant air interface employed in 4G and 5G broadband wireless communication systems as well as modern WiFi local area networks.

8.4 Sub-Carrier Spacing (SCS)

A brief description of specifications for different Sub-Carrier Spacings (SCS) in 5G NR (Release 15) is shown in Table 8.1.

Table 8.1: OFDM Parameters for 5G NR (Release 15)

Parameter	15 kHz	30 kHz	60 kHz	120 kHz	240 kHz
Useful symbol duration	66.67 μ s	33.33 μ s	16.67 μ s	8.33 μ s	4.17 μ s
Cyclic prefix length	4.69 μ s	2.34 μ s	1.17 μ s	0.59 μ s	0.29 μ s
Total symbol duration	71.35 μ s	35.68 μ s	17.84 μ s	8.92 μ s	4.46 μ s

A comparison of LTE vs NR specs is shown in Figure 8.22. Notice the higher carrier frequencies, variable Sub-Carrier Spacings (explained in Section 8.4), wider bandwidths, downlink and uplink waveforms, and other such differences.

The carrier frequencies for NR range from low microwave frequencies to higher mmWave frequencies. Based on what we learned about OFDM before, there are multiple factors at play that determine what ranges of Sub-Carrier (SCS) spacing Δ_F are supported by the standard.

Consider the following relation reproduced from Eq (8.9).

$$\Delta_F = \frac{1}{T_u}$$

This implies that a large SCS translates to a shorter useful symbol time T_u , i.e., both the OFDM symbol duration and cyclic prefix length become smaller. This makes the system susceptible to more delay spread that distorts the signal in terms of Inter-Symbol Interference (ISI) and Inter-Carrier Interference (ICI). As a consequence, the narrower the SCS, the more resilient the system becomes in multipath channels. However, there are some other factors that put a lower limit on how small the SCS can be. We discuss two of them below.

Doppler Shift

With densely packed subcarriers, symbol times are long. However, the maximum duration after which the channel changes is given by coherence time T_C which puts an upper limit on how close the subcarriers can come. In frequency domain, a large Doppler spread also creates extra Inter-Carrier Interference (ICI) that hurts closely spaced subcarriers more than widely spaced ones.

LTE (3GPP Rel-15)		NR
Frequency Band	Sub-6 GHz	FR1: 410 MHz - 7 GHz FR2: 24 GHz – 52 GHz
Subcarrier Spacing	15 kHz	2 ⁿ .15 kHz
Maximum Bandwidth	20 MHz	FR1: 5, 10, 15, 20, 25, 30, 40, 50, 60, 80, 100 MHz FR2: 50, 100, 200, 400 MHz
Waveform	DL: CP-OFDM UL: SC-FDMA	DL: CP-OFDM UL: CP-OFDM, DFT-s-OFDM
Modulation	DL: Up to 256 QAM UL: Up to 64-QAM	DL: Up to 256 QAM UL: Up to 256 QAM
Max No. of Subcarriers	1200	3276
MIMO	Up to 8x8	Up to 8x8
Channel Coding	Data: Turbo Code Control: TBCC	Data: LDPC Code Control: Polar Code
Duplexing	FDD, Static TDD	FDD, Static TDD, Dynamic TDD

Figure 8.22: A comparison of LTE vs NR specs

Finally, the impact is different on high band as compared to low or mid bands. In Chapter 6, we studied how the Doppler shift increases with higher frequencies. This implies that the channel changes faster within the same time as compared to lower frequencies.

Phase Noise

A Local Oscillator (LO) of a Tx/Rx generates a sinusoidal signal for upconversion or downconversion of a modulated waveform. In an ideal world, a perfect sinusoid has a spectrum that is a single impulse. In a real world, the sinusoid is not perfect and is perturbed by rapid random fluctuations in phase that generated a mountain-like spectrum instead of a simple impulse. In general, the higher the carrier frequency, the larger the phase noise. For a narrow value of SCS (i.e., the subcarriers are closer to each other), there is more overlap between those mountain-shape spectra and this larger phase noise at higher frequencies can distort the signal and makes the demodulation process difficult for the Rx as the demodulated symbols are spread out in the Rx constellation.

Putting all this together, the SCS should be as small as possible above a given threshold that is determined by signal distortion in the presence of phase noise and Doppler.

The NR solution to this SCS spacing problem is to offer a range of SCS (in multiples of 15 kHz, the SCS in LTE) to accommodate different scenarios. The exact formula is given by

$$\Delta_F = 15 \cdot 2^\mu \text{ kHz}, \quad \mu = 0, 1, 2, 3, 4$$

We can see that the SCS in NR ranges from $15 \cdot 2^0 = 15$ kHz to $15 \cdot 2^4 = 240$ kHz. The resultant segmented bandwidth can be visualized as in Figure 8.23.

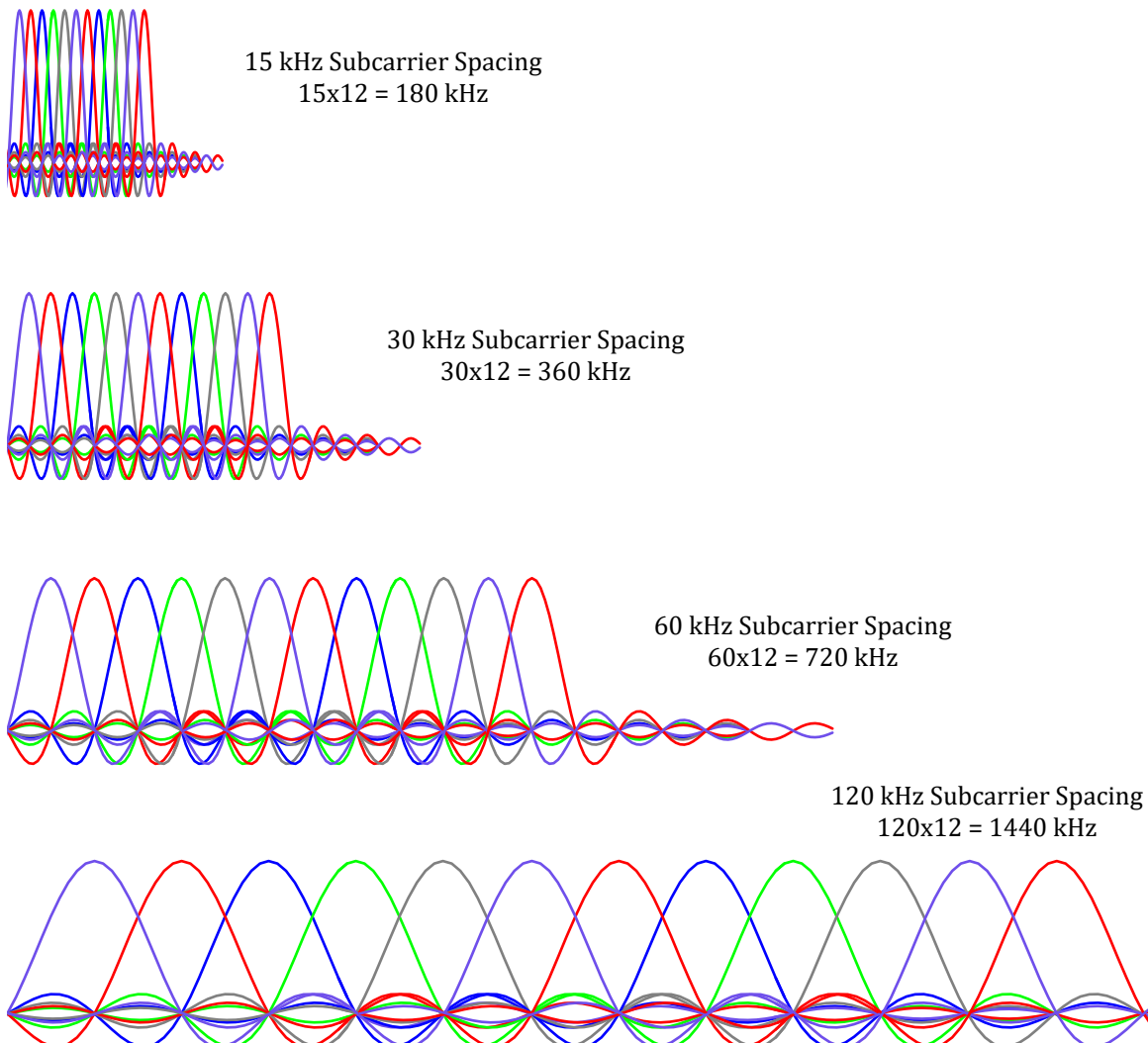


Figure 8.23: NR subcarrier numerology

8.5 DFT-Precoded OFDM

One of the drawbacks of an OFDM waveform is its high Peak to Average Power Ratio (PAPR).

- This high PAPR arises from the fact that a set of N QAM symbols are taken into time domain through an iFFT operation that basically generates a combination of complex sinusoids scaled by those symbols. Due to the variations between the symbol values and the sinusoids with different frequencies, the output waveform can have a large variance in amplitudes.
- This reduces the power amplifier efficiency that results in faster battery drainage in a mobile terminal. The effect on base station performance is less critical.

To mitigate this problem at the mobile terminal, NR allows DFT-Precoded OFDM or DFT-spread-OFDM (DFT-s-OFDM) on the user side. A block diagram of such a scheme is drawn in Figure 8.24 from a Tx viewpoint. It is quite similar to the OFDM Tx block diagram at the top of Figure 8.21 with one critical difference: the presence of a DFT block after the modulation. Let us discuss the role it plays in keeping the waveform PAPR low.

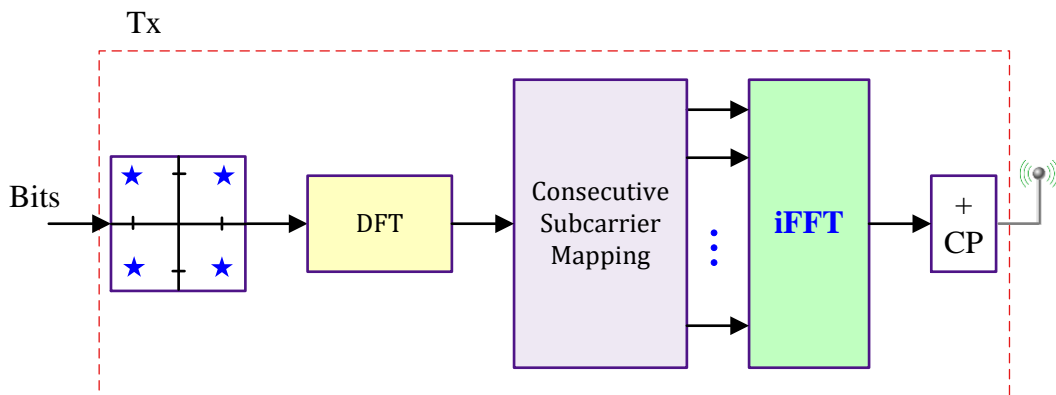


Figure 8.24: A block diagram for DFT-Precoded OFDM

The modulation symbols are first input to a DFT (i.e., FFT), the output of which is mapped on subcarriers and given as input to the iFFT operation. Looking at the constellation diagrams of any QAM modulation scheme, the amplitude variations are not too large. Since a transform followed by an inverse transform tends to have a canceling effect (they exactly cancel each other if they are of the same size), the output of the iFFT operation has a PAPR not much different than the input to the DFT operation, i.e., the input QAM symbols. To recap, if the modulation symbols are input to an M -point DFT and the output is mapped on contiguous subcarriers that are then input to an N -point iFFT, the overall waveform has a low PAPR value that makes it suitable for the user equipment. For this reason, while the downlink waveform in the NR standard is OFDM, the standard allows both OFDM and DFT-Precoded OFDM on the uplink.

8.6 The Small Picture

In high rate wireless systems, multipath effect becomes the major bottleneck due to resource intensive time domain equalization techniques.

- This problem is overcome in time domain by transmitting the same information in several low rate parallel streams.
- Such an expansion in time segments in frequency domain the available bandwidth into many parallel frequency flat channels.
- Since convolution in time is multiplication in frequency, equalization for each narrow slice requires just a single division operation, significantly reducing the computational load of the equalizer.

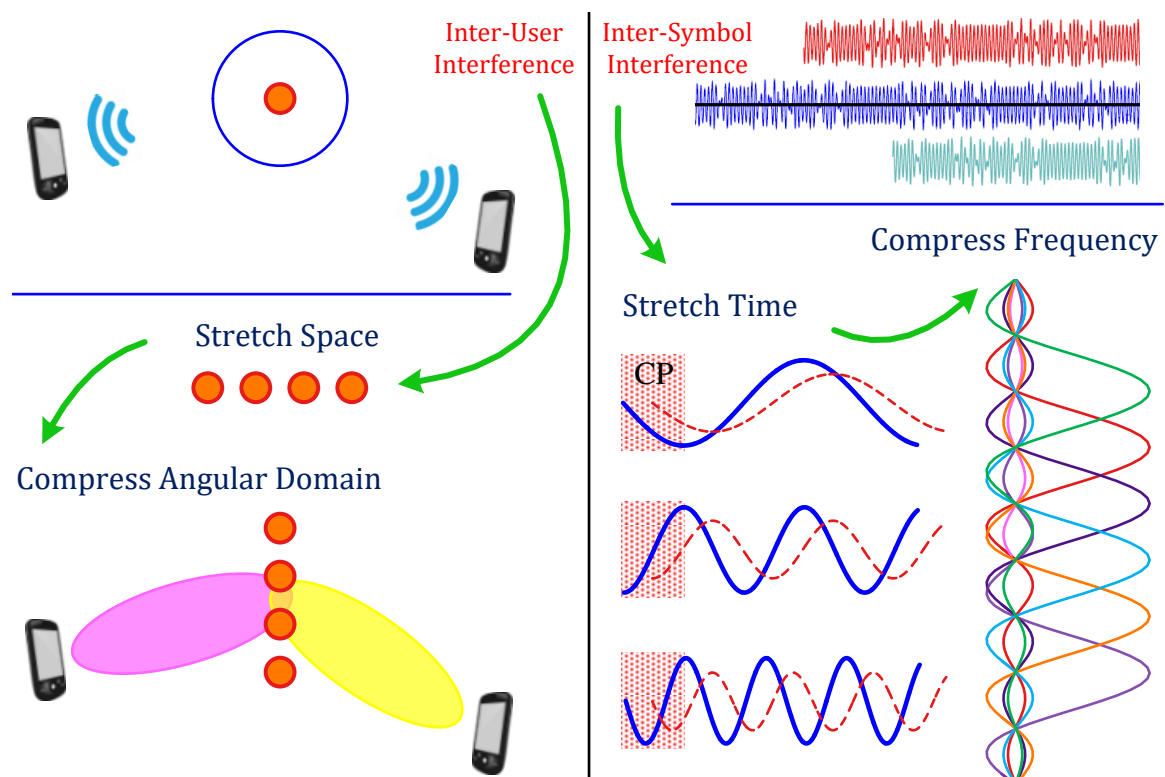
Viewed from another angle, OFDM employs a set of complex sinusoids in time domain that *samples the channel in frequency domain* at discrete intervals in frequency, see Figure 8.18. I find the similarity of this perspective with a single-carrier time domain waveform very fascinating and beautiful.

One Page Summary

While the figures only take *one* page, I decided to include a brief description to explain the ideas further. The reader should go through the respective chapters to fully appreciate how this page summarizes the understanding of 5G cellular systems. There are three main themes in this regard.

1. Stretch in One Domain to Compress in Another

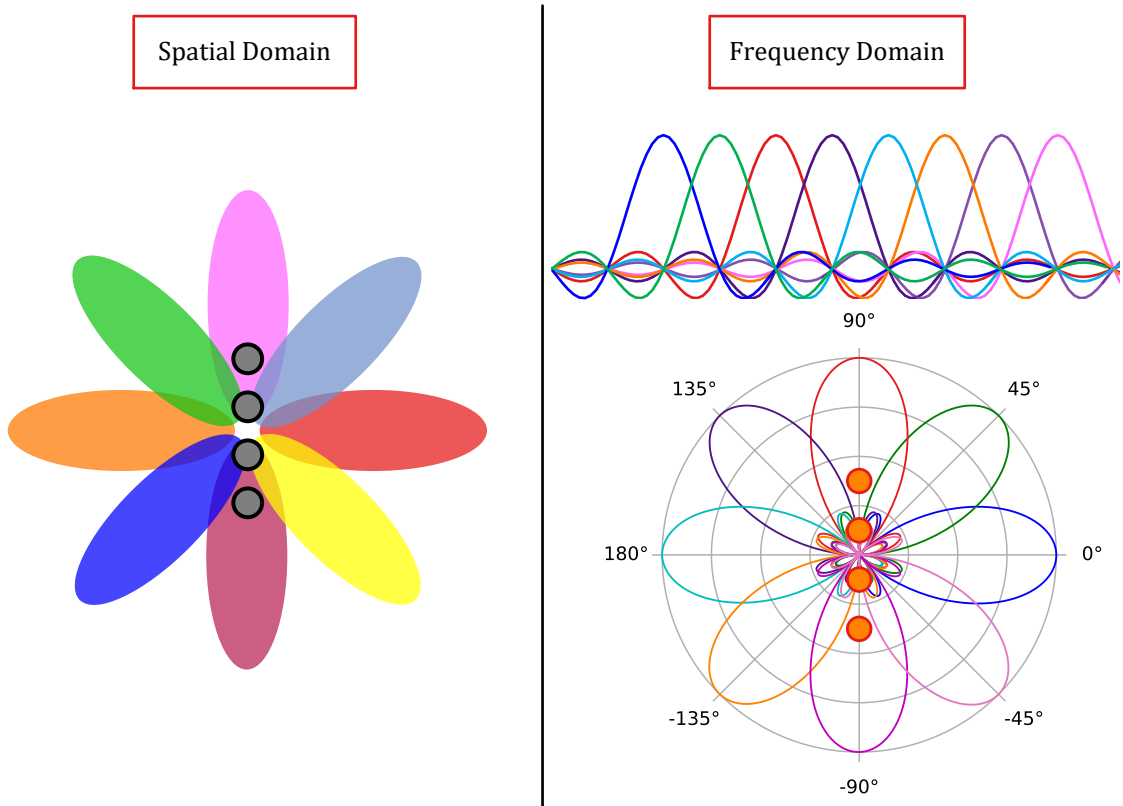
There are three villains in a cellular system: (1) Inter-User Interference (2) Inter-Symbol Interference (3) Fading. The fight against the first two relies on the same principle: Stretching in one domain produces compression in the other.



- To handle Inter-User Interference, an antenna array stretches the signal in space to compress the angle for narrow beams.
- To handle Inter-Symbol Interference, OFDM stretches the signal in time to compress the spectrum for narrow subcarriers.

2. The Two Flowers

Following the above procedure, classical beamforming creates pointed beams in space that separates the cell users in angular domain (generalized beamforming does the same in a mathematical sense). Similarly, OFDM creates pointed beams in spectrum that separates the modulation symbols in frequency domain. The resemblance between the two is visible in the figure when the OFDM subcarriers are also bent into a polar pattern. The blue subcarrier on the left points at 0° in the polar plot and subsequent colors follow the order in a similar manner.



3. Going Massive

Another theme is going massive to solve the problems. (a) This is done in the number of antennas in massive MIMO to combat the third villain mentioned above, i.e., fading, through channel hardening and favorable propagation. (b) mmWave bands are chosen for deploying massive amounts of bandwidths. (c) The LDPC codes introduce a massive parity check matrix that ultimately translates into better coding gains. (d) Finally, the system is evolving towards massive cell density that in the limit approaches a cell-free (user centric) architecture.

Bibliography

- [1] C. Shannon, *A mathematical theory of communication*, Bell System Technical Journal, 27, 1948.
- [2] Q. Chaudhari, *Wireless Communications from the Ground Up - An SDR Perspective*, KDP, 2018.
- [3] K. McClaning, *Wireless Receiver Design for Digital Communications*, 2nd Edition, Scitech Publishing, 2012.
- [4] E. Larsson, P. Stoica, *Space-Time Block Coding for Wireless Communications*, Cambridge University Press, 2003.
- [5] D. Tse, P. Viswanath, *Fundamentals of Wireless Communication*, Cambridge University Press, 2005.
- [6] M. Dohler et al., *Is the PHY layer dead?*, IEEE Communications Magazine, Vol. 49, 2011.
- [7] T. Marzetta, Non-Cooperative Cellular Wireless with Unlimited Number of Base Station Antennas, IEEE Transactions on Wireless Communications, Vol. 9, No. 11, Nov 2010.
- [8] T. Marzetta et al. *Fundamentals of Massive MIMO*, Cambridge University Press, 2016.
- [9] P. Delos, B. Broughton, J. Kraft, Phase Array Antenna Patterns, Analog Dialogue, Vol. 54, No. 2, May 2020.
- [10] J. Andrews, A. Ghosh, R. Muhamed, *Fundamentals of WiMAX - Understanding Broadband Wireless Networking*, Prentice Hall, 2007.
- [11] E. Björnson, J. Hoydis and L. Sanguinetti, *Massive MIMO Networks: Spectral, Energy, and Hardware Efficiency*, Foundations and Trends in Signal Processing: Vol. 11: No. 3-4, 2017.
- [12] T. Rappaport, R. Heath, R. Daniels, J. Murdock, *Millimeter Wave Wireless Communications*, Pearson, 2014.
- [13] R. Mailloux, *Phased Array Antenna Handbook*, 2nd ed., Artech House, 2005.
- [14] C. Balanis, *Antenna Theory: Analysis and Design*, 3rd ed., Wiley-Interscience, 2005.
- [15] P. Hindle et al., 5G Phased Array Technologies, Microwave Journal, Sep 2019.

- [16] S. Buzzi and C. D'Andrea, *Massive MIMO 5G Cellular Networks: mm-Wave vs μ -wave frequencies*, ZTE Communications, Vol. 15, No. S1, 2017.
- [17] D. Costello, G. Forney, *Channel coding: The road to channel capacity*, Proceedings of the IEEE, Vol. 95, 2007.
- [18] J. Hagenauer, E. Offer, L. Papke, *Iterative decoding of binary block and convolutional codes*, IEEE Transactions on Information Theory, Vol. 42, No. 2, Mar 1996.
- [19] N. Varnica, K. Gunnam, *IEEE Tutorial on LDPC Decoding, VLSI Architectures and Implementations*, Flash Memory Summit Conference, Santa Clara, Aug 2013.
- [20] H. Asplund, D. Astely, P. Butovitsch, T. Chapman, M. Frenne, F. Ghasemzadeh, M. Hagstrom, B. Hogan, G. Jongren, J. Karlsson, F. Kronestedt, E. Larsson, *Advanced Antenna Systems for 5G Network Deployments, Bridging the Gap Between Theory and Practice*, Academic Press, 2020.

About the Author



Qasim Chaudhari is an independent consultant and trainer with expertise in wireless communications, Software Defined Radio (SDR) and Digital Signal Processing (DSP). As the founder of <https://wirelesspi.com>, he focuses on explaining concepts through beautiful figures, simple mathematics and intuitive reasoning. After obtaining a PhD in Electrical Engineering from Texas A&M University, he worked in different research labs on DSP algorithms development for real world demonstrations of wireless systems such as a MIMO-OFDM testbed, low-SNR receivers and phase of arrival based localization. You can reach him at info@wirelesspi.com.
